

CHEMICAL COMPOSITION OF ATMOSPHERIC PARTICLES AS A TOOL TO
IDENTIFY SOURCES AFFECTING AEROSOL POPULATION IN THE
EASTERN BLACK SEA ATMOSPHERE

A THESIS SUBMITTED TO
THE GRADUATE SCHOOL OF NATURAL AND APPLIED SCIENCES
OF
MIDDLE EAST TECHNICAL UNIVERSITY

BY

İLKER BALÇILAR

IN PARTIAL FULFILLMENT OF THE REQUIREMENTS
FOR
THE DEGREE OF DOCTOR OF PHILOSOPHY
IN
ENVIRONMENTAL ENGINEERING

MARCH 2018

Approval of the thesis:

**CHEMICAL COMPOSITION OF ATMOSPHERIC PARTICLES AS A TOOL
TO IDENTIFY SOURCES AFFECTING AEROSOL POPULATION IN THE
EASTERN BLACK SEA ATMOSPHERE**

submitted by **İLKER BALÇILAR** in partial fulfillment of the requirements for the degree of **Doctor of Philosophy in Environmental Engineering Department, Middle East Technical University** by,

Prof. Dr. Halil Kalıpçılar
Dean, Graduate School of **Natural and Applied Sciences** _____

Prof. Dr. Kahraman Ünlü
Head of Department, **Environmental Engineering** _____

Prof. Dr. Gürdal Tuncel
Supervisor, **Environmental Engineering Dept., METU** _____

Examining Committee Members:

Prof. Dr. Ayşegül Aksoy
Environmental Engineering Dept., METU _____

Prof. Dr. Gürdal Tuncel
Environmental Engineering Dept., METU _____

Prof. Dr. Gülen Güllü
Environmental Engineering Dept., Hacettepe University _____

Prof. Dr. Duran Karakaş
Environmental Engineering Dept., AİBU _____

Assoc. Prof. Dr. Tuba Hande Bayramoğlu
Environmental Engineering Dept., METU _____

Date: March 19, 2018

I hereby declare that all information in this document has been obtained and presented in accordance with academic rules and ethical conduct. I also declare that, as required by these rules and conduct, I have fully cited and referenced all the material and results that are not original to this work.

Name, Last name: İlker Balcılar

Signature :

ABSTRACT

CHEMICAL COMPOSITION OF ATMOSPHERIC PARTICLES AS A TOOL TO IDENTIFY SOURCES AFFECTING AEROSOL POPULATION IN THE EASTERN BLACK SEA ATMOSPHERE

Balcılar, İlker

Ph.D., Department of Environmental Engineering

Supervisor: Prof. Dr. Gürdal Tuncel

March 2018, 250 pages

Daily size distributed particulate matter samples were collected at a rural station on Eastern Black Sea region between March 2011 and December 2013. Particulate matter samples were analyzed for trace elements by ICP-MS and ED-XRF and for black carbon by Aethalometer. Mean concentrations of trace elements in the fine fraction varied between 0.0011 ng m⁻³ for Tm and 1382.42 ng m⁻³ for SO₄²⁻, while mean concentrations in the coarse fraction varied between 0.0017 ng m⁻³ for Tm and 1441.5 ng m⁻³ for Si. The dominant sectors of air masses arriving the Eastern Black Sea region were N, NE and E in summer and SE, S, SW and W in winter. Air masses were classified into eight clusters regarding their wind speed and direction. Rainfall was found as the only local meteorological parameter affecting concentrations of species. The average contribution of episodes to the concentrations of elements was 60%. Source apportionment of PM was carried out by PMF model and seven sources were resolved. Power plant emissions were found to be the major contributor to PM_{2.5} (50%). The second largest source was the anthropogenic source with a contribution of 17%. Crustal factors were also remarkable sources with 15% contribution in total.

Urban pollution emission were accounted for 13% of PM_{2.5} mass. The iron and steel plant emission and oil processing emission were accounted 2% and 3% of PM_{2.5} mass, respectively. Potential source regions of resolved sources were determined by potential source contribution function analysis.

Keywords: Eastern Black Sea, Long-range Transport, Trace Element, Positive Matrix Factorization, Potential Source Contribution Function.

ÖZ

DOĞU KARADENİZ ATMOSFERİNDEKİ AEROSOL POPÜLASYONUNU ETKİLEYEN KAYNAKLARIN BELİRLENMESİNDE ATMOSFERİK PARÇACIKLARIN KİMYASAL BİLEŞİMİNİN BİR ARAÇ OLARAK KULLANILMASI

Balcılar, İlker

Doktora, Çevre Mühendisliği Bölümü

Tez Yöneticisi: Prof. Dr. Gürdal Tuncel

Mart 2018, 250 sayfa

Günlük boyut dağılımlı partikül madde örnekleri Doğu Karadeniz Bölgesi'nde kırsal bir istasyonda Mart 2011 ve Aralık 2013 tarihleri arasında toplanmıştır. Örnekler eser element içeriği için ICP-MS ve ED-XRF ile, siyah karbon içeriği için Atelometre cihazı ile analiz edilmiştir. Elementlerin ortalama konsantrasyonları ince fraksiyonda Tm ve SO₄²⁻ için sırasıyla 0.0011 ng m⁻³ -1382.42 ng m⁻³ aralığında değişirken, kaba fraksiyonda Tm ve Si için sırasıyla 0.0017 ng m⁻³ -1441.5 ng m⁻³ aralığında değişmiştir. Doğu Karadeniz Bölgesi'ne ulaşan hava kütlelerinin hakim yönü yaz aylarında kuzey, kuzeydoğu ve doğu iken kış aylarında ise güneydoğu, güney, güneybatı ve batı sektörleridir. Hava kütleleri rüzgâr hızlarına ve geliş yönleri göre sekiz farklı kümeye ayrılmıştır. Yerel meteorolojik faktörlerden sadece yağmurun elementlerin konsantrasyonlarını etkilediği tespit edilmiştir. Episodların elementlerin konsantrasyonlarına olan ortalama katkısı %60 olmuştur. Partikül maddeyi etkileyen kaynakları bulmak için PMF modeli kullanılmış ve yedi kaynak ayrıştırılmıştır. Enerji santrali emisyonları PM_{2.5} kütlelerinin %50'sini oluşturarak en büyük katkıya sahiptir. Katkısı ikinci sırada yer alan antropojenik kaynaklı emisyonlar PM_{2.5} kütlelerinin

%17'sini oluřturmuřtur. Toprak fakt6rleri toplamda %15'lik katkı ile dikkat çekmektedir. Őehir kaynaklı emisyonların $PM_{2.5}$ kütlesine katkısı %13 olmuřtur. Demir çelik fabrikaları ve petrol rafinesi emisyonları sıyasıyla $PM_{2.5}$ kütlesine %2'lik ve %3'lük katkı yapmıřtır. PMF ile ayrıřtırılan kaynakların kaynak potansiyel kaynak katkı fonksiyonu analizi ile belirlenmiřtir.

Anahtar Kelimeler: Doęu Karadeniz, Uzun Mesafeli Tařınım, Eser Element, Pozitif Matriks Fakt6rizasyonu, Potansiyel Kaynak Katkı Fonksiyonu

To Begüm and Ayda

ACKNOWLEDGEMENTS

I would like to express my sincere gratitude to the following people for their tremendous help and support. Without their encouragement and guidance, I would never have been able to realize this work.

First and foremost, I would like to express my greatest appreciation to my enthusiastic supervisor Prof. Dr. Gürdal Tuncel. As you might guess, PhD is a long journey with ups and downs, mostly downs. He made this tough journey bearable. His never-ending energy and work enthusiasm became my greatest motivation in this process. I wish to thank his not only for his tremendous academic support and valuable guidance but also for providing me so many wonderful opportunities. I am very lucky to have the opportunity to do a PhD under his guidance.

I would like to thank to my committee members Prof. Dr. Ayşegül Aksoy, Prof. Dr. Gülen Güllü, Prof. Dr. Duran Karakaş and Assoc. Prof. Dr. Tuba Hande Bayramoğlu for their encouragement, insightful comments and valuable suggestions.

I would like to extend my gratitude to the financial support from The Scientific and Technological Research Council of Turkey (TÜBİTAK) BİDEB for my one year research in USA.

I extend my sincere thanks to Dr. Güray Doğan, Dr. Derya Deniz Genç Tokgöz, and Dr. Fatma Öztürk who are former graduates of our group for sharing their knowledge and experiences.

A special acknowledgement goes to my dear friends of many years: Ebru Koçak, Elif Küçük, Selcen Ak, and Nilüfer Ülgüdür. They were true friends since we met in 2010. I would like to thank you guys for your motivation, encouragement and especially for

all the fun we have had in the last eight years. You were always there to when I need you.

To my family, particularly my parents and brothers and sister, thank you for your love, support, and unwavering belief in me. Without you, I would not be the person I am today.

Finally, I would like to thank my wife, Begüm, and our little girl, Ayda, for their love, patience and support. My wife has given me the hope and encouragement to continue my research and to be an academician. I owe you everything. I dedicate this Ph.D. thesis to you, my girls.

The author gratefully acknowledges the support from TÜBİTAK ÇAYDAG (Project Code: 108Y306).

TABLE OF CONTENTS

ABSTRACT	v
ÖZ	vii
ACKNOWLEDGEMENTS	x
TABLE OF CONTENTS	xiii
LIST OF TABLES	xvii
LIST OF FIGURES	xix
LIST OF ABBREVIATIONS	xxiii

CHAPTERS

1 BACKGROUND	1
1.1 Aim of the Study	4
2 LITERATURE REVIEW	7
2.1 Particulate Matter	7
2.2 Size Distribution of Particulate Matter in the Atmosphere	8
2.3 Sources of Particulate Matter	11
2.3.1 Natural Sources	12
2.3.2 Anthropogenic Sources	14
2.4 Trace Elements	17
2.5 Environmental Effects of Particulate Matter	19
2.5.1 Health Effects of Particulate Matter	19
2.5.2 The Effects of Particulate Matter on Haze Formation	20
2.5.3 Effects of Particulate Matter on Hydrological Cycle	21
2.5.4 The Role of Particulate Matter in Climate Change	23
2.6 The Long Range Transport of Particulate Matter	24
2.7 National and International Air Quality Standards	25
2.8 Source Apportionment of Particulate Matter	27

2.9	Aerosol Studies in Black Sea	30
3	MATERIAL AND METHODS	33
3.1	Sampling.....	33
3.1.1	Sampling Location	33
3.1.2	Sampling Equipment	34
3.1.3	Sample Handling	40
3.2	Analytical Techniques.....	41
3.2.1	Gravimetric Analysis.....	41
3.2.2	Black Carbon Analysis.....	41
3.2.3	Trace Element Determination	43
3.2.3.1	ED-XRF Analysis	43
3.2.3.2	ICP-MS Analysis.....	46
3.2.3.2.1	Preparation of Samples for ICP-MS Analysis	46
3.2.3.2.2	Analysis	49
3.3	Quality Assurance and Quality Control for ED-XRF and ICP-MS Analysis	51
3.3.1	Method Detection Limit	51
3.3.1.1	Method Detection Limit of ED-XRF	52
3.3.1.2	Method Detection Limit of ICP-MS	53
3.3.2	Blank Analysis	54
3.3.2.1	ED-XRF Blank Analysis	55
3.3.2.2	ICP-MS Blank Analysis	56
3.3.3	SRM Analysis	63
3.3.3.1	ED-XRF SRM Analysis	63
3.3.3.2	ICP-MS SRM Analysis	64
3.3.4	Replicate and Repeated Analysis of test Samples by ICP-MS	65
3.3.5	Comparison of ED-XRF and ICP-MS Data Sets	66
3.4	Source Apportionment	69
3.4.1	Positive Matrix Factorization (PMF)	69
3.4.2	Back Trajectory Modeling	72
3.4.3	Potential Source Contribution Function (PSCF).....	74
4	RESULTS AND DISCUSSION	77

4.1	General Characteristic of the Data Set	77
4.1.1	Data Set	77
4.1.2	Distribution Characteristic of Data Set	82
4.1.3	Coarse to fine concentration ratios of elements	88
4.2	Comparison with Literature	91
4.3	Flow Climatology	100
4.3.1	Residence Time Analysis	100
4.3.2	Contribution of Wind Sectors to the Residence Time of Trajectories ..	106
4.3.3	Cluster Analysis	113
4.4	Relation between Elemental Concentrations and Local Meteorology	128
4.4.1	Relation Between Wind Speed and Concentrations of Species	131
4.4.2	Relation Between Temperature and Concentrations of Species	132
4.4.3	Relation Between Local Rain and Concentrations of Species	135
4.5	Temporal Variations of Pollutants	140
4.5.1	Short Term Variations	141
4.5.2	Long Term Variations	148
4.6	Source Apportionment	158
4.6.1	Enrichment Factor	158
4.6.2	Contribution of Forest Fires	166
4.6.3	Dust Transport to the Eastern Black Sea Region	173
4.6.4	Positive Matrix Factorization and Potential Source Contribution Function	182
5	CONCLUSIONS AND RECOMMENDATIONS	215
	REFERENCES	221
	CIRRICULUM VITAE	247

LIST OF TABLES

TABLES

Table 2.1 Elemental composition of atmospheric particulate matter	18
Table 2.2 National and international air quality standards for 6 criteria air pollutants	26
Table 2.3 National air quality standards for benzene, As, Cd, Ni, and Benzo(a)pyrene	26
Table 3.1. Different measurement conditions used in the spectrometer during analysis of a sample	45
Table 3.2 Three phase digestion program	47
Table 3.3. ICP-MS Operating Parameters.....	51
Table 3.4. ED-XRF MDL of elements and percent BDL in each fractions.....	52
Table 3.5 ICP-MS MDL of elements and percent BDL in each fractions.....	53
Table 3.6 Average field blank concentrations and percent contributions to size fractions.....	56
Table 3.7 Average field blank concentrations and standard deviations (ng 50ml ⁻¹)..	57
Table 3.8 NIST SRM 2783 certified and measured concentrations of elements and percent error	63
Table 3.9. NIST SRM 1648a certified and measured concentrations of elements and percent error	64
Table 3.10 Comparison of ED-XRF and ICP-MS for the measured common elements	66
Table 4.1 Statistical summary of concentration (ng m ⁻³) of trace elements, black carbon and PM mass of fine fraction aerosols	79
Table 4.2 Statistical summary of concentration (ng m ⁻³) of elements, black carbon and PM mass of coarse fraction aerosols	81
Table 4.3 Distribution types of elements in the fine and coarse fraction.....	84

Table 4.4 Comparison of current study with the other studies in the literature (concentrations in ng m^{-3})	95
Table 4.5 Percent contribution of each wind sector for 100, 500, 1500 m arrival height back trajectories and combined back trajectories.....	107
Table 4.6 Number and percentage of trajectories allocated in each cluster	116
Table 4.7 Median concentrations of measured species (ng m^{-3}) and K-W test p-values	120
Table 4.8 Long term (1961-2016 years) average temperature, relative humidity, total rainfall and wind speed at Gümüşhane meteorological station.....	129
Table 4.9 Elemental concentration vs wind speed regression p-values	131
Table 4.10 Elemental concentration vs temperature regression p-values	133
Table 4.11 Mean and median concentrations of elements in rainy and non-rainy days (ng m^{-3}).....	136
Table 4.12 Comparison of median concentrations of species on non-rainy and rainy days with Mann-Whitney test and p-values	139
Table 4.13 Baseline concentration of elements and percent concentrations accounted by episodes	143
Table 4.14 Summer and winter concentrations of elements in fine fraction (concentrations are in ng m^{-3}).....	150
Table 4.15 Summer and winter concentrations of elements in coarse fraction. (concentrations are in ng m^{-3}).....	151
Table 4.16 Categories assigned to species	183
Table 4.17 Bootstrap factors mapped to base factors.....	185

LIST OF FIGURES

FIGURES

Figure 2.1 Size distribution and formation mechanisms of aerosols	10
Figure 2.2 US national summary of particulate matter (PM) emissions by source sector	13
Figure 2.3 PM _{2.5} source attribution results for seven urban sites in the US.....	15
Figure 2.4 Results of a PM ₁₀ source apportionment study performed at a roadside location in New York City in April 1992	16
Figure 2.5 (a) sulfur deposits in different regions of Turkey and (b) contribution of foreign sources to precipitated amounts.....	32
Figure 3.1 Location of the sampling station	35
Figure 3.2 PM ₁₀ pre impactor and holder	37
Figure 3.3 Filter holder and polycarbonate filters.....	38
Figure 3.4 Constant flow pump used in SFU	39
Figure 3.5 Microwave digestion system	48
Figure 3.6 Open digestion vessels placed on hot place.....	48
Figure 3.7 Sub-boiling distillation unit	49
Figure 3.8 Coarse fraction sample to blank ratio for elements	59
Figure 3.9 Fine fraction sample to blank ratio for elements	60
Figure 3.10 Trace element ratios of purified and commercially available HNO ₃	62
Figure 3.11 Elemental ratios of repeated analysis of test samples.....	67
Figure 3.12 Elemental ratios of replicate analysis of test samples	68
Figure 3.13 The study domain used in PSCF analysis.....	75
Figure 4.1 Log-normal distribution examples of selected elements	86
Figure 4.2 Right skewed distribution examples of selected elements	87
Figure 4.3 Coarse-to-fine median concentration ratios (C/F) of elements.....	90
Figure 4.4 Comparison of current study with the other studies in the literature.....	96

Figure 4.5 Distribution of iron and steel plants in Europe	99
Figure 4.6 The study domain used in residence time analysis	102
Figure 4.7 Residence time analysis for trajectories 100m, 500m, 1500m arrival heights and combined trajectories.....	104
Figure 4.8 Differences between summer and winter residence times of air masses for 100m, 500m, 1500m arrival heights and combined back trajectories.....	105
Figure 4.9 Study domain used in the calculation of contribution of wind sectors... ..	106
Figure 4.10 Percent contribution of wind sectors to residence time of trajectories arriving to the station.....	109
Figure 4.11 Seasonal variations of percent contributions of wind sectors.....	111
Figure 4.12 Comparison of seasonal contributions of wind sectors at different parts of Turkey	112
Figure 4.13 Selection of optimum number of clusters for combined trajectories....	114
Figure 4.14 Cluster centroids of clusters calculated for combined trajectories	115
Figure 4.15 Trajectories allocated to different clusters.....	119
Figure 4.16 Cluster median concentrations of selected crustal elements.....	122
Figure 4.17 Cluster median concentrations of pollution derived elements.....	123
Figure 4.18 Cluster median concentrations of elements with mixed origin.....	124
Figure 4.19 Median concentrations of crustal elements in Clusters 1 and 5.....	127
Figure 4.20 Annual, summer and winter wind roses.....	130
Figure 4.21 Log-log scatter plots of elements against wind speed	132
Figure 4.22 Binary correlations between concentrations of selected elements and temperature.....	134
Figure 4.23 Median concentration ratios of species on non-rainy rainy days.....	138
Figure 4.24 Frequency histogram for calculation of most frequently occurring value	142
Figure 4.25 Percent concentrations accounted by episodes annually	146
Figure 4.26 Baseline concentrations of elements Amasra, Antalya and Torul stations	147
Figure 4.27 Summer-to-winter median ratios of elements in fine and coarse fractions	153

Figure 4.28 Monthly variation in concentrations of selected crustal elements at Eastern Black Sea.....	155
Figure 4.29 Anthropogenic elements with higher concentrations in summer	156
Figure 4.30 Anthropogenic elements, which do not show a well-defined seasonal variation.....	157
Figure 4.31 Crustal enrichment factors of elements in PM ₁₀ and PM _{2.5} fractions...	160
Figure 4.32 EF _c -Al diagram for crustal elements	162
Figure 4.33 EF _c -Al diagram of anthropogenic elements.....	164
Figure 4.34 EF _c -Al diagram of elements with mixed origin.....	165
Figure 4.35 Time series plots of K concentration and enrichment factor	168
Figure 4.36 Trajectories and locations of forest fires during K episode days.....	171
Figure 4.37 Fire day – to – non fire day ratios of concentrations and enrichment factors of elements	172
Figure 4.38 Dream model outputs for selected dust days at Torul station.....	175
Figure 4.39 Modis optical depth satellite images for selected dust days at Torul station	176
Figure 4.40 OMI Aerosol Index satellite images for selected dust days at Torul station	177
Figure 4.41 Back trajectories for selected dust days at Torul station	178
Figure 4.42 Selected Dust episode days along with Al and Si time series	179
Figure 4.43 Comparison of (a) dust and non-dust days, (b) trace element composition of dust arriving from Middle East + Arabic Peninsula and Sahara	181
Figure 4.44 Scaled residuals of some selected elements.....	186
Figure 4.45 Observed and predicted concentrations of selected species	187
Figure 4.46 Observed and predicted concentrations of PM _{2.5} mass.....	188
Figure 4.47 Diagnostic figures for factor 1, which includes Factor loadings, fractions of elemental concentrations explained, Seasonal variation in factor scores and crustal enrichment factors of elements	190
Figure 4.48 Trajectories corresponding to highest 30% of g-scores of each factor.	191
Figure 4.49 Distribution of PSCF values computed using trajectories that correspond to highest 30% of factor 1 scores as “polluted” trajectories	192
Figure 4.50 Contribution of each factor to PM _{2.5} mass at Eastern Black Sea.....	193

Figure 4.51 Diagnostic figures for factor 2, which includes Factor loadings, fractions of elemental concentrations explained, Seasonal variation in factor scores and crustal enrichment factors of elements	196
Figure 4.52 Distribution of PSCF values computed using trajectories that correspond to highest 30% of factor 2 scores as “polluted” trajectories	197
Figure 4.53 Diagnostic figures for factor 3, which includes Factor loadings, fractions of elemental concentrations explained, Seasonal variation in factor scores and crustal enrichment factors of elements	200
Figure 4.54 Distribution of PSCF values computed using trajectories that correspond to highest 30% of factor 3 scores as “polluted” trajectories	201
Figure 4.55 Diagnostic figures for factor 4, which includes Factor loadings, fractions of elemental concentrations explained, Seasonal variation in factor scores and crustal enrichment factors of elements	203
Figure 4.56 Distribution of PSCF values computed using trajectories that correspond to highest 30% of factor 4 scores as “polluted” trajectories	204
Figure 4.57 Diagnostic figures for factor 5, which includes Factor loadings, fractions of elemental concentrations explained, Seasonal variation in factor scores and crustal enrichment factors of elements	206
Figure 4.58 Distribution of PSCF values computed using trajectories that correspond to highest 30% of factor 5 scores as “polluted” trajectories	207
Figure 4.59 Diagnostic figures for factor 6, which includes Factor loadings, fractions of elemental concentrations explained, Seasonal variation in factor scores and crustal enrichment factors of elements	209
Figure 4.60 Distribution of PSCF values computed using trajectories that correspond to highest 30% of factor 6 scores as “polluted” trajectories. Locations of Refineries in the region are marked on the map	210
Figure 4.61 Diagnostic figures for factor 7, which includes Factor loadings, fractions of elemental concentrations explained, Seasonal variation in factor scores and crustal enrichment factors of elements	213
Figure 4.62 Distribution of PSCF values computed using trajectories that correspond to highest 30% of factor 7 scores as “polluted” trajectories	214

LIST OF ABBREVIATIONS

AAS	Atomic Absorption
B.C.	Black Carbon
CCN	Cloud Condensation Nuclei
CLRTAP	Convention on Long-range Transboundary Air Pollution
CMB	Chemical Mass Balance
CWT	Concentration Weighted Trajectory
ED-XRF	Energy Dispersive X-ray Fluorescence
FA	Factor Analysis
IC	Ion Chromatography
ICP-MS	Inductively coupled plasma mass spectrometry
INAA	Instrumental Neutron Activation Analysis
ME	Multilinear Engine
MLR	Multiple Linear Regression
NOAA	US National Oceanic and Atmospheric Administration
PCA	Principle Component Analysis
PIXE	Proton Induced X-ray Emissions
PGAA	Prompt Gamma Activation
PM	Particulate Matter
PMF	Positive Matrix Factorization
PSCF	Potential Source Contribution Function
TÜBİTAK	Türkiye Bilimsel ve Teknolojik Araştırma Kurumu
US EPA	United States Environmental Protection Agency
WHO	World Health Organization

CHAPTER 1

BACKGROUND

The regional transport of pollutants through atmosphere and this way damaging the forest and lake ecosystems has been one of the most important agenda items in Europe and in other parts of the world. The most important indication of this is the Convention on Long-range Transboundary Air Pollution (CLRTAP), which is the first international binding treaty, signed by the European Countries and by Turkey as State Party in 1979 and additional protocols developed later on this convention. The air pollution problem is dealt by the convention on a regional basis. The concept of regional air pollution has led to very comprehensive work not only in Mediterranean Basin but also in almost all of the world. As a result, there are many studies in the Eastern Mediterranean Region, Mediterranean and Aegean regions today.

The literature in Mediterranean and Eastern Mediterranean basin have studied the chemical and physical characteristics of existing aerosol population in the basin. Now, there is a broad database for Mediterranean particle composition. The studies (e.g., Güllü et al., 2000; Koçak et al., 2007; Koçak et al., 2012; Koulouri et al., 2008; Öztürk et al., 2012; Pey et al., 2013) showed that Mediterranean particles have four main components; a crustal component; an anthropogenic component; a sea salt component; a biogenic component. The source locations for crustal component were arid regions at North Africa and Middle East, while for anthropogenic component the source locations were industrialized regions located at the north of the basin. The anthropogenic component of Western and Eastern Mediterranean aerosol was studied extensively to identify source types affecting the basin and to determine the locations of these sources. The modeling studies (e.g., Barnaba and Gobbi, 2004; Spyridaki et al., 2006) also investigated the physical and radiative characteristics of Eastern (Fotiadi et al., 2006; Ichoku et al., 1999) and Western (Esteve et al., 2012; Mallet et

al., 2011) Mediterranean particles. Lidar network was also established around the basin (Balis et al., 2003).

Studies to investigate chemical composition of Black Sea particles are not as abundant as the studies in the Mediterranean region. There are a few data sets generated to determine the pollutant levels and the sources and locations of these pollutants in the Black Sea atmosphere. The first data set was generated from 19 aerosol samples collected at two research ships in 1988 by analyzing approximately 40 element and ion by using Instrumental Neutron Activation Analysis (INAA), Atomic Absorption Spectrometry (AAS) and Ion Chromatography (IC) techniques (Hacısalıhoğlu et al., 1992). Although the number of samples is very small, it is an important data set because of the large number of parameters analyzed and the only study that the Eastern and Western Black Sea aerosol compositions were compared. Another dataset generated in the region is the dataset generated by analyzing daily collected rainwater and aerosol samples in a station established in Amasra between 1993 and 1997 for trace 40 elements and ions by using INAA, AAS and IC methods (Alagha and Tuncel, 2003; Karakaş and et al., 2004). Another dataset generated in the Black Sea region is the dataset obtained by analyzing samples collected in July 1992 at a ship using AAS and IC techniques (Kubilay et al., 1995). In addition to these studies, daily aerosol samples were collected from April 2006 to March 2008 at a rural site established by our group in Kırklareli and collected samples were analyzed for about 50 elements and ions using ICP-MS and IC techniques (Tokgöz, 2013).

All the evaluations related to the Black Sea atmosphere are based on above data sets. The most current data set in Black Sea Region was generated by Tokgöz (2013). But, the study was conducted on the Bulgarian border of Turkey in Western Black Sea and the concentrations and compositions of the pollutants are different in the Eastern and Western Black Sea (Hacısalıhoğlu et al., 1992). However, one thing to note here is that this difference was seen in the samples collected in 1988. Everything that we know about Eastern Black Sea Region is based on analysis of five aerosol samples collected in 1988. The situation in the region today may have changed greatly, but there is no

data to evaluate it. So there are still gaps in knowledge associated with the Eastern Black Sea atmosphere.

Reliable scientific data on anthropogenic emissions are necessary for the construction of applicable policies and regulation of man-made emissions. The literature associated with temporal coverage of trace element concentrations of Eastern Black Sea atmosphere is very limited and outdated. Identification of more sources with available receptor modelling techniques needs more parameters and more samples to be used as tracers. For this reason, higher temporal coverage (sample) is useful in resolution of more sources in source apportionment studies. The generation of data set will fill the gaps in the current knowledge of pollution profile of Eastern Black Sea Region. But, the measurements of trace elements alone cannot be used directly by policy makers to formulate optimal abatement strategies to achieve ambient air quality standards. The delineation of contribution of local sources and distant sources is a crucial step in forming balanced and cost effective strategies for dealing complex air pollution problem in a region. This study will not only provide pollution profile of Eastern Black Sea region to the scientific community, but also it will provide invaluable information on source types affecting the aerosol population in the Eastern Black Sea Region, contribution of these to the measured levels of pollutants and locations of these sources to the policy makers.

In this study, results obtained from daily size distributed particulate matter samples collected between March 2011 and December 2013 at rural site on the Eastern Black Sea basin were studied extensively. The data set generated in this work is one of the extensive studies at the Black Sea region and the most extensive study in Eastern Black Sea region due to the temporal coverage. The data generated in this work is invaluable to identify types and locations of the sources affecting the region. In this investigation, the atmospheric long-range transport of natural and anthropogenic species to the Eastern Black Sea region was studied.

1.1 Aim of the Study

The main objectives of this study are as follows:

- a) **Determination of concentration of pollutants:** Most of the aerosol studies were conducted on Central or Western Black Sea basin. The available literature in Eastern Black Sea is very limited and outdated. Due to the expected spatial variability of the atmospheric concentrations, the data generated at this part of the basin will be very beneficial to identify sources and source regions. The trace element data obtained in this study will be compared with other studies to assess to extend of the pollution level in the Eastern Black Sea.
- b) **Determination of long-range transport patterns of pollutants to the Eastern Black Sea region:** The flow climatology of Eastern Black Sea region will be determined by analyzing back trajectories of air masses. General flow patterns of back trajectories and concentrations of trace elements will be combine to understand the transport mechanisms of pollutants.
- c) **Investigations of relation between local meteorological parameters and concentration of pollutants:** Local meteorological parameters (wind speed, temperature and rain) can provide information on contribution of local sources. The dependency of pollutants on local meteorological parameters will be investigated to determine the contribution of local sources.
- d) **Determination of temporal variations of pollutants:** The short and long term variations of pollutants is a very strong clue for the transport mechanisms of the pollutants of to the region. Episodic and seasonal variations of the pollutants will be investigated to understand factors controlling these variations.

e) **Determination of source types and source regions affecting the concentrations of pollutants in the Eastern Black Sea region:** The contributions forest fires and different desert dusts to the pollutant concentrations will be investigated using the marker species. The types of sources responsible for the pollutant concentrations will be evaluated. For this purpose, Positive Matrix Factorization will be used to identify sources and to determine the contribution of sources. The source regions of identified sources by Positive Matrix Factorization will be determined using Potential Source Contribution Function analysis.

CHAPTER 2

LITERATURE REVIEW

2.1 Particulate Matter

Aerosols are suspensions of solid or liquid particles in the atmosphere. The particulate portion of an aerosol is referred to as particulate matter, or PM. Particulate matter is a generic term applied to chemically heterogeneous discrete liquid droplets or solid particles. The metric used for describing PM is the micron, or micrometer (μm). The PM in an aerosol can range in size from 0.001 to greater than 100 microns in diameter (Spurny, 1999).

Particulate matter has a great importance in air pollution studies and has been identified as one of the 6 common pollutants (priority pollutants) by the US Environmental Protection Agency (US EPA). The other priority pollutants are ground-level ozone (O_3), carbon monoxide (CO), sulfur dioxide (SO_2), nitrogen dioxide (NO_2) and lead (Pb). In conjunction with this definition, particulate matter and other priority pollutants are monitored and regulated in accordance with the National Open Air Quality Standards (NAAQS) established under Clean Air Act law (US EPA, 2018). In our country, pollutants are regulated with Article 6 of the Environment Law and Air Quality Assessment and Management Regulation in accordance with the European Union Air Quality Directives.

When the deaths and serious health problem caused by air pollution and the knowledge gained from epidemiological and toxicological studies on the air pollution are considered, we can conclude that the particulate matter has serious effects on human health and the environment. The fact that the World Health Organization (WHO) has ranked the particulate matter air pollution as the 13th leading cause of mortality

worldwide is also an indicative of the effects of particulate matter (Anderson et al., 2012).

2.2 Size Distribution of Particulate Matter in the Atmosphere

Understanding the size distribution of particulate matter in the atmosphere is of great importance for understanding the sources, behavior and formation mechanisms of particulate matter. The level of health and environmental effects of particulate matter are directly related to its dimensions. As the diameters of particles become smaller, they become more hazardous for health, because they can move more deeply into the respiratory system. In addition, as the residence time increases with the decreasing diameter, the environmental impacts become larger. (Fuzzi et al., 2015; Radke et al., 1991; World Health Organization, 2003)

Particulate matter consists of particles of very different density and shape. Therefore, it is not possible to consider all particles as spheres and to define their diameters accordingly. For this reason, the particles in the atmosphere are defined by the "aerodynamic diameter". The aerodynamic diameter is defined as the diameter of the spherical body, which has the same behavior as the real particles, with an equivalent velocity of settling and a density of 1 gr cm^{-3} of the real particles (DeCarlo et al., 2004).

Particulate matter is divided into two classes by US EPA, coarse and fine, and this classification is used globally. Coarse particles represent particles smaller than $10 \mu\text{m}$ (PM_{10}), and fine particles represent particles smaller than $2.5 \mu\text{m}$ ($\text{PM}_{2.5}$) (US EPA, 2016a). Contrary to particle size classification done by US EPA, Whitby (1978) proposed a trimodal particle size classification. According to this trimodal classification, particulate matter are mainly classified into Aitken nuclei mode ($D < 0.01 \mu\text{m}$), accumulation mode ($0.01 \mu\text{m} < D < 2.0 \mu\text{m}$) and coarse particle mode ($D > 2.0 \mu\text{m}$).

The particles forming the Aitken nuclei mode are formed by gas-particle transformation, and the residence times of such particles in the atmosphere are very

short due to their very high coagulation rates. The particles in the accumulation mode either consist of gas-particle transformation, as in the case of Aitken Particles, or growth and coagulation of particles in the core mode. Coarse particle mode ($D > 2\mu\text{m}$) is usually formed by mechanical processes such as friction, abrasion (Jacob, 2000).

Mechanisms leading to aerosol formation are shown in Figure 2.1 (Whitby and Sverdrup, 1980). The formation mechanisms are important, because the dimensions (aerodynamic diameters) of the resulting particles depend on the formation type. Most of the aerosol mass is in the accumulation and coarse particle modes. This is related to the formation mechanisms of the particles. The majority of particles in the Aitken and accumulation modes are secondary particles. In other words, these particles have not been emitted from any source, they are formed by reactions of different gases in the atmosphere. As can be understood from this, the most important dimension range for the health effects and transport of particles is the accumulation mode that is between $0.01\mu\text{m}$ and $2.0\mu\text{m}$. Particles in the accumulation mode generally consist of sulfate, nitrate, ammonium, organic compounds and elemental carbons. Since the particles in this group are formed during transformation of gas to particulate and combustion processes, the process is complicated.

The particles in the coarse aerosol group are generally consist of dust (calcium carbonate, silica, metal oxides) and sea salt (Jacob, 2000). Coarse particles are one of the important component of the atmosphere due to their light-scattering properties and their production in large quantities. Coarse particles' residence time in the atmosphere are shorter than smaller particles, since they settle rapidly due to their large mass.

As mentioned before, the particles in the accumulation mode is the most important group of particles. One reason for this is their chemically active surfaces are very large. This characteristic is also seen in the Aitken nuclei particles, but the life of the particles in Aitken nuclei group is much shorter, making the particles in the accumulation mode more important.

The majority of the particles we know as pollutants in the atmosphere are secondary particles. The formation mechanisms of secondary particles are very complex, but in general, they are low vapor pressure products formed in the reactions of the precursor gases in the atmosphere. Secondary particle nuclei begins to grow just after they have formed. Growth rates continues until they reach a value between 1 and 20 nm h⁻¹. Due to the size of such particles, health effects are important. Secondary particles can reach the lowest level of the respiratory system, since they have small dimensions. These particles can also be transported to long distances, since they are resistant to scavenging from the atmosphere due to their diameters.

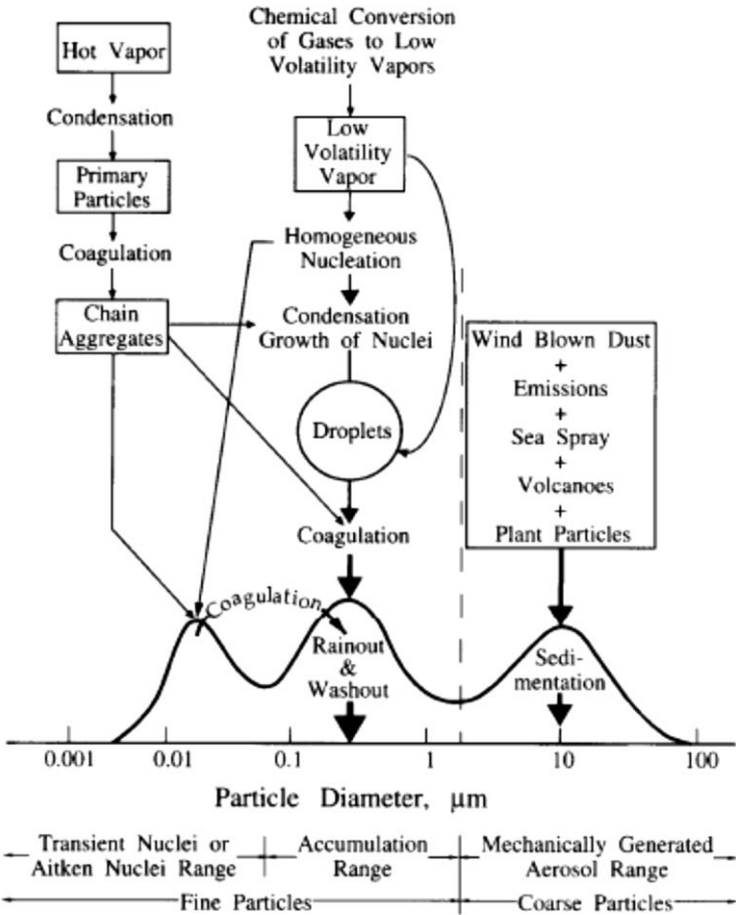


Figure 2.1 Size distribution and formation mechanisms of aerosols (Whitby and Sverdrup, 1980)

2.3 Sources of Particulate Matter

Particulate matter has a wide variety of natural and anthropogenic sources. Components of these sources are both primary (directly emitted) and secondary (formed in the atmosphere) (National Research Council, 2010). Soil, sea salt and volcanoes are the best-known natural resources. On the other hand, fossil fuel combustion and industrial emissions are the best-known anthropogenic sources. In some cases, it is not easy to distinguish between natural and anthropogenic sources. For example, soil is a natural particulate matter source. The particles lofted by the wind constitute a significant part of the aerosol mass on a global scale. However, it is not possible to conclude that every dust lofted by the wind has a natural source. The increasing desertification due to human activities can increase the mass concentrations of soil particles in the atmosphere regionally or locally. No matter the soil is a natural source, the particles formed in such desertification processes are not natural. Another example is the forest fires. If the forest fire occurs due to natural causes such as lightning, it is considered a natural source. However, forest fire started by humans is an anthropogenic source, not a natural source.

The chart prepared by US EPA (Figure 2.2) shows the US national summary of PM_{2.5} and PM₁₀ emissions by sources. According to these results, the largest PM_{2.5} source in the US is fires, followed by dust particles and agricultural emissions. The most obvious source is the dust particles for PM₁₀ emissions and followed by agricultural emissions and fire emissions in the US. It can be also concluded that the natural sources generally emit coarse particles, while anthropogenic sources emit fine particles.

Ninety percent of the mass of the particulate matter in the atmosphere comes from natural sources (Voiland, 2010); but the remaining 10% of the particulate matter, which is considered anthropogenic, dominates the air downwind of urban and causes greater human and environmental impacts (National Research Council, 2010; Voiland, 2010). The underlying reason for this is the particulate matter emissions from anthropogenic sources are predominantly attributed to fine and very fine particle

groups, so that the longer the atmospheric lifetimes, the greater the number and density in the atmosphere (AQEG, 2005).

2.3.1 Natural Sources

The most common natural sources of particulate matter are wind-blown dust particles, sea and ocean-origin salt crystals, volcanic-borne particles and natural forest fires. Dust particles and salt crystals are the two most important ones of these sources.

The mineral dust, one of the two most important natural sources, is emitted into atmosphere from soil erosions, dust storms, resuspension of soil particles. The largest source of natural mineral dust is the Sahara Desert (Karanasiou et al., 2012). Such emissions contribute greatly to the particulate matter air pollution and account for the largest proportion of the PM₁₀ emissions (Fuzzi et al., 2015). As a result, these sources are responsible for the emissions of mineral oxides and crustal elements such as iron, aluminum, silicon, calcium, potassium, and magnesium. (Appel et al., 2013; Houghton et al., 2001; Perraud et al., 2012). Fuzzi et al. (2015) indicated that 75% of dust emissions are emitted from natural sources while the remaining 25% is emitted by anthropogenic sources. These emissions have become increasingly important in recent years due to the Saharan dust storm events and their transport are known to play a role in exceedances of particulate matter air quality standards in European cities (Querol et al., 2009)

Marine and ocean-borne particulate matter, in other words sea-spray aerosols (SSA), has an important place in air pollution studies because of forming the largest fraction of the mass of global particulate matter budget with a large contribution of 3 to 30 Pg year⁻¹ (Lewis and Schwartz, 2004), as well as effect on the global radiative budget due to absorbing or scattering properties of the solar radiation, and effect on the formation of the cloud condensation nuclei (CCN) (Greythe et al., 2014; Houghton et al., 2001). The most important component of sea salt aerosols is sodium chloride (NaCl), as well as ions and organic substances such as K⁺, Mg²⁺, Ca²⁺, SO₄²⁻ (O'Dowd et al., 2004).

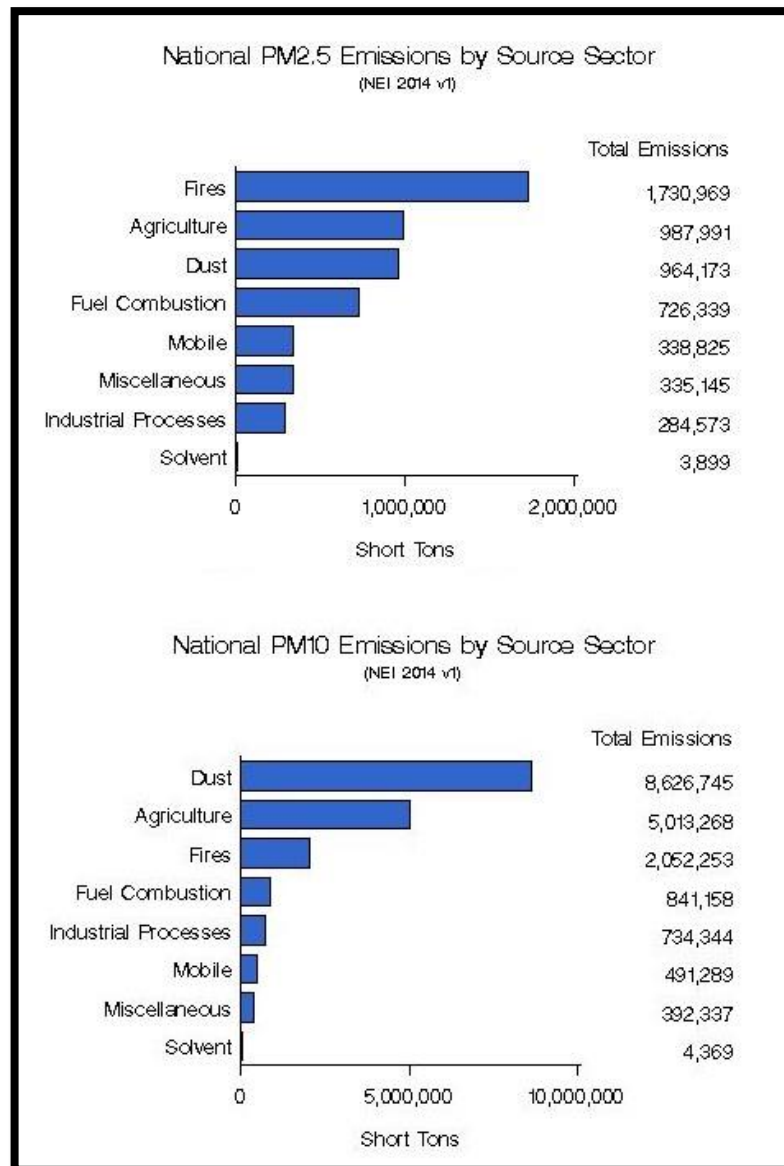


Figure 2.2 US national summary of particulate matter (PM) emissions by source sector (US EPA, 2017a)

Volcanic eruptions also contribute to the formation of particulate matter as another natural source. Essentially two substances are emitted from volcanic eruptions; the first is the volcanic ash rich in iron and magnesium, and the second is sulfur in the gas phase, mostly in the form of SO₂ (Houghton et al., 2001). Depending on the power of the volcanic eruptions, the ashes emitted from these explosions can be transported to the free troposphere and even to the stratosphere. In addition to direct bursts of

volcanic ash, volcanic ash can sink into the clinker by wind and can be transported in the atmosphere (Langmann, 2013). In addition, volcanic ash can be resuspended by wind and can be transported in the atmosphere (Langmann, 2013).

Forest fire is a natural source that emits various gasses and particulate matter complexes through the combustion of wood and various organics. Forest fire emissions form a significant part of the combustion related emissions. Hinds (1999) stated this amount as 20 Tg year⁻¹. Most of the particulate matter emissions in forest fires consist of incomplete combustion products and mostly contribute to the organic carbon and black carbon fractions of the particulate matter (Franzi et al., 2011; Radke et al., 1991; Urbanski et al., 2009).

2.3.2 Anthropogenic Sources

Anthropogenic (man-made) particulate matter sources are divided into two; as stationary sources and mobile sources. Stationary sources consist of residential, commercial, agricultural and industrial sources, while mobile sources consist of motor vehicles such as automobiles, airplanes, trains, and vessels (National Research Council, 2010; US EPA, 2015).

Fossil fuel combustion is the leading factor in man-made particulate matter emissions. This combustion can take place in different forms, including motor vehicles, power plants using fossil fuels, domestic heating, and in industrial plants. (National Research Council, 2010; US EPA, 2015).

Traffic-related emissions include direct and indirect vehicle emissions, tire and brake wear emissions, and indirect emission from resuspended road dust (European Commission, 1997). With the use of fossil fuels in motor vehicles, many trace elements such as Fe, Al, Ca, Na, K, Ba, Se, S, Mn, and Pb are emitted into atmosphere (Hung et al., 2009; Omidvarborna et al., 2009; Robert et al., 2007)

The distribution of important direct and indirect source contributors to the traffic-related particulate matter emissions in Albany, Birmingham, Houston, Long Beach, El Paso, and Westbury cities from a study conducted by Gertler (2005) is shown in Figure 2.3.

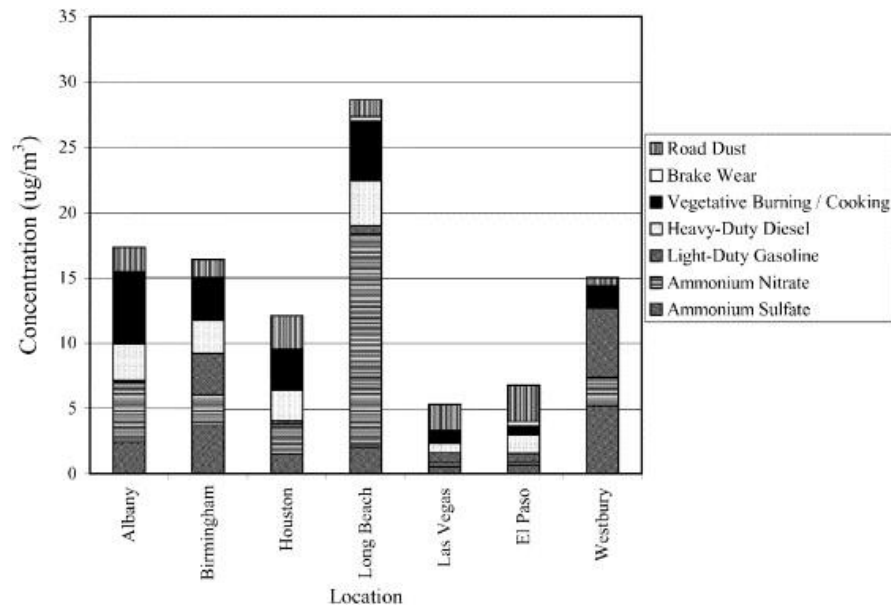


Figure 2.3 PM_{2.5} source attribution results for seven urban sites in the US (Gertler, 2005)

Obviously, the most important of these sources is the exhaust gas emissions from vehicles. Fossil fuels such as gasoline and diesel used in vehicles are one of the main sources of particulate matter emissions as well as many products due to incomplete combustion. From these fuels, various researches show that diesel emissions have more contribution to the urban particulate pollution than others (Schauer, 2003; Zhu et al., 2002). A study by Gertler (2005) at a roadside area in New York City in 1992 also supports this. The results obtained in this study are shown in Figure 2.4.

Power plants, one of the main sources of all types of air pollutants, have a significant effect on the particulate matter emissions, and in particular have great influence on the fine particulate matter emissions (European Commission, 1997). In particular, coal

burning power plants are responsible for the large part of the power plant emissions. According to the report of the US Environmental Cooperation Commission, of the 250 power plants that make the most contribution to the particulate matter emissions in the US, 241 (96.4%) were using coal as fuel while 7 (2.8%) were using liquid fuel (fuel oil) and 2 (0.8%) were using natural gas (Miller and Van Atten, 2005). The main components of particulate matter emissions from coal burning power plants are identified as SiO_2 , Al_2O_3 , Fe_2O_3 (Zhang et al., 2005).

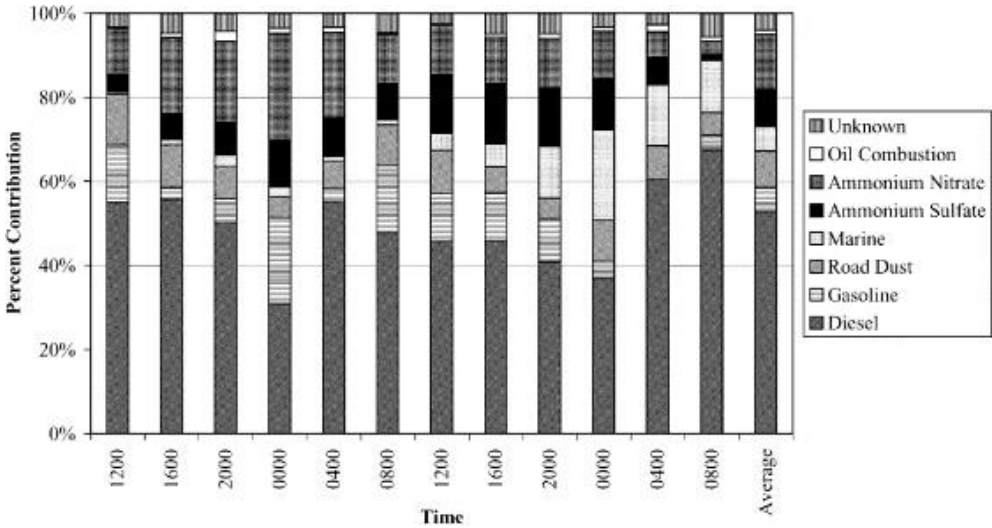


Figure 2.4 Results of a PM₁₀ source apportionment study performed at a roadside location in New York City in April 1992 (Gertler, 2005)

Domestic heating, which is another source of particulate matter based on fossil fuel combustion, also exhibits similar characteristics to the power sources mentioned above. The reason is that these fuels have high carbon and sulfur content due to their complex chemical structure, resulting in emittance of particulate matter in the form of incomplete combustion products (Energy Information Administration, 1999).

Most of the domestic heating particulate matter emissions are due to wood and coal combustion. Such fuels have high carbon and sulfur content due to their complex chemical structure and emit particulate matter emission as products of incomplete combustion (Energy Information Administration, 1999). Contrary to these fuels,

natural gas emits much lower levels of particulate matter and other dangerous pollutants due to its simple chemical structure, low carbon and sulfur contents (US EPA, 1995). This is also confirmed by the comparison of particulate matter emissions per unit energy output. Accordingly, the amount of particulate matter emissions for 1 billion BTU energy production is 7 lb for natural gas, 84 lb for oil and 2744 lb for coal. Hence, natural gas emissions are 392 times cleaner than coal emissions in terms of particulate matter emissions (Energy Information Administration, 1999).

The emissions from industrial processes are also one of the sources contributing to the atmospheric particulate matter load. As a matter of fact, emissions from industrial processes contributed 23% of the total particulate matter emissions in the UK (Passant et al., 2002). The authors listed the major industrial processes that contribute to the particulate matter pollution as iron and steel plants, blast furnaces, cement production, lime production, glass production, construction, and quarrying. As a result of these industrial processes, dangerous trace elements such as As, Cd, Cr, Cu, Pb, Zn, Hg, Ni, Se, and V are emitted into the atmosphere (Passant et al., 2002).

2.4 Trace Elements

In order to ensure that the precautions to be taken to reduce pollutant emissions in a region are accurate, effective and not costly, the contribution of sources to the pollutant levels must be correctly determined. Organic and inorganic pollutants are frequently used in identifying the pollution source types and determining levels of contribution. Most of the trace elements are emitted into atmosphere from their sources (natural or anthropogenic) on particulate matter and remain on the particles during their transport to the remote areas. Because of these conservative behaviors of trace elements, they can be measured at any size fractions (Çetin et al., 2007; Kulkarni et al., 2007) and used as natural tracers to identify the sources of pollution (Güllü et al., 1998). The trace elements in the aerosols may be emitted from natural and/or anthropogenic sources. Table 2.1 lists the natural and anthropogenic source types and the trace elements emitted from these sources. From each of the natural and anthropogenic sources, one or more trace elements are emitted to the atmospheres in different

compositions. Depending on the ratio of each trace element in aerosols, the type of source can be identified. This is further discussed in the following parts of the manuscript. It has been shown that the natural sources of the trace elements are generally windblown dust and sea salt particles; and anthropogenic sources are such as motor vehicles, industrial processes, and incineration plants. (Morawska and Zhang, 2002). Therefore, the number of measured trace elements is important in identification of sources and determination of their contributions (Artaxo et al., 1998; Thurston et al., 2011).

Table 2.1 Elemental composition of atmospheric particulate matter (Morawska and Zhang, 2002)

Emission Source	Characteristic elements emitted
Road transport	
Motor vehicle emissions	Br, Pb, Ba
Engine wear	Fe, Al
Tire wear	Zn
Road dust	EC, Al, Si, K, Ca, Fe, Zn
Industrial facilities	
Oil-fired power plants	V, Ni
Refuse incineration	Zn, Sb, Cu, Cd, Hg
Coal combustion	Se, As, Cr, Co, Cu, Al, S, Pa, Ca
Refineries	V
Non-ferrous metal smelters	As, In, Ni, Cu
Iron and steel plants	Pb
Plant producing Mn metal and Mn chemicals	Mn
Copper refinery	Cu
Incinerators	
Waste incinerators	Zn, Sb, Cu, Cd, Hg, K, Pb
Wood smoke	Ca, Na, K, Fe, Br, Cl, Cu, Zn
Mineral and raw material processes	
	Mg, Al, K, Mn, Fe, Se
Sea spray	
	Na, Cl, S, K
Suspended dust particles	
	Si, V, Cr, Ca, Ti, Sr, Al, Mn, Se

2.5 Environmental Effects of Particulate Matter

Particulate matter pollution has many environmental effects as well as health effects. These environmental effects can be summarized briefly as the degradation of visibility, the effect on hydrological cycle through the formation of cloud condensation nuclei (CCN), and the effects on climate change (US EPA, 2017b; World Health Organization, 2003)

2.5.1 Health Effects of Particulate Matter

Poor air quality has been regarded as a sign of bad health throughout history and has become an undesirable situation. Especially in the last century, after the fatal air pollution incidents, it has become a serious interest and research topic (Anderson et al., 2012). The first major fatal case recorded in the past occurred in the Meuse Valley, an important heavy industrial zone in Belgium. Between December 1st and 5th, 1930, a thick fog layer covered the sky in the region and more than 60 people died due to respiratory diseases (Nemery et al., 2001).

The incident in the Meuse Valley was the first known major event, but the incident in 1952 in London was the most well-known incident in the world and it has been a milestone in air pollution research. In this incident, also known as The Great Smog, a dense dark SO₂-containing fog and black smoke layer covered the London skies for about a week and killed about 4,000 more people on average (Laskin, 2006). This catastrophe has become a milestone in atmospheric research and has revealed that the air pollution can be fatal, and serious work has begun on this subject. Following this, the Clean Air Act came into force in the United Kingdom in 1956, and similar laws came into force in the United States and around world after 1970s (Anderson et al., 2012; Laskin, 2006).

The most important criterion in defining the health effects of particulate matter is the aerodynamic diameter of the particles, because the residence time of the particles in

the atmosphere and the extent of their effect to the human body depend on the size of the particles (US EPA, 2016b). Since the particles larger than 10 μm are scavenged from atmosphere in a short time by wet or dry deposition and are captured in the upper respiratory system, the health effects on humans are low, and the PM₁₀ standard has been set accordingly (Anderson et al., 2012). However, fine particles, smaller than 2.5 μm , pose a major threat to human health because they can penetrate into the respiratory system and reach the lungs and even can enter into the bloodstream.

Particulate matter is the most fundamental risk factor of the air pollution on human health because it has more effect on human health than all other priority pollutants (Kim et al., 2015). The reason being is that the chemical composition of the particulate matter varies in a wide range; nitrates, sulphates, acids, organic substances and heavy metals (World Health Organization, 2003). Major health problems caused by particulate matter include premature infant deaths, non-fatal heart attacks, cardiac dysrhythmia, asthma, lung function loss, shortness of breath, and respiratory system irritation (Anderson et al., 2012; Kim et al., 2015; US EPA, 2016b; World Health Organization, 2003).

Abdolahnejad et al. (2017) reported that every 10 $\mu\text{g m}^{-3}$ increase in PM₁₀ concentration causes an increase of 6% in mortality rate in Europe. World Health Organization (2013) also reported that the daily all-cause mortality increases 0.2–0.6% per 10 $\mu\text{g m}^{-3}$ increase of PM₁₀, while long-term risk of cardiopulmonary mortality increases 6–13% per 10 $\mu\text{g m}^{-3}$ increase of PM_{2.5}. In addition, more than 25,000 new cases of chronic bronchitis, more than 290,000 cases of bronchitis in children, more than 0.5 million asthma attacks and over 16 million cases of restricted activity have been reported in adults throughout Austria, France and Switzerland (Künzli et al., 2000)

2.5.2 The Effects of Particulate Matter on Haze Formation

Visibility range is defined as the furthest distance that is visible with the naked eye in the open-air (Zhao et al., 2013). It is known that the particulate matter in the

atmosphere impairs the visibility range. This impairment is due to the scattering and absorption of visible light by suspended particles. This case is defined as haze (Cheng et al., 2013). The particles in the atmosphere appear as haze in three different ways;

1. When there is enough sunlight, the atmosphere turns into a turbulent state and the pollutants in the atmosphere mixed well to form a homogeneous haze.
2. In cold winter months, when there is wind, the pollutants appear as a coherent cloud of smoke.
3. If there is no wind and pollutants are emitted into the stagnant atmosphere, a hazy layer forms and new layers continue to build up as long as the stagnant weather conditions continue.

Although haze formation is affected both by natural and anthropogenic sources, it can be concluded that anthropogenic sources primarily responsible for haze formation, since fine particles contribute to this formation more. Gasoline and diesel emissions from motor vehicles, power plants, especially coal burning power plants, and various industrial activities are known to responsible for the formation of haze and the visibility degradation (Malm, 1999). The visibility degradation problem is more prevalent and more intense in crowded urban areas because the major constituents responsible for haze formation in the particulate matter such as, sulfates, nitrates and various organics, present in higher amounts in such areas. Zhao et al. (2013) revealed that the visibility range in the Yangtze River Delta, known as one of the busiest city clusters in China, has decreased from 25 km to 20 km over the past 30 years due to extensive haze formation in this area.

2.5.3 Effects of Particulate Matter on Hydrological Cycle

In a particle free atmosphere, supersaturations of $\geq 400\%$ is necessary for water vapor to condense and form water droplets, which is not possible under atmospheric conditions (Seinfeld and Pandis, 2006). Therefore, particles that serve as condensation nuclei (CN) are required to form water droplets in the atmosphere. Cloud condensation nuclei (CCN) is defined as the particles active at a certain supersaturation to form cloud droplets.

There are many different types of atmospheric particles that can act as CCNs. The composition of these particles can be composed of many different substances such as dust or clay, black carbon from biomass or forest fires, sea salt from sea sprays, sulphate from volcanic activity, and organic matter formed by oxidation of organic compounds. Since the hygroscopic properties of these different components are very different, the ability of the particles to form cloud droplets varies according to the composition. For example, sulphate and sea salt particles are very hygroscopic, whereas soot and mineral particles are hydrophobic.

Although the fresh soot particles are known to be hydrophobic, they are aged in the atmosphere and shifted to a hydrophilic structure and act as condensation nuclei. In a laboratory-scale study, it was observed that the soot particles injected into the experimental setup acted as a condensation nuclei following an activation period of 40 minutes (Ma and Kim, 2014).

Particles that act as a condensation nuclei in the atmosphere can have natural or anthropogenic sources, as well as be primary particles (directly emitted) or secondary particles (Kalivitis et al., 2015; Kerminen et al., 2012; Merikanto et al., 2009). The formation of new particles in the atmosphere starts at 1 to 2 nm in diameter, but then grows rapidly through coagulation to form condensation nuclei (Fuzzi et al., 2015; Kerminen et al., 2012). Modeling studies have shown that the new particle formation (secondary particles) is responsible for a significant proportion of condensation nuclei amount in the atmosphere (Fuzzi et al., 2015; Kalivitis et al., 2015; Kerminen et al., 2012). Merikanto et al. (2009) showed that 31%-45% of the low level cloud condensation nuclei's at 0.2% supersaturation were formed through nucleation. In addition, in this study, it was reported that 55% of the condensation nuclei (45% entered from free troposphere and 10% nucleated directly in the boundary layer) were formed by nucleation at 0.2% supersaturation in the marine boundary layer. Another study showed that 45% - 78% of the low cloud condensation nuclei at 0.2% supersaturation was through nucleation (Westervelt et al., 2014).

2.5.4 The Role of Particulate Matter in Climate Change

Like all other air pollutants, the atmospheric emissions of particulate matter undoubtedly plays a role in climate change. The most obvious effect of particulate matter emissions is the effects on Earth's radiation budget (US EPA, 2016c). However, the way the particulate matter affects the radiation budget varies depending on various factors. These factors are the size, shape and chemical composition of the particles. In addition to these factors, also temporal and spatial variances play a role (Jimoda, 2012).

Aerosols affect the radiation budget of the earth by scattering or absorbing solar radiation. In the case of solar radiation scattered, particles make a negative change in the radiation budget, making the earth cooler. This happens when low carbon content particles such as sulfate particles and sea salt particles predominates (Buseck. and POsfai, 1999). In the case of solar radiation absorbed, particles make a positive change in the radiation budget, making the earth warmer. This happens when the black carbon content (mostly from combustion emissions) predominates in desert dust particles (Fuzzi et al., 2015).

Particles can affect the climate directly and indirectly. The direct effect, known as direct radiative forcing effect, is the interaction of particles with solar radiation and terrestrially re-emitted infrared radiation (Charlson et al., 1992). The indirect effect, known as indirect radiative forcing effect, is the alteration of the planetary albedo (Twomey, 1991). One example to this is the black carbon. It alters the planetary albedo. When black carbon is deposited on snow and ice surfaces, it alters the albedo by darkening the snow and ice surfaces. Thus, land and mountain glaciers absorb more radiation and they melt faster (Fuzzi et al., 2015; National Research Council, 2010). Haywood and Boucher (2000) estimated the radiative forcing for sulfate as -0.26 to -0.82 W m^{-2} , for black carbon as $+0.16$ to $+0.42 \text{ W m}^{-2}$, and for mineral dust $+0.9$ to -0.46 W m^{-2} .

2.6 The Long Range Transport of Particulate Matter

Long range transport of air pollutants means the mobilization of air pollutants from their initial location to downwind locations through wind. This way, they may reach thousands of kilometers away from their source. Pollution levels in cities are caused by two factors, local sources and pollutants or precursors transported through a long range. However, pollution in rural areas are predominantly caused by long range transport as local sources are scarce or non-exist.

Long range transport allows the formation of secondary pollutants as it provides the time required by chemical reactions. Because of this, unless a given pollutant is chemically inactive and is considered as a primary pollutant, both atmospheric chemistry and long range transport should be thought to affect its fate. This also results in the spatial distribution of secondary pollutants being smoother compared to that of the primary pollutants as atmospheric chemistry occurs alongside atmospheric dispersion.

Among the important factors linked to long range transport is the residence time or atmospheric lifetime of a pollutant. This residence time refers to the average time it takes for a pollutant to be removed from the atmosphere. Its value depends on the removal rate rather than the overall abundance of the pollutant (Seinfeld and Pandis, 2006).

The common occurrence of long range transport is referenced in many studies around the world investigating the sources of PM pollution and the manner long range transport affects the PM levels in urban centers. Various studies of North American acid rain and photochemical smog phenomena have indicated that long range transport is an important factor in determining the pollutant concentrations (Brankov et al. 2003; Gálvez 2007; Keeler et al. 1990; Zeng and Hopke 1989). A study conducted by Vet and Ro (2008) showed that between 56% and 83% of wet deposition of non-sea-salt SO_4^{2-} and NO_3^- is caused by long range transport from the US. A different study

suggested that about 65% to 70% of the summer PM_{2.5} in greater Toronto is caused by long range transport (Brook et al., 2002).

In Europe, the European Monitoring and Evaluation Program (EMEP) provides the framework for long range transport of air pollutants. It was seen from various studies that most of the PM pollution in both urban and rural areas of Europe is caused by long range transport (Abdalmogith and Harrison, 2005; Birmili et al., 2010; Cabello et al., 2012; Mantas et al, 2014; Paschalidou et al. 2015; Remoundaki et al., 2013). A study showed that dust from African deserts frequently transported to Europe (Kalivitis et al., 2007). Similarly, Cabello et al. (2012) showed that Eastern Spain is regularly subjected to dust from Africa. Another study indicated that air masses arriving to the south of Athens, Greece were linked to the episodes in the Wider Metropolitan Area, showing long range transport of Saharan dust combined with sea salt (Paschalidou et al., 2015). Saharan dust was also found to be the source of about 3 to 5% of PM_{2.5} pollution reaching much higher values during dust emissions from the Sahara desert (Mantas et al. 2014; Remoundaki et al. 2013).

2.7 National and International Air Quality Standards

Air pollution, which is a consequence of urbanization brought about by modern life, has an impact on global scale as well as local and regional. Since air pollution has important effects on human health, great importance is given to air quality all over the world. In order to solve air pollution problems and determine strategies, both the scientific community and the relevant authority have focused on monitoring and analyzing the atmospheric pollutant concentrations (Kyrkilis et al., 2007). Air pollution regulations aim to define and establish air quality targets to prevent or reduce the harmful effects of air pollution on the environment and human health, and to ensure that the air quality is assessed on the basis of defined methods and criteria.

In our country, air pollutants are regulated with Article 6 of the Environment Law and Air Quality Assessment and Management Regulation in accordance with the European Union Air Quality Directives (96/62/EC, 99/30/EC, 2000/69/EC, 2002/3/EC and

2004/107/EC) (Resmi Gazette, 2008). The national ambient air quality standards along (Resmi Gazette, 2008) with US EPA (US EPA, 2016d) and EU (European Commission, 2017) standards by the year 2018 for 6 criteria air pollutants are given in Table 2.2.

Table 2.2 National and international air quality standards for 6 criteria air pollutants

	Averaging Time	USEPA L.V.	EU L.V.	National L.V.
CO	8 hours	10 mg m ⁻³	10 mg m ⁻³	10 mg m ⁻³
Pb	1 year	0.15 µg m ⁻³ **	0.5 µg m ⁻³	0.6 µg m ⁻³ (in 2019)
NO₂	1 hour	188 µg m ⁻³ *	200 µg m ⁻³	260 µg m ⁻³
O₃	8 hours	140 µg m ⁻³ *	120 µg m ⁻³	120 µg m ⁻³ (in 2022)
PM_{2.5}	24 hours	35 µg m ⁻³	25 µg m ⁻³ ***	--
PM₁₀	24 hours	50 µg m ⁻³	50 µg m ⁻³	50 µg m ⁻³
SO₂	1 hour	196.5 µg m ⁻³ *	350 µg m ⁻³	380 µg m ⁻³

L.V.: Limit Value

*converted to µg m⁻³

**averaging time is 3 months

***averaging time is 1 year

The limit values set in our country are higher than the limit values set by the EU and US EPA. In addition, there is no restriction in our legislation on PM_{2.5}. However, it is targeted that these limit values will be in line with the limit values set by EU air quality directives. Beside these 6 criteria pollutants, Turkey set limit values for other air pollutants such as Benzene, As, Cd, Ni, and Benzo(a)pyrene in accordance with EU directives (see Table 2.3). These limit values will be effective from on 2020 and 2021 (Resmi Gazette, 2008).

Table 2.3 National air quality standards for benzene, As, Cd, Ni, and Benzo(a)pyrene

	Averaging Time	Limit Value	From on
Benzene	1 year	5 µg m ⁻³	2021
As	1 year	6 ng m ⁻³	2020
Cd	1 year	5 ng m ⁻³	2020
Ni	1 year	20 ng m ⁻³	2020
Benzo(a)pyrene	1 year	1 ng m ⁻³	2020

2.8 Source Apportionment of Particulate Matter

Two different approaches, source oriented and receptor oriented, have been used to determine sources of pollutants and source contributions to the level of atmospheric pollution in a region. Numerical models are the main tools used in source oriented approach. In this approach, also known as dispersion modeling, meteorological and topographic information, emission inventory, source information are used as input parameters and the concentration of contaminants in the atmosphere is calculated by simulating the transport of pollutants in the atmosphere. Despite the widespread use of numerical modeling, the uncertainty of the results can be high due to the insufficient or incorrect source inventory of pollutants.

Receptor oriented models can be used as an alternative method of identifying sources and distributing the observed concentrations of contaminants to these sources. Receptor models do not require emission, topography and meteorological information. Receptor modeling is an experimental method that involves the measurement of natural tracers of sources in the collected samples and identification of the sources by means of statistical tools applied later. Since receptor models are independent of meteorological conditions and emission rate changes, it is possible to simultaneously calculate the contribution of different types of pollutant sources to atmospheric air pollution (US EPA, 2005).

Trace elements are used as natural tracers in source apportionment studies by means of receptor modeling. But, it is not possible to characterize each source with a single trace element because each source type does not have a single tracer that is not emitted from other sources. Therefore, sources are characterized by a set of elements, referred to as "source profiles". Although the natural tracers of sources seem like trace elements, in fact it is the proportion of the trace elements. Especially in regional studies it becomes more difficult to identify the source types, as pollutants come from distant sources and many emissions will interfere with each other during their transport. For this reason, the use of statistical tools with high reliability is very important in source apportionment studies by means of receptor modeling.

Depending on the statistical tool used, various receptor models are defined. The most commonly used receptor models since 1980s in order to identify probable sources of the total aerosol mass and composition measured in the receiving atmosphere, are the multivariate statistical approaches called Principle Component Analysis (PCA), Multiple Linear Regression (MLR), Factor Analysis (FA), Chemical Mass Balance (CMB), UNMIX, Positive Matrix Factorization (PMF), Multilinear Engine (ME) (Kuntasal, 2005; Han et al., 2005).

Among these models, CMB differs from other models. Concentration of an element measured at any receptor point in CMB is considered as a linear combination of the emissions of the same elements from different sources and measured concentrations are separated into components (amounts coming from different sources) by applying "least square fit". CMB technique has some advantages and disadvantages over other receptor modeling techniques. The most important advantage of CMB is that it can be applied to each sample separately. Therefore, large data sets are not required to apply CMB. However, the most important disadvantage is the need for source profiles. Source profiles are the elemental composition of particles that are emitted from each source. Since it is not possible to measure the composition of the emissions at each source in the studies done, the need for the source profiles is a big disadvantage. But, US EPA has created SPECIATE database, US EPA's repository of volatile organic gas and particulate matter speciation profiles for air pollution sources, in order to overcome this problem (Subramoney et al., 2013).

Other receptor modeling techniques such as FA, PCA, PMF and MLR are based on the variance relationship between the parameters used (Watson et al., 2002). FA and CMB are the earliest receptor models and have been used since the early 80s (Gordon, 1988). PMF (Paatero and Tapper, 1994) is a newer method than other receptor models. Although the PMF has recently been developed, it has found a wide range of uses due to its advantages over conventional methods such as FA, PCA or CMB (Karanasiou et al., 2009; Kim et al., 2003; Liu et al., 2003; Reff et al., 2007; Viana et al., 2008). The major advantage of PMF over other receptor models is that it is based on variance analysis and gives quantitative results and the uncertainty of each parameter is

evaluated individually. This last statement points to a very important advantage of the method. The data sets of trace elements or organic compounds may have large missing data points. Some of these missing data points are due to the pollutant concentrations are below the detection limit. The other part is either due to the measured values are below the blank levels or the fact that the parameter is not measured in some samples. Statistical methods used in multivariate analysis of variance methods such as FA and PCA do not accept missing data points in the data set. Therefore, if there are unmeasured or below method detection limit values, which are often found in the dataset, then the sample is either completely removed from the analysis, or replaced with a data generated by an approximation technique for missing data points. (Wang et al., 2006; Yendra et al., 2013). Both of these approaches are undesired. When the samples have missing data points removed, sometimes no data left to apply FA or PCA. Moreover, if it is taken into account that these data sets are generated with a great deal of labor and money, it does not seem to be a good approach to remove the missing data points. Although there are different types of data approximation methods, it should be noted that no data generated with this way is a true data, (Palmer and Royall, 2010; Wang et al., 2006; Yendra et al., 2013). For these reasons, PMF, which handles the missing data points in the data set better, has a considerable advantage. In PMF, missing data points are replaced with half of the method detection limit and the uncertainty of this data is kept very high. By this way, the contribution of these data to model optimization is minimal, since high uncertainties are assigned to them and it is not necessary to remove the sample from PMF analysis. Another advantage of the PMF technique is that it gives quantitative results. In multivariate analysis of variance such as FA and PCA, the concentration data are normalized in the first step, so concentration information is lost and the results are only qualitative.

Back trajectory statistics is another type of receptor modeling. Receptor modeling can provide very comprehensive information about types of emissions that form an aerosol mass, but they cannot determine source locations of emissions. To obtain such information, it is necessary to combine the concentration data with the back trajectory information. Determination of source locations by this process is generally known as back trajectory statistics. The potential source contribution function (PSCF), which is

a type of back trajectory statistic, is also used in this work and has been discussed extensively in later chapters. For this reason, the PSCF technique is not discussed here. PSCF and other back trajectory statistics methods are widely used in the literature (Gildemeister et al., 2007; Lee and Hopke, 2006; Zhao and Hopke, 2006; Xie et al., 1999).

2.9 Aerosol Studies in Black Sea

The Black Sea region shows similar features in terms of regional air pollution with the Mediterranean, but studies done in this region are much more limited. Even though the studies done in Black Sea composed of a few datasets, the generated datasets were highlighted some points about this region. The knowledge gained from these studies is summarized below. One of the first points revealed in relation to the Black Sea atmosphere is that the SO_4^{2-} ion concentrations measured in both aerosols (Hacısalıhoğlu et al., 1992) and in rainwater (Alagha et al., 2003) are very high, as it is in the Eastern Mediterranean region. Unfortunately, there is not enough data available to evaluate the SO_4^{2-} concentration decline over time in this region. The high concentration of SO_4^{2-} in the Black Sea region attracted the attention of researchers in a study conducted in Georgia in the 1980s (Dzubay et al., 1984). The fact that high concentrations of SO_4^{2-} are still measured in very different places of Black Sea region, as it in Eastern Mediterranean region, indicates that the SO_4^{2-} level in the Black Sea does not decrease as much as it is in Europe.

Another point revealed from the studies is that the trace element and ion concentrations measured in the Black Sea atmosphere are comparable to those measured in the Mediterranean (Doğan et al., 2010). On the other hand, pollutant levels measured in the Black Sea atmosphere are twice as high as those measured in the regions of the Anatolian Plateau (Türküm et al., 2008). Similarly, aerosol concentrations measured on the Mediterranean coast are also higher than those measured in the Anatolian Plate, indicating that the pollutant transport to this region is highly complex.

Another point that has been revealed about the Black Sea aerosol is that the concentrations of the pollutants are different in the Eastern and Western Black Sea. The concentrations of the anthropogenic elements and ions measured in the samples collected on Western Black Sea region were two times higher than the concentrations measured in samples collected on Eastern Black Sea (Hacısalıhoğlu et al., 1992). However, one thing to note here is that this difference was seen in the examples collected in 1988.

In a modeling study conducted by Pervan in 1991, it was shown that the majority of the SO_4^{2-} concentration calculated in Turkey's Thrace and Eastern the Black Sea was originating from distant sources and Turkey's contribution was very small (Pervan, 1991). The contribution of domestic and foreign sources to the sulfur levels calculated in Turkey and the distribution of sulfur deposition obtained in this model study in different regions of Turkey is shown in Figure 2.5. Likewise, in a short period of work in Georgia by Dzubay et al. (1984), it was concluded that the concentration of anthropogenic elements was high and it was suggested that the sources of anthropogenic elements were the smelting plant located in Mikopol or Zestafoni. The fact that the Mn originating from the metal industry is as high in the Eastern Black Sea region as it is the Western region also confirms that this region is affected by the smelting plants in Russia. As can be noted, the evaluations made are based on very old data. The situation in the region today may have changed greatly, but there is no data to evaluate it.

Another information revealed from studies in the Black Sea atmosphere is that aerosol compositions show short (daily) and long-term (seasonal) changes. It was concluded that the most important reason for these variations were the changes in precipitation (Alagha et al., 2003; Karakaş et al., 2004,). Although the most prominent source of measured pollutants in the Black Sea region was dust, it was concluded that marine and anthropogenic sources were also had important influences. (Karakaş et al., 2004; Türküm et al., 2008). In study conducted by Doğan et al. (2010), it was reported that anthropogenic pollutants were originated from Western Europe and Turkey by means of local and long range transport. The main source regions of soil elements were local,

Africa, former USSR countries, Western European, and Middle Eastern countries, while for anthropogenic species source regions were Western and Eastern Europe and Russian Federation and Turkey (Alagha and Tuncel, 2003; El-Agha, 2000; Hacısalihoğlu et al., 1992; Karakaş et al., 2004; Türküm et al., 2008). The results revealed from these studies were obtained from samples collected on Western Black Sea. The only study including the Eastern Black Sea region was carried out by Hacısalihoğlu et al. (1992). In the study, samples were collected on a ship that traveled from the West Black Sea to the East Black Sea. However, the number of samples collected in the study was limited to five.

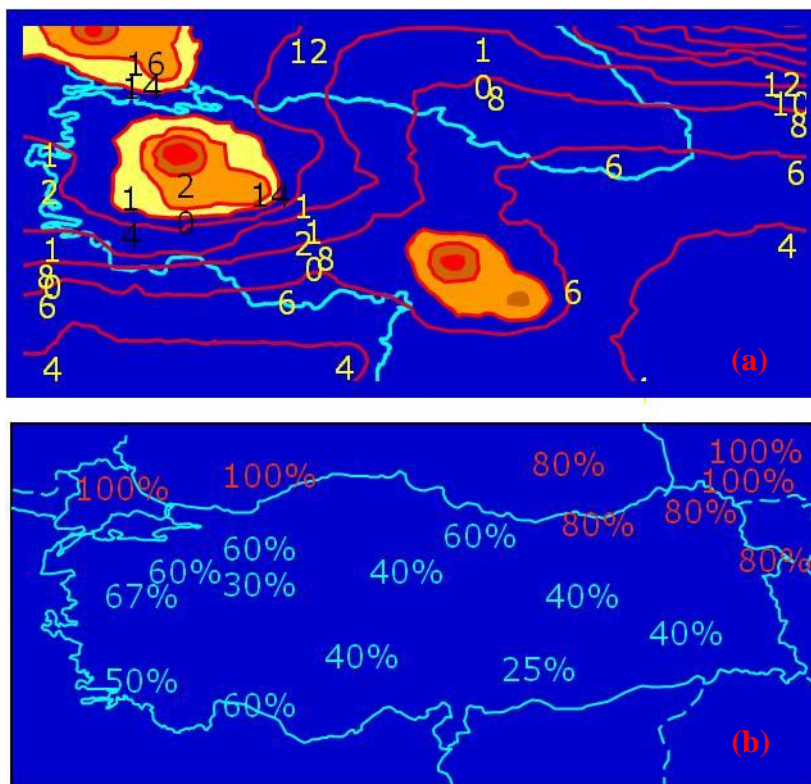


Figure 2.5 (a) sulfur deposits in different regions of Turkey and (b) contribution of foreign sources to precipitated amounts

CHAPTER 3

MATERIAL AND METHODS

3.1 Sampling

3.1.1 Sampling Location

Sampling location selection is an important step in all fields of environmental studies. It becomes more crucial in long-range transport studies where trace levels of airborne pollutants are measured. In long-range transport studies, the purpose is to measure airborne pollutants originating from distant sources rather than local sources. Therefore, sampling site should not be under influence of any kinds of local sources. It should be away from large agglomeration(s), power plants and major roads. Other requirements also should be taken into consideration in selection of sampling location in rural areas include:

1. Availability of power for sampling equipment,
2. Adequate protection for sampling equipment,
3. Capable people to change samples.

The station was planned for a TÜBİTAK project (Project Code: 108Y306) to study long-transport of pollutants to Eastern Black Sea region and to compare the measured concentrations of pollutants with other stations operated under the same project at different parts of Turkey. Therefore, various places on the Eastern Black Sea region were visited to find a sampling location, which fits above criteria. After these visits, a timber-storage depot of the General Directorate of Forestry (40°32'33.84"N and 39°16'56.80"E) located approximately 5 km southeast of Torul town of Gümüşhane province was selected as the sampling location where the station to be established.

Sampling point was approximately 75 km from the Black Sea and 200 km from the Georgian border and at an altitude of 1115 m from the sea level. Location of the station and some pictures of it are given in Figure 3.1.

The nearest settlement area to the station is Torul town, which had a population of 5000 at that time (TUİK, 2017). The biggest agglomeration close to sampling station is the Gümüşhane city (Population 41604), which is approximately 30km to the south of the station. There is also no significant industrial activity within a circle of 50 km radius around the station.

Daily PM sampling was started on March 2011 and ended on December 2013. During this sampling period, total 357 daily aerosol samples were collected.

3.1.2 Sampling Equipment

Daily, coarse ($PM_{2.5-10}$) and fine ($PM_{2.5}$), aerosol samples were collected using a Gent Stacked Filter Unit (SFU). Variety of samplers are available to collect size separated aerosol samples and dichotomous sampler is one of them. Stack Filter Unit is cheaper than "dichotomous sampler" and is designed for the same purpose. The sampling system is based on the principle of collecting particles on two different pore sized filters ($8.0\ \mu\text{m}$ and $0.4\ \mu\text{m}$) located in series when air is drawn at a rate of $16.7\ \text{L min}^{-1}$. Particles with a diameter larger than $2.5\ \mu\text{m}$ are retained on the top filter ($8.0\ \mu\text{m}$ pore size) and $PM_{2.5}$ particles are retained on the bottom filter ($0.4\ \mu\text{m}$ pore size). Not all filters have this feature. When a membrane filter is referred with pore size, for example $2.0\ \mu\text{m}$ pore size, actually the average pore size is mentioned. There are many different diameter of pores in the membrane filters, but their average values are expressed as the pore size. The filter used in this study is made of polycarbonate and known by the brand name "NUCLEPORE". Such filters are formed by first thinning the polycarbonate layers with alpha particles and then etching the thinned portions with acid. The most important feature of these filters is that all the pores on them have the same dimensions. Only Nuclepore filters can provide the desired size separation.

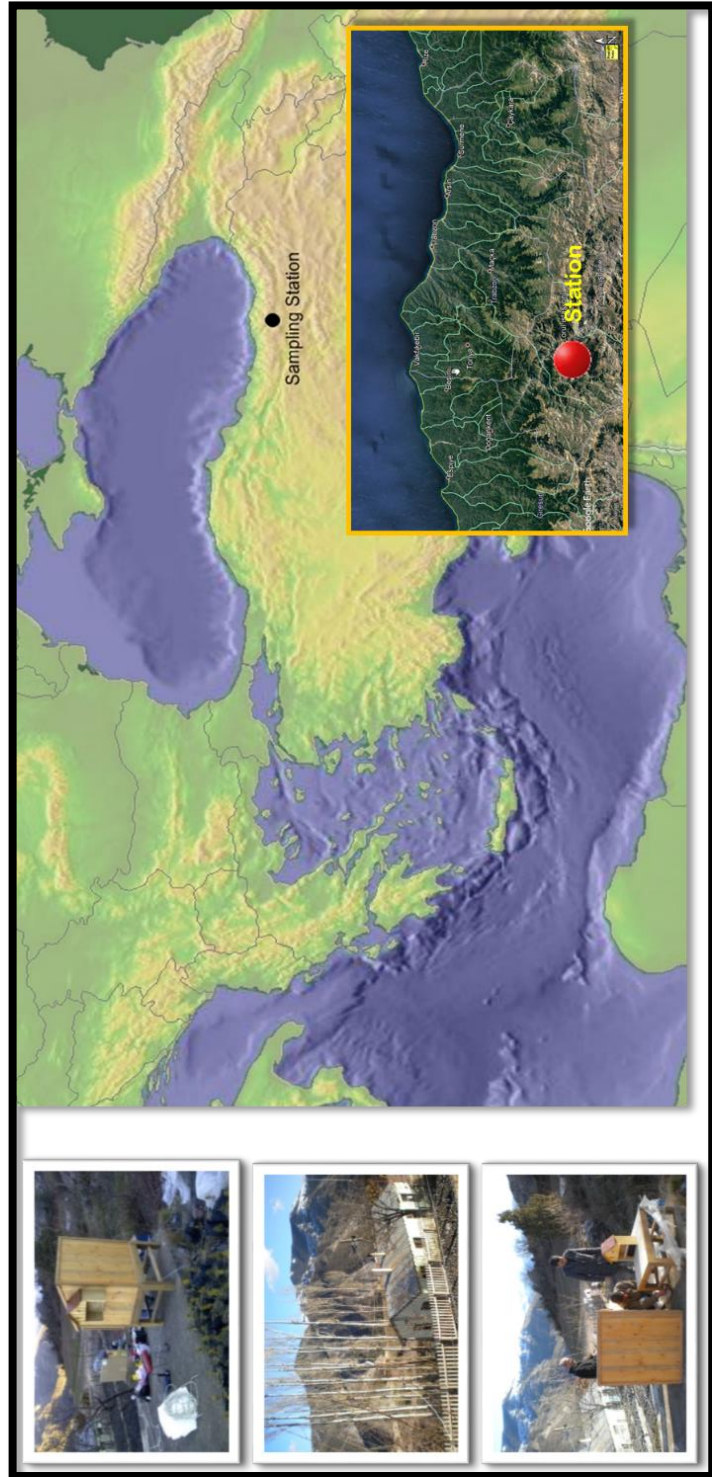


Figure 3.1 Location of the sampling station

The "Stack Filter Unit" and its components are shown in Figure 3.2, Figure 3.3 and Figure 3.4. The system consists of a filter unit (Figure 3.2 and Figure 3.3) and a constant flow pump (Figure 3.4). In filter unit, two Nuclepore filters with different pore sizes placed in series. When the flow rate of the air passing through these filters is fixed to 16.7 L min^{-1} , particles with aerodynamic diameter greater than $2.5 \mu\text{m}$ are collected on the top filter and particles with aerodynamic diameter less than $2.5 \mu\text{m}$ are collected on the bottom filter (Hopke et al., 1997). This system has been widely used in the literature due to its relatively low price (Al-Momani et al., 2005; Artaxo et al., 1999; Graham et al., 2004; Yatin et al., 2000).

A special filter holder, which is another component of SFU and allows two filters to be placed in series, is available from NILU (NILU, Model 9634). Another component of SFU is a PM_{10} pre-impactor which has a cut point at $10 \mu\text{m}$. When the flow rate of SFU is fixed to 16.7 L min^{-1} , particles with aerodynamic diameter greater than $10 \mu\text{m}$ are held at the pre-impactor and are not allowed to reach filters.

The constant flow pump used (Marathon Electric, Model 5KH36KNAS510X) in the SFU especially designed for this task and equipped with a flow meter. It has capability of vacuuming up to 100 L of air per minute and it can be adjusted to desired flow rate by the user. The flow meter (F&J Model) allows to monitor instant flow rate, total sampling time, and total volume of air sampled during the sample collection. The total volume air parameter is the most important parameter in such studies, because the volume of air used in the calculation of the concentrations of species.



Figure 3.2 PM₁₀ pre impactor and holder



Figure 3.3 Filter holder and polycarbonate filters.

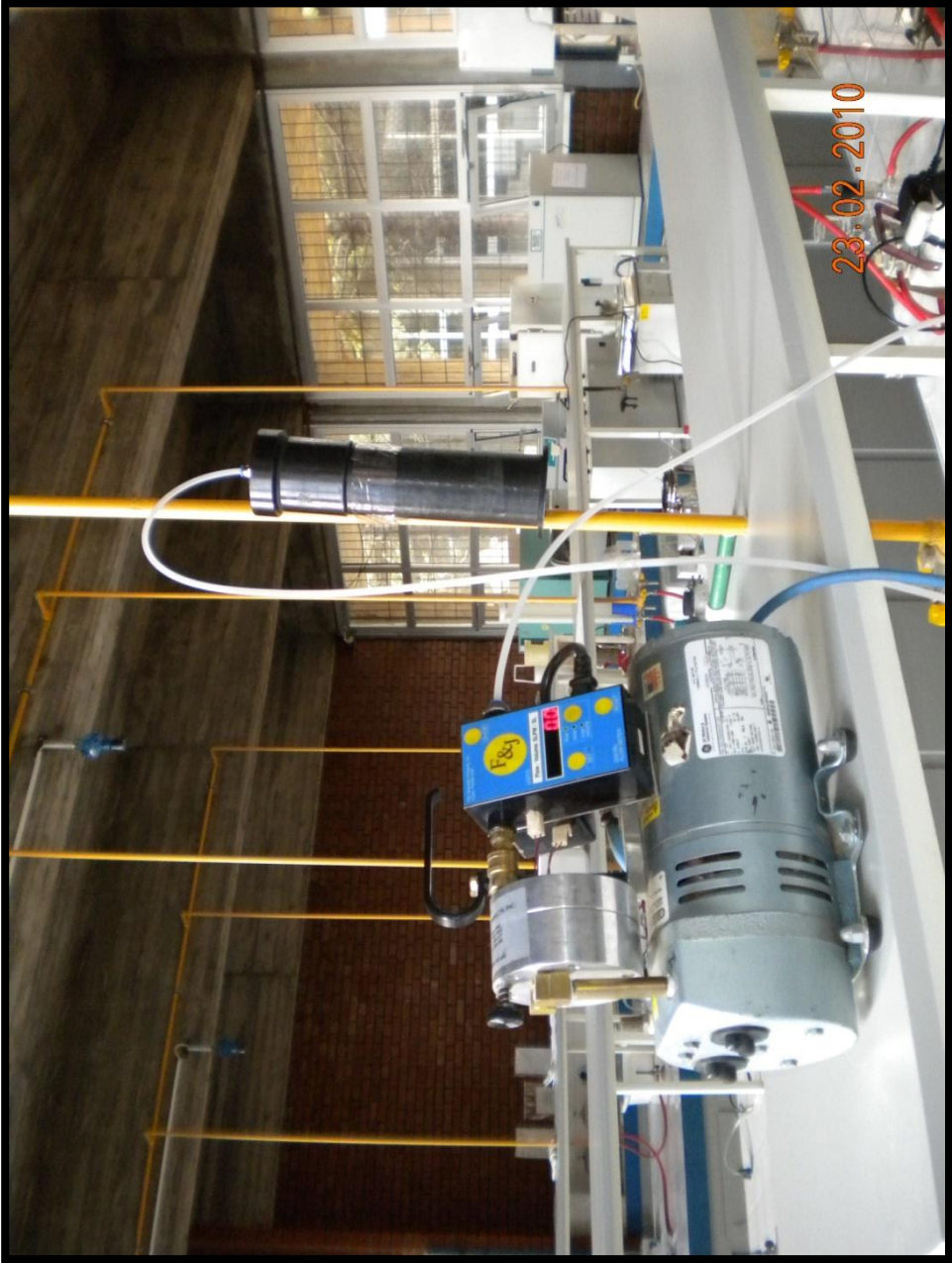


Figure 3.4 Constant flow pump used in SFU

3.1.3 Sample Handling

Size separated particle samples were collected at 24-hour periods. Sampling was started every day approximately at 10:00 and ended approximately at 10:00 the next day. When the sampler was stopped; volume, time, and final flow rate values were read from the information screen on the pump and the observed meteorological events (precipitation, wind etc.) in the 24-hour sampling process and filter numbers were recorded in the relevant places on the "Filter Information Form". After this process, the filter holder was removed from the PM₁₀ pre-impactor and placed in polyethylene bags together with the "Filter Information Form" of the relevant filters. Polyethylene bags were sealed with heat to prevent possible contamination during transport. A fresh filter holder, prepared for sampling, was placed in the PM₁₀ pre-impactor and sampling was started for that day. Collected samples were sent to the laboratories every 7 days.

Loading of the filter holders for sampling and unloading them from after sampling was done in a clean area in the METU Environmental Engineering Department. Air in the clean room was filtered through High Efficiency Particulate (HEPA) filters, which captures particles with diameters 0.1 μm, with 0.9999999 efficiency.

Since the measured concentrations are expected to be at trace levels, all the necessary precautions were taken in order to minimize the contamination at each step of sampling. Powder-free gloves and plastic tweezers were used during loading and unloading of filters to minimize possible contamination. Before and after sampling coarse and fine pore filters were placed in different petri dishes and conditioned in the constant humidity chamber ($26 \pm 4\%$) with 25 ± 5 °C temperature for 24 hours.

After conditioning, filters were numbered and weighed using a precision scale. Conditioned filters were placed on filter holders by placing coarse filters at top and fine filters at bottom. Loaded filter holders were placed in polyethylene bags and heat-sealed before they were sent to the station.

3.2 Analytical Techniques

In this study, coarse and fine filters, first, were weighed gravimetrically to determine the PM mass collected on them. Next, black carbon content on filters were analyzed using an Aethalometer. Finally, filters were analyzed for their trace element composition using Energy Dispersive X-ray fluorescence and Inductively Coupled Plasma Mass Spectrometry techniques.

Detailed information about each analytical technique is in given following sections.

3.2.1 Gravimetric Analysis

As stated before, both coarse and fine filters were conditioned in constant humidity ($26\pm 4\%$) and temperature ($25\pm 5^\circ\text{C}$) chamber for 24 hours before filters were sent to station and after sampling. Just after each conditioning step, filters were weighed with a microbalance. Coarse and fine filters both have 47 mm diameter, which means samples were collected on a relatively small surface area (17.35 cm^2), particularly when it is compared with filters used in Hi-Vol samplers (516.1 cm^2). At a flow rate of 16.7 L min^{-1} , approximately 24 m^3 of air were sampled in a 24-hr sampling day, which is also significantly smaller than air sampled by a Hi-Vol sampler in a 24-hr sampling period ($1200 - 1400\text{ m}^3$). Therefore, amount of PM mass collected on coarse and fine fraction filters were at microgram levels.

In this study, filters were weighed with Sartorius MC- 5 microbalance with 0.001 mg sensitivity. Before weighting, static electricity of filters was eliminated by placing by an ionizer by the filter. Collected PM mass on filters were calculated by subtracting initial weigh of filter from weigh of filter after sampling.

3.2.2 Black Carbon Analysis

After gravimetric analysis, both coarse and fine filters were analyzed for their Black Carbon (B.C.) content by using Aethalometer (Magee Scientific, Model OT21), which

is located at METU Environmental Engineering Department. Concentration of B.C. ($\mu\text{g m}^{-3}$) in samples was calculated in accordance with the following equations:

$$\text{Attenuation} = 100 * \ln\left(\frac{T_o}{T}\right) \quad \text{Equation 3.1}$$

$$\text{BC density } (\mu\text{g cm}^{-2}) = \frac{\text{Attenuation}}{\sigma} \quad \text{Equation 3.2}$$

$$\text{BC } (\mu\text{g m}^{-3}) = \frac{\text{BC density } (\mu\text{g cm}^{-2}) * A_F}{V_F} * c_f \quad \text{Equation 3.3}$$

where;

T_o is transmission intensity of reference filter,

T is transmission intensity of sample filter,

σ is specific attenuation coefficient ,

A_F is exposed area,

V_F is volume of air passed through the sample filter,

c_f is correction coefficient.

The working principle of Aethalometer is based on optical properties of B.C. Along with sample filter a reference filter, in this case field blanks were used, to measure B.C. content of the sample filter. Aethalometer first measures transmission intensities of blank filter and sample filter at 880 nm, and attenuation of sample filter is calculated using Equation 3.1. At this point the assumption is that the light attenuation at the sample filter decreases with its' B.C. loading. By using Equation 3.2, B.C. content of sample filter is calculated. In order to calculate the B.C. density, specific attenuation coefficient is needed. The specific attenuation coefficient (σ) at 880 nm was given as $16.6 \text{ m}^2 \text{ g}^{-1}$ by the manufacturer. In last step, BC concentration was calculated by using Equation 3.3. Khan et al. (2010) reported the correction coefficient (c_f) as 1.1, since the B.C. collection efficiency of the Nuclepore filter is $> 90\%$.

3.2.3 Trace Element Determination

As stated previously, the sampling station was operated under a TÜBİTAK project and the collected samples were analyzed by Energy Dispersive X-ray fluorescence (ED-XRF) for the project. Trace elements are used as natural tracers in source apportionment studies by means of receptor modeling. But, it is not possible to characterize each source with a single trace element because each source type does not have a single tracer that is not emitted from other sources. Identification of more sources with available receptor modelling techniques needs more parameters and more samples be used as tracers. For this reason, collected samples were analyzed with Inductively Coupled Plasma Mass Spectrometry (ICP-MS) to increase the number of parameters.

ICP-MS is a very powerful multi-element technique, but it has a traditional weakness for some elements. Unfortunately, two of these elements are Al and Fe, which are very important marker elements for crustal material. Because of this and reason mentioned above, samples were first analyzed by ED-XRF, which is a non-destructive technique, then digested and analyzed by ICP-MS. Comparison of results demonstrated that agreement between the two techniques were acceptable for most of the elements including Fe and S, but not so good for Al and few other elements. These elements were also detected in smaller number of samples in ICP-MS measurements. Because of these reasons, XRF data were used for this small group of elements including Na, Mg, Al, Ca, Mn, Ni, As, and Pb.

3.2.3.1 ED-XRF Analysis

Analysis of filters was performed using an Energy Dispersive X-ray fluorescence spectrometer (ED-XRF) in Sarayköy Nuclear Research and Training Center of the Turkish Atomic Energy Authority in Ankara. The XRF were able to detect 17 elements, including Na, Mg, Al, Si, S, K, Ca, Ti, V, Cr, Mn, Fe, Ni, Cu, Zn, As, and Pb in samples.

Energy dispersive-XRF analysis is a powerful multi-element analysis technique. It allows qualitative and quantitative analysis of elements in a sample (Al-Eshaikh et al., 2011). There are few important advantages of XRF over other analytical techniques. First of all it is a multi-element technique which can analyze > 30 elements (at least in theory) in sample. It is also non-destructive, which means you can take a sample analyzed by XRF and analyze it with another analytical tool. It is also a very fast analytical tool. Analysis time can be as low as one minute. However it should be noted that analysis time is a strong function of concentrations of elements in the sample. Since particle loading on sample filters were very low, four different excitation programs were run for different groups of elements, and analysis time 17 minutes/sample.

The technique has also some disadvantages against comparable multi-element analytical methods. The most notable disadvantage is its sensitivity. It is not very sensitive for samples where elemental concentrations are low (like this study's samples). It is also a surface technique.

In an X-ray fluorescence spectrometer, the photons emitted from an of X-ray source are directed onto the sample to be analyzed. X-ray photons displaces an inner-shell of the atom, leaving behind a vacancy at the inner shell, thus exciting the atom to a higher energy state. The atom fills the vacancy that the displaced electron left behind with the electrons from outer shells of the atom to go back to its low energy state (so called ground state). During the drop of electron from a higher to lower shell to fill vacancies, atom loses energy. This energy, which is equal to the difference in energies of two shells. The emitted energy is the characteristic X-ray (Mathys et al., 2001). This characteristic X-ray is unique to each element, in other words, it is the fingerprint of the element. Detecting the wavelength of the X-ray allows us to determine the element. Intensity of the emitted X-ray, on the other hand, is related with the mass of that element in the sample.

The main components of the ED-XRF used in this study consist of a radiation source, a silver anode X-ray tube, a sample chamber, an amplifier, and a liquid nitrogen-cooled

lithium-drifted silicon solid-phase detector. Silver anode X-ray tube, which is used for excitation of elements, has of 1000 μ A maximum current and 50 kV maximum voltage specifications.

One of the main factors controls the measurement time of the XRF is the exposure time (Huang et al., 2016). Since excitation of elements with X-ray depends on atomic numbers, different excitation conditions should be used for different elements. In the spectrometer used in this study, four different analysis conditions were applied during the 17-minute long analysis of a sample to provide optimal conditions for different elements. Analysis conditions used in the spectrometer are given in Table 3.1. As can be seen from Table 3.1, different elements were analyzed in different conditions and their concentrations were calculated.

Table 3.1. Different measurement conditions used in the spectrometer during analysis of a sample

Parameter	Condition Number			
	1 (VLE)	2 (S)	3 (St)	4 (ME)
Tube Voltage (keV)	2.5	10	15	22.6
Tube Current (mA)	900	900	1000	494
Analysis Time (s)	150	100	100	100
Energy Range Analyzed	Na - K	K - Cr	Cr - Fe	Fe - Mo
Elements Analyzed	Mg, Al, Si, P, S	K, Ca	Ti, Cr, Mn	Fe, Ni, Cu, Zn, Pb

VLE: Very Light Elements; **S:** Solids; **St:** Steels; **ME:** Medium Elements

One of the methods used in the calibration of the ED-XRF is the use of standards, which are prepared by addition of standard solutions on to filter medium (Braziewicz et al., 2004). Various types of SRMs are available by NIST for this purpose. However, the matrix of the SRM used in this study should match with the matrix of the sample. In this study, National Institute of Standards and Technology (NIST) SRM 2783 was used as standard for calibration of ED-XRF. SRM 2783 is a deposited air particulate

matter sample on polycarbonate filter and is reduced in particle size to simulate PM_{2.5} (National Institute of Standards & Technology, 2011).

3.2.3.2 ICP-MS Analysis

ICP-MS is one of the most sensitive multi-element analytical technique which can be purchased and operated in any laboratory. There are few other comparable multi-element techniques, including instrumental neutron activation (INAA), prompt gamma activation (PGAA), proton induced x-ray emission (PIXE) and x-ray fluorescence (XRF). The INAA and PIXE have comparable detection limits with ICP-MS. However, one cannot buy an INAA or PIXE system. You must have access to a research nuclear reactor to use INAA and you must have proton accelerator to use PIXE. You cannot have these facilities in your lab. The only comparable instrument that you can install to your lab is XRF. However, XRF measures smaller number of elements and its detection limits are not as low as those of ICP-MS. Because of these advantages, ICP-MS found tremendous use in analytical community.

3.2.3.2.1 Preparation of Samples for ICP-MS Analysis

One of the most important steps of the ICP-MS analysis technique is the sample preparation step. PM samples collected on the polycarbonate filters should be converted to aqueous solution before aspirating into the ICP-MS. In this study, sample filters for trace element analysis were first digested with a HNO₃-HF mixture using a BERGHOF SW-2 model microwave digestion system. This system is depicted in Figure 3.5. The three-step digestion program used in the microwave is given in Table 3.2.

There are 10 teflon digestion vessels in the microwave turret shown in Figure 3.5. Nine of these vessels were used for the filter digestion and one of them is used for the filter blanks.

Table 3.2 Three phase digestion program

Step	Time (min)	Temperature (°C)	Power (W)
1	9	100	40 %
2	10	140	80 %
3	9	180	90 %

For digestion of the sample filters, first the filters were put into vessels and then 5 ml HNO₃ and 1 ml HF were added to the teflon digestion vessel shown in Figure 3.5. With the program shown in Table 3.2, the samples could be digested in approximately 30 minutes. However, the resulting solution contains HF. Since HF can damage of ICP-MS's optics system, which is made of glass and quartz, it is necessary to evaporate the HF entirely before the samples are aspirated to ICP-MS. After microwave digestion sample mixture was transferred to Teflon open digestion vessels and evaporated until 1 ml of mixture left by placing the vessels on hot plate (Figure 3.6). Then, 5 mL of ultrapure HNO₃ was added to the Teflon vessels, and the mixture were again evaporated until 1 ml left. This procedure was repeated one more time to ensure complete removal of HF.

After removal process of HF, content of the vessel was transferred to volumetric flask and the volume was adjusted to 50 mL with nanopure water which has a resistance of 18.2 MΩ – cm at 25 °C. Then the diluted solution was filtered through Sartorius cellulose acetate filter paper, which had 0.45 mm pore, to remove soot carbon residuals.

Since trace element levels measured in PM samples are very low, the acids and water used must be very pure to avoid contamination. Merc suprapur grade HF and nanopure water was used in the sample preparation step of the ICP-MS analysis. High amounts of HNO₃ is required during the sample preparation for ICP-MS analysis and in this case, the cost of HNO₃ is an important criterion. ISO grade 65 % HNO₃ is a cheaper alternative to suprapur grade 65 % HNO₃. However, the trace element levels in the ISO grade is higher than the ones in suprapur grade. Therefore, ISO grade 65 % HNO₃ was further purified by using an AHF, Model SAP-902 sub-boiling distillation unit.

The unit used for this purpose is shown in Figure 3.7. Trace elements levels in purified HNO_3 were compared with commercially available suprapur grade HNO_3 and discussed in Section 3.3.2.2.



Figure 3.5 Microwave digestion system



Figure 3.6 Open digestion vessels placed on hot place



Figure 3.7 Sub-boiling distillation unit

3.2.3.2.2 Analysis

PM samples collected in this study were analyzed for trace elements in approximately 50 major and minor trace elements. Elements measured include Li, Be, Na, Mg, Al, S, K, Ca, Ti, V, Cr, Mn, Fe, Co, Ni, Cu, Zn, Ge, As, Se, Rb, Sr, Y, Zr, Ag, Cd, Sn, Sb, Te, Cs, La, Pr, Nd, Sm, Eu, Gd, Tb, DY, Er, Tm, Yb, Lu, Hf, Ta, Tl, Pb, and Bi. Samples were analyzed using Perkin Elmer DRC II Model ICP-MS which is located at the Central Laboratory of the Middle East Technical University.

Inductively Coupled Plasma Mass Spectrometry (ICP-MS) is an analytical technique that allows extremely fast and precise measurement of elements in solid and liquid samples (Montaser, 1998). ICP-MS instrument consists of sample introduction system which composes of nebulizer, spray chamber and ICP torch, plasma, mass analyzer, detector and computer. Analyte from the sample vial is pumped into the nebulizer

where aerosol is formed as a result of mixing with argon gas. Larger droplets pass through the cool spray chamber. By this way, they can be removed from the aerosol. On the other hand, the fine aerosol is dragged into the central channel of the plasma where argon stream is present in a quartz tube or torch. Due to the travel through the high temperature argon plasma, aerosol droplets are subjected to drying, decomposition, vaporization and atomization. The removal of one electron from each atom results in the production of positively charged ions in the plasma. Sampling orifice extracts the ions into the interface. The ions next extracted into vacuum region, where the ion lenses and mass analyzer are located. The positive ions are separated from the unwanted neutral species via electrostatic lenses. In order to achieve this separation, these lenses bend the positive ions into the mass analyzer system and quadrupole mass spectrometer, one of the components of the mass analyzer system, uses mass to charge ratio for the separation. The mass of interest is scanned by the quadrupole across the mass range and is passed to the detector. The detector generally is an electron multiplier detector. The electronic signals are counted and stored and mass spectrum in which the intensity of the given mass is proportional to concentration of isotope at that mass is created via this detector.

The most appropriate physical conditions for ICP-MS measurements should be established in the laboratory. For this purpose, the temperature was kept between 15 - 30 °C and the maximum temperature change per hour has not exceeded 2.8 °C. It was ensured that the humidity in the laboratory is between 30% and 50% and that it did not go beyond these limits. The air entering the ICP-MS laboratory was filtered to minimize particulate matter levels in the laboratory. This is especially important for the accurate determination of soil-derived elements such as Fe, Ca, K, Na, which are abundant in the atmosphere. The pH value of the cooling water used should be kept between 6.5 - 8.5 and care was taken to ensure that the heavy metals in the water are below 1 ppm. The pressure of the cooling water was 344 ± 13 kPa.

After taking all the necessary precautions, ICP-MS was started up and the analytical conditions was selected. Analytical conditions include selection of isotopes, method, and instrumental parameters. Optimized parameters were stored once they created for

the analysis and same parameters were used during analysis of the samples. Optimized operating parameters used in the ICP-MS analysis is in given in Table 3.3.

Table 3.3. ICP-MS Operating Parameters

a) Instrumental Parameters	
RF power (kW)	1100 Watts
Argon gas flow (L min ⁻¹)	
• Plasma	15
• Auxiliary	1.2
• Nebulizer	0.97
Peristaltic pump (rpm)	18
Sample uptake rate (1 ml min ⁻¹)	~1
b) Data acquisition parameters	
Measurement mode	Scanning (Standard)
Number of measurements per peak	50 ms
Mass range (m/z)	5-270 amu
Integration time	1000 ms
Number of repetitions	3
Time per sample measurement	4 min 22 s (including 40 s sample flush)

3.3 Quality Assurance and Quality Control for ED-XRF and ICP-MS Analysis

3.3.1 Method Detection Limit

Method detection limit (MDL) is defined as “the minimum concentration of an analyte in a sample determined with a 99% confidence level that concentration is distinguishable from method blank results” by US.EPA (2017c). Different procedures have been reported in the literature to calculate method detection limit (Bennet et al., 2005; Gatari et al., 2005). In this study, for both ED-XRF and ICP-MS analysis method detection limit of each element was calculated as the three times of the standard deviation, obtained from 10 replicate analysis of the blank filters (Lopes et al., 2006).

3.3.1.1 Method Detection Limit of ED-XRF

Method detection limit calculated for each element in ED-XRF analysis and percent below detection limit (BDL) of corresponding elements in the coarse and fine fractions are given in Table 3.4.

Table 3.4. ED-XRF MDL of elements and percent BDL in each fractions

	MDL (ng m⁻³)*	Coarse % BDL	Fine % BDL
Na	6.97	9.59	9.96
Mg	10.91	0.74	7.01
Al	70.30	13.28	24.72
Si	147.76	10.33	25.09
S	57.08	2.58	0.00
K	3.40	0.00	2.95
Ca	78.18	1.85	20.30
Ti	7.44	19.93	26.57
V	0.87	4.43	2.21
Cr	2.89	16.24	17.34
Mn	3.61	8.86	12.55
Fe	67.48	9.23	9.59
Ni	0.75	13.28	7.38
Cu	4.36	16.24	17.71
Zn	9.44	9.59	11.44
As	0.51	59.04	57.93
Pb	6.00	25.83	36.53

*The average sampled volume was taken as 24 m³.

Method detection limit of the elements varied between 0.51 ng m⁻³ (As) and 147.76 ng m⁻³ (Si). %BDL of elements showed different patterns in different size fractions. Crustal elements, Al, Si, Fe, and Ca, had %BDL were less than 10% in coarse fraction whereas their % BDL values were higher (greater than 20%), in fine fraction. Elements with mixed sources, including Ti, V, Cr, Ni, had higher %BDLs in fine fraction. Among measured anthropogenic elements, As and Pb had the highest %BDL in both fractions. % BDLs for As and Pb was observed as 58 % and 37 %, respectively.

The concentrations of the remaining elements were above the MDL in nearly all the samples.

3.3.1.2 Method Detection Limit of ICP-MS

Calculated MDL for each element in ICP-MS analysis and percent BDL for corresponding elements in different size fractions are given in Table 3.5. Method detection limit of the elements varied between 0.007 ng m⁻³ (Tm) and 18.1067 ng m⁻³ (Zn). %BDLs of elements in different size fractions followed similar patterns as they did in ED-XRF. %BDL of crustal elements, Al, Fe, and Ca, in coarse fraction varied between 0% and 2.58% whereas their %BDLs varied between 0% and 22.25% in fine fraction. The concentrations of elements with mixed origin such as Ti, Cr, and Ni were above the MDL in nearly all the samples. Only exception to this was V, which had 16.77% BDL in coarse fraction and 18.96% BDL in fine fraction. Anthropogenic elements, S, Zn, As, Cd, and Ag had lower %BDLs in fine fraction compared to ones in coarse fraction. Only Pb and Cu did not follow this pattern, their %BDLs were higher in the fine fraction.

Table 3.5 ICP-MS MDL of elements and percent BDL in each fractions

	MDL (ng m ⁻³)*	Coarse %BDL	Fine %BDL		MDL (ng m ⁻³)*	Coarse %BDL	Fine %BDL
Li	0.1469	21.29	23.90	Zr	0.9270	33.55	57.42
Be	0.0336	30.32	36.81	Ag	0.0942	0.65	0.27
Na	0.2125	32.26	54.12	Cd	0.1259	42.58	19.51
Mg	0.0527	8.39	14.56	Sn	0.8779	34.19	48.35
Al	0.1502	2.58	22.25	Sb	0.0073	0.65	0.27
Si	0.0672	21.94	28.30	Te	0.0086	9.03	7.42
S	0.0686	1.94	0.00	Cs	0.0022	3.87	6.04
K	0.1344	58.06	60.71	La	0.0294	3.23	12.64
Ca	0.3907	0.00	0.00	Pr	0.0044	7.74	17.86
Ti	3.0931	0.00	0.82	Nd	0.0168	10.32	21.70
V	0.1910	16.77	18.96	Sm	0.0048	1.94	11.54
Cr	2.2480	0.00	0.00	Eu	0.0021	0.65	6.87
Mn	0.2692	4.52	4.67	Gd	0.0019	1.94	3.57
Fe	0.0159	0.00	0.27	Tb	0.0008	7.74	23.63
Co	1.7553	69.68	82.42	Dy	0.0052	9.68	29.40

	MDL (ng m⁻³)*	Coarse %BDL	Fine %BDL		MDL (ng m⁻³)*	Coarse %BDL	Fine %BDL
Ni	0.8908	0.00	0.00	Er	0.0035	15.48	38.19
Cu	1.9721	12.26	29.95	Tm	0.0007	20.00	33.24
Zn	18.1067	14.84	8.24	Yb	0.0026	10.97	34.62
Ge	0.0027	3.23	3.30	Lu	0.0005	1.94	5.22
As	0.6677	43.87	38.74	Hf	0.0111	11.61	37.09
Se	0.4760	8.39	8.52	Ta	0.0057	32.26	35.44
Rb	0.2005	32.90	42.86	Tl	0.0017	8.39	5.22
Sr	2.3253	47.74	47.80	Pb	5.0721	29.68	54.67
Y	0.0274	16.77	35.16	Bi	0.0057	7.10	7.69

*The average sampled volume was taken as 24 m³.

3.3.2 Blank Analysis

Since blank samples have significant effects on uncertainty in sampling and measurements, blank levels of the elements in this study were very carefully monitored. Throughout the study, different types of blank samples were collected/prepared. Following blanks were analyzed in the course of the study:

- Filter blanks: Blank sample measurements for the determination of elemental levels in clean filters,
- Reagent blanks: Blank sample measurements for the determination of elemental levels in acids and water,
- Field blanks.

ED-XRF is a non-destructive method therefore, reagent blanks and filter blanks are not necessary in the ED-XRF analysis, only the field blanks were analyzed along with the sample filters. In ICP-MS analysis, sample filters first digested then analyzed. Therefore, all the blank types mentioned above were analyzed along with the samples.

Filter blanks were prepared and analyzed along with samples at ICP-MS using exactly the same procedures. As mentioned before, one clean filter was put in to teflon vessels at each set of microwave digestion procedure (9 sample filters and 1 clean filter). In

total 60 filters were prepared. In this way, trace element variability of clean filters were monitored at each digestion set.

Reagent blanks were used to monitor the contribution of acids and water used during the digestion of samples. 12 acid blanks and 10 DI water blanks were prepared and analyzed with the samples.

Field blanks were the main blanks in this study. Because, they include all the possible contaminations from processes followed during the sample collection and analysis of the samples. Eighteen field blanks were collected during the study period. Field blanks were weighed, recorded, and sent to the field like sample filters. However, sampler was operated only for 5 minutes when field blanks were loaded to sampler. After this step, field blanks were treated as sample filters and same processes were applied to them.

3.3.2.1 ED-XRF Blank Analysis

Collected field blanks were treated as samples and were analyzed under same conditions with samples. Average elemental composition of field blanks are given Table 3.6. The average concentrations of the elements in coarse and fine fractions and the percentage subtraction of the field blanks from the concentration in the coarse and fine fractions are also given in the Table 3.6.

As can be seen from Table 3.6, elements can be divided into two groups according to their blank values. The first group consist of Mg, Al, Si, S, K, Ca, Ti, Mn, Fe, Ni. Blank concentrations for these elements were less than 10% of their average concentrations. The exception to this group elements was S. Blank concentration of S was a very small fraction, 4%, of the average S concentration in the fine fraction. However, S blank concentration in the coarse fraction was 22% of the measured S levels in the samples

Table 3.6 Average field blank concentrations and percent contributions to size fractions

	Average Blank Conc. ng cm^{-2}	Coarse		Fine	
		Average Sample Conc. ng cm^{-2}	% BLK	Average Sample Conc. ng cm^{-2}	% BLK
Na	86 ± 34	801	11	405	21
Mg	16 ± 9	1432	1	690	2
Al	41 ± 9	3871	1	1719	2
Si	123 ± 117	11136	1	4404	3
S	246 ± 77	1138	22	5713	4
K	39 ± 16	1364	3	931	4
Ca	90 ± 71	8162	1	2759	3
Ti	17 ± 8	2072	1	197	8
V	5 ± 7	150	3	24	21
Cr	25 ± 9	183	14	145	17
Mn	9 ± 6	221	4	128	7
Fe	334 ± 98	7518	4	4629	7
Ni	1.03±0.34	19	5	32	3
Cu	23 ± 9	76	30	76	30
Zn	68 ± 69	203	33	220	31
As	0.84 ± 0.45	3	33	3	29
Pb	46 ± 27	50	92	68	68

Second group is consisted of remaining elements Na, V, Cr, Cu, Zn, As, Pb and these elements high blank concentrations, ranging from 11% to 92% of the measured levels in the samples. Thus, statistical uncertainties of this group will be high.

3.3.2.2 ICP-MS Blank Analysis

After the filter blanks analyzed with ED-XRF, same field blanks were digested with the same procedure used in the digestion of samples and analyzed along with samples. Average field blank concentrations and corresponding standard deviations of the measured elements is given in Table 3.7.

Sample-to-blank ratios of measured elements were also calculated based on the concentrations of samples and field blanks for both coarse and fine size fractions and given Figure 3.8 and Figure 3.9, respectively.

Table 3.7 Average field blank concentrations and standard deviations (ng 50ml⁻¹)

	AVG±STD		AVG±STD
Li	2.96±1.76	Ag	6.15±1.13
Be	0.97±0.4	Cd	1.97±1.51
Na	4.97±2.55	Sn	6.34±10.54
Mg	2.4±0.63	Sb	0.96±0.09
Al	9.68±1.8	Te	0.09±0.1
S	3.37±0.82	Cs	0.04±0.03
K	2.66±1.61	La	1.01±0.35
Ca	19.63±4.69	Pr	0.12±0.05
Ti	141±37.12	Nd	0.35±0.2
V	2.45±2.29	Sm	0.26±0.06
Cr	208.75±26.98	Eu	0.18±0.02
Mn	4.2±3.23	Gd	0.13±0.02
Fe	0.81±0.19	Tb	0.02±0.01
Co	28.31±21.06	Dy	0.12±0.06
Ni	76.29±10.69	Er	0.11±0.04
Cu	49.43±23.67	Tm	0.02±0.01
Zn	456.07±217.28	Yb	0.07±0.03
Ge	0.31±0.03	Lu	0.02±0.01
As	9.9±8.01	Hf	0.44±0.13
Se	15.76±5.71	Ta	0.07±0.07
Rb	4.63±2.41	Tl	0.04±0.02
Sr	51.7±27.9	Pb	95.64±60.86
Y	0.62±0.33	Bi	0.11±0.07
Zr	24.93±11.12		

Sample-to-blank ratios in the coarse fraction ranged from 1-2 for As, Be, K, Se, Ge, Ag and S, from 2-10 Rb, Mg, Sr, Cr, Tm, Er, Ca, Na, Lu, Eu, Sm, Yb, Zr, Zn, Y, Ni, Ti, Sb, Dy, Tb, Tl, Li, Hf, La, Gd, Pr, Sn, Ta, Co, Nd, V, Pb, Al, Bi and Cu, from 11-47 Fe, Te, Cs, Mn, and Cd. Sample blank ratios were less than two for As, Be, K, Se, Ge, Ag and S, indicating that the blanks have a significant contribution on observed levels of these elements in the coarse fraction. However, As, Ag, and S have their

majority of mass in the fine fractions. Therefore, contribution of high blank levels was not high for fine fraction As, Ag, and S.

Sample to blank ratios in the fine fraction ranged from 1-2 for Be, Co, Zr, Er, Se, Tm, Mg, Sr, K, Hf, Lu, Al, Ca, and Ge, 2-10 Yb, Eu, Ti, Ag, Pb, Y, As, Sn, Na, Dy, Tb, Rb, Zn, Li, Gd, Cr, La, S, Ta, Sb, Sm, Pr, Bi, Nd, Fe, V, Ni, Tl, and Cd from 10-23 Cu, Cs, Te, and Mn. However, sample-to-blank ratios were less than two for Be, Co, Zr, Er, Se, Tm, Mg, Sr, K, Hf, Lu, Al, Ca, and Ge, indicating that the blanks have a significant contribution on observed levels of these elements in the fine fraction.

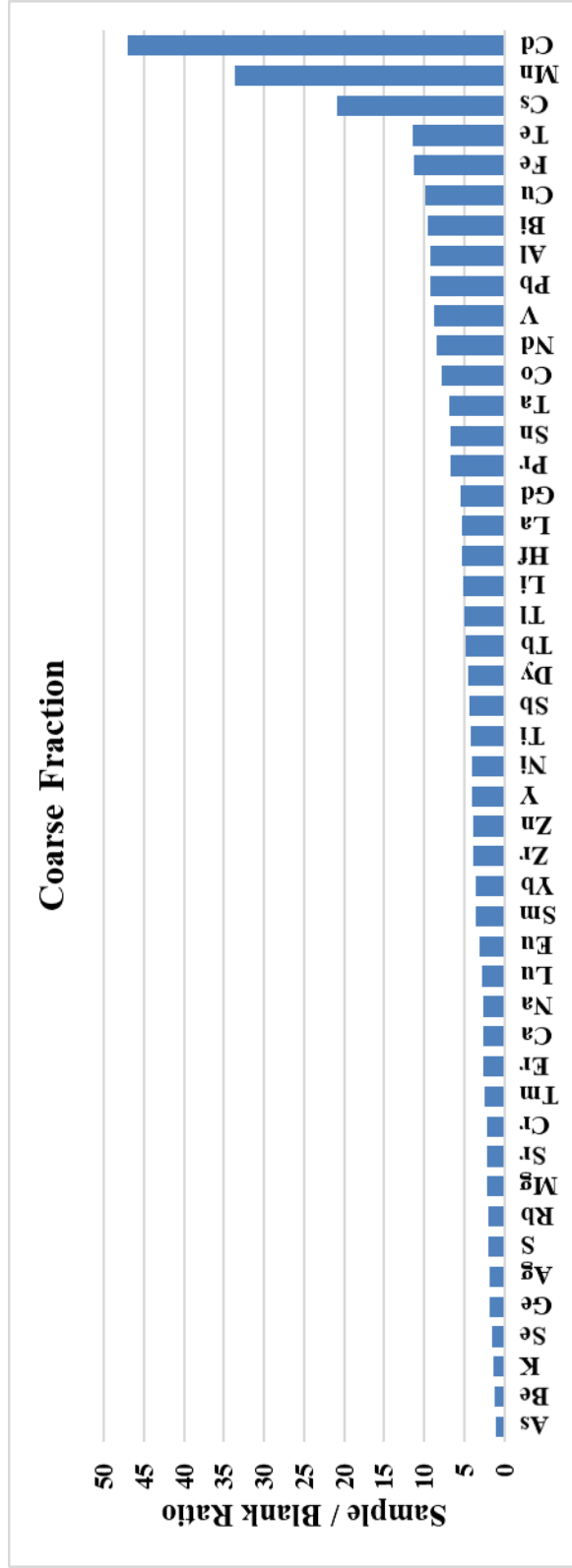


Figure 3.8 Coarse fraction sample to blank ratio for elements



Figure 3.9 Fine fraction sample to blank ratio for elements

As stated in Section 3.2.3.2.1, ISO grade HNO₃ was further purified with a sub-boiling distillation system to avoid high cost of HNO₃. In order to compare the trace elements levels in the purified HNO₃ with the commercially available suprapur grade HNO₃, 10 blanks were prepared from each acid and analyzed with ICP-MS under the same conditions with the samples. Ratios of trace elements in the acids depicted in Figure 3.10.

The ratios of trace elements varied between 0.17 and 2.63 for Be and Sr, respectively. Majority of the elements had a ratio less than one. Mg, Zn, Fe, and Co were slightly higher than one (1.00 to 1.37). Ratios of Rb and Sr were higher than two, 2.18 and 2.63, respectively. This comparison of the element levels in both acids indicated that the sub-boiling system have a good performance for majority of elements, except for Sr and Rb.

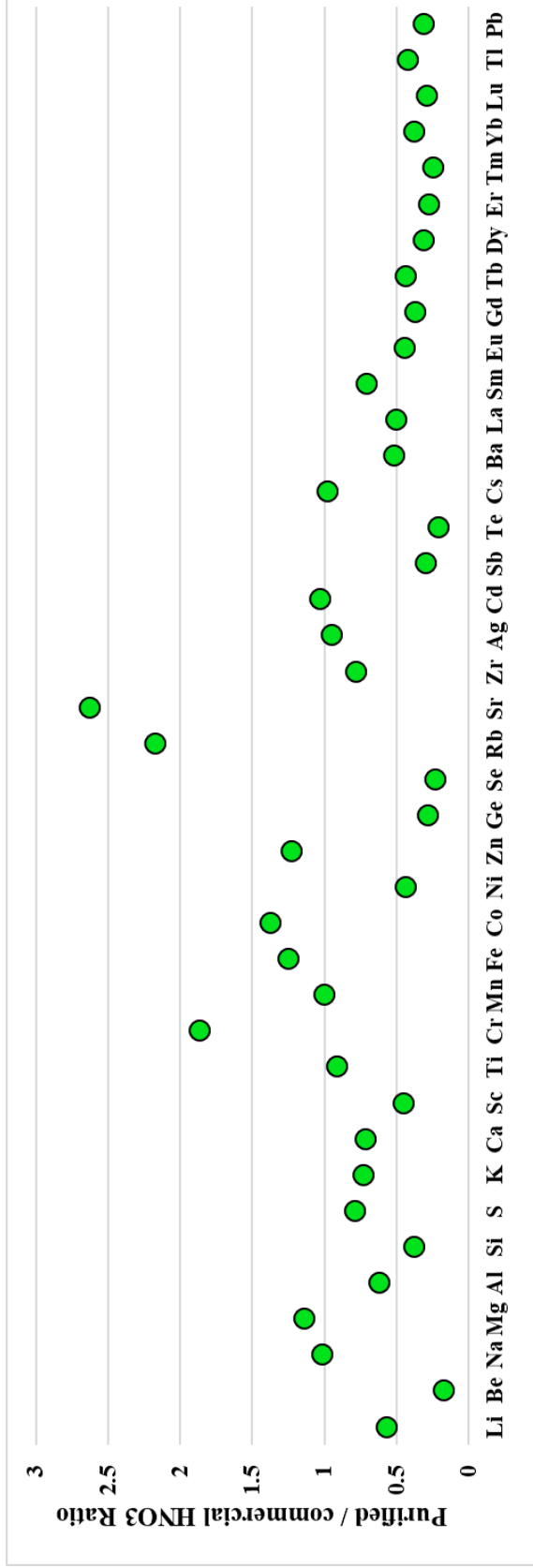


Figure 3.10 Trace element ratios of purified and commercially available HNO₃

3.3.3 SRM Analysis

In order to test the accuracy of the analyses, Standard Reference Materials (SRMs) were analyzed and measured trace element levels of the SRMs were compared with the certified levels of the SRMs. Please note that this approach makes it possible to evaluate the errors caused by the calibration of the instrument rather than the total error in study.

3.3.3.1 ED-XRF SRM Analysis

NIST SRM 2783 particulate matter reference filter was used to determine the accuracy of the ED-XRF analysis. This reference filter is analyzed along with the sample filters under same ED-XRF conditions. The certified concentrations of the elements in the SRM, measured concentration of the corresponding element, and the percent error calculated for each element are given in Table 3.8.

Calculated error for Si, Al, Mn, Na, Pb were lower than 5%. The errors calculated for K, As, Ca, Fe, Mn, Na, Ni, Ti, Zn and Cr were between 5% and 10%. The error percentages for S, Mg, and V were between 10 and 15%, %, which are reasonable and indicate that there is no gross calibration errors in the course of XRF measurements.

Table 3.8 NIST SRM 2783 certified and measured concentrations of elements and percent error

	Certified (ng filter⁻¹)	Measured (ng filter⁻¹)	%Error
S	1050	915	12
Si	58600	59186	1
Al	23210	24138	4
As	11.8	12.4	5.6
Ca	13200	12400	6
Cr	135	147	9
Cu	404	355	12
Fe	26500	28100	6

	Certified (ng filter⁻¹)	Measured (ng filter⁻¹)	%Error
K	5280	4900	7
Mg	8620	9800	14
Mn	320	330	4
Na	1860	1760	5
Ni	68	73	8
Pb	317	325	3
Ti	1490	1400	6
V	48.5	53.8	11
Zn	1790	1660	7

3.3.3.2 ICP-MS SRM Analysis

The accuracy of the ICP-MS analysis was verified using the NIST SRM 1648a (urban particulate matter). NIST SRM 1648a was digested by the same procedure applied to samples and then analyzed by ICP-MS under the same conditions (SRM 2783 particulate matter reference filter was too expensive to digest). Measured and certified concentrations of elements are given in Table 3.9.

Table 3.9. NIST SRM 1648a certified and measured concentrations of elements and percent error

	Unit	Certified	Measured	% Error
Cd	mg kg ⁻¹	72	70.88	1.56
Mn	mg kg ⁻¹	822	782.25	4.84
Sb	mg kg ⁻¹	44	39.17	10.99
Sr	mg kg ⁻¹	207	196.35	5.14
Al	%	3.43	3.18	7.24
Ca	%	5.84	5.47	6.33
Fe	%	3.92	3.80	3.04
S	%	5.51	4.62	8.53
K	%	1.056	0.96	9.52
Mg	%	0.813	0.75	8.30
Zn	mg kg ⁻¹	4800	4677.75	2.55
Rb	mg kg ⁻¹	51	45.15	11.47
Co	mg kg ⁻¹	17.93	17.12	4.55

Calculated error percentages for Cd, Mn, Fe, Zn, and Co were lower than 5%. The errors calculated for Sr, Al, Ca, S, K, and Mg were between 5% and 10%. The error percentages for Sb and Rb were between 10 and 12%. The comparison demonstrated that as in XRF analysis calibration errors were not significant for ICP analysis as well. However, please note that although > 40 elements are measured with ICP, comparison is limited to elements that had certified values in the SRM

3.3.4 Replicate and Repeated Analysis of test Samples by ICP-MS

ICP-MS analysis of samples was tested by two approaches:

1. Repeated analysis: Collected PM samples were digested for ICP-MS analysis in two batches. After the samples were digested in the first batch, the resulting 50 ml volume was divided into two and one portion was sent for the analysis, when the second batch was digested, saved sample from the first batch was sent with the second batch of samples. Eight samples were saved from the first batch and were sent with the second batch. This repeated analysis was done to test batch-to-batch variations of ICP-MS analysis.
2. Replicate analysis: Nine random samples were selected among the digested samples and these samples were divided into two. Each portion was assigned with different bottle numbers and analyzed with ICP-MS in the same batch. This approach was done to ensure the repeatability of the ICP-MS analysis.

Elemental ratios of the test samples from repeated and replicate analysis are depicted in Figure 3.11 and Figure 3.12, respectively.

In repeated analysis ratios of repeated Li, Na, Al, K, Ti, V and Cr measurements were consistently smaller than unity. However, although variability was high, ratios were around unity for rest of the elements. For replicate analysis which is a measure of variability in the same batch, ratios for Li, Mg, Al, K and Ca were around unity, but concentrations of Ti, V, Cr and Mn were consistently higher unity, indicating problems with measurement of these elements in the same batch.

These seven elements are the ones that were analyzed by ICP-OES due to their high concentrations in samples. For the remaining elements that were measured by ICP-MS, even though spreads are large, for some elements in both repeated and replicate analysis of the test samples, they all center around unity, indicating there was no substantial error in ICP-MS measurement.

3.3.5 Comparison of ED-XRF and ICP-MS Data Sets

As stated previously, ED-XRF and ICP-MS were the main analytical techniques employed to determine the chemical composition of PM samples collected in this study. Na, Mg, Al, S, K, Ca, Ti, V, Cr, Mn, Fe, Ni, Cu, Zn, As, Pb were the common elements measured both by ED-XRF and ICP-MS. In this section of this study, these common elements are compared in terms of their number of observance in each technique and given in Table 3.10.

Table 3.10 Comparison of ED-XRF and ICP-MS for the measured common elements

ED-XRF		ICP-MS	
Elements	N	Elements	N
Na	195	Na	168
Mg	176	Mg	162
Al	196	Al	148
S	267	S	343
K	241	K	201
Ca	216	Ca	328
Ti	154	Ti	284
V	17	V	327
Cr	184	Cr	324
Mn	184	Mn	284
Fe	86	Fe	340
Ni	134	Ni	271
Cu	72	Cu	236
Zn	103	Zn	307
As	162	As	62
Pb	118	Pb	212

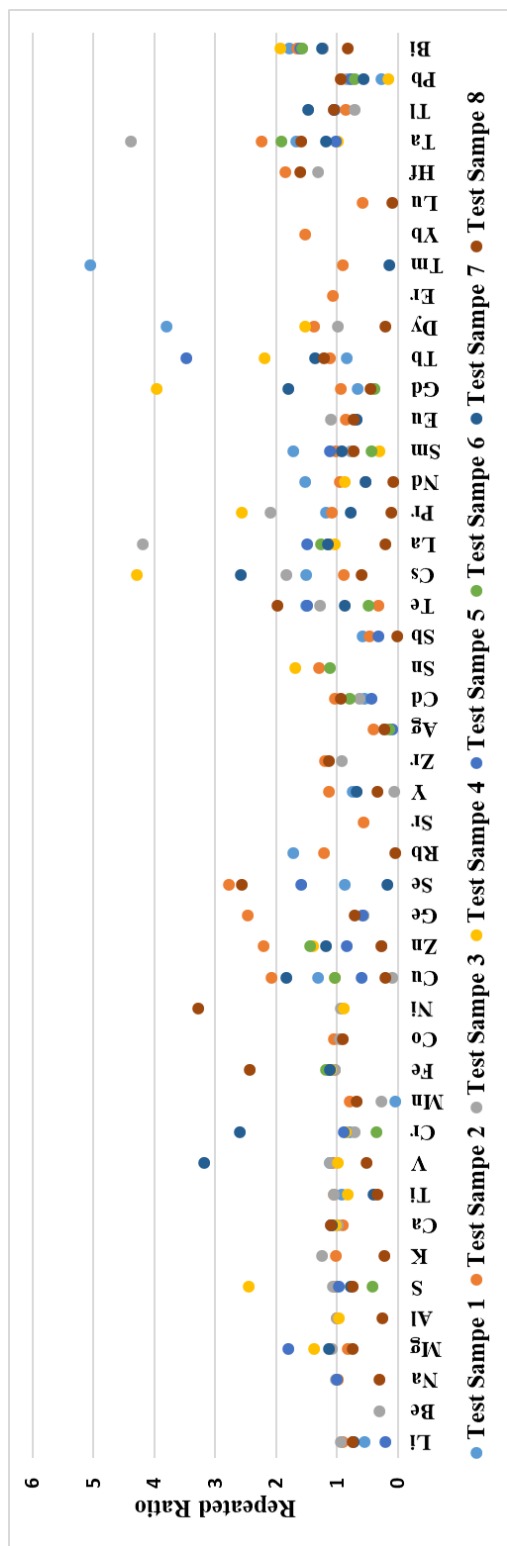


Figure 3.11 Elemental ratios of repeated analysis of test samples

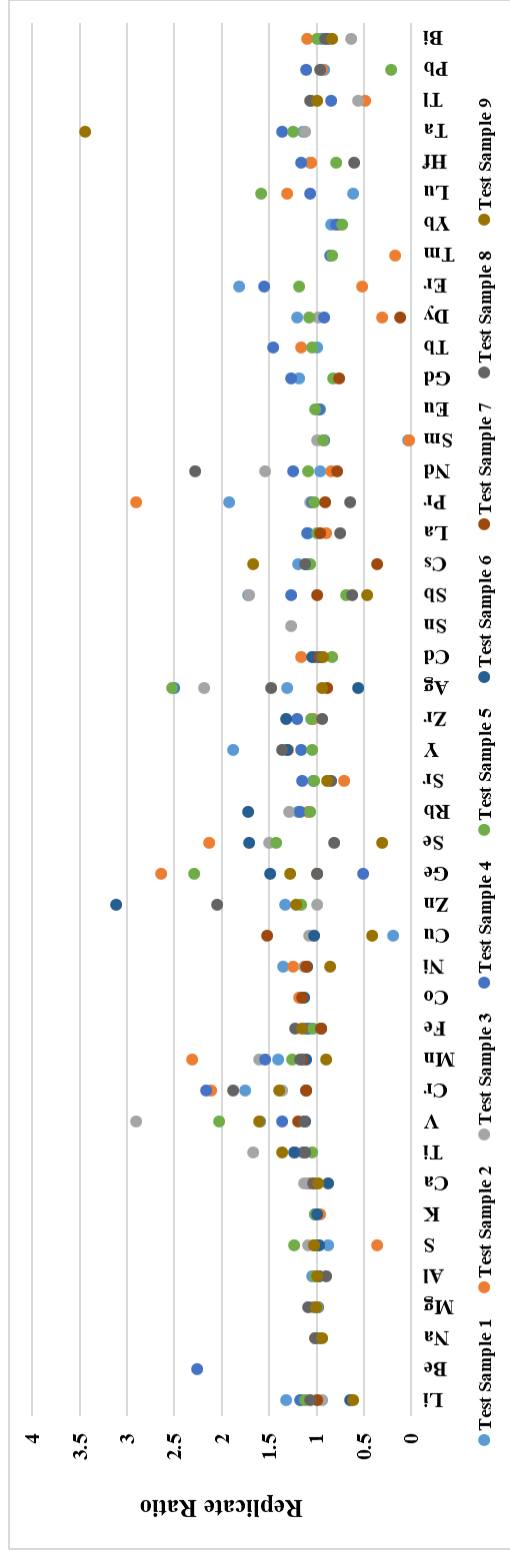


Figure 3.12 Elemental ratios of replicate analysis of test samples

Comparison of results demonstrated that agreement between the two techniques were acceptable for most of the elements including Fe and S, but not so good for Al and few other elements. These elements were also detected in smaller number of samples in ICP-MS measurements. Because of these reasons, XRF data were used for this small group of elements including Na, Mg, Al, Ca, Mn, Ni, As, and Pb.

3.4 Source Apportionment

In this study, different techniques, including Enrichment Factor calculations (EF), Positive Matrix Factorization (PMF), and Potential Source Contribution Function (PSCF) were used for the source apportionment of the PM collected at the Eastern Black Sea region of Turkey.

3.4.1 Positive Matrix Factorization (PMF)

The Positive Matrix Factorization (PMF) model, one of the multivariate receptor models, was used to identify the sources contributing and the contributions of these sources to the aerosol population at the Eastern Black Sea atmosphere. PMF was developed in early 90s by Paatero and Tapper (1993, 1994) and Paatero, (1997). Following the release of the PMF by US EPA, it has become the most widely used source apportionment method (Hopke, 2016).

The PMF is based on the solution of the receptor modeling problem shown in Equation 3.4.

$$X = GF + E \quad \text{Equation 3.4}$$

In the equation, X represents the data matrix, F represents the source profiles, G represents the source contributions, and E represents the unmodeled portion. Factor analysis models aim to identify G and F matrices. Equation 3.4 can be written for each data point as follows:

$$x_{ij} = \sum_{k=1}^p g_{ik} f_{kj} + e_{ij} \quad \text{Equation 3.5}$$

In Equation 3.5, x_{ij} is the concentration of j^{th} species on the i^{th} sample, g_{ik} is the contribution of the k^{th} factor to the i^{th} sample, f_{kj} is the fraction of the k^{th} factor that is species j , e_{ij} is the residual for the j^{th} species at the i^{th} sample.

The main purpose of the Positive Matrix Factorization model is to minimize the ratio of the unmodeled portion to the uncertainty defined for each data by utilizing an explicit least-squares formulation. This process can be defined with an objective function (Q) as follows:

$$Q = \sum_{i=1}^n \sum_{j=1}^m \left(\frac{e_{ij}}{s_{ij}} \right)^2 \quad \text{Equation 3.6}$$

In the Equation 3.6, s_{ij} represents the uncertainty of j^{th} species on the i^{th} sample. In an ideal model, the objective function Q is expected to be zero. However, the Q value can be high, especially in aerosol samples where the environmental background noise is high.

In this study, the EPA PMF 5.0 model developed by the United States Environmental Protection Agency (US. EPA) (Norris, 2014) was used. In this model, two different Q values are reported. The first one is Q(true). The Q(true) value is calculated including all data points in the data set. The second reported Q value is Q(robust). Q(robust) is calculated excluding the data points that the uncertainty-scaled residuals greater than +4 and less than -4. In a successful run, it is expected that the Q(true) and Q(robust) values are close to each other, in other words the ratio of e_{ij}/s_{ij} calculated for all data points should be between -4 and +4

In PMF model, the species that cannot be well modeled or whose the signal to noise ratio less than one are assigned as "weak" and the uncertainties associated to these species in the model are multiplied by three. However, if these species are still not well

modeled, they are removed from the model. The theoretical Q value is calculated using non-weak data points by Equation 3.7.

$$Q_{theo} = (ixj) - (i + j)xN \quad \text{Equation 3.7}$$

In this equation, K is the number of non-weak data points (sample number \times specie number), N is the number of factors, i is the number of samples, and j is specie number in the data set. The theoretically calculated Q value is expected to be close to $Q(\text{true})$ value.

The $Q/Q(\text{theoretical})$ value is calculated for each specie and for each data day / point, as described above, in the PMF model to show how efficiently each species are modeled or not modeled. The $Q/Q(\text{theoretical})$ ratio expected to be at most two (Norris, 2014).

In order to get the most feasible solution in the PMF model, firstly the distributions of the e_{ij}/s_{ij} ratios obtained for each specie should show a normal distribution in the range of ± 3 . Either data points that do not show this distribution should be removed from the model or the number of factors should be increased.

Another model performance criterion is the comparison of measured concentrations and predicted (modeled) concentrations scatter plots. This plot is used to check if the model fits the individual species well. In this plot, it is expected that the points scatter around the 1:1 line. If a specie do not have a strong correlation between measured and predicted concentrations, then the specie should be down-weighted by assigning its category as “weak” or should be removed from the model.

The third model performance criteria is time series analysis of the measured and predicted concentrations. This analysis is important to assess the model performance in certain periods. The low-performance data points of the species should be removed from the model or the specie should be removed completely from the model.

If the above mentioned criteria are successfully completed, the next step is to examining the Q/Q (theoretical) values for each specie and sample. If there is no problem, the factors should be identified by examining factor profiles (F-loadings) and factor contributions (G-Score) of each source. If the factors cannot be defined correctly, the number of factors should be increased. However, it should be avoided to divide a factor into two while increasing the number of factor. For this, the correlation between the G-scores of the factors should be examined. Correlation between factors should not be observed. Contrary to expectations, in some cases correlation between some factors are observed. Such situations need to be scrutinized clearly. In this case, the correlation between G-scores of the factors is partially eliminated by applying the F-Peak. Similarly, F-Peak is also eliminate correlation between factor profiles.

3.4.2 Back Trajectory Modeling

The transport of pollutants from one place to another in the atmosphere is called long-range transport. Air pollution in a country is not only affected by its own sources, but can also be affected by sources of air pollution in another country. Investigating the long-range transport of airborne pollutants is important in understanding the air pollution in a region and developing effective control strategies for it.

Ambient air quality at a location is determined by the amount of emissions and meteorological conditions. However, the relationship between these two factors is quite complex. As a pollutant reside in the atmosphere, it is dispersed, diluted, settled and under goes to chemical and / or photochemical reactions (Mayer, 1999). For this reason, establishing a relationship between the emission and concentration of a pollutant in the atmosphere is quite difficult (Fenger, 1999). While surface winds are used to determine the effect of local pollutants, synoptic scale air movements (upper atmospheric air movements) are used to determine the effect of the pollution sources at a remote location. It is known that synoptic scale air movements affect long-range transport of pollutants. Back trajectory analysis is a common technique used to determine synoptic scale air movements (Brankov et al., 1998; Dorling et al., 1992; Katsoulis, 1999; Stohl et al., 2002). A back trajectory is a set of vectors that

demonstrates the latitude, longitude, and altitude of an air mass in the atmosphere. There are different models that calculate the back trajectory movements of air masses. The most common ones are FLEXTRA (Stohl et al., 1995), ECMWF (Molteni et al., 1996) and HYSPLIT (Draxler and Hess, 1998).

In this study, the HYbrid Single-Particle Lagrangian Integrated Trajectory (HYSPLIT) Version 4 (Stein et al., 2015) model developed by US. National Oceanic and Atmospheric Administration (NOAA) was used for the calculation of back trajectories. The model calculation method is a hybrid between the Lagrangian approach, using a moving frame of reference for the advection and diffusion calculations as the trajectories or air parcels move from their initial location, and the Eulerian methodology, which uses a fixed three-dimensional grid as a frame of reference to compute pollutant air concentrations (Stein et al., 2015).

Back trajectory calculations with HYSPLIT is done on a daily basis through its web interface. However, in such studies where the sample numbers are high, the time required to calculate back trajectories on a daily basis could be very long. Therefore, some Geographical Information Systems (GIS) based softwares that can calculate back trajectories weekly and / or monthly are available. In this study, back trajectories were calculated with TrajStat Version 1.2.2.6, a GIS based software, developed by Wang et al. (2009). TrajStat also has capabilities of view, query, and cluster the trajectories and when combined with measurement data it can compute the potential source contribution function (PSCF) and concentration weighted trajectory (CWT) analyses (Wang et al., 2009).

Selection of back trajectory length is an important criterion in trajectory modeling. Back trajectory length should be long enough to cover the regions of interest and meanwhile should not be too long to minimize trajectory errors. As the length of the trajectory increases, spatial and temporal errors in the meteorological data also increase (Fast and Berkowitz, 1997). Previous studies in our research group showed that five-day long back trajectories are long enough to cover the major source regions that

thought to be affecting Eastern Black Sea atmosphere and they are not long enough to cause unreasonably high uncertainties.

Five-day back trajectories starting from the sampling station at 19:00 UTC at three different altitudes, namely 100, 500 and 1500 meter were calculated for sampling period. Reanalysis meteorological data archive of the NOAA was used as input data for back trajectory calculations. Isentropic vertical motion method type was selected in the model calculation. For each arrival heights, 357 back trajectories were calculated.

3.4.3 Potential Source Contribution Function (PSCF)

Receptor models determine contribution of a source by identifying the nature of the source, rather than determining the geographical location of a source that is contributing the pollution at a region. In order to reveal such information, measured concentrations and geographical information should be combined in some way. Geographical information is usually obtained from back trajectories. The method for determination of the location of sources affecting the aerosol population at a receptor by combining back trajectories and measurement data is called trajectory statistics. In this study, Potential Source Contribution Functions (PSCF), which is a type of trajectory statistics, was used. The concept of PSCF was introduced to determine geographical regions that may have a higher probability of being source areas.

The Potential Source Contribution Function (PSCF) analysis begins by dividing the study domain into the $1^{\circ} \times 1^{\circ}$ grids. The study domain used in PSCF analysis extends from west of UK (20°W) to Center of Asia (60°E) in North East direction and from Siberia (75°N) to middle of Africa (15°N) and shown in Figure 3.13. Total number of cells (grids) in the study domain was 4800. Back trajectories calculated in the TrajStat software were divided into hourly segments. Each positions of the segments of a back trajectory was assigned to one of the grids, depending on their coordinates. Since 5-day back trajectories were used in this study, there were 121 segments for each trajectory. Calculated segments for each arrival height were 43197.

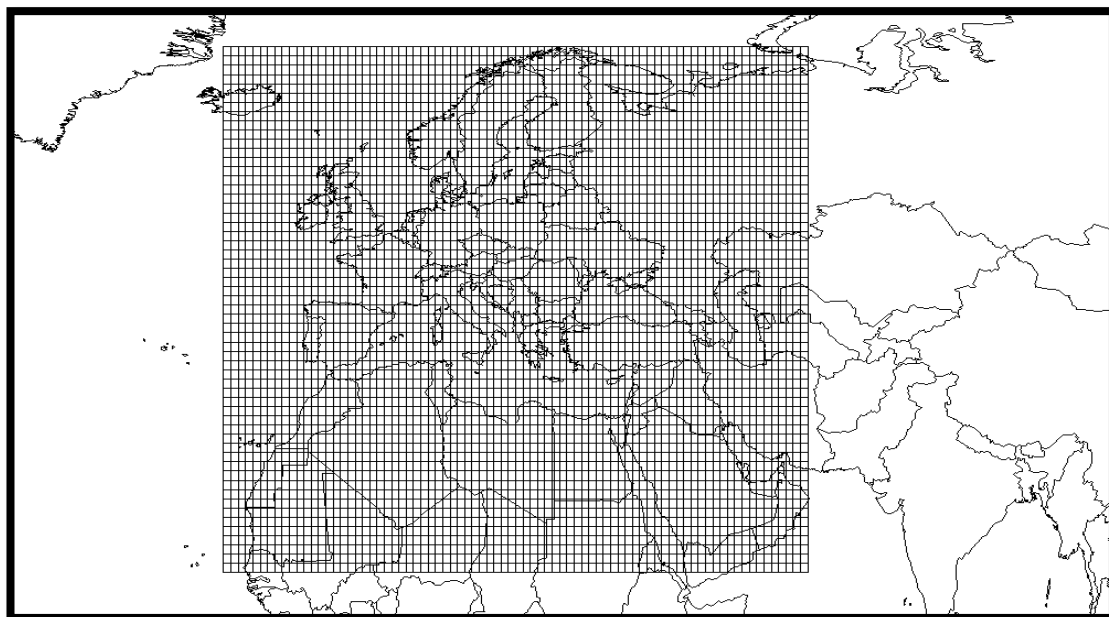


Figure 3.13 The study domain used in PSCF analysis

PSCF value of grid cell ij for a specie or a factor, obtained from PMF analysis, is calculated with Equation 3.8. In order to calculate the PSCF value of a grid cell, MAPINFO, a GIS based software, was used. First, the coordinates of segments of all trajectories calculated in TrajStat were assigned to grid cells, and then the number of segment in each grid was counted. This counting calculates the n_{ij} value in Equation 3.8. A second counting was required to calculate m_{ij} value. m_{ij} represents the number of segments in grid cell ij that belong to back trajectories assigned to highest 40% concentration of a specie or a factor. Trajectories correspond to highest 40% concentration of a specie or a factor was selected and copied to another file. Second counting was done only with this group trajectory. PSCF value of grid ranges between 0 and 1. If a grid has a PSCF value of 1, then this means that every segment in that cell corresponds to high concentration of a specie.

$$PSCF_{ij} = \frac{m_{ij}}{n_{ij}} \quad \text{Equation 3.8}$$

A high PSCF value, approaches 1, of grid indicates that the grid is the potential source region and a low PSCF value, approaches 0, indicates the grid is unlikely to be a source region.

As in all models, there are uncertainties in the PSCF. If the number of n_{ij} in the grid is small, then the calculated PSCF value for this grid will only depend on a few segments and PSCF value of this grid can be high. Such high values may not be statistically significant and this may not mean that the area covered by the grid cells is a strong potential source region. Thus, uncertainties of the PSCF value due to few segments will be high. The uncertainties of PSCF is dealt with two methods. The first method (Plaisance et al., 1997; Zeng and Hopke, 1989) is the weighting of PSCF value of a grid cell depending on the number of segment it contain. The second method is the non-parametric bootstrapping approach proposed by Hopke et al. (1995) and Lupu and Maenhaut (2002). This approach test the statistical significance of each PSCF value of grid cells of the study domain.

In this study, the uncertainties of PSCF is dealt with the weighting method given in Equation 3.9 (Zhao and Hopke, 2006).

$$W(n_{ij}) = \begin{cases} 0.15 & n_{ij} \leq n_{avg}/2 \\ 0.5 & n_{avg}/2 < n_{ij} \leq n_{avg} \\ 0.75 & n_{avg} < n_{ij} \leq 2 \times n_{avg} \\ 1.0 & n_{ij} > 2 \times n_{avg} \end{cases} \quad \text{Equation 3.9}$$

where;

$W(n_{ij})$ is the weighting function

n_{avg} is the average number of segments in the whole study domain

In this method, PSCF value of a grid cell is multiplied with a $W(n_{ij})$ value depending on the number of segment it contains. Thus, the weight of a grid cells with small number of n_{ij} is minimized.

CHAPTER 4

RESULTS AND DISCUSSION

4.1 General Characteristic of the Data Set

4.1.1 Data Set

The concentration of elements in PM samples collected on Eastern Black Sea region of Turkey (Torul, Gümüşhane) from March, 2011 to December, 2013 are presented in this study. Different analytical techniques, ICP-MS, ED-XRF, and Aethalometer, were used to determine the elemental composition of aerosol samples. In both coarse (PM_{2.5-10}) and fine (PM_{2.5}) fraction samples, concentrations of 10 elements (Na, Mg, Al, Si, Ca, K, Mn, Ni, As, Pb) were determined using ED-XRF, concentrations of 39 elements (Li, Be, SO₄²⁻, Ti, V, Cr, Fe, Co, Ni, Cu, Zn, Ge, Se, Rb, Sr, Y, Zr, Ag, Cd, Sn, Sb, Te, Cs, La, Pr, Nd, Sm, Eu, Gd, Tb, Dy, Er, Tm, Yb, Lu, Hf, Ta, Tl, Bi) were determined using ICP-MS, black carbon (B.C.) content was determined using Aethalometer and particulate mass (PM) concentration was determined gravimetrically.

Arithmetic means with associated standard deviations, median values, maximum and minimum values for all measured species in fine and coarse fraction samples are given in Table 4.1 and Table 4.2, respectively. Number of samples are also provided in the tables.

Standard deviations listed in Table 4.1 and Table 4.2 are higher than the corresponding mean values. Variations in meteorological events, changes in the air mass transport patterns and the variations in the source strengths are the main factors for the large variability of the atmospheric concentrations of measured species (Güllü et al., 2000). Such high standard deviations are not unusual for atmospheric trace element data sets. Almost all of the trace elements in the tables have mean concentrations almost twice

the median value and this indicates log-normal and other skewed distributions of trace elements (Koçak et al., 2004). Distribution characteristics of the measured trace elements in this study are discussed in details at Section 4.1.2.

Data completeness is challenging in atmospheric trace element data sets, especially when the sampling is performed with low volume samplers detection frequency of trace elements is an important problem. With a Stack Filter Unit, a type of low volume sampler, approximately 24 m³ air is drawn and passed through the filters during a 24 hours sampling, hence small amount of particulate mass is collected on the filters. Another factor that causes this problem is the partitioning of elements between fine and coarse size fractions. Coarse fraction is dominated by elements arise from soil and crustal materials, whereas fine fraction is dominated by anthropogenic species (National Research Council, 1980). Therefore, blanks subtraction of crustal elements will be high in the fine fraction (because most of their mass occurs in coarse fraction), while blank subtraction of anthropogenic elements will be high in the coarse fraction (because most of their mass occurs fine fraction). Even though all the necessary precautions such as using low-blank filters and reagents were taken, due to these reasons it resulted in fairly large blank subtraction and small frequency of detection for some of the elements.

Mean concentrations of trace elements in the fine fraction varied between 0.0011 ng m⁻³ for Tm and 1382.42 ng m⁻³ for SO₄²⁻. Eighteen species, including Co, Pb, Be, Zr, Ni, Sn, Eu, Hf, Er, As, Mn, Mg, Na, Lu, Al, Sr, Tm, Rb were detected in less than 60% of the samples; 23 species, including Ca, Yb, B.C., Si, K, Ge, Cu, Sm, Y, Ag, Tb, Dy, Gd, La, Pr, Ta, Ti, Li, Nd, Te, Se, Sb, Zn were detected in between 60% and 90% of the samples and 8 species, namely Bi, Tl, Cr, Cd, V, Cs, Fe, SO₄²⁻ were found at least in 90% of the samples. The species with high missing data points were handled more carefully than other elements in statistical tests and source apportionment models, since the uncertainties associated to these species were high.

Table 4.1 Statistical summary of concentration (ng m^{-3}) of trace elements, black carbon and PM mass of fine fraction aerosols

	Arithmetic Mean	Median	Maximum	Minimum	N
PM_{2.5}*	10.39 ± 21.14	7.30	303.83	0.25	344
B.C.	269.04 ± 702.34	194.80	10313.20	0.90	217
Li	0.595 ± 3.65	0.218	60.85	0.001	289
Be	0.0282 ± 0.0408	0.0181	0.40	0.001	123
Na	31.07 ± 39.29	25.76	473.83	1.17	192
Mg	69.36 ± 145.49	38.88	1771.18	0.87	173
Al	179.45 ± 357.68	111.51	4457.38	0.51	193
Si	436.51 ± 850.87	299.38	11522.96	2.97	226
SO₄²⁻	1382.43 ± 2948.53	954.03	46410.45	32.98	343
K	90.62 ± 148.84	68.88	2137.56	0.92	235
Ca	274.55 ± 530.77	155.21	5601.03	0.52	212
Ti	8.79 ± 11.78	4.70	84.69	0.02	284
V	0.619 ± 1.8	0.32	24.28	0.002	327
Cr	11.37 ± 12.48	7.06	94.31	0.18	324
Mn	11.96 ± 16.16	8.28	171.42	0.21	179
Fe	172.96 ± 290.45	83.38	2603.61	0.28	340
Co	2.76 ± 2.87	1.58	11.96	0.002	110
Ni	3.7 ± 15.93	1.99	185.87	0.04	134
Cu	4.25 ± 8.38	1.75	95.35	0.01	236
Zn	30.66 ± 23.37	27.22	115.95	0.13	307
Ge	0.025 ± 0.088	0.015	1.34	0.0001	235
As	0.226 ± 0.348	0.184	4.79	0.005	162
Se	0.514 ± 0.343	0.473	2.33	0.01	294
Rb	0.673 ± 1.352	0.133	8.73	0.0003	210
Sr	3.49 ± 7.7	1.17	69.07	0.01	197
Y	0.0604 ± 0.0862	0.0257	0.71	0.0002	242
Zr	2.13 ± 2.49	1.61	12.58	0.001	127
Ag	0.565 ± 0.969	0.304	11.85	0.002	242
Cd	0.523 ± 1.095	0.144	8.66	0.001	325
Sn	0.672 ± 1.362	0.233	11.59	0.01	141
Sb	0.131 ± 0.218	0.093	2.84	0.0005	301
Te	0.0523 ± 0.0644	0.0429	0.69	0.0001	292
Cs	0.0229 ± 0.0368	0.0140	0.50	0.0001	335
La	0.152 ± 0.229	0.073	2.68	0.0002	273
Pr	0.0222 ± 0.0337	0.0100	0.32	0.00002	274
Nd	0.0790 ± 0.1180	0.0371	1.12	0.0001	291
Sm	0.0511 ± 0.1059	0.0173	0.98	0.0005	236
Eu	0.0265 ± 0.0491	0.0111	0.37	0.0001	144
Gd	0.0177 ± 0.0254	0.0090	0.24	0.00004	265
Tb	0.0022 ± 0.0031	0.0013	0.03	0.00001	244
Dy	0.0129 ± 0.0202	0.0069	0.21	0.00002	245

	Arithmetic Mean	Median	Maximum	Minimum	N
Er	0.0079 ± 0.0111	0.0043	0.10	0.0002	161
Tm	0.0011 ± 0.0013	0.0007	0.01	0.00003	209
Yb	0.0063 ± 0.0088	0.0034	0.08	0.0001	214
Lu	0.0013 ± 0.0016	0.0007	0.01	0.00003	192
Hf	0.0508 ± 0.0580	0.0297	0.29	0.0006	145
Ta	0.0129 ± 0.0390	0.0077	0.51	0.0001	278
Tl	0.0104 ± 0.0179	0.0071	0.23	0.0002	319
Pb	4.1 ± 5.31	2.80	43.12	0.15	115
Bi	0.0221 ± 0.0302	0.0164	0.32	0.000004	318

* $\mu\text{g m}^{-3}$, N: Number of samples

The chemical composition of fine and coarse fraction are generally quite different (National Research Council, 1980). The composition and sources of coarse fraction are well known and do not vary greatly one sampling point to another. The coarse fraction is dominated by elements that mainly arise from soils and other crustal materials, whereas fine fraction is dominated by anthropogenic species, since their size is generally less than $2.5 \mu\text{m}$ (Tokgöz, 2013). Therefore, 154 out of 352 coarse fraction samples were analyzed for their elemental composition to check whether there was a modification to this general pattern and summary statistics of the trace elements in the analyzed coarse fraction samples are given in Table 4.2.

Mean concentrations of trace elements in the coarse fraction varied between 0.0017 ng m^{-3} for Tm and 1441.5 ng m^{-3} for Si. Thirteen species, including Ni, Pb, Co, As, Ag, Mn, Be, Sn, Sr, Zr, Al, Ge, Mg were detected in less than 60% of the samples; 27 species, including Eu, Na, Si, K, Hf, B.C., Rb, Ca, Zn, Cd, Er, Tm, Sb, SO_4^{2-} , Ta, Lu, Cu, Li, Se, Tl, Cr, Y, Te, Sm, Yb, Bi, Tb were detected in between 60% and 90% of the samples and 9 species, namely La, Pr, Dy, V, Nd, Gd, Ti, Cs, Fe were found at least in 90% of the samples.

Table 4.2 Statistical summary of concentration (ng m⁻³) of elements, black carbon and PM mass of coarse fraction aerosols

	Arithmetic Mean	Median	Maximum	Minimum	N
PM_{2.5-10}*	9.7 ± 18.31	5.98	193.66	0.04	147
B.C.	109.52 ± 122.93	86.00	999.10	3.90	104
Li	0.66 ± 1.2	0.257	8.58	0.0003	127
Be	0.0263 ± 0.0214	0.0209	0.09	0.001	76
Na	68.85 ± 100.75	40.21	794.57	1.02	97
Mg	167.42 ± 457.19	62.54	3295.08	10.45	91
Al	458.06 ± 1156.67	197.23	8706.09	16.17	88
Si	1441.5 ± 4428.91	493.81	33038.73	36.01	97
SO₄²⁻	556.68 ± 555.26	359.99	3000.14	31.22	121
K	132.46 ± 208.53	80.32	1918.87	12.63	98
Ca	802.14 ± 1622.22	442.80	15325.40	46.32	110
Ti	17.17 ± 17.67	10.78	78.26	0.16	145
V	0.889 ± 1.316	0.47	9.07	0.002	141
Cr	10.61 ± 12.56	5.85	86.13	0.40	132
Mn	26.28 ± 105	8.76	909.20	0.49	74
Fe	349.82 ± 496.33	156.56	2279.36	10.95	153
Co	5.79 ± 9.75	2.05	41.12	0.004	48
Ni	3.44 ± 5.19	1.63	19.79	0.02	29
Cu	7.24 ± 14.91	1.98	96.68	0.01	125
Zn	45.23 ± 32.45	42.06	118.25	0.32	111
Ge	0.0169 ± 0.0164	0.0118	0.09	0.0003	89
As	0.198 ± 0.224	0.147	1.31	0.005	54
Se	0.531 ± 0.573	0.413	5.66	0.0016	128
Rb	0.332 ± 0.395	0.248	3.26	0.001	106
Sr	3.43 ± 6.66	2.00	56.40	0.03	83
Y	0.0957 ± 0.1312	0.0584	1.14	0.0002	132
Zr	5.74 ± 6.74	3.09	31.61	0.01	84
Ag	0.644 ± 1.736	0.133	10.12	0.01	71
Cd	0.532 ± 1.222	0.125	8.39	0.001	111
Sn	1.83 ± 3.39	0.60	18.91	0.002	81
Sb	0.162 ± 0.259	0.065	1.48	0.001	114
Te	0.0414 ± 0.0277	0.0389	0.20	0.001	132
Cs	0.0378 ± 0.1314	0.0182	1.53	0.0001	149
La	0.213 ± 0.268	0.144	1.83	0.003	139
Pr	0.0339 ± 0.0491	0.0182	0.40	0.0002	139
Nd	0.125 ± 0.18	0.069	1.56	0.0003	141
Sm	0.0339 ± 0.0452	0.0185	0.33	0.00001	133
Eu	0.0285 ± 0.0408	0.0103	0.16	0.000004	94
Gd	0.0278 ± 0.04389	0.0164	0.35	0.0003	141
Tb	0.0036 ± 0.0047	0.0024	0.04	0.00005	137
Dy	0.0199 ± 0.0282	0.0120	0.25	0.00003	140

	Arithmetic Mean	Median	Maximum	Minimum	N
Er	0.0110 ± 0.0144	0.0072	0.12	0.0002	111
Tm	0.0017 ± 0.002	0.0012	0.02	0.00003	113
Yb	0.0091 ± 0.0125	0.0052	0.11	0.0001	133
Lu	0.0018 ± 0.0019	0.0014	0.02	0.0001	124
Hf	0.125 ± 0.157	0.064	0.74	0.0006	99
Ta	0.0191 ± 0.0316	0.0079	0.17	0.0002	122
Tl	0.0076 ± 0.0079	0.0045	0.03	0.0003	130
Pb	4.96 ± 8.01	2.62	45.18	0.25	37
Bi	0.0353 ± 0.0362	0.0207	0.15	0.00	136

* $\mu\text{g m}^{-3}$, N: Number of samples

4.1.2 Distribution Characteristic of Data Set

Fluctuations in the meteorological conditions and emission strength variations determines the distribution characteristics of aerosol composition over a time period. Frequency distributions of airborne pollutants are useful to understand processes influence the ambient levels of pollutants and to estimate the number of exceedance of a critical concentration level while developing control strategies (Lu and Fang, 2002).

During the transport of pollutants from source regions to receptor site, due to successive mixing and dilution pollutants results in a log-normal distribution of the ambient concentrations, even though the emission strength of sources are constant. As presented in Table 4.1 and Table 4.2, arithmetic mean values of species are greater than corresponding median values, this suggesting log-normal distribution of species (log-normal distributions of pollutants were also observed in numerous aerosol studies in our research group, some examples are Al-Momani et al. (1998); Güllü et al. 1998; Öztürk et al. (2012); Tokgöz, (2013); Yatin et al., (2000)). Since the concentrations of species right skewed as a result of very high concentrations, arithmetic mean of species concentrations are no longer representative for data population.

In this study, STATGRAPHICS Centurion (version 16.1) software was used test the goodness-of-fit of the data to log-normal distribution by applying the Kolmogorov-Smirnov (K-S DN) test. The Kolmogorov-Smirnov goodness-of-fit test measures the maximum distance between the cumulative distribution of the data and that of the fitted

distribution (STATGRAPHICS Centurion XVI User Manual, 2010). STATGRAPHICS test the null hypothesis that the selected specie comes from a lognormal distribution with a pre-defined confidence interval and displays a p-value. If the p-value is greater than the pre-defined confidence interval (null hypothesis is accepted), then the data can be assumed to have a log-normal distribution. In this study, a 95% confidence interval was chosen for the test and all species have p-value greater than 0.05 were assumed to have a log-normal distribution.

The Kolmogorov-Smirnov test was applied to elements in both fine and coarse fractions and calculated p-value and distribution type in each size fraction is given in Table 4.3. As can be seen from Table 4.3, that majority of elements followed a log-normal distribution with 95% confidence level. Frequency histograms of some selected elements, Fe, Pb, Mn, with log-normal distribution are given in Figure 4.1. The elements that did not follow log-normal distribution were again tested for other types of right skewed distributions with the Kolmogorov-Smirnov test. The Kolmogorov-Smirnov test showed that these elements followed Weibull, or log-logistic distributions with 95% confidence level. Some examples to other types of right skewed distributions are given in Figure 4.2. As can be seen from Figure 4.2, frequency histograms of K, Al and Na were also skewed right.

Since median values, which is insensitive to extreme values (Jones et al., 2008), represent right skewed distributed data sets better than arithmetic mean values, throughout the manuscript median values of elements are used.

Table 4.3 Distribution types of elements in the fine and coarse fraction

	Fine Fraction		Coarse Fraction	
	p-value	Distribution Type	p-value	Distribution Type
B.C.	0.004	log-logistic	0.040	log-logistic
Li	0.037	log-logistic	0.014	log-logistic
Be	0.548	log-normal	0.353	log-normal
Na	0.050	log-logistic	0.566	log-normal
Mg	0.711	log-normal	0.351	log-normal
Al	0.001	Weibull	0.540	log-normal
Si	0.021	log-logistic	0.483	log-normal
SO₄²⁻	0.029	log-logistic	0.832	log-normal
K	0.091	log-normal	0.838	log-normal
Ca	0.001	log-logistic	0.555	log-normal
Ti	0.036	Weibull	0.348	log-normal
V	0.010	log-logistic	0.526	log-normal
Cr	0.754	log-normal	0.379	log-normal
Mn	0.171	log-normal	0.665	log-normal
Fe	0.061	log-normal	0.700	log-normal
Co	0.004	Weibull	0.174	log-normal
Ni	0.082	log-normal	0.748	log-normal
Cu	0.417	log-normal	0.430	log-normal
Zn	0.000	Weibull	0.000	Weibull
Ge	0.058	log-normal	0.786	log-normal
As	0.003	log-logistic	0.088	log-normal
Se	0.006	Weibull	0.010	Weibull
Rb	0.452	log-normal	0.055	log-normal
Sr	0.453	log-normal	0.328	log-normal
Y	0.166	log-normal	0.046	Weibull
Zr	0.007	Weibull	0.188	log-normal
Ag	0.036	Weibull	0.561	log-normal
Cd	0.121	log-normal	0.670	log-normal
Sn	0.544	log-normal	0.546	log-normal
Sb	0.017	log-logistic	0.721	log-normal
Te	0.000	log-logistic	0.030	Weibull
Cs	0.004	log-logistic	0.016	log-logistic
La	0.163	log-normal	0.095	log-normal
Pr	0.226	log-normal	0.569	log-normal
Nd	0.174	log-normal	0.297	log-normal
Sm	0.560	log-normal	0.205	log-normal
Eu	0.105	log-normal	0.124	log-normal
Gd	0.436	log-normal	0.593	log-normal
Tb	0.284	log-normal	0.256	log-normal
Dy	0.135	log-normal	0.144	log-normal
Er	0.182	log-normal	0.427	log-normal
Tm	0.168	log-normal	0.074	log-normal

	Fine Fraction		Coarse Fraction	
	p-value	Distribution Type	p-value	Distribution Type
Yb	0.160	log-normal	0.917	log-normal
Lu	0.093	log-normal	0.296	log-normal
Hf	0.032	Weibull	0.382	log-normal
Ta	0.029	log-logistic	0.760	log-normal
Tl	0.013	log-logistic	0.921	log-normal
Pb	0.410	log-normal	0.908	log-normal
Bi	0.00	log-logistic	0.279	log-normal

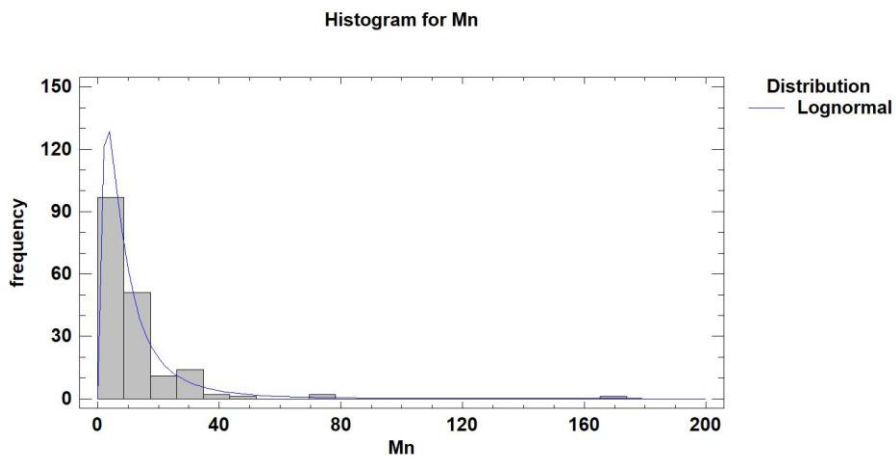
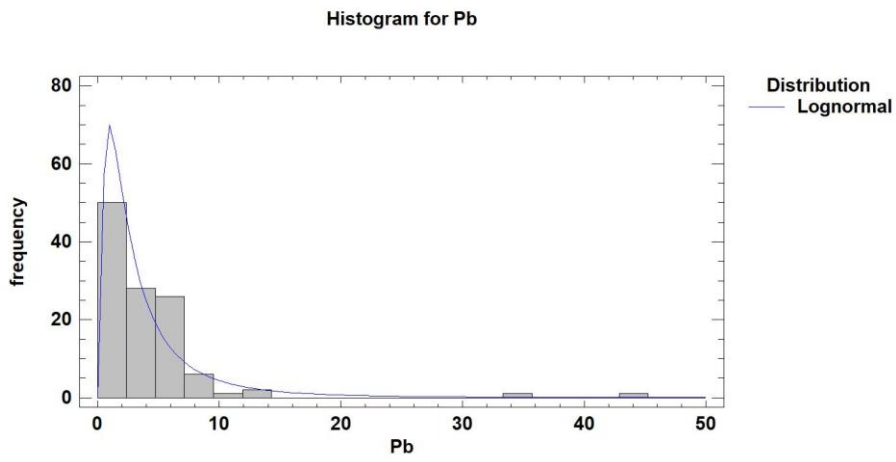
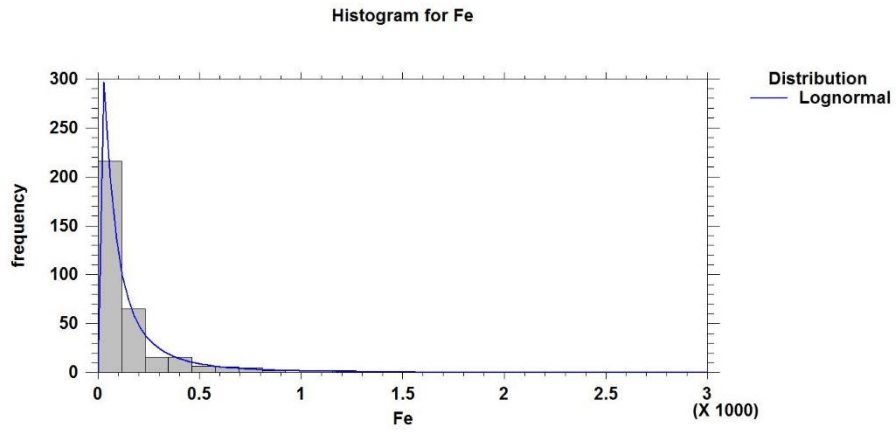


Figure 4.1 Log-normal distribution examples of selected elements

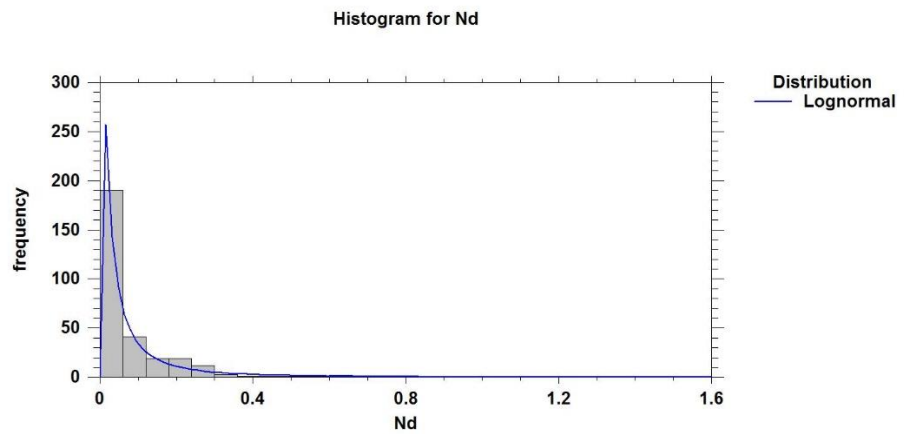
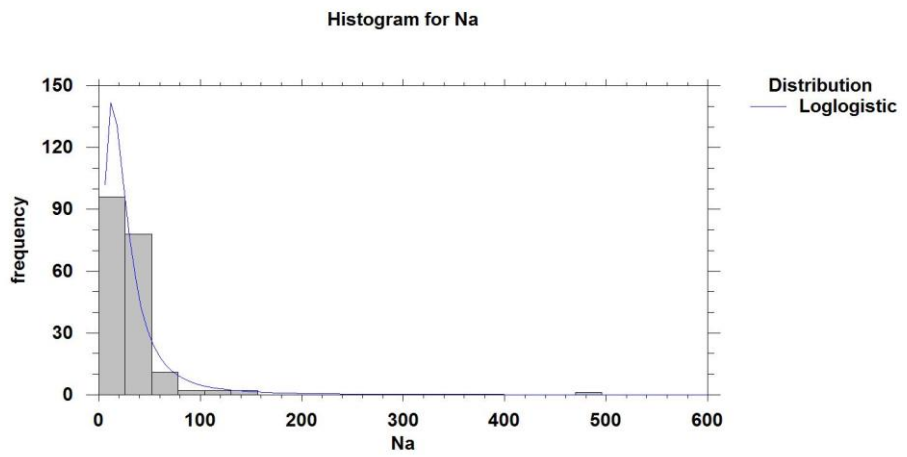
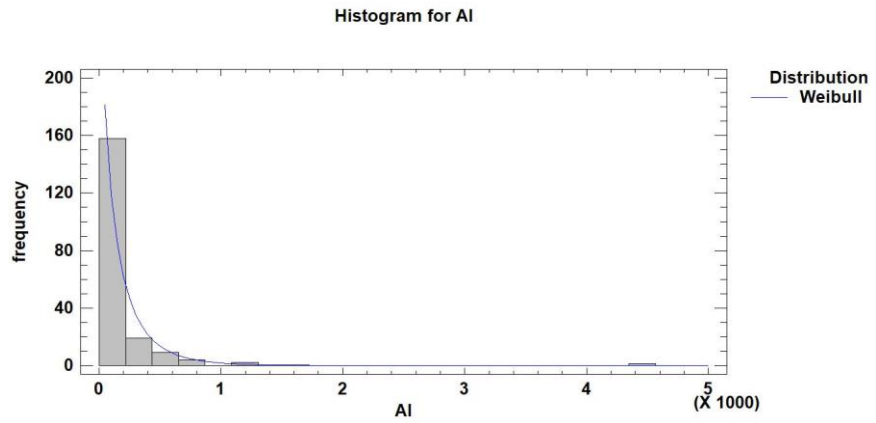


Figure 4.2 Right skewed distribution examples of selected elements

4.1.3 Coarse to fine concentration ratios of elements

The mass of trace elements occurs in different size fractions depending their source types. Elements that arises from soil, such as Al, Fe, and Si, and sea salt tracers Na and Mg have large aerodynamic diameters, whereas elements released from anthropogenic activities, such as S, As, Pb, and Cd, have relatively smaller aerodynamic diameters ($<2.5 \mu\text{m}$). Therefore, evaluating the coarse-to-fine concentration ratios (C/F) of trace elements gives preliminary information about their sources.

Coarse-to-fine ratios of trace elements at the Eastern Black Sea region is depicted in Figure 4.3. C/F ratios of elements were varied between 0.38 for SO_4^{2-} and 2.85 for Ca. As stated previously, 154 out of 352 coarse samples were analyzed for their elemental composition. Therefore, C/F ratios of elements were calculated with the corresponding fine fraction samples of the coarse fraction samples using the median concentrations. Please note that the fine fraction dataset for which the C/F ratio is discussed is smaller than the dataset provided in Section 4.1.1.

Crustal elements, Al, Fe, Si, and Ca, were mainly distributed in the coarse fraction of the aerosol. Their C/F ratios were greater than 1. This is an expected behavior for crustal elements since they are arisen from soil and other crustal materials (Almedia et al., 2005). C/F ratio of Na, a marine element, was greater than 1, which is similar to that observed in lithophilic elements. Please note that this does not mean Na is originating from soil. The C/F ratio of the Na would be >1 , even though there is no crustal contribution. Because, sea salt particles are also coarse.

In a large part of the anthropogenic elements, C/F ratio was less than 1, which was an expected behavior of anthropogenic elements as reported in previous studies (Barbaro, 2016; Çelik, 2014; Kuloğlu and Tuncel, 2005; Munzur, 2008). The exceptions to this pattern were Cu, Zn and Sn, their C/F ratios were 1.10, 1.55 and 2.58, respectively. Even though the C/F ratio of copper was close to unity, C/F ratios of Sn and Zn were high, and this indicated the masses of Sn and Zn were present in the coarse fraction at a certain level. Such high C/F ratios of anthropogenic species have been observed in

previous studies (Çelik, 2014; Kuloğlu and Tuncel, 2005; Munzur, 2008). This situation is thought to be substantially due to coagulation of fine particles containing these elements onto coarse particles.

Cr, Ni, Mn, K, V, Ti have mixed sources and their measured concentrations are accounted for both crustal and anthropogenic sources. C/F ratio of mixed origin elements is a good indicator of which source type is more likely to contributing. In case of anthropogenic sources are more dominant than crustal origin the C/F ratio will <1 , in contrary case the ratio will be >1 .

C/F ratios of these elements can be divided into two groups based on C/F ratios. First group is consisted of Ni and Cr, C/F ratios of these elements were 0.82 and 0.83, respectively. This indicates that the contribution of anthropogenic sources to Ni and Cr concentrations is more dominant in the Eastern Black Sea atmosphere.

Second group is consisted of Mn, K, V, and Ti. C/F ratios of these elements are >1 . In fact, this is a much more expected behavior of elements that have both crustal and anthropogenic sources. Coarse-to-fine ratios >1.0 for these elements indicate that the contribution of coarse crustal particles on their measured concentrations are more dominant than contributions of anthropogenic sources in Eastern Black Sea atmosphere.

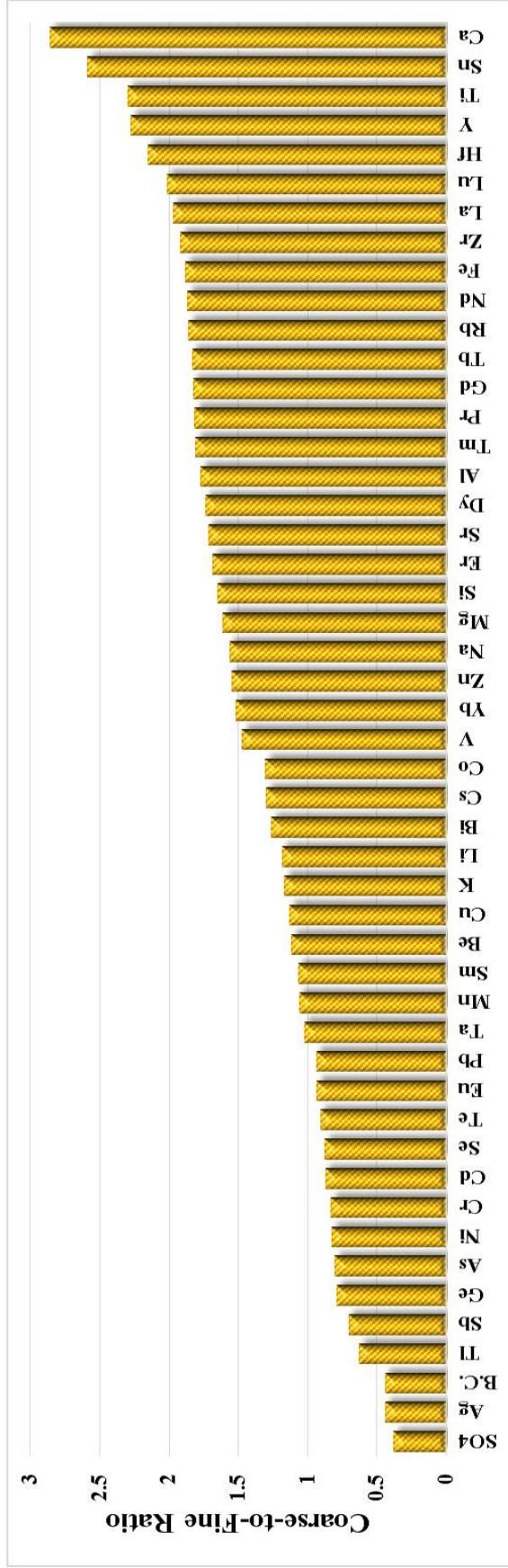


Figure 4.3 Coarse-to-fine median concentration ratios (C/F) of elements

4.2 Comparison with Literature

Comparison of observed concentrations of elements with earlier observations of trace elements reported from comparable sites is important in terms of assessing the extend of the pollution in a study area. Since the sampling station was located at a rural area, the literature data was also selected from rural sites. Comparison was done with studies conducted in the Mediterranean Sea basin and also other parts of the Turkey. The selected literature studies for the comparison are Antalya, Turkey (Öztürk et al., 2012), Kırklareli, Turkey (Tokgöz, 2013), Eastern Black Sea, Turkey (Hacısalihoğlu et al., 1992), Mersin, Turkey (Koçak et al, 2007a), Amasra, Turkey (Karakaş, 1999), Cyprus (Bari et al., 2009), Northern Greece (Samara et al., 2005), Ashdod, Israel (Mamane et al., 2008), Northwest Italy (Padoan et al., 2016), and Southeast Spain (Galindo et al., 2017).

Short description of literature studies used for comparison is given below:

1- Antalya, Turkey (Öztürk et al., 2012)

Concentrations of trace elements and major ions were measured in aerosol samples collected using a high volume PM₁₀ sampler at a rural site on the Mediterranean coast of Turkey, 20 km to the west of Antalya (30°34'30.54" E and 36°47'30.54"N), between 1993 and 2001. Trace element composition of the collected were determined with ED-XRF and ICP-MS; major ions were determined by using Ion Chromatography (IC).

2- Kırklareli, Turkey (Tokgöz, 2013)

Daily total suspended particulate matter samples were collected with a high volume sampler between April 2006 and March 2008 at a rural station, which is 5 km to Turkish-Bulgarian border (41° 57.996' N and 27° 23.670' E), at Kırklareli province. Collected samples were analyzed for 50+ trace element composition with ICP-MS, ions by IC and black carbon by Aethalometer.

3- Eastern Black Sea, Turkey (Hacısalihoğlu et al., 1992)

Daily particulate samples were collected using a high volume sampler on a ship that traveled from the West Black Sea to the East Black Sea in 1988. The total number of samples collected in the Black Sea was 19. Only five particulate samples were collected on Eastern Black Sea and the data generated from these samples are used in comparison. Particulate samples were analyzed for 36 element and ion by using Instrumental Neutron Activation Analysis (INAA), Atomic Absorption (AAS) and ion chromatography techniques.

4- Mersin, Turkey (Koçak et al, 2007a)

PM_{2.5} and PM_{2.5-10} samples were collected using a Gent-type PM₁₀ stacked filter unit at a rural site on the coast of the Eastern Mediterranean, Erdemli (36° 33' 54"N and 34° 15' 18"E), Turkey. 562 aerosol samples were collected during April 2001 and April 2002 with a 24 hr temporal resolution. Water-soluble ions were measured with IC and concentrations of trace elements measured with proton-induced X-ray emission (PIXE).

5- Amasra, Turkey (Karakaş et al, 2004)

Sampling station was implemented at a rural site on the Western Black Sea coast of Turkey. Station was at 20 km east of Amasra city and 3.5 km to Black Sea and 3.5 to Black Sea (41° 47 N' and 32° 29'E). Daily PM₁₀ sampling was done with a PM₁₀ high volume sampler between April 1995 and July 1997. Collected samples were analyzed with atomic adsorption spectrometry, instrumental neutron activation analysis, IC and UV/VIS spectrometry for about 46 elements and major ions.

6- Cyprus (Bari et al., 2009)

In the study, sampling was performed at three different characteristic sites (traffic, residential and rural) to identify the contribution of different sources to the PM₁₀

concentrations. For a valid comparison the rural site, which is also within the network of the Co-operative Programme for Monitoring and Evaluation of the Long-range Transmission of Air Pollutants (EMEP), near the Agia Marina village was selected. Daily PM₁₀ samples were collected using a gravimetric reference low volume sampler, LVS3, during November 2002 and August 2003. Twelve trace elements were analyzed by XRF, major ions by IC and two elements (Pb and Ni) by graphite furnace atomic absorption spectrometry.

7- Northern Greece (Samara et al., 2005)

A limited number of daily TSP samples, 3 samples per month, in total 35 samples, were collected with a high volume sampler at a rural Petrana station (40° 17' N' and 21° 52' E) on the Northern Greece between November 2000 and November 2001. TSP samples were analyzed for 27 trace elements by XRF. S concentration was converted to SO₄²⁻ for a valid comparison

8- Ashdod, Israel (Mamane et al., 2008)

The study was focused on the characterization of fine and coarse particles over a midsize industrial city Ashdod on the East Mediterranean coast. For this purpose, 2 sampling stations, an urban and a rural, were operated 3 weeks in November 2004 and July 2005. Coarse and fine fraction PM samples were collected with a dichotomous sampler. Collected samples were analyzed with XRF for 25 trace elements. For a valid comparison, observed concentrations of trace elements of PM₁₀ data at the rural sampling station was used. S concentration was converted to SO₄²⁻ for a valid comparison.

9- Northwest Italy (Padoan et al., 2016)

Daily PM₁₀ samples were collected in 2011 at five different sites on the Northwest Italy. Among these stations the rural Saliceto station was selected for the comparison. Twenty-eight PM₁₀ samples (one week in February, May, August and November) were

collected using a size selective low volume sampler at Saliceto station and were analyzed with a high resolution ICP-MS for 25 trace elements.

10- Southeast Spain (Galindo et al., 2017)

PM₁ and PM₁₀ samples were collected at Mt. Aitana (38°38'56.8"N 0°15'55.2"W; 1558 m above sea level) on the southeast coast of Spain for 18 months between March 2014 and September 2015. The PM₁₀ samples were collected using a high volume sampler with a 24 hr duration and three samples per week. Samples were analyzed for ions by IC, for trace elements by ED-XRF. Observed concentrations of trace elements of PM₁₀ data was used for the comparison.

Measured concentrations of trace elements in this study and selected studies are given in Table 4.4 and are also shown in Figure 4.4 for visual comparison. For comparison of observed concentrations of elements of this with those reported for other comparable sites, arithmetic mean values of elements were used in Table 4.4 and Figure 4.4, since most of the previous results were reported as arithmetic means. Both PM_{2.5} data and PM₁₀ data are used for comparison, since PM₁₀ was usually reported in previous studies. But, it should be kept in mind that PM₁₀ data was not as large as PM_{2.5} data, since a portion of coarse fraction samples were analyzed.

It should be noted that the concentrations are highly dependent on the distance between source and the sampling station. Another important factor affecting the comparability of different data sets is the year that the sampling performed. Particularly, the concentration of anthropogenic elements decreases over time due to taken measures. For this reason, it is necessary to consider the reduction in concentrations of pollutants over time, when comparing the results obtained in a study conducted 2013 with the results obtained in a study conducted in the beginning of 2000s or in a study conducted in the 1990s.

Table 4.4 Comparison of current study with the other studies in the literature (concentrations in ng m⁻³)

	This Study (PM _{2.5})	This Study (PM ₁₀)	Antalya Turkey	Kırklareli Turkey	Eastern Black Sea	Mersin Turkey	Amasra Turkey	Cyprus	Northern Greece	Ashdod Israel	Northwest Italy	Southeast Spain
Na	31.1	110	2241	550	3900	3430	380	1357				250
Mg	69.4	275.1	538	650		490	150	189	150		173	52
Al	179.5	724.3	661	920	330		320	471	340	270	123	
SO₄²⁻	1382.4	1848.6	7927	5800	4300	4950	4900	4554	1710	2850		1504
K	90.6	224.3	536	460	101	360	180	353	280	240	459	65
Ca	274.6	1340.2	1422	1600		1890	410	1784	5370	1330	735	413
Ti	8.8	27.4	32	67		27	32	108	44	34	19	20
V	0.6	1.4	3.17	3.8	1.8	8.7	2.7		3.3	5.5	3.2	4
Cr	11.4	22.2	6.77	33	8.3	5.7	1.3	6	8.2	1.7	3.2	
Mn	12	40.4	8.93	26	17	7.6	11	36	18	8.3	7.1	6
Fe	173	505.8	400	710	290	350	280	470	690	360	259	173
Ni	3.7	7.4	2.52	8.6	3	3.7	1.6	6	6.4	3.1	3.3	3
Cu	4.2	11.7		9.8			170	6	22	2.6	1.7	1
Zn	30.7	78.9	17	58	26	9.7	16	12	40.8	38	26.1	6
As	0.2	0.3	0.82	1	0.33		1.6		4.7		0.4	
Pb	4.1	12	52	32	37		17	26	9.7	18.5	6.2	1
			Öztürk et al., 2012	Tokgöz, 2013	Hacısalıhoğlu et al., 1992	Koçak et al., 2007a	Karakaş et al., 2004	Bari et al., 2009	Samara et al., 2005	Mamane et al., 2008	Padoan et al., 2016	Galindo et al., 2017

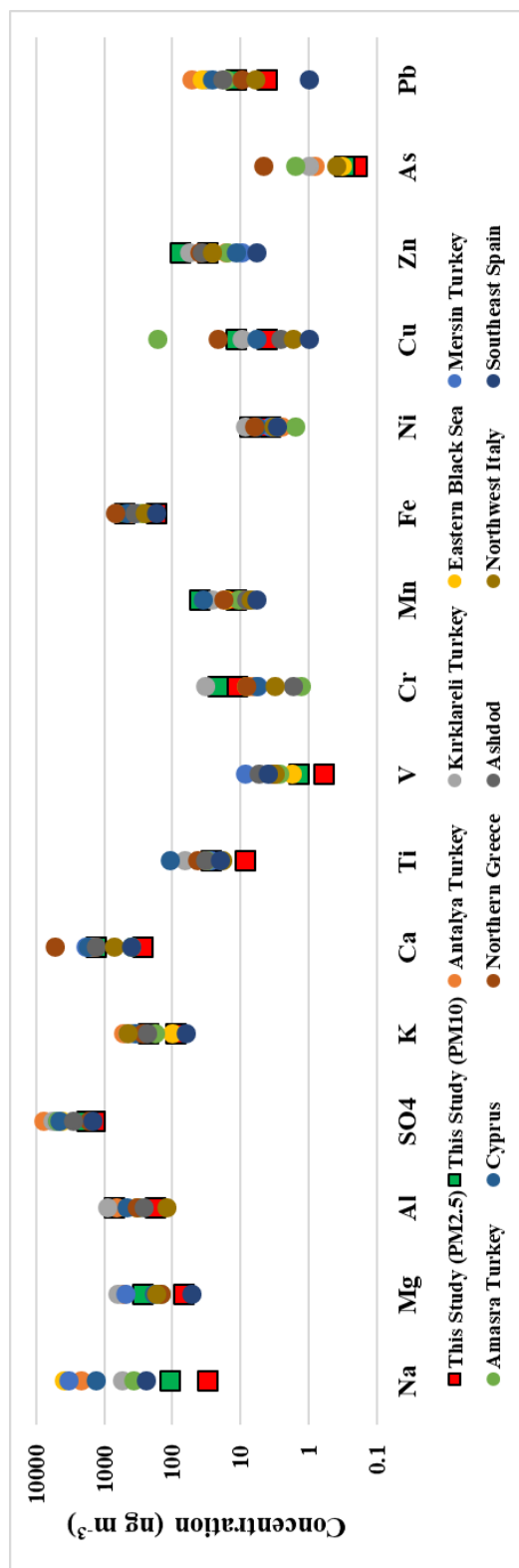


Figure 4.4 Comparison of current study with the other studies in the literature

The concentrations of a great majority of elements in the PM_{2.5} size fraction in this study, as expected, were lower compared to corresponding concentrations reported in other sampling sites. This is obviously due to partitioning of masses of trace elements into different size fractions. Since the masses of elements partitioned, their observed levels in the PM_{2.5} size fraction will be low compared the ones in PM₁₀ or TSP fractions.

Concentrations of soil-related elements, Mg, Al, K, Ca, and Fe, in this study are comparable with the ones reported in other sampling sites. It has been well document that the stations in the Mediterranean Sea basin are under the strong dust transport from North Africa (Gerasopolous et al., 2006; Koçak et al., 2007b; Mitsakou et al., 2008; Querol et al., 2009). Thus, elevated levels of soil-related elements are expected in the Mediterranean Sea basin than Black Sea basin. But, the Al concentration measured in this study is among the highest concentrations reported in other sampling sites. It is also interesting that the highest Al concentration is measured in Kırklareli station, another Black Sea station. However, this is due to the fact that TSP was collected in Kırklareli station. Transport form other arid regions that resulted in such high Al concentration in the sampling site is further investigated in the following sections of the manuscript. Other lithophilic elements are not significantly different than the reported concentrations at other sites.

Sodium, a sea salt marker, is fairly low compared to the reported levels in other sampling sites. Concentration of Na is heavily dependent on the distance between sampling site and coastline; the distance between the Torul sampling station and Black Sea coastline was approximately 75 km. Sea salt particles generated on the sea surface by bubble bursting. The particles generated by bubble bursting are coarse and they scavenged from atmosphere within few kms from coastline. Some of the sampling site selected for comparison was very close to the coastline or the samples were collected during a cruise of a ship. Therefore, the contribution of sea salt to the reported levels of Na was high at these sampling sites; highest at Eastern Black Sea study conducted by Hacısalıhoğlu et al. (1992), whereas the contribution of sea salt was low in this study. This difference is the main reason for such low levels of Na.

Concentrations of pollution-derived elements differ from one element to another. Concentrations of SO_4^{2-} , V, As and Pb are lower than the concentrations measured in the Mediterranean basin. Concentrations of anthropogenic species Cr, Mn, Ni and Zn measured in this study are higher than those measured concentrations at Mediterranean stations. The reason for the differences in concentrations of anthropogenic elements is that the concentration of these elements depends on whether there is a nearby source region at the sampling site or not. Since the only source of all lithophilic elements is dust, if one these elements is high, usually others are also high or if one is low, usually others are also low. But, this is not valid for anthropogenic elements since they are released from different sources. An interesting point is that the concentrations of elements such as Cr, Mn, Ni, Zn, which are among the highest when compared to other stations in Mediterranean basin, are all elements that originate from the metal industries. The most important iron and steel plants in Europe are shown in Figure 4.5.

World's largest metal industries are located to the north of the Black Sea, at Donetsk region on the east of Ukraine, and near Moscow, and at Ural Mountains. Also, other large iron and steel plants are located at Ereğli and Karabük on the Black Sea coast of Turkey and at Rustavi in Georgia. Obviously, the Donetsk region is the most important source region for Cr, Mn, Ni, and Zn because of its proximity to the sampling point and the size of the facilities at this region. A global emission inventory study by Pacyna and Pacyna (2001) was pointed that these regions are important resource regions for elements such as Cr, Mn. It was also concluded that these regions affect aerosol composition in the Black Sea (Hacısalıhoğlu et al., 1992; Dzubay et al 1984). Therefore, the concentration of elements such as Cr, Mn, Ni and Zn in the Eastern Black Sea region may be higher than the other regions in the Mediterranean, due to proximity of the source regions discussed above.

The comparison of two data sets generated at Eastern Black Sea in 2013 (this study) and in 1988 (Hacısalıhoğlu et al., 1992) has important implications in terms of change concentrations of pollutants over time. But, it should be noted that the data set generated by Hacısalıhoğlu et al. (1992) is based on analysis of only five particulate samples.

The measured concentrations of SO_4^{2-} and Pb in 2013 are lower than those levels in 1988. The most obvious reason for the different levels of SO_4^{2-} and Pb in this study and the study conducted by Hacısalıhoğlu et al. (1992) is the different times in which data sets were generated. The actions taken for SO_2 emissions at source regions decreased the regional SO_4^{2-} concentrations. Switching to unleaded fuel and installing catalytic converters to cars decreased the Pb concentrations. Concentrations of Cr, Mn, Ni and Zn, which are associated with iron and steel plants, measured in this study are higher than those levels reported by Hacısalıhoğlu et al. (1992). Important source regions around the Black Sea basin for these elements are discussed above and Hacısalıhoğlu et al. (1992) stated the influence of sources at these regions. Even though both data sets were generated on Eastern Black Sea, in the current study the samples were collected 75 km inland from the Black Sea and Hacısalıhoğlu et al. (1992) collected samples on a ship during its cruise hundreds of km away from the coastline. Therefore, the sources regions affecting the observed levels of Cr, Mn, Ni and Zn may not be same for both data sets. This is investigated in the following sections of the manuscript.



Figure 4.5 Distribution of iron and steel plants in Europe (URL1)

4.3 Flow Climatology

Flow climatology, a type of trajectory statistics method, has been widely used to characterize the source areas of pollutants (for example; Eneroth et al., 2003; Harris and Kahl, 1990; Moody et al., 2014). There are two important factors that determine the concentrations of pollutants at a receptor site. The first one is the origin of the air masses that arrive at the sampling point, and the second one is the frequency of flow of air masses from that location. Flow climatology provides information on these two factors. In other words, flow climatology provides an improved understanding of typical air-flow patterns and when combined with the measured concentrations of pollutants, it provides preliminary information on the possible locations of source regions of pollutants that contribute to the observed levels.

In this part of the manuscript, three different approaches were used for a better understanding of air-flow patterns in the Eastern Black Sea region. These approaches are residence time analysis, wind sector contributions, and cluster analysis. Back trajectories are used to calculate flow climatology of a region. Back trajectories are calculated for 3 different arrival height, 100m, 500m and 1500m, at the sampling station for whole sampling period March 2011 to December 2013. Since all the trajectories below the boundary layer will contribute to the observed levels of trace elements, a new group of trajectory called combined back trajectories is defined and it is defined as the combination of 100m, 500m and 1500m trajectories. The number of back trajectories calculated for the whole sampling period for each arrival height and combined back trajectories were 976 and 2928, respectively.

4.3.1 Residence Time Analysis

Residence time analysis is an approach that shows the spatial distribution of how much air masses spent time over a region as they travel to the region (Ashbaugh et al., 1985). The probability of pollution transport from a particular region increases as the residence time of air masses increases over a particular region, because air masses

spend enough time to pick up pollution. This does not apply to all cases, air masses will bring pollution in case of sources are present at that particular region.

In this approach, MapInfo software was used to calculate residence times of air masses. First, the study domain divided into $1^{\circ} \times 1^{\circ}$ grids. The study domain used in residence time analysis, shown in Figure 4.6, extends from west of UK (20°W) to Center of Asia (60°E) in North East direction and from Siberia (75°N) to middle of Africa (15°N). Then the segments of the back trajectories were assigned to grids according to their coordinates (longitude and latitude). Please note that segment is the hourly position of trajectory as longitude, latitude and height. The number segments in each grid cell were counted at MapInfo and each segment was color coded depending on number of segments assigned to it. This counting process was repeated for each arrival heights (100m, 500m and 1500m) and combined back trajectories. The maps generated for each arrival height and combined trajectories shown in Figure 4.7.

The residence time of air masses increase around the sampling point, since trajectories are intercepted at the station. However, the spatial distribution of residence time is not symmetrical around the station. The residence time values in the north-westerly direction are higher than those in the south at the same distance.

The patterns of residence times of air masses identical in all arrival height; they do not show much differences. Of course, as the arrival height increases, more remote regions starts to contribution to the residence time of air masses. In the calculations done with 100 and 500 m arrival height trajectories, air masses do not spend much time on France and Spain. The calculation done with 1500 m arrival height trajectories indicate that the air masses spend a little time on France and Spain too. That means, if the pollutants are transported from France and Spain to the station, this transport is occurred with the 1500 m arrival height trajectories.

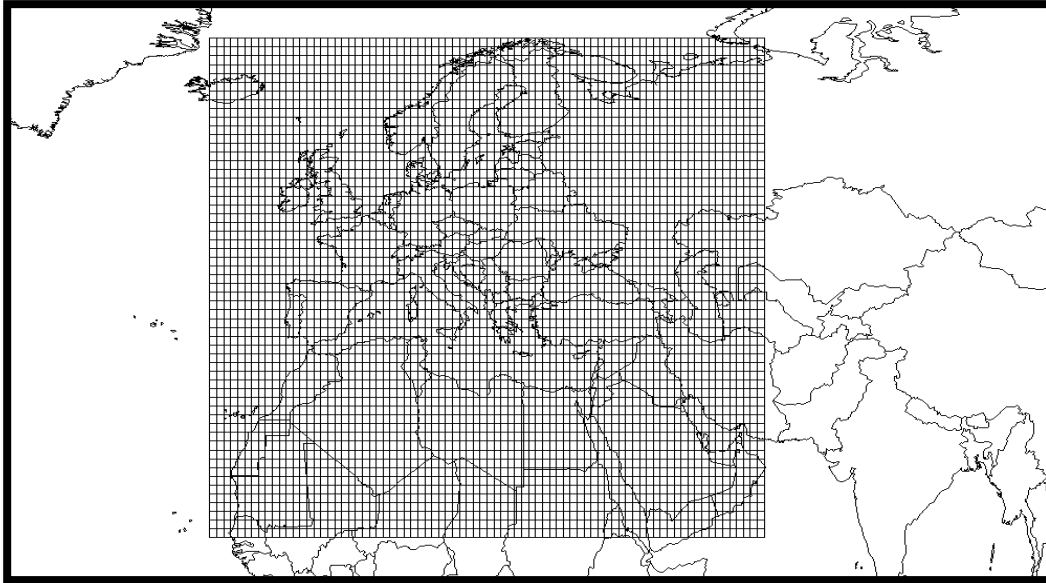


Figure 4.6 The study domain used in residence time analysis

Seasonal variations of residence times of air masses were also investigated. In order to do this, first the year was divided into two seasons as summer and winter. The division is based on the rainfall amount. Approximately 70% of the rainfall is recorded in winter season. Summer is the period between May and October, and winter is the rest of the year. Then the trajectories are assigned to seasons according to their arrival time at the station. The counting of segments was done for each season for each arrival height. For example, for a particular grid cell: 1st counting was done for segments of trajectories assigned to summer season, 2nd counting was done this time for segments of trajectories assigned to winter season. After the counting, the difference between the values of each season was calculated and the grid was color coded accordingly. If the value of the grid cell is positive, this means that the air masses reside more in summer season than winter season. If the value is negative, this means that trajectories spent more time in winter season in that grid.

The thematic maps created for summer and winter differences of residence time of each arrival height and combined trajectories are depicted in Figure 4.8. There are not very big variances among different arrival heights, patterns are identical. But, the maps depicted interesting summer and winter variations. There are systematic

differences in the summer and winter distributions of air masses. In summer, air masses spend more time in the north, east, and north-east of the station, while air masses spend more time in the south during the winter season. It is necessary to pay attention to one point here. The fact that air masses spend more time in the southern in the winter does not mean that the air masses come more frequent from south sector other sectors. For example, air masses spend less time in the southern sectors than in the northern sectors. This is the case for both winter and summer seasons. But, the air masses spend much higher time in the southern sector than in summer.

The observed difference between summer and winter means that the probability of pollutant transport from the north is higher in summer. Likewise, transport from countries like Georgia, Iran at the east should not be ignored, especially during the summer months.

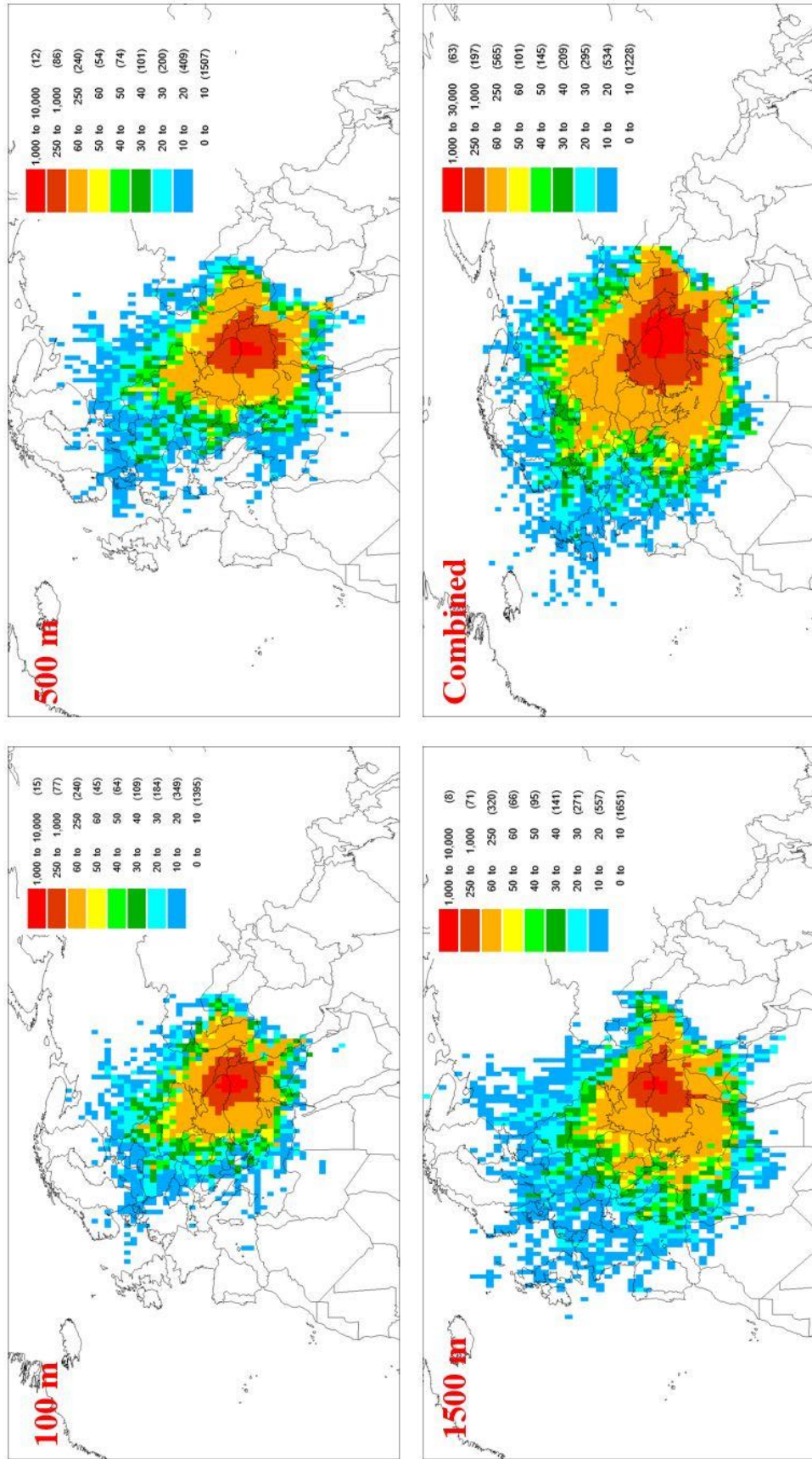


Figure 4.7 Residence time analysis for trajectories 100m, 500m, 1500m arrival heights and combined trajectories

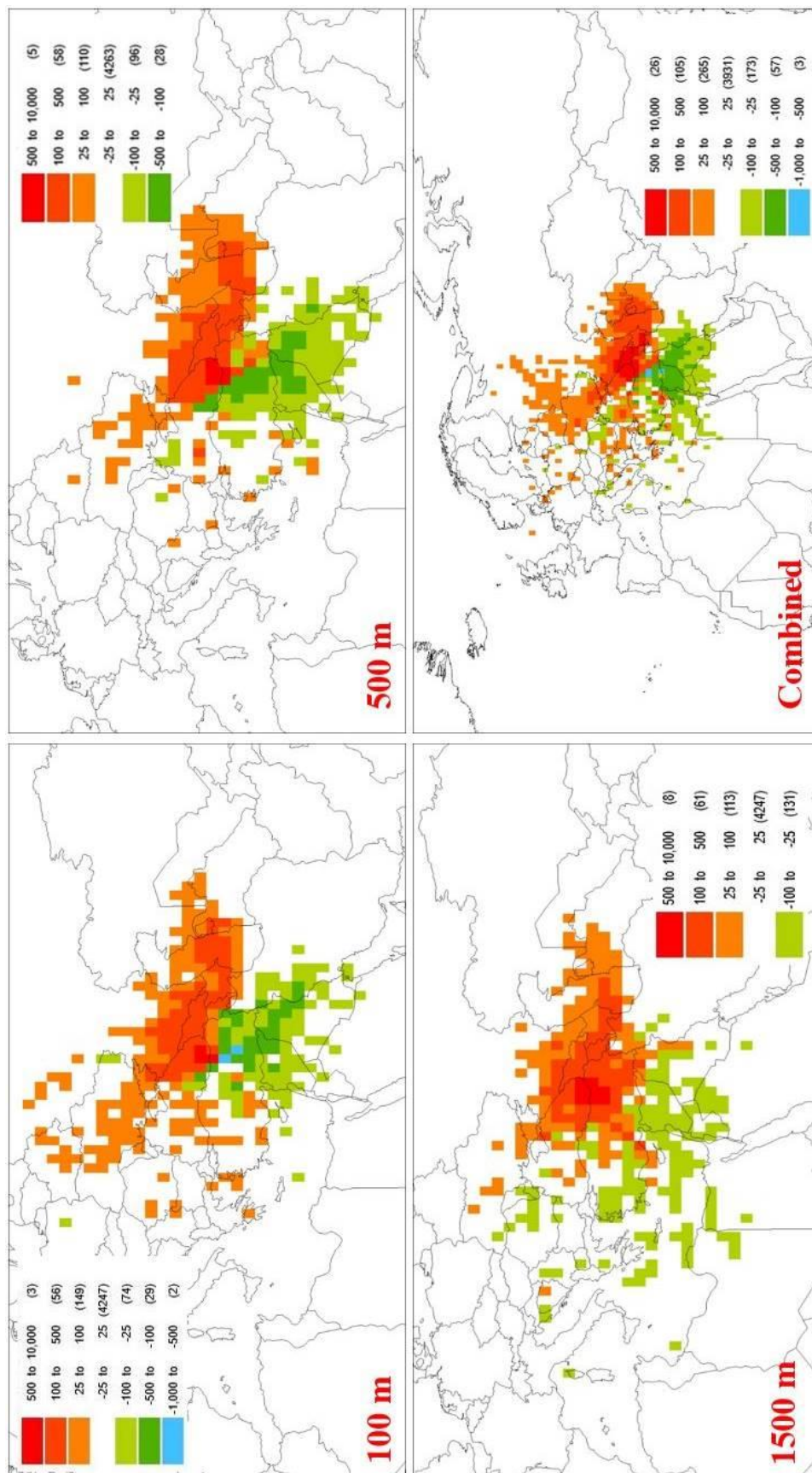


Figure 4.8 Differences between summer and winter residence times of air masses for 100m, 500m, 1500m arrival heights and combined back trajectories

4.3.2 Contribution of Wind Sectors to the Residence Time of Trajectories

In the previous section, the spatial distributions of residence times of air masses was shown. At this section of the manuscript, the contribution of wind sectors to the residence time of trajectories, which is a more conventional in the literature, were calculated and shown.

In order calculate percent contribution of each wind sector, MapInfo software was used, but the study domain used in the residence time analysis was divided into 8 wind sector as East (E), NE (Northeast), N (North), NW (Northwest), W (West), Southwest (SW), S (South), and SE (Southeast). The study domain used in the calculation of contribution of wind sector to the residence time is shown in Figure 4.9. Then, the segments in each wind sector were counted and divided by the total number segments for each arrival heights. This calculates the percent contribution of each wind sector to the residence time of trajectories.

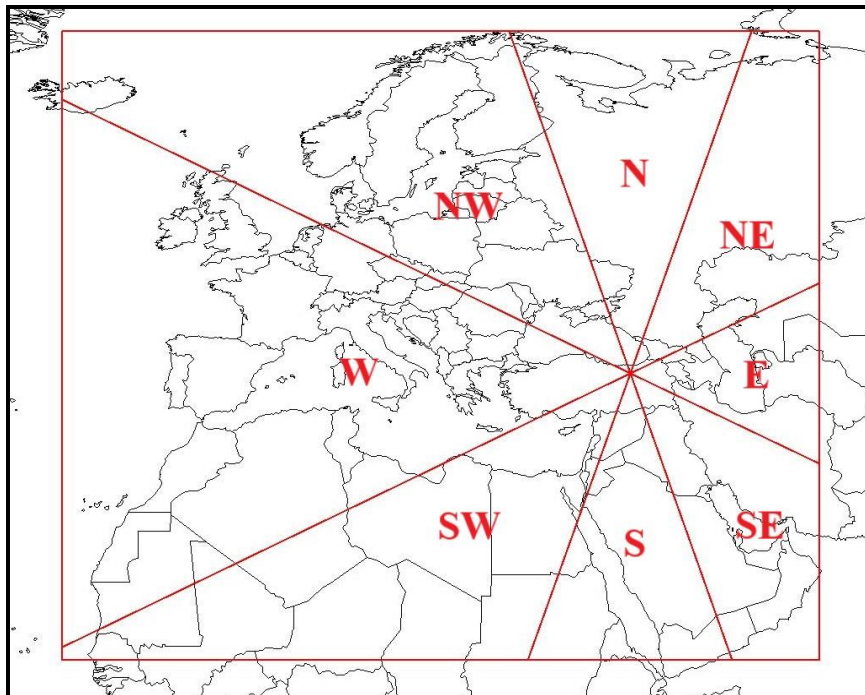


Figure 4.9 Study domain used in the calculation of contribution of wind sectors

Percent contribution of each wind sector to the residence time of back trajectories is given in Table 4.5 and as visual shown in Figure 4.10.

Table 4.5 Percent contribution of each wind sector for 100, 500, 1500 m arrival height back trajectories and combined back trajectories

Wind Sector	100m	500m	1500m	Combined
N	12.2%	10.7%	8.0%	10.2%
NE	10.4%	9.7%	5.9%	8.7%
E	14.7%	14.2%	10.0%	12.9%
SE	9.9%	8.8%	4.9%	7.9%
S	5.9%	5.6%	4.7%	5.4%
SW	8.9%	10.0%	14.0%	11.1%
W	14.9%	18.1%	32.2%	21.7%
NW	23.2%	22.9%	20.3%	22.2%

The distribution of trajectory segments in the different wind sectors for 100 m and 500 m arrival heights of are not different. However, when the distributions of the segments in the 1500 m arrival height are examined, differences were observed. The percentage contribution of the segments to the W sector at 1500 m arrival height was very high compared to ones at 100 m and 500 m arrival heights (1500 m 32%, 100 m 15% and 500 m 18%). In contrast, at 1500m arrival height the contribution of segments to the N, NE E, and SE sectors was less than those at other arrival heights. Air masses traveling from the W sector are thought to bring pollutants from Europe, therefore the role of trajectories with 1500m arrival height in this transport of pollutants will be higher than other arrival heights. The movement of air masses generally from the W and NW sectors points out that the sources in Ukraine and Russia. Taking into account the presence of large industrial facilities and non-effective emission controls in Ukraine, it is expected that the Eastern Black Sea region where the station located will be significantly affected by source areas in Ukraine. High contribution of anthropogenic content from these sectors was documented by Herut et al. (2001), Lelieveld et al. (2002), and Sciare et al. (2003) in the Mediterranean basin.

Seasonal variations of the contribution of wind sectors to the residence times of back trajectories were also investigated. In order to calculate seasonal variations, the procedure used in the residence time analysis was used, but this time the counting was done for wind sector. Figure 4.11 shows the summer and winter percent contribution of wind sector at different arrival heights.

Significant differences were observed on summer and winter contributions of wind sectors. The contribution of N, NE and E sectors were obviously high in the summer. On the other hand, SE, S, SW and W sectors of air masses were higher in the winter season. This pattern is same with the one previously observed at the seasonal variations of residence time analysis. This difference is an important feature of the region in terms of flow climatology and provides important information on possible pollutant transport. The pattern did not change much with the increasing arrival heights; it was same in 100m, 500m, and 1500m arrival heights.

Flow climatology calculated for the Eastern Black Sea region was compared with those calculated for other regions of the Black Sea and the Mediterranean region. The first one is this study's station at Torul. Second one Dereköy station (Tokgöz, 2013) at the Western Black Sea. Third one was Amasra station (Tuncer, unpublished data) approximately at the mid-point of Torul and Dereköy station on Black Sea coast. Last one was the Marmaris station (Tuncer, unpublished data), which represents the Mediterranean region. The comparison is shown in Figure 4.12.

Flow patterns in different regions of Turkey in general is not very different. At all stations residence times in W, NW, N and NE sectors are higher than other sectors. Again both the N and NE sectors are higher in summer, whereas S, SE, SW and W sectors are higher in winter. In other words, the flow pattern calculated for East Black Sea regions applies to all parts of Turkey.

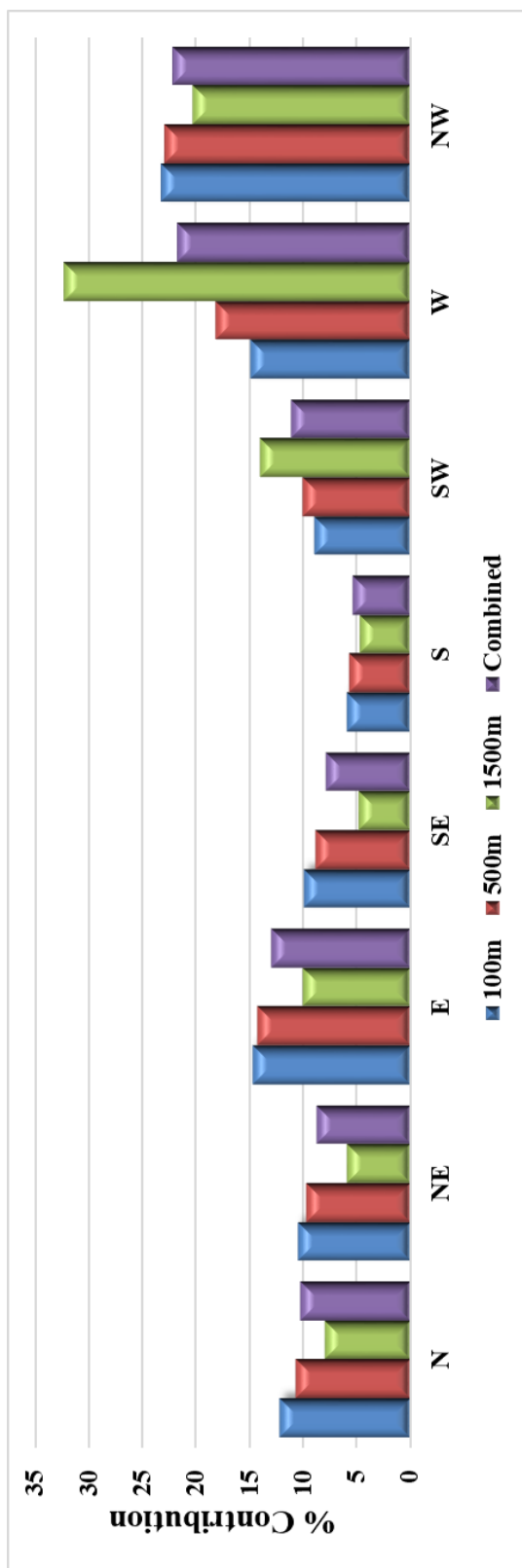


Figure 4.10 Percent contribution of wind sectors to residence time of trajectories arriving to the station

One point to note is that comparison was made on sector-by-sector basis taking only into account the directions relative to stations. It is not clear how the residence time of trajectories change as they move away from the station.

By taking into account transport of pollutants from the regions that the air spend more time is likely to occur, flow pattern similarities in different parts of Turkey do not mean that the same source regions affect the stations. For example, the air masses from the NW sector in the Torul station are very important because they will pick up emissions from the major industrial areas in Ukraine to the station. In contrast, the NW sector in Dereköy represents air masses from Bulgaria and Romania. Hence, the flow pattern similarities in different parts of Turkey does not mean the source regions are same for different parts of Turkey.

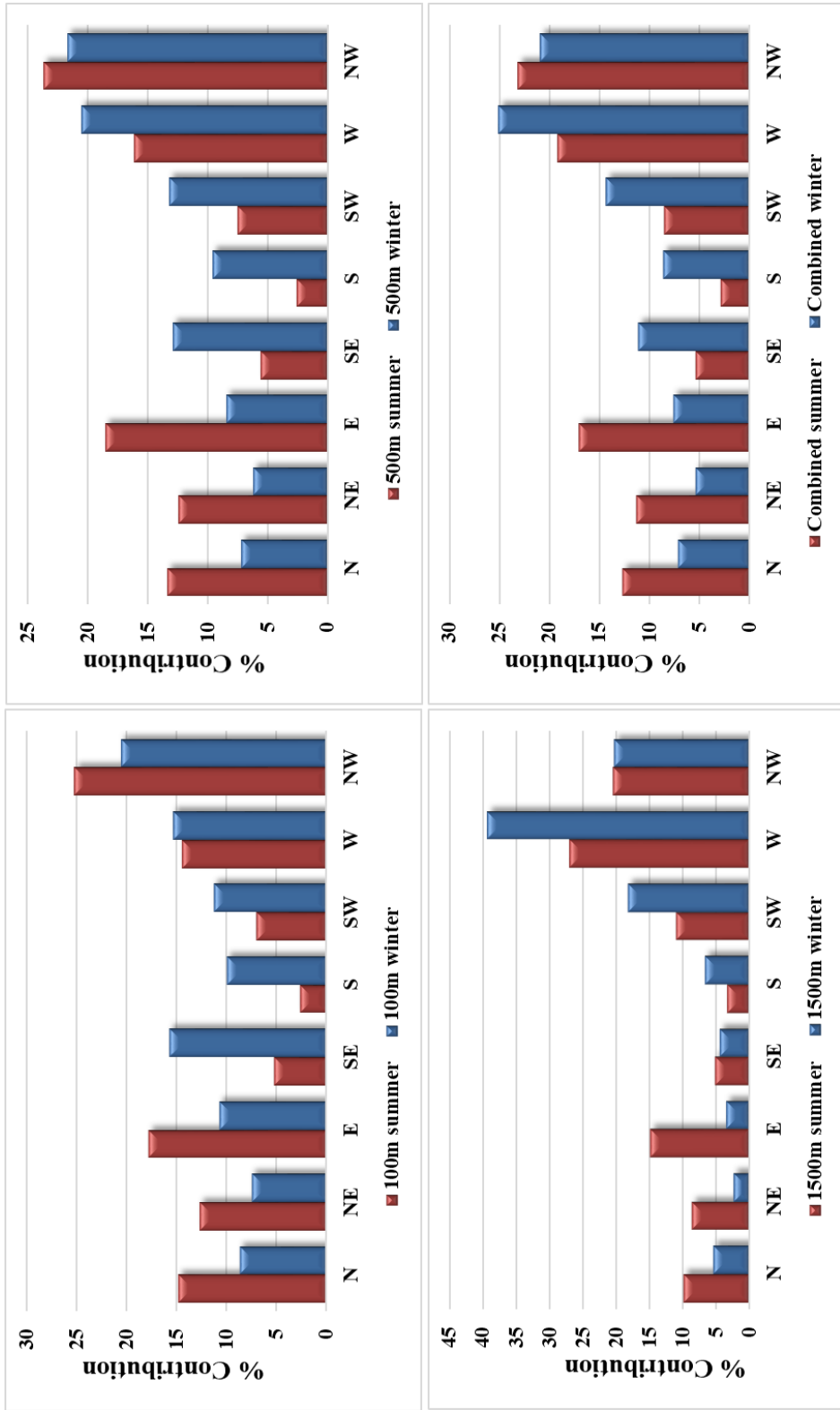


Figure 4.11 Seasonal variations of percent contributions of wind sectors

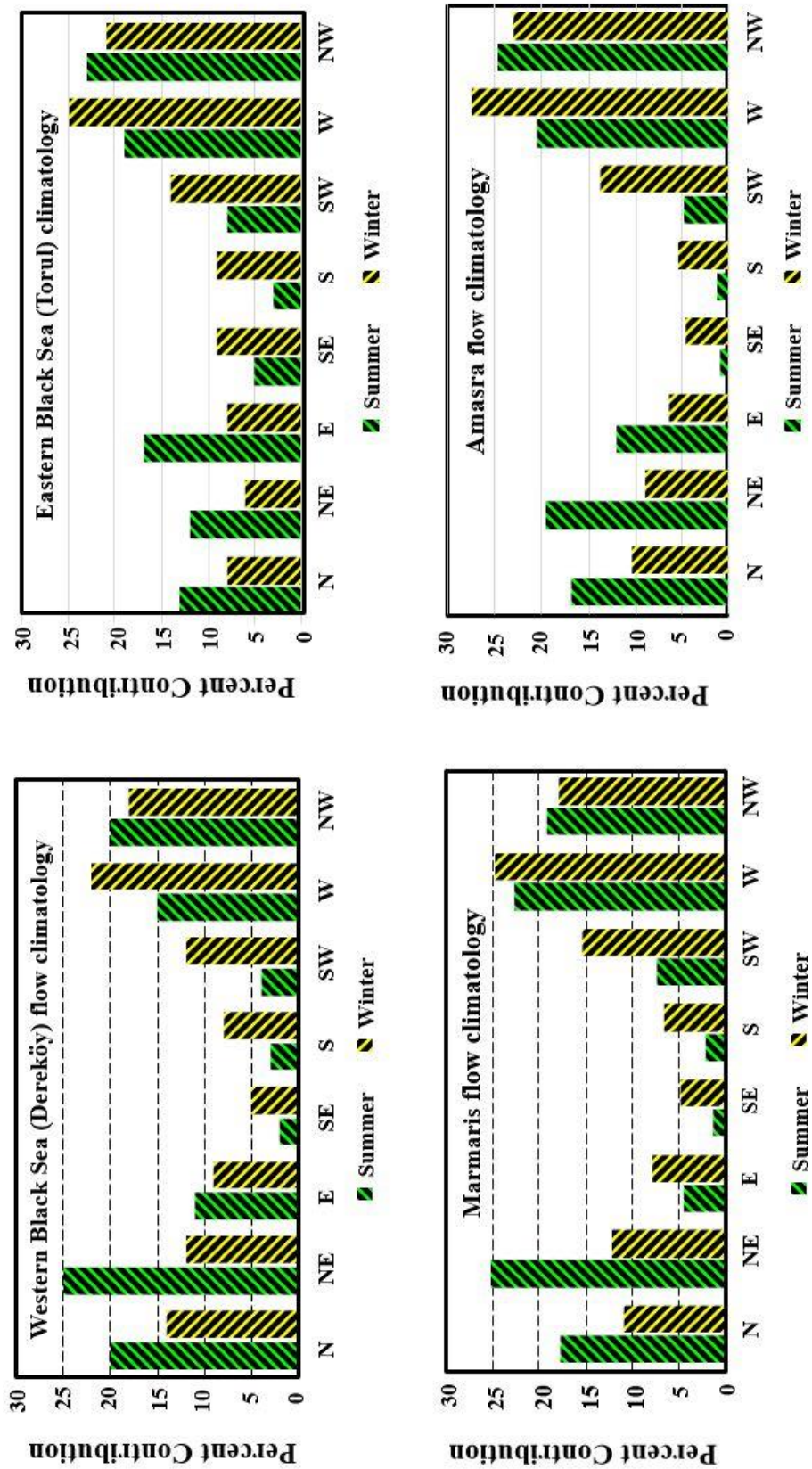


Figure 4.12 Comparison of seasonal contributions of wind sectors at different parts of Turkey

4.3.3 Cluster Analysis

In air pollution studies trajectories are examined with various techniques to understand the atmospheric transport patterns. Throughout the manuscript different techniques are used to examine trajectories. In this part, the efforts is to combine the air flow patterns and observed levels of species with the so-called technique Cluster Analysis to establish source-receptor relation. Wang et al. (2009) defined Cluster Analysis as a multivariate technique that combines the flow climatology and pollutant transport pathways with particle or gas measurements at a sampling station.

The first step of Cluster Analysis is to form cluster of trajectories which have similar length (transport speed) and curvature (direction) (Abdalmogith and Harrison, 2005). The generated clusters should be homogenous and distinctly different from each other. Different algorithms have been developed to form clusters; some examples are Brankov et al. (1998); Dorling et al. (1992); Harris and Kahl, (1990); and Sirois and Bottenheim, (1995).

In this study, TrajStat software was used to form clusters in Cluster Analysis. The software uses Ward's hierarchical method (Ward, 1963) to form clusters by combining the nearest trajectories. TrajStat uses Euclidean distance algorithm to define the distance between trajectories using latitude and longitude of the trajectories.

Determining the optimum number clusters that best describe the significantly different air-flow patterns in the study period is subjective. In order to overcome this, a two-step method was used. In the first step, a method developed by Brankov et al. (1998) was used to determine the optimum number of clusters. According to this method, different number of cluster calculated and percentage change in total root-mean-square deviation (TRMSD) is examined when decreasing number of clusters, for example 20 clusters to 19 clusters. The authors concluded that 5% change in TRMSD was significantly large to have a manageable number of clusters.

Since all the 100m, 500m, and 1500m arrival height back trajectories will contribute to the observed levels of trace elements, different number of clusters for combined back trajectories were calculated. Starting from 20 clusters the number of clusters were decreased by merging the two clusters according to their coordinates. This process was continued until 3 clusters. In each decrease percentage change in total root-mean-square deviation was calculated. Percentage change in TRMSD against the number of clusters plot is show in Figure 4.13. Five percent change in TMRSD was also used as a threshold value in this study.

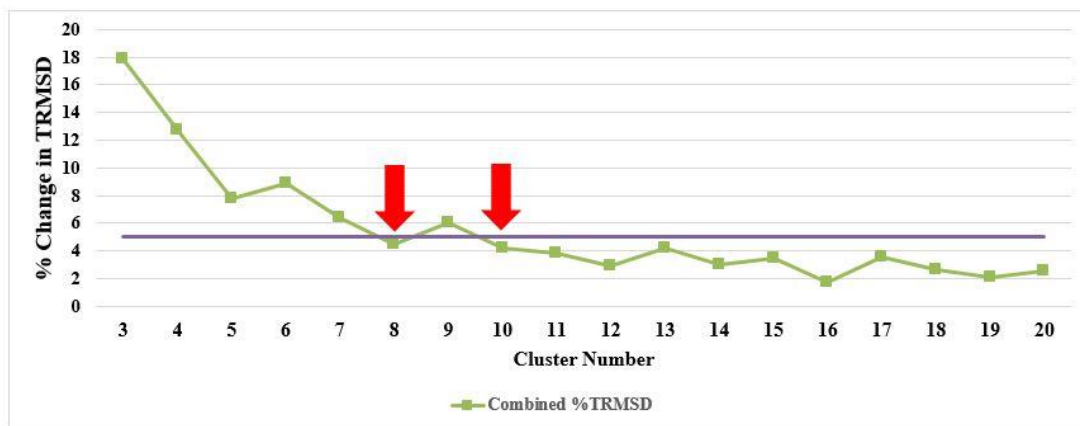


Figure 4.13 Selection of optimum number of clusters for combined trajectories

Percent change in TMRSD exceeds 5% threshold value at 9 and 7 cluster. Therefore, merging clusters should be stopped at 10 or 8. Since two different number of clusters suggested by the methodology developed by Brankov et al. (1998), a second method, which was the visual inspection of cluster, was used. In this method, starting from a number, the number of clusters are increased. The criteria used in visual inspection method is when the number of clusters increased, it should not split an existing cluster into two that has same speed and curvature. Starting from 3 clusters, the number of clusters was increased to 20 and each of them visually inspected. It was seen that after 8 cluster every new cluster split an existing into two and did not add much information to the existing ones. Therefore, the optimum number of clusters was determined as 8 that best describes significantly different air-flow patterns in the Eastern Black Sea region.

Cluster centroids calculated by TrajStat for each cluster are given in Figure 4.14. Cluster centroid is the center of mass of all of the trajectories of each cluster. The centroid can be considered as the average of the elements (coordinates and speed) of trajectories in that particular cluster. The number of trajectories assigned to cluster and there are given in Table 4.6.

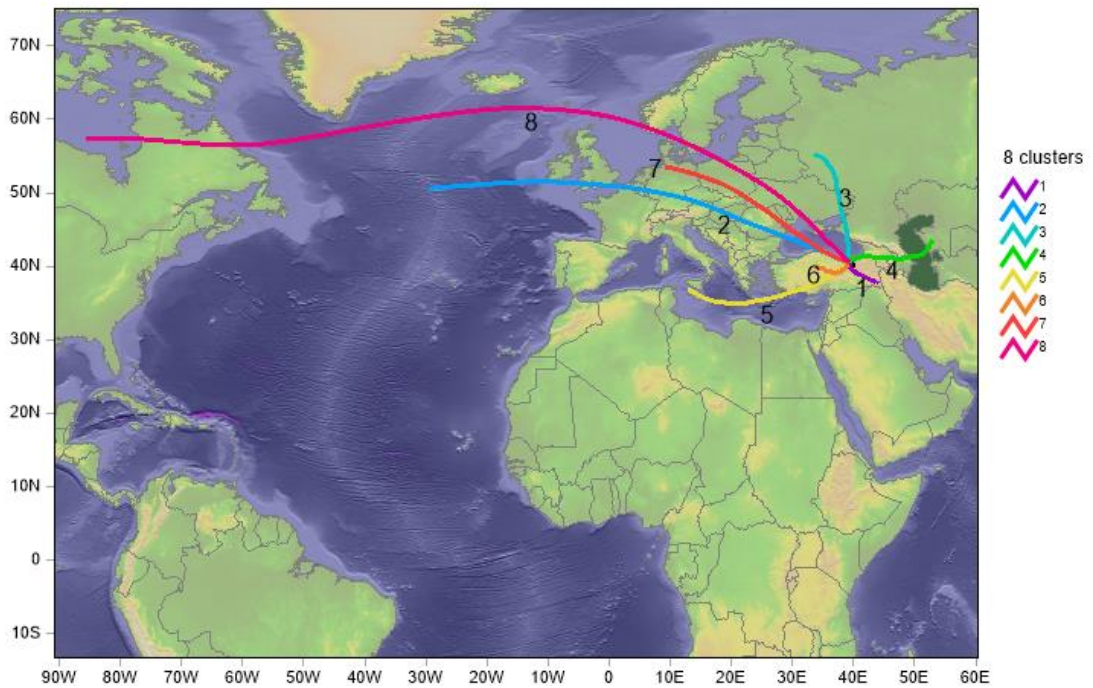


Figure 4.14 Cluster centroids of clusters calculated for combined trajectories

There were two local trajectory groups (6 and 1). There was a trajectory cluster from the south (5). There were four trajectory clusters from West, Northwest, and North (2, 3, 7 and 8). There was also a trajectory cluster from the East (4).

The directional distributions and length (speed) of cluster have very interesting implications. 1 and 6, the shortest length clusters, are expected to transport airborne pollutants to the station from the local sources in the region. However, since there are not too many local sources in the region, it is difficult to predict how much these two

short-length clusters would carry the airborne pollutants to the station. But, the next section which discusses the variation of elemental concentrations among the clusters will show that the air movements, especially, in the cluster 1 carry the anthropogenic origin of the particles to the station. Cluster 1 and 6 accounts for the majority of trajectories. In total 1071 trajectories were calculated at different arrival heights. These southerly Clusters accounted for 522 trajectories (approximately 49% of all trajectories). Therefore, Cluster 1 and 6 play a very significant role in the aerosol composition in the region, because air masses spend half of their time over the regions that the Cluster 1 and 6 cover.

Table 4.6 Number and percentage of trajectories allocated in each cluster

Cluster	Trajectory Number	Ratio
1	263	24.60%
2	44	4.10%
3	74	6.90%
4	176	16.40%
5	136	12.70%
6	259	24.20%
7	104	9.70%
8	15	1.40%

Cluster 1 has another point to note. Previously when the dust transport to the Turkey was mentioned, only the transport of well known “Saharan dust” from North Africa came to mind. However, the importance of the dust transports from the Arabian Peninsula and from the Middle East have been increasing in recent years. This transport have been probably important in the past, but there were not any sampling stations in Eastern and Southeastern Anatolia. Now, we can identify the dust transport from the Arabian Peninsula and the Middle East much more easily and certainly with the help of samplings all around the Anatolia. Cluster 1 contains trajectories that bring the dust from these areas to Torul.

Cluster 5 contains another trajectory group from the south. This cluster accounts for 136 trajectories, this is approximately 13% of all trajectories. Since the cluster centroid

is close to Africa, a considerable part of the trajectory in this group will spend time over Africa. In case of a transport from Sahara, the trajectories in Cluster 5 will bring the dust to Torul.

Another cluster that is considered as interesting is Cluster 4. This cluster contains trajectories from the east. The movement of air masses from the east usually is not the case in the region. Therefore, our knowledge on particles transported from east and their compositions is very limited. The trajectories in Cluster 4 are important because they may provide information which will improve our limited knowledge. Cluster 4 accounts for 176 trajectories. This is 16% of the total trajectories.

The remaining four clusters (2, 3, 7, and 8) contain trajectories arriving to the station from the West and Northwest. The total number of trajectories in these four clusters are 237, which is 22% of the total trajectories. The trajectories associated to these clusters are expected to carry pollutants to the region as they cross over industrial zones in Eastern and Western Europe and arrive to the station. However, the fact that the mentioned industrial zones are far from the sampling station poses question marks on at what portion the pollutants transported from these zone will be effective on the levels of pollutants in the Eastern Black Sea region. Among these clusters, Cluster 8 has the fastest air movement, hence fetch from Canada and Atlantic. Transport of organic and inorganic forest fire emissions from Canada to Europe has been investigated in recent years (Forster et al., 2001; Müller et al., 2005; Trickl et al., 2015). Even though Cluster 8 contains a few trajectories (15), their chemical composition should be examined carefully.

Cluster centroids along with the associated trajectories are given in Figure 4.15. It can be concluded that trajectories in Cluster 1 may bring crustal particles from arid regions at Southern Turkey; trajectories in Cluster 5 may bring Saharan dust to the station; the 8th cluster is the only group that may bring transoceanic pollutants, even with a small number of trajectories; Cluster 4 could provide information about sources located east of Turkey which we have limited knowledge so far.

Another point worth mentioning is that the trajectories in Cluster 3 has the potential to bring pollutants to the east of Ukraine, an important industrial source zone in the region.

The second step of the cluster analysis is the relation of measured concentrations of species with clusters. Variation of concentrations of species among the clusters can be very informative as it provides clues about potential sources areas. The PM_{2.5} fraction median concentrations of the elements in each cluster are provided in Table 4.7. The median concentrations of elements was tested with Kruskal Wallis (K-W) test using STATGRAPHICS Centurion (version 16.1) software to check whether there was a significant differences on median concentrations of element in different clusters. Kruskal Wallis test tests the null hypothesis that the medians are all equal with a 95% confidence interval and displays a p-value. If the p-value is less than 0.05 (null hypothesis is rejected), there is a statistically significant difference amongst the medians at the 95.0% confidence level. The p-value of each element is also provided in Table 4.7. At least one of the median concentrations of all elements in Table 4.7 were significantly different than other with few exceptions. Only median concentrations of Co, Cu, Ge, Sr, Sm, Eu, Hf did not show significant differences between clusters.

The median concentrations of some element groups in the clusters are also shown in Figure 4.16 for crustal elements, in Figure 4.17 for pollution derived elements and in Figure 4.18 for mixed origin elements.

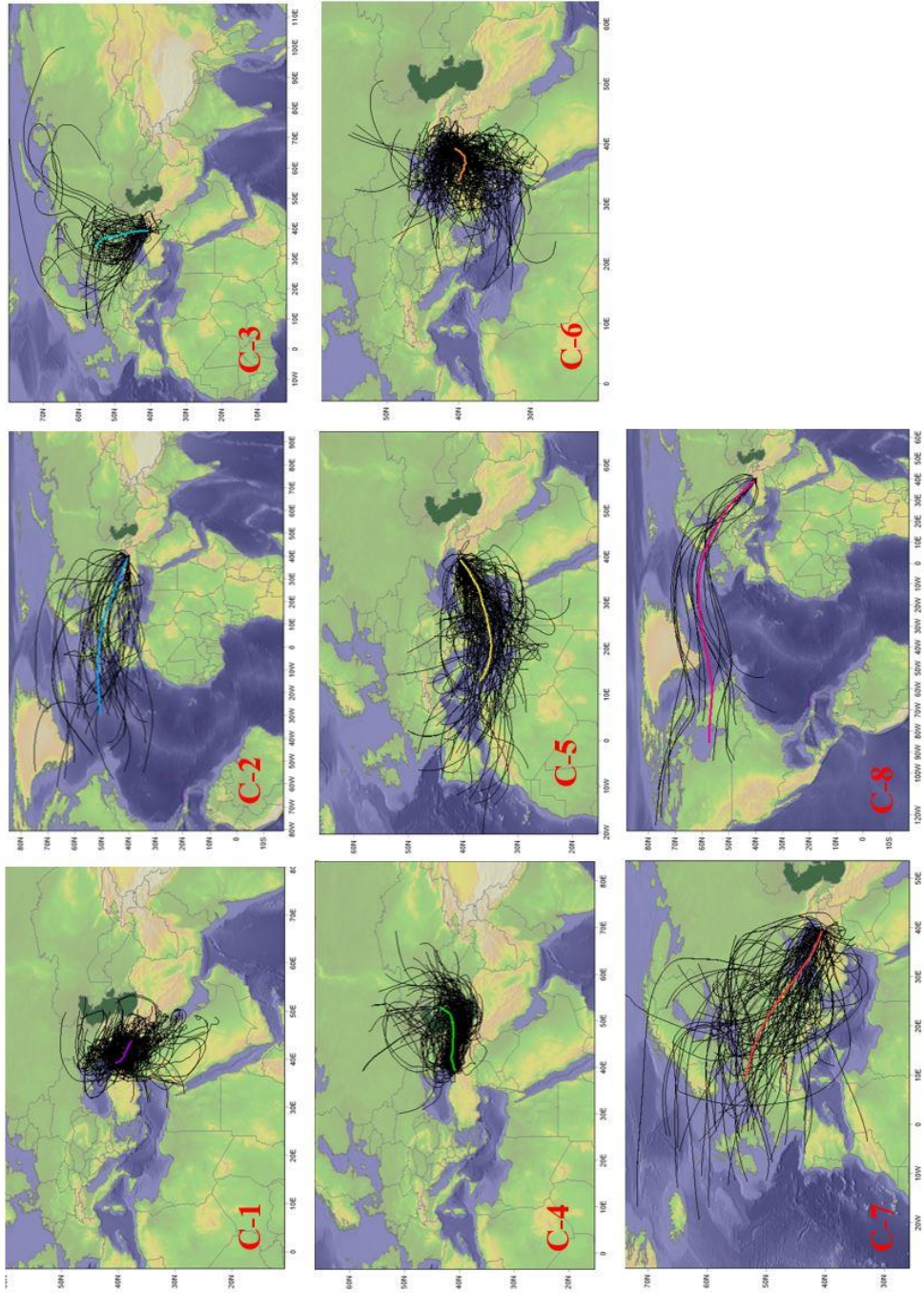


Figure 4.15 Trajectories allocated to different clusters

Table 4.7 Median concentrations of measured species (ng m⁻³) and K-W test p-values

	Cluster 1	Cluster 2	Cluster 3	Cluster 4	Cluster 5	Cluster 6	Cluster 7	Cluster 8	p-value
PM _{2.5} *	7.4445	5.3889	7.5800	9.1633	7.5500	6.6984	6.8007	5.1300	7.76E-08
BC	169.8000	163.9518	150.2115	251.9000	251.2000	166.0500	172.0626	437.0000	0.008
Li	0.1752	0.2474	0.1924	0.2893	0.2043	0.2603	0.1745	0.0387	0.01715
Be	0.0179	0.0180	0.0112	0.0174	0.0113	0.0192	0.0264	0.0331	0.02701
Na	22.3225	23.5135	33.7501	26.6292	27.7419	19.0064	27.3532	50.4877	0.01006
Mg	50.3991	24.6184	15.6113	35.6897	63.6276	41.9036	21.7434	14.1245	1.02E-12
Al	139.7008	67.8693	110.3405	114.1887	167.1729	100.1431	66.7678	31.2172	9.2E-05
Si	345.6034	245.9574	176.5171	308.1116	398.0848	268.6144	159.0478	96.4283	0.00033
SO ₄	1004.4021	777.5022	1288.7244	1499.3595	782.6406	762.6111	951.5094	724.4733	2.86E-11
K	81.7552	48.2749	68.6491	81.7852	74.0047	61.2545	46.4375	91.3001	0.00105
Ca	156.5334	122.2541	103.0701	146.8015	231.9480	159.4938	130.0395	60.8844	0.00063
Ti	6.3551	2.4235	2.7689	4.5798	5.7151	4.6227	2.9746	2.9746	0.0004
V	0.4062	0.2369	0.2711	0.4555	0.3263	0.2549	0.2204	0.2294	1.39E-09
Cr	9.4139	8.7130	7.6607	5.3101	9.5246	6.4462	7.1753	8.6031	0.00039
Mn	8.5487	5.0825	9.3328	8.8859	7.2641	6.6170	10.6650	4.1911	0.01604
Fe	98.2023	74.0372	85.1627	81.9343	89.4804	77.5887	70.2805	93.9179	0.0352
Co	1.1783	1.1402	3.2406	2.0843	0.3146	4.3791	0.7569	4.6630	0.07229
Ni	1.7913	1.4007	2.7903	1.6784	2.4927	1.9773	2.6886		0.04788
Cu	1.3557	1.5148	1.1232	1.4658	2.2340	1.9973	2.0704	4.2998	0.06691
Zn	27.8399	26.0332	28.6592	24.7705	27.7938	23.7359	28.9309	36.4584	0.0027
Ge	0.0173	0.0171	0.0142	0.0175	0.0120	0.0123	0.0108	0.0127	0.47471
As	0.2127	0.1309	0.1820	0.2181	0.1573	0.1606	0.2043	0.1973	0.0023
Se	0.3957	0.5055	0.5316	0.5204	0.4155	0.5022	0.4311	0.5972	0.00118
Rb	0.1746	0.2230	0.1157	0.1158	0.2551	0.0897	0.1556	0.0538	0.02249

	Cluster 1	Cluster 2	Cluster 3	Cluster 4	Cluster 5	Cluster 6	Cluster 7	Cluster 8	p-value
Sr	1.1236	1.3274	2.4336	0.7031	1.4212	1.1522	1.4212	1.1069	0.07622
Y	0.0380	0.0157	0.0195	0.0193	0.0572	0.0232	0.0169	0.0012	8.26E-07
Zr	0.7652	3.1348	2.2993	1.7715	0.7167	1.8504	2.1669	1.7288	0.01821
Ag	0.3139	0.2048	0.2582	0.3807	0.3640	0.3040	0.2208	0.3484	0.02536
Cd	0.1213	0.1179	0.2145	0.2611	0.1276	0.1618	0.1266	0.0483	1.1E-05
Sn	0.3556	0.2634	0.2239	0.2044	0.1785	0.2330	0.1862	1.6404	0.0027
Sb	0.0924	0.0962	0.0899	0.1221	0.0752	0.0777	0.0970	0.0548	0.00144
Te	0.0474	0.0440	0.0605	0.0429	0.0400	0.0387	0.0481	0.0228	0.0017
Cs	0.0156	0.0125	0.0208	0.0167	0.0138	0.0119	0.0152	0.0161	0.00075
La	0.1139	0.1084	0.0399	0.0471	0.1501	0.0632	0.0474	0.2592	1.2E-06
Pr	0.0138	0.0094	0.0052	0.0069	0.0154	0.0098	0.0051	0.0045	6.91E-07
Nd	0.0504	0.0219	0.0196	0.0374	0.0594	0.0360	0.0226	0.0047	2.3E-05
Sm	0.0176	0.0166	0.0171	0.0127	0.0206	0.0174	0.0177	0.0129	0.73967
Eu	0.0077	0.0178	0.0099	0.0106	0.0092	0.0172	0.0107	0.0130	0.22448
Gd	0.0110	0.0094	0.0083	0.0068	0.0130	0.0076	0.0087	0.0087	0.00072
Tb	0.0015	0.0016	0.0010	0.0008	0.0024	0.0012	0.0016	0.0022	0.0001
Dy	0.0088	0.0100	0.0041	0.0051	0.0078	0.0053	0.0064	0.0078	0.00031
Er	0.0067	0.0027	0.0021	0.0027	0.0071	0.0028	0.0067	0.0022	0.00024
Tm	0.0009	0.0005	0.0005	0.0006	0.0010	0.0006	0.0004	0.0010	0.003
Yb	0.0035	0.0034	0.0034	0.0021	0.0050	0.0033	0.0044	0.0017	0.00607
Lu	0.0005	0.0008	0.0009	0.0006	0.0011	0.0007	0.0003	0.0008	0.00625
Hf	0.0201	0.0885	0.0518	0.0180	0.0274	0.0415	0.0384	0.0593	0.05512
Ta	0.0090	0.0061	0.0093	0.0076	0.0080	0.0058	0.0071	0.0136	0.00016
Tl	0.0087	0.0059	0.0096	0.0091	0.0071	0.0055	0.0079	0.0065	4.4E-05
Pb	2.4354	1.6647	5.6857	3.3653	2.1602	2.1748	4.4554		0.00011
Bi	0.0175	0.0152	0.0177	0.0220	0.0112	0.0142	0.0172	0.0293	1.88E-08

* $\mu\text{g m}^{-3}$

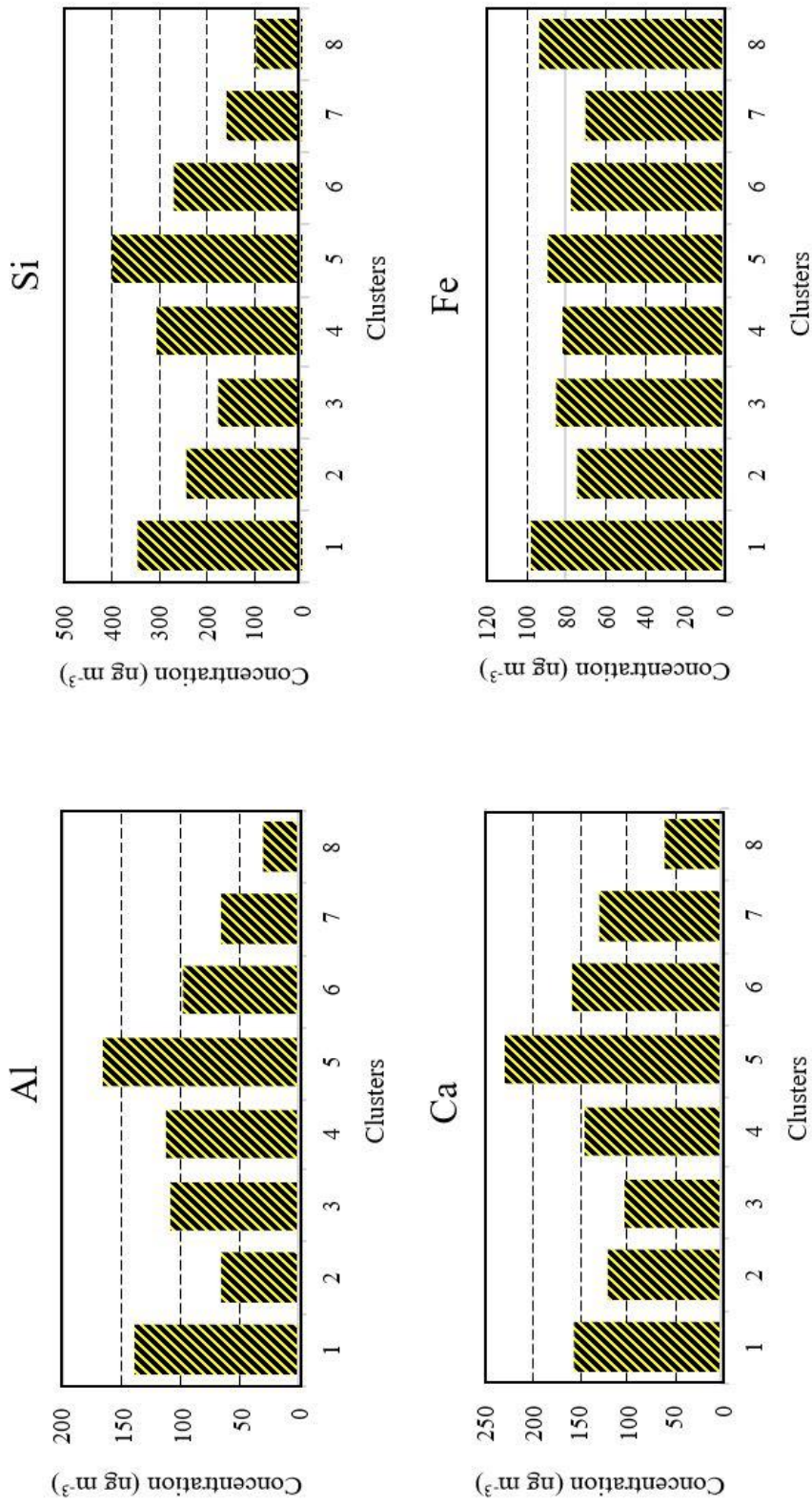


Figure 4.16 Cluster median concentrations of selected crustal elements

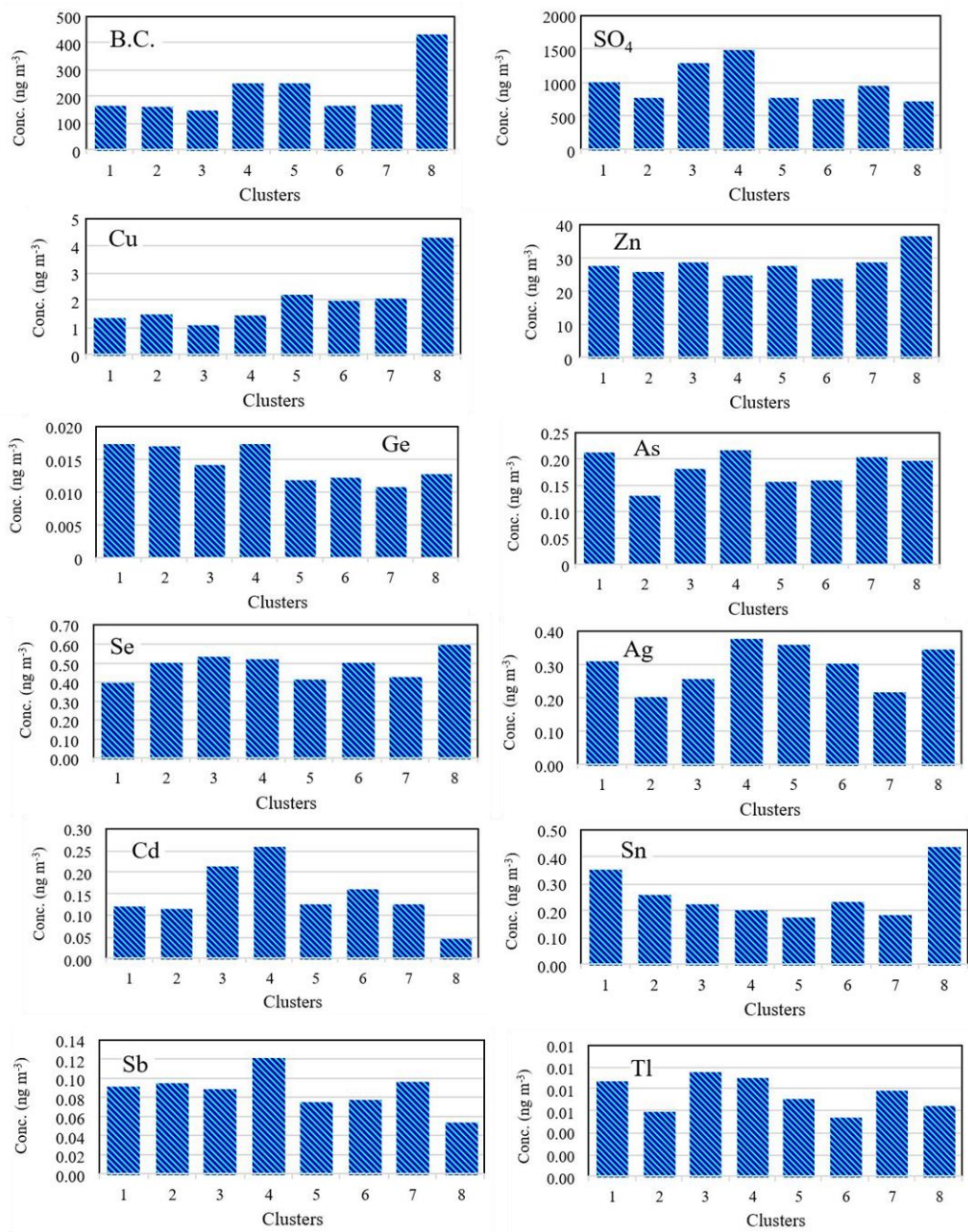


Figure 4.17 Cluster median concentrations of pollution derived elements

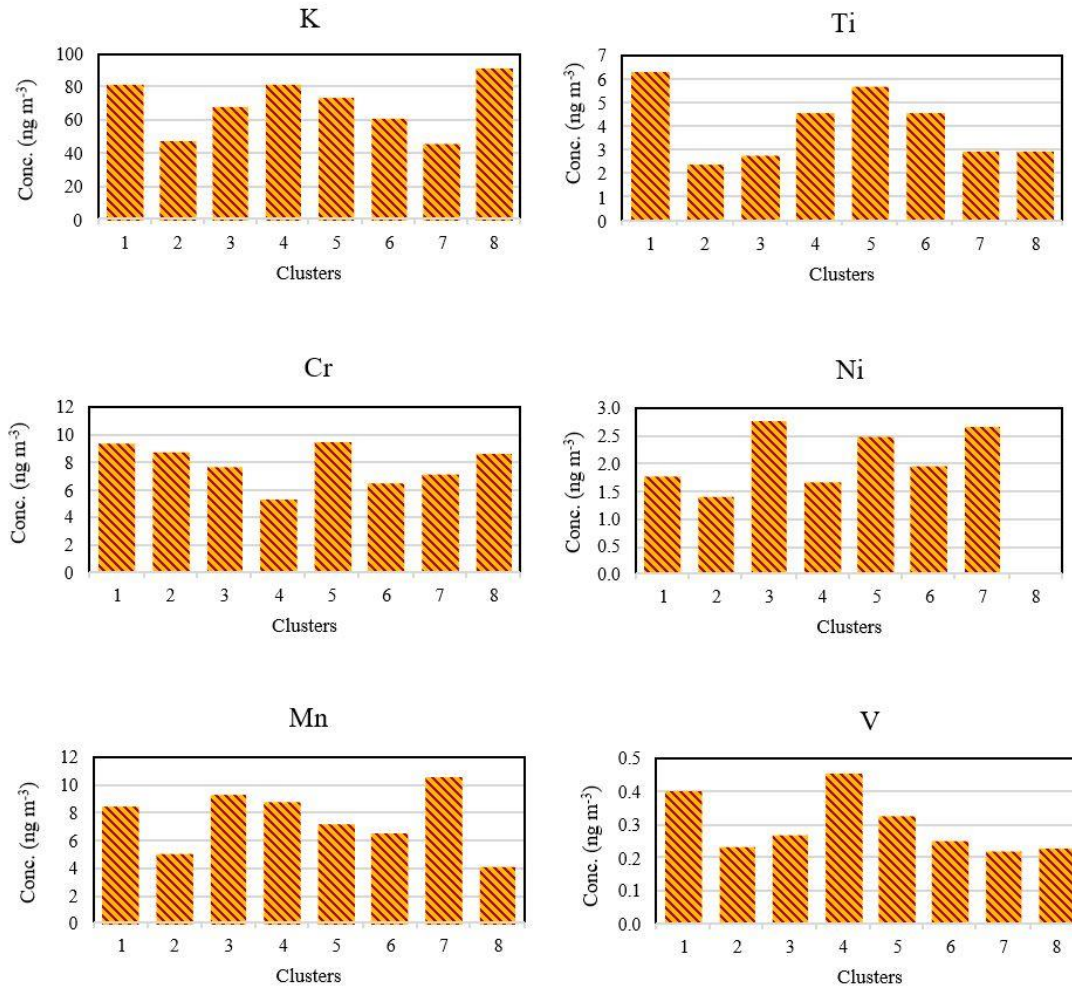


Figure 4.18 Cluster median concentrations of elements with mixed origin

The median concentrations of some selected crustal elements in the clusters are shown in Figure 4.16. Only 4 elements is selected for the figure, but the remaining crustal elements also followed similar trends. Cluster 5 and Cluster 1 are the clusters that contribute the most to the observed concentrations of crustal elements, which is not surprising. As can be seen from Figure 4.15, Cluster 1 contains a southward-extending trajectory group. Such air movements are expected to bring the dust originating from Middle East and the Arabian Peninsula to the Black Sea region. As can also be seen from Figure 4.15, the vast majority of the Cluster 5 trajectories spent their time over North Africa. Therefore, the trajectories in Cluster 5 includes air movements, which may bring Saharan dust from Africa to the Black Sea region. In order to check whether

there was a difference between Saharan and Middle East and/or the Arabian Peninsula dust Box-and Whisker plots of the soil-related elements were prepared and shown in Figure 4.19. The Box and Whisker plot was prepared with log-transformed data because of the large differences between the concentrations of the elements. As can be seen, the concentrations of crustal elements are generally higher in Cluster 5. The difference is very consistent in rare earth elements. For all rare earth elements without an exception, the Cluster 5 concentrations are higher than the Cluster 1 concentrations. For some rare earth elements such as Y, La, Tb, Yb and Lu, the ratio of Cluster 5/Cluster 1 concentrations ranges from 1.4 to 2.1, while for other rare earth elements the ratio of Cluster 5/Cluster 1 concentrations ranges from 1.1 to 1.2. But, for all rare earth elements without exception Cluster 5/Cluster 1 concentration ratios are greater than 1.

The cluster median values of the anthropogenic elements are shown in Figure 4.17. Since different anthropogenic elements have different sources, different elements can be high in different clusters. But, there are some characteristics that are common to most of the elements. Most of the elements are high in Cluster 4. The most obvious examples are B.C., SO_4^{2-} , Ge, As, Se, Ag, Cd, Sb, and Tl. Cluster 4 represents movement of air masses from east. These air masses are expected to bring pollutants emitted in the source regions of Azerbaijan, Georgia and Iran to the station. Likewise, the median concentrations of a large part of the anthropogenic elements are also high in Cluster 3. B.C., SO_4^{2-} , As, Se, Cd and Tl concentrations in Cluster 3 are higher than those in other clusters. Cluster 3 represents trajectories from the northwest to the Eastern Black Sea region. It is not surprising that the concentrations of pollution-derived elements are high in Cluster 3, because these air masses pass over Ukraine and arrive the sampling station. Industrial zones in the east of Ukraine has emerged as an important source region affecting every part of Turkey at most of studies done in our group. Therefore, it is not surprising that the median concentrations of anthropogenic elements are high in Cluster 3, since the region is very close to the station and the trajectories of Cluster 3 arrive to the station through this region.

The third trajectory group with a high median concentrations of B.C., Cu, Zn, Ag, Se and Sn. is Cluster 8. This cluster is also a trajectory group in which anthropogenic element concentrations are expected to be high. As can be seen from Figure 4.17, the trajectories in Cluster 8 has the fastest movement of air masses. These trajectories arrive from North America, even from the Pacific coast of the US to the Eastern Black Sea within five days. As stated before, there is considerable evidence that pollutants emitted into the atmosphere from large forest fires, known as boreal forest fires, in Canada are transported to Europe. Thus, the trajectories in Cluster 8 can similarly bring such pollutants to the Eastern Black Sea region where the station is located. This does not mean that the elements with high median concentration in this cluster arrive from North American. All the trajectories in this group arrive to Black Sea region through Europe. For this reason, the sources of the pollution derived elements at the cluster may also be in Europe. An obvious point is that Cluster 8 is a trajectory group that brings pollutants to the Eastern Black Sea region. The particles and the elements associated to these particles are measured in this study. It is no surprise that the air masses bring pollutant-derived elements to the Eastern Black Sea region also bring other pollutants that was not measured.

The median concentrations of the elements with both anthropogenic and natural (soil) sources, such as Ti, V, Mn, K, are shown in Figure 4.18. The median concentrations of the elements in this group are high in both Clusters 1 and 5, which bring crustal elements to the region and high in Clusters 3, 4, and 8, which bring the anthropogenic elements to the region.

It should be noted that the median values of the anthropogenic elements and the mixed origin elements are not expected to be high in the same clusters, since they have different sources. But, this is not the case for the soil-related elements, since they are released from same source.

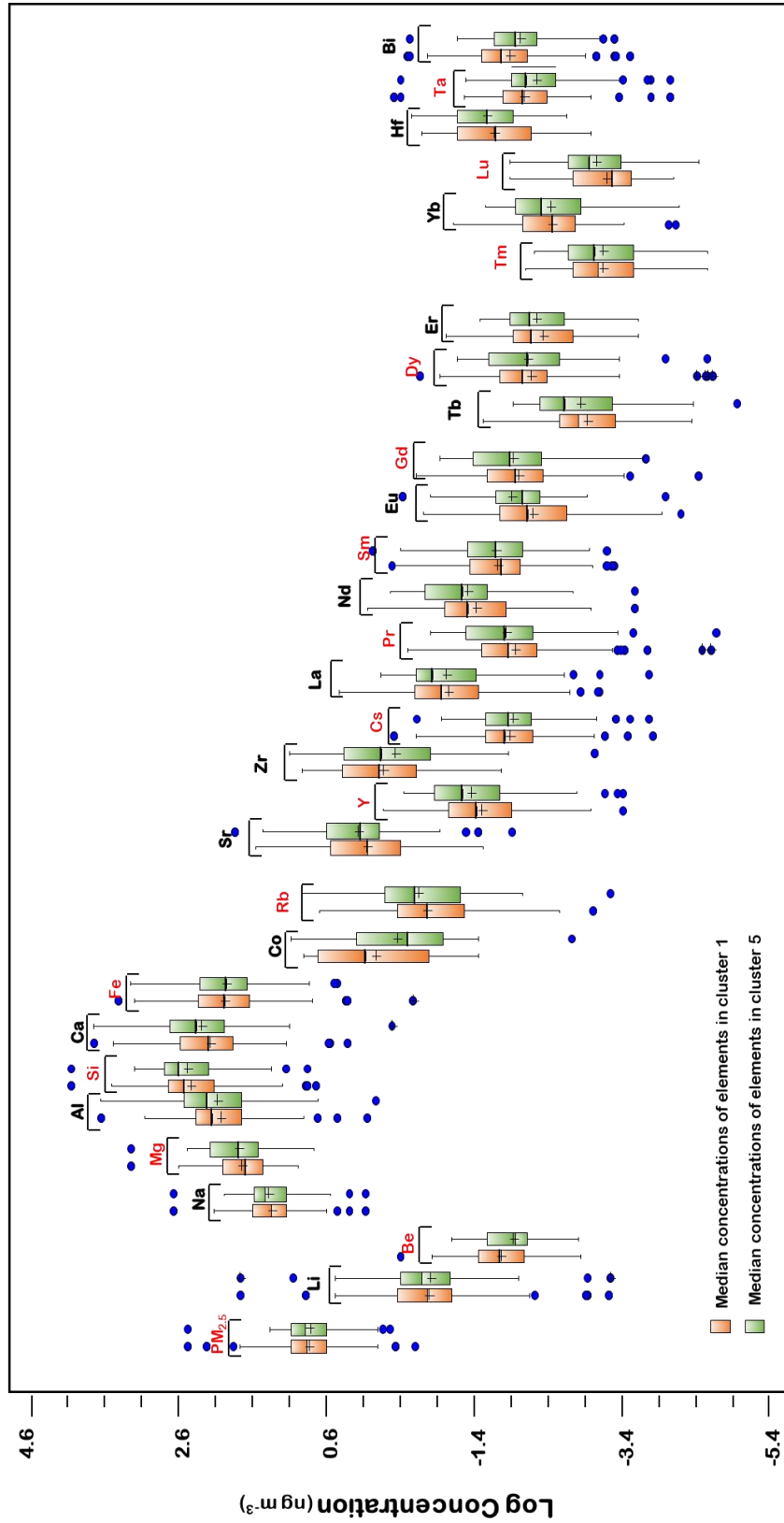


Figure 4.19 Median concentrations of crustal elements in Clusters 1 and 5

4.4 Relation between Elemental Concentrations and Local Meteorology

The main focus of this study is monitor long-range transported pollutant emissions, therefore most of the discussions given are based on the upper atmospheric air movements, rather than surface meteorology. However, surface meteorology can provide information on contribution of local sources if there are sources around the vicinity of the station. In such cases, the meteorological data obtained from the local meteorological stations become important. In this section of the manuscript, the effort is to investigate the relation of local meteorological parameters with pollution.

The meteorological station in Torul has been operated since 2014. Therefore, meteorological data was obtained from the Gümüşhane station, which was the closest station to sampling site. The 55-year meteorological parameters obtained from Gümüşhane meteorological station are given in Table 4.8.

Torul is located at a mountain region, Zigana-Trabzon Mountains to the north, Çimen Mountains to the south, Giresun Mountains to the west and Pulur, Soğanlı Mountains to the east. Torul has a humid continental climate with cold and snowy winters and warm summers. January is the coldest month with $-1.7\text{ }^{\circ}\text{C}$ mean temperature and mean temperature in winter is $-0.6\text{ }^{\circ}\text{C}$. On the other hand, August is the warmest month with $20.3\text{ }^{\circ}\text{C}$ mean temperature and mean summer temperature is summer is $19.2\text{ }^{\circ}\text{C}$. July and August are the only months that the mean temperatures are above $20\text{ }^{\circ}\text{C}$ and rest of the months in Torul have temperatures below $20\text{ }^{\circ}\text{C}$. The amount of mean rainfall ranges from 12.4 mm (for July) to 60.4 (for April) and the total rainfall amount is 464.2 mm , which is smaller than the Black Sea mean (2200 mm) The highest rainfall is observed at spring season with a 172.2 mm mean, which is the 37.1% of the mean annual rainfall. July and August are the only months mean wind speed $\geq 2.0\text{ m s}^{-1}$. Rest of the months wind speed is below 2.0 m s^{-1} . The mean relative humidity is around 60% during the year at Gümüşhane station.

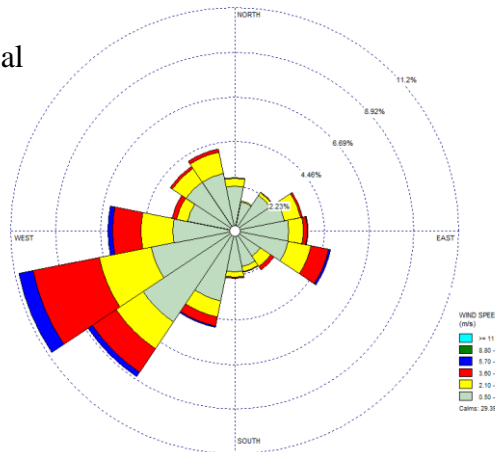
The annual, summer, and winter wind roses along with percent local wind frequencies and average wind speed during the sampling period (2011 to 2013) are shown in Figure 4.20.

Table 4.8 Long term (1961-2016 years) average temperature, relative humidity, total rainfall and wind speed at Gümüşhane meteorological station

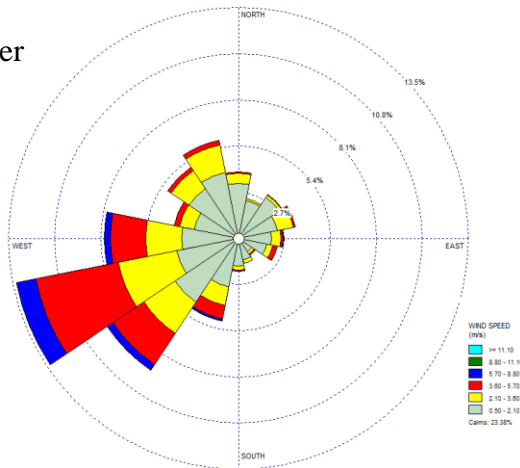
	Temperature (°C)	Relative Humidity (%)	Rainfall (mm)	Wind Speed (m s ⁻¹)
January	-1.7	66.2	36.6	1.1
February	-0.5	65.8	32.8	1.2
March	3.8	58.3	43.8	1.6
April	9.4	58.2	60.4	1.5
May	13.7	60.9	68	1.2
June	17.2	58.4	46.8	1.7
July	20.2	54.9	12.4	2.0
August	20.3	56.5	12.9	2.1
September	16.7	55.3	22.2	1.6
October	11.4	57.7	45.2	1.1
November	5.1	66.8	42.3	0.8
December	0.4	65.0	40.8	0.9

The figure shows that most of the local winds blew between west and south of the sampling station. WSW and SW are the dominant wind sectors at Eastern Black Sea region regardless of the season. At summer season frequencies from WSW and SW are 13.5%, 9.4%, respectively. During winter months frequencies of these wind sector decreased to 8.70% and 8.5%. But, the contribution of ESE sector (7.2%) more apparent in winter sector. The frequency of Northerly winds are less than 5% regardless of the seasons.

Annual



Summer



Winter

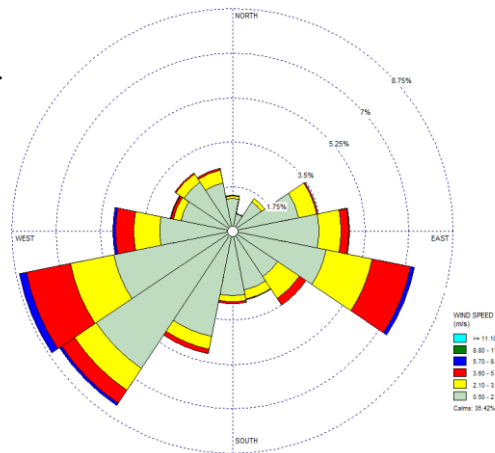


Figure 4.20 Annual, summer and winter wind roses

4.4.1 Relation Between Wind Speed and Concentrations of Species

The relation between wind speed and daily concentrations of species in PM_{2.5} fraction were investigated at STATGRAPHICS using simple regression test. This test tests the correlation between daily concentrations of species and wind speed at a 95% confidence level and displays a p-value. The results of the test tabulated at Table 4.9. As can be seen from Table 4.9, all the p-values are greater than 0.05 and there is no statistically significant relation between wind speed and daily concentrations of species at a 95% confidence level. Scatter plots some selected elements from different origins are depicted in Figure 4.21. The scatter plots of the species in Figure 4.21 also confirm the lack of relation of the wind speed and daily concentrations of species.

Table 4.9 Elemental concentration vs wind speed regression p-values

	p-value			p-value	
PM_{2.5}	0.8287	no relation	Y	0.415	no relation
B.C.	0.0891	no relation	Zr	0.828	no relation
Li	0.114	no relation	Ag	0.1347	no relation
Be	0.8648	no relation	Cd	0.9114	no relation
Na	0.8527	no relation	Sn	0.0717	no relation
Mg	0.0769	no relation	Sb	0.0624	no relation
Al	0.3836	no relation	Te	0.6515	no relation
Si	0.1559	no relation	Cs	0.9229	no relation
SO₄²⁻	0.7818	no relation	La	0.568	no relation
K	0.3555	no relation	Pr	0.1166	no relation
Ca	0.6141	no relation	Nd	0.3007	no relation
Ti	0.9453	no relation	Sm	0.3191	no relation
V	0.3127	no relation	Eu	0.1464	no relation
Cr	0.1882	no relation	Gd	0.1539	no relation
Mn	0.7866	no relation	Tb	0.3748	no relation
Fe	0.0974	no relation	Dy	0.1307	no relation
Co	0.0708	no relation	Er	0.4779	no relation
Ni	0.264	no relation	Tm	0.9936	no relation
Cu	0.2	no relation	Yb	0.8334	no relation
Zn	0.1036	no relation	Lu	0.0726	no relation
Ge	0.0676	no relation	Hf	0.9008	no relation
As	0.4217	no relation	Ta	0.1429	no relation
Se	0.6078	no relation	Tl	0.3157	no relation
Rb	0.6221	no relation	Pb	0.386	no relation
Sr	0.5298	no relation	Bi	0.8443	no relation

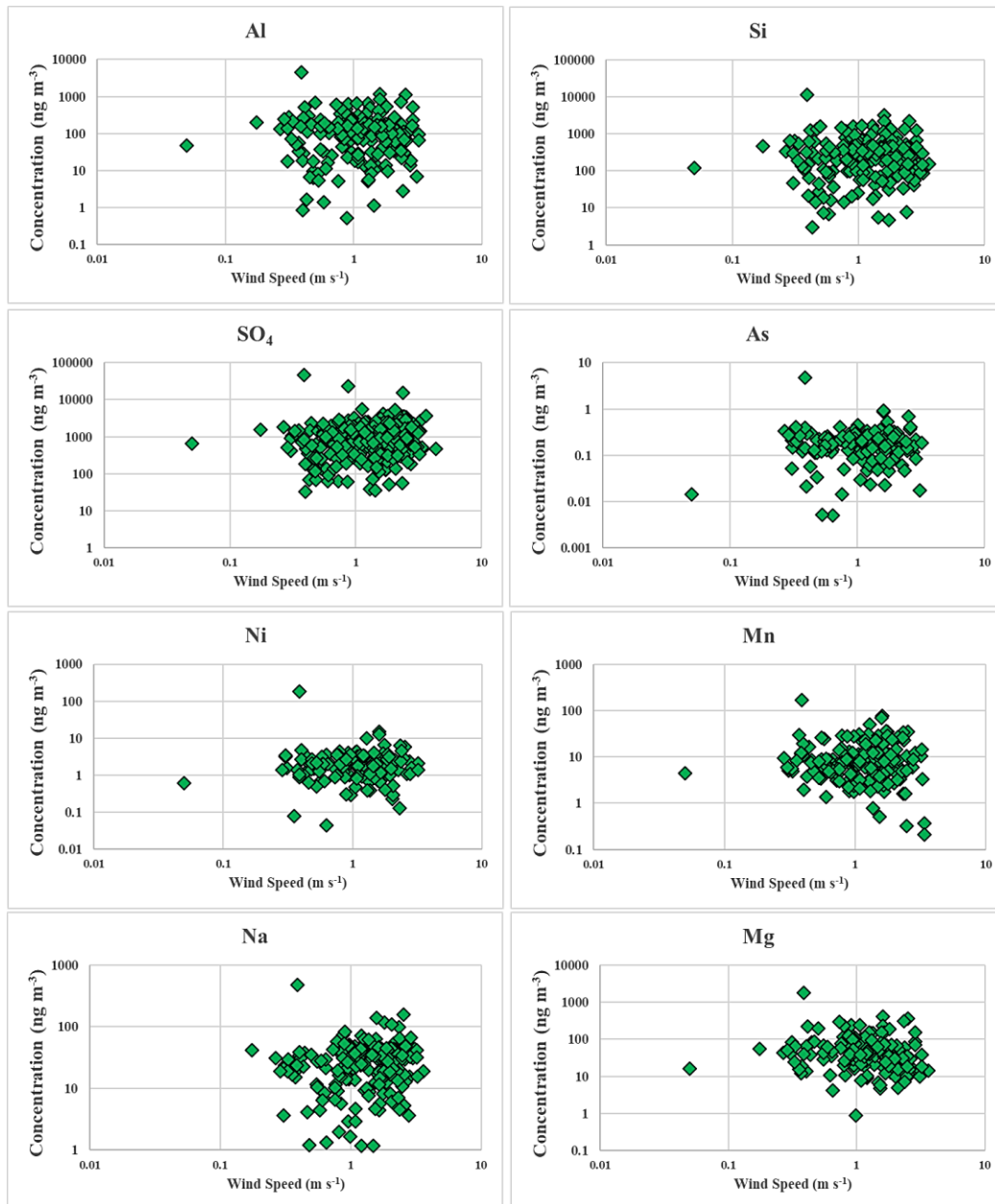


Figure 4.21 Log-log scatter plots of elements against wind speed

4.4.2 Relation Between Temperature and Concentrations of Species

Temperature is another local surface meteorological parameters that affect the measured concentration of species. The relation between temperature and daily concentrations of species in PM_{2.5} fraction were investigated at STATGRAPHICS using simple regression test. The results of the test are tabulated in Table 4.10. As can

be seen from Table 4.10, all the p-values are greater than 0.05 and there is no statistically significant relation between temperature and daily concentrations of species at a 95% confidence level. Scatter plots of temperature and daily concentrations of some selected species from different origins are depicted in Figure 4.22.

Table 4.10 Elemental concentration vs temperature regression p-values

	p-value			p-value	
PM_{2.5}	0.338	no relation	Y	0.0829	no relation
B.C.	0.8803	no relation	Zr	0.1335	no relation
Li	0.7269	no relation	Ag	0.6944	no relation
Be	0.2214	no relation	Cd	0.0978	no relation
Na	0.4341	no relation	Sn	0.1939	no relation
Mg	0.5917	no relation	Sb	0.2492	no relation
Al	0.8346	no relation	Te	0.3095	no relation
Si	0.5644	no relation	Cs	0.1202	no relation
SO₄²⁻	0.3208	no relation	La	0.6563	no relation
K	0.4305	no relation	Pr	0.0753	no relation
Ca	0.9725	no relation	Nd	0.0897	no relation
Ti	0.8438	no relation	Sm	0.0658	no relation
V	0.8567	no relation	Eu	0.1998	no relation
Cr	0.5142	no relation	Gd	0.0221	no relation
Mn	0.3001	no relation	Tb	0.0759	no relation
Fe	0.8139	no relation	Dy	0.0687	no relation
Co	0.6657	no relation	Er	0.3864	no relation
Ni	0.4708	no relation	Tm	0.0571	no relation
Cu	0.1123	no relation	Yb	0.055	no relation
Zn	0.8321	no relation	Lu	0.1711	no relation
Ge	0.8684	no relation	Hf	0.7877	no relation
As	0.7701	no relation	Ta	0.8008	no relation
Se	0.2662	no relation	Tl	0.1252	no relation
Rb	0.1486	no relation	Pb	0.9101	no relation
Sr	0.0931	no relation	Bi	0.1091	no relation

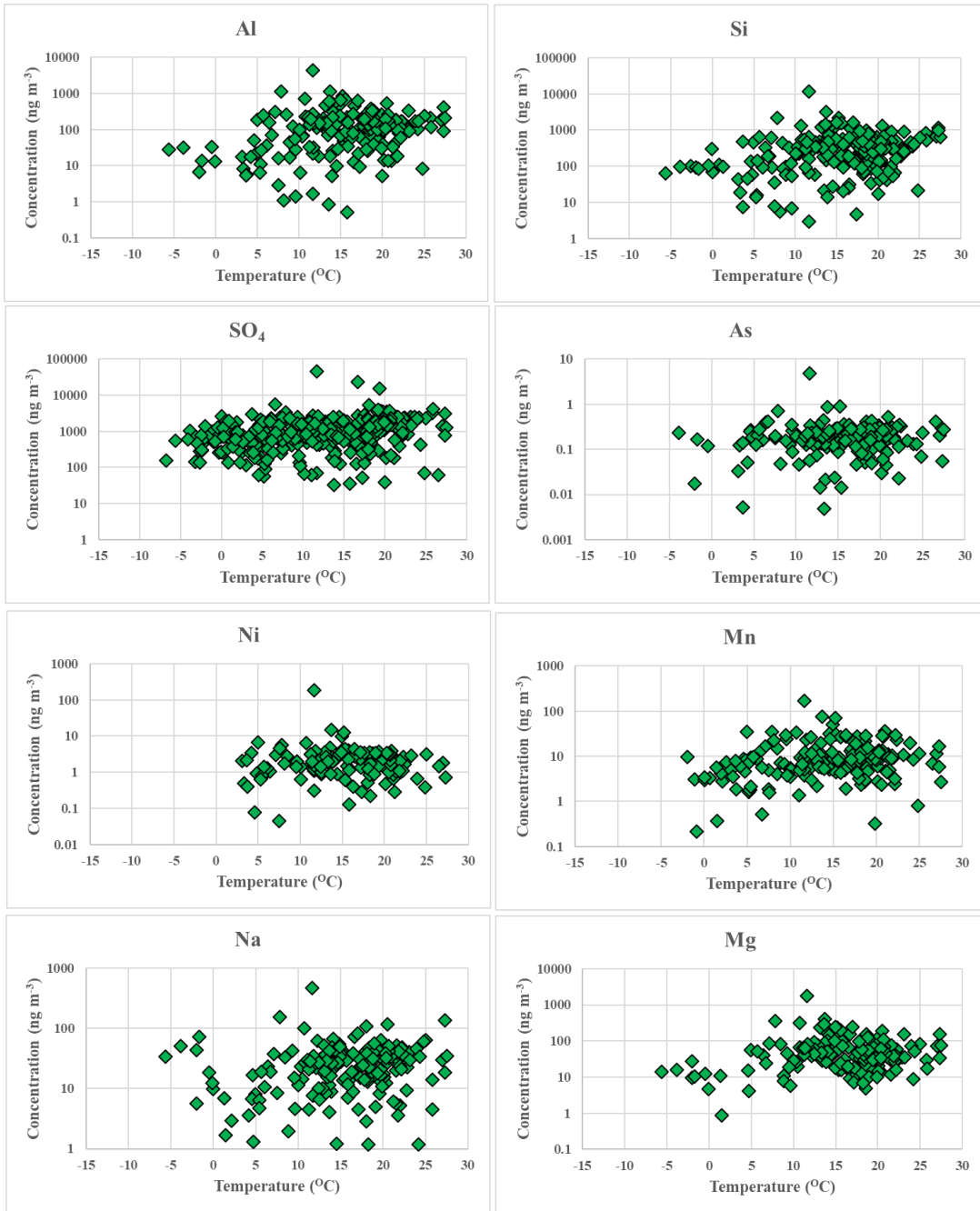


Figure 4.22 Binary correlations between concentrations of selected elements and temperature

In Figure 4.22, it seems if there were a relation between temperature and daily concentrations of Al, Si, and SO_4^{2-} species. However, the relation between temperature and daily concentrations of these species are not direct. Please note that there were no statistically relation between temperature and daily concentrations of species at 95%

confidence level. Precipitation is the main reason for the indirect relation between temperature and concentrations of crustal species Al and Si. Torul has a continental climate, hence wet and cold winter months, dry and warm summer months. During cold and wet winter season the soil is damp or ice covered and resuspension of local soil is less likely. However, during dry and warm summer months resuspension of soil is much easier. The indirect relation of temperature and concentrations of SO_4^{2-} is due to higher solar flux during temperature. The gas-phase oxidation of SO_2 increases with the higher solar flux during warm summer months.

4.4.3 Relation Between Local Rain and Concentrations of Species

Rain is the main determining factor for observed variability of the elemental concentrations. Particles can be scavenged from atmosphere either at the vicinity of the station by local rain events or they can be removed during their long range transport to the station site by rain events on the path of air masses. At this part of the manuscript the efforts is determine the effect of local rain events on observed concentrations of elements in $\text{PM}_{2.5}$ fraction by diving the samples into two sets as samples corresponding to rainy and non-rainy days. Key statistics of concentrations of species and their median concentrations ratio on non-rainy and rainy days are given in Table 4.11. The median concentration ratios of species on non-rainy and rainy days are depicted in Figure 4.23.

The median concentration ratios of elements on non-rainy and rainy days varied between 0.74 (for Ag) and 1.86 (for Er). Even though the non-rainy day-to-rainy day median ratios of elements varied between 0.74 and 1.86, majority of the elements have ratios around one. This indicates that the local rain events were not effective on the majority of the elements.

Table 4.11 Mean and median concentrations of elements in rainy and non-rainy days (ng m⁻³)

	Rainy			Non-rainy			Non-rainy/Rainy Ratio
	AVG ± STD	Median	Count	AVG ± STD	Median	Count	
PM_{2.5} ($\mu\text{g m}^{-3}$)	10.185 ± 27.28	6.547	122	10.512 ± 16.828	7.75	222	1.18
B.C.	387.495 ± 1265.909	171.831	64	219.491 ± 144.746	196.9	153	1.15
Li	0.905 ± 6.098	0.191	98	0.397 ± 0.998	0.242	191	1.27
Be	0.025 ± 0.022	0.018	45	0.03 ± 0.048	0.018	78	1.02
Na	31.646 ± 66.05	16.356	49	30.874 ± 24.033	29.095	143	1.78
Mg	101.087 ± 258.198	45.338	45	58.208 ± 68.509	37.841	128	0.83
Al	226.642 ± 600.518	110.766	55	160.64 ± 184.271	113.254	138	1.02
Si	550.725 ± 1427.715	278.832	66	389.391 ± 417.363	300.099	160	1.08
SO₄²⁻	1307.11 ± 4205.97	766.89	119	1422.44 ± 1977.35	1072.53	224	1.40
K	105.051 ± 255.997	60.818	69	84.616 ± 63.24	73.216	166	1.20
Ca	379.395 ± 845.507	157.809	60	233.162 ± 323.532	153.015	152	0.97
Ti	7.992 ± 10.7	4.585	88	9.145 ± 12.223	4.762	196	1.04
V	0.529 ± 1.689	0.24	112	0.667 ± 1.855	0.378	215	1.58
Cr	12.969 ± 15.671	7.52	117	10.471 ± 10.128	6.898	207	0.92
Mn	14.145 ± 24.562	8.389	57	10.932 ± 9.895	8.251	122	0.98
Fe	141.106 ± 216.531	75.148	121	190.554 ± 322.8	87.855	219	1.17
Co	2.692 ± 2.72	1.585	42	2.804 ± 2.952	1.576	68	0.99
Ni	7.297 ± 29.072	2.148	39	2.228 ± 1.838	1.977	95	0.92
Cu	3.987 ± 6.653	1.433	87	4.402 ± 9.242	1.875	149	1.31
Zn	31.988 ± 22.229	29.948	111	29.905 ± 23.957	24.551	196	0.82
Ge	0.034 ± 0.148	0.016	80	0.02 ± 0.019	0.014	155	0.89
As	0.28 ± 0.696	0.157	45	0.205 ± 0.126	0.197	117	1.25
Se	0.466 ± 0.297	0.428	106	0.541 ± 0.363	0.503	188	1.18
Rb	0.56 ± 1.049	0.136	59	0.717 ± 1.451	0.132	151	0.97

	Rainy			Non-rainy			Non-rainy/Rainy Ratio
	AVG \pm STD	Median	Count	AVG \pm STD	Median	Count	
Sr	3.181 \pm 5.941	1.152	63	3.634 \pm 8.395	1.189	134	1.03
Y	0.052 \pm 0.07	0.024	74	0.064 \pm 0.092	0.027	168	1.12
Zr	1.792 \pm 1.724	1.406	43	2.298 \pm 2.78	1.655	84	1.18
Ag	0.665 \pm 1.362	0.382	82	0.514 \pm 0.679	0.283	160	0.74
Cd	0.515 \pm 1.176	0.131	112	0.527 \pm 1.05	0.15	213	1.14
Sn	0.331 \pm 0.483	0.189	55	0.891 \pm 1.664	0.261	86	1.39
Sb	0.11 \pm 0.202	0.076	96	0.14 \pm 0.225	0.101	205	1.32
Te	0.051 \pm 0.061	0.04	109	0.053 \pm 0.067	0.045	183	1.11
Cs	0.02 \pm 0.03	0.012	114	0.024 \pm 0.04	0.016	221	1.28
La	0.147 \pm 0.171	0.071	93	0.154 \pm 0.253	0.076	180	1.06
Pr	0.019 \pm 0.026	0.01	92	0.024 \pm 0.037	0.01	182	0.94
Nd	0.068 \pm 0.091	0.039	97	0.085 \pm 0.129	0.037	194	0.94
Sm	0.05 \pm 0.093	0.017	78	0.052 \pm 0.112	0.017	158	1.03
Eu	0.024 \pm 0.043	0.011	49	0.028 \pm 0.052	0.013	95	1.21
Gd	0.016 \pm 0.022	0.009	89	0.018 \pm 0.027	0.009	176	1.03
Tb	0.002 \pm 0.002	0.001	83	0.002 \pm 0.003	0.001	161	1.61
Dy	0.01 \pm 0.014	0.006	79	0.014 \pm 0.022	0.007	166	1.13
Er	0.006 \pm 0.008	0.003	51	0.009 \pm 0.012	0.005	110	1.87
Tm	0.001 \pm 0.001	0.001	64	0.001 \pm 0.001	0.001	145	1.40
Yb	0.005 \pm 0.007	0.003	66	0.007 \pm 0.009	0.003	148	0.98
Lu	0.001 \pm 0.002	0.001	72	0.001 \pm 0.001	0.001	120	1.46
Hf	0.045 \pm 0.044	0.029	49	0.054 \pm 0.064	0.03	96	1.04
Ta	0.014 \pm 0.041	0.009	94	0.013 \pm 0.038	0.007	184	0.81
Tl	0.008 \pm 0.019	0.005	112	0.011 \pm 0.017	0.009	207	1.76
Pb	4.218 \pm 5.576	3.413	37	4.046 \pm 5.184	2.765	78	0.81
Bi	0.021 \pm 0.03	0.017	110	0.023 \pm 0.03	0.016	208	0.99

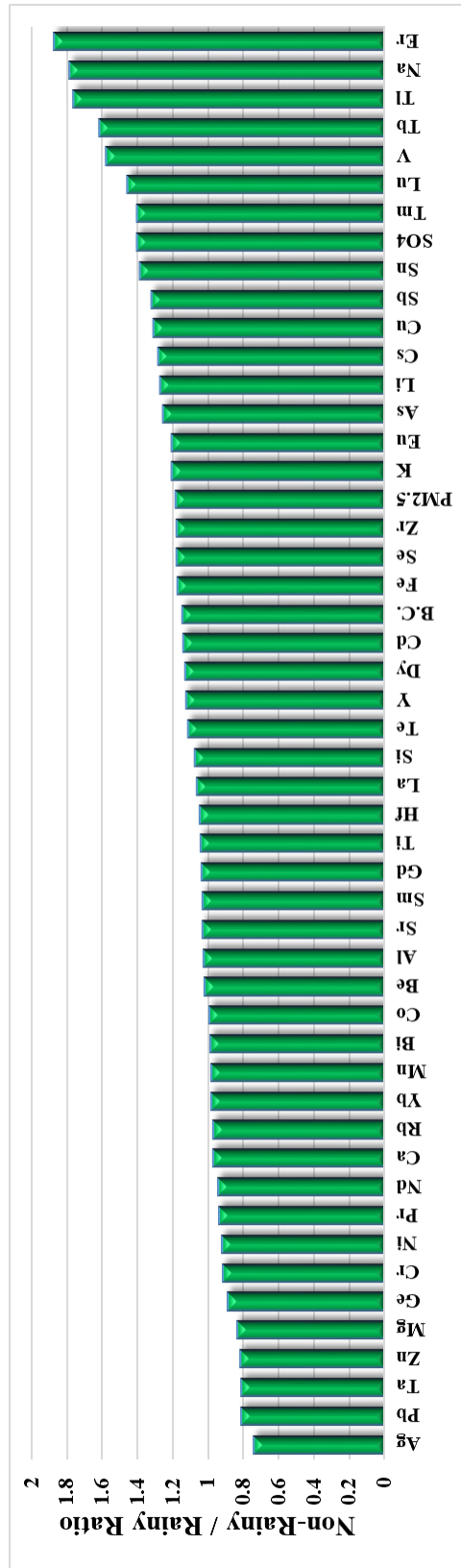


Figure 4.23 Median concentration ratios of species on non-rainy rainy days

In order to check which elements effected significantly from local rain events, median concentrations of species in PM_{2.5} fraction on non-rainy and rainy was tested with Mann-Whitney test using STATGRAPHICS software. Mann-Whitney test tests the null hypothesis that the medians of two samples are equal with a 95% confidence interval and displays a p-value. If the p-value is less than 0.05 (null hypothesis is rejected), there is a statistically significant difference between the medians at the 95.0% confidence level. The results of Mann-Whitney test tabulated in Table 4.12.

Table 4.12 Comparison of median concentrations of species on non-rainy and rainy days with Mann-Whitney test and p-values

	p-value		p-value
PM_{2.5}	0.0673	Y	0.4700
B.C.	0.7044	Zr	0.6930
Li	0.1620	Ag	0.2890
Be	0.8790	Cd	0.3298
Na	0.0192	Sn	0.0077
Mg	0.1318	Sb	0.0262
Al	0.5651	Te	0.7073
Si	0.5660	Cs	0.0517
SO₄	0.0016	La	0.9852
K	0.1301	Pr	0.5535
Ca	0.9376	Nd	0.5609
Ti	0.4585	Sm	0.5642
V	0.0011	Eu	0.6040
Cr	0.5692	Gd	0.3868
Mn	0.4093	Tb	0.0516
Fe	0.0739	Dy	0.1092
Co	0.9143	Er	0.0857
Ni	0.6105	Tm	0.1823
Cu	0.7563	Yb	0.5727
Zn	0.2190	Lu	0.0474
Ge	0.6803	Hf	0.8985
As	0.0882	Ta	0.5506
Se	0.1352	Tl	0.0000
Rb	0.8537	Pb	0.8551
Sr	0.9051	Bi	0.5244

The particles that are brought to the receptor site from distant sources can be scavenged from atmosphere both at the vicinity of the station by local rain events and during their long range transport to the station site by rain events on the path of air masses. During several days-long travel of air masses, they pass through several rain events. At each rain event particles they carry are washed out, and then they pick up new particles from other source areas. These newly acquired particles may also be washed up in the next rain event. This process continues and whatever left in the air mass when it reaches the station is sampled. On the other hand, particles that are emitted from more nearby sources will not be wet scavenged as effectively, because they will arrive to the station at a shorter time. Proximity of the sources to the station determines how the particles affected from local rain events. This is the case for majority of the elements in Table 4.12. Their non-rainy and rainy days median concentrations are not statistically different.

Na, SO_4^{2-} , V, Sn, Sb, Lu, and Tl are the exceptions to the mechanism above. According to the Mann-Whitney test median concentrations of Na, SO_4^{2-} , V, Sn, Sb, Lu, and Tl on non-rainy and rainy days were significantly different at the 95.0% confidence level. Concentrations of these species decreased significantly during local rain events. This indicates that these species have nearby sources compared to sources of other species. Among these species sodium is a marine element and the distance between sampling station and Black Sea is 75 km. The potential locations of the remaining elements will be discussed in the source apportionment section of the manuscript. Another reason for the significant differences on the non-rainy and rainy day median concentrations of some elements is the water solubility property. Some species for example, Na and SO_4^{2-} , are highly soluble in water. During the local rain events the compounds of Na and SO_4^{2-} dissolve in the rain droplets and scavenged from the atmosphere more efficiently.

4.5 Temporal Variations of Pollutants

Temporal variations of concentrations of species depend on several factors including; the existing sources, transport pattern, and meteorological factors. Since most of these

parameters change in time, chemical composition of PM show temporal variations. Temporal variations of species are generally studied for two different time scales as it is in this study. Short term variations are the episodic changes in concentrations, whereas long term variations are the average changes in time scales of seasons (Karakaş et al, 2004).

4.5.1 Short Term Variations

Trace element data is very episodic in nature due to frequent changes in air mass movements that brings pollutants and natural constituents to receptor. When upper atmospheric transport occurs from a polluted sector, concentrations of pollutants measured at the receptor will be high. However, when air mass movements is shifted to a clean sector, pollutant concentrations drop rapidly generating an episode. These episodes are frequent and that is why trace element data shows right-skewed distributions (such as log-normal).

In this section, episodic nature of trace element data generated at Torul station is discussed. Concentrations of elements and other pollutants measured at a receptor has two components in their measured concentrations. One of these components is the baseline levels of species which are the concentrations that occurs in whole region and do not change very much in time and space. Superimposed on these baseline concentrations there are episodes, which are transient, because pollutants associated with these episodes, are brought to receptor by air masses, which passes over source areas. When air mass movement to receptor change direction, they disappear. Depending on frequency of air mass movement from source areas and distance between the receptor and sources, episodes can account for a large fraction of measured concentrations.

Please note that, episodes can be reduced in magnitude and frequency or even can be eliminated entirely by taking regulatory actions to reduce emissions at source areas, but baseline concentrations will not be affected at the same pace. Consequently, one has to know baseline concentrations of elements and other pollutants to understand

how much average concentration of a pollutant can be decreased by proper regulatory actions at sources.

There are different ways to estimate baseline levels of elements. In one approach time series plots of elements can be prepared and episode days are visually excluded from baseline data. In the second approach the peak concentration as best-fitted frequency distribution is adopted as baseline level of that element. This approach is illustrated in Figure 4.24. When there is sufficiently large data set, baseline concentrations of elements estimated by both histogram and time-series approach produce similar results. This histogram approach was adopted, because it is more quantitative and more robust than the other one. This approach is not invented in this work. It is first used by Husain et al. (1982), than by Olmez (1997). The histogram approach to calculate baseline concentrations were also frequently used in our group to calculate baseline levels of elements at Eastern Mediterranean (Güllü et al., 1998; Öztürk et al., 2012) and at Central Black Sea basin (Karakaş et al., 2004).

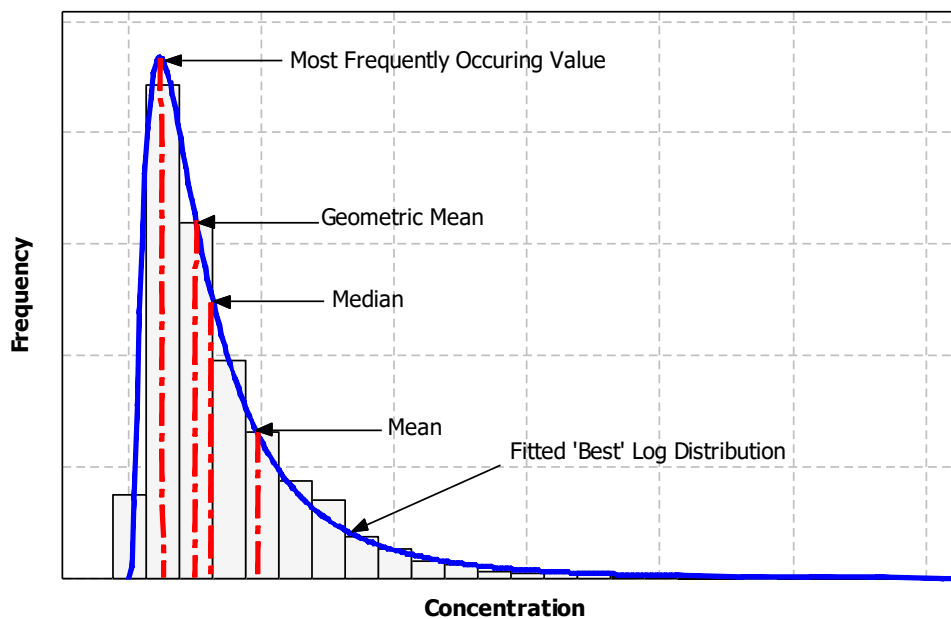


Figure 4.24 Frequency histogram for calculation of most frequently occurring value

Baseline concentrations of elements measured in PM_{2.5} fraction are given in Table 4.13, together with percentage of element concentrations that are accounted for by episodes. Baseline concentrations are significantly smaller than average concentrations of elements, indicating the high contribution of episodes.

Table 4.13 Baseline concentration of elements and percent concentrations accounted by episodes

Elements	Baseline Concentration (ng m ⁻³)	% Concentrations Accounted by Episodes		
		Annual	Summer	Winter
Ni	2.4565	30.4	30.9	28.9
Li	0.7524	36.1	35.3	40.8
Ta	0.0075	41.2	42.7	36.4
As	0.1191	42.5	45.8	36.9
Ge	0.0150	43.5	43.2	44.0
V	0.2821	48.1	47.8	48.7
Se	0.2759	49.9	49.1	50.9
Te	0.0242	49.9	50.4	49.1
B.C.	112.8530	50.4	50.4	50.5
Sm	0.1411	52.2	50.9	72.4
SO ₄ ²⁻	564.2630	53.1	55.4	49.1
Cs	0.0084	55.6	60.7	45.0
Ca	81.8833	56.0	55.0	58.3
Mn	3.8894	56.1	60.7	48.5
Tl	0.0038	56.7	57.0	56.2
Na	11.6684	56.8	58.1	52.5
Mg	20.4708	58.4	57.5	61.2
Sn	0.1411	59.0	56.7	63.4
Si	153.5310	59.3	59.4	58.8
Cu	1.1285	61.7	55.5	70.8
Sr	0.7524	61.7	67.3	52.6
Cd	0.0940	62.1	64.5	58.2
Sb	0.0376	62.5	63.6	60.7
Al	51.1771	63.5	62.9	65.4
K	25.5885	63.7	65.7	59.5
Pb	0.9724	64.9	69.3	57.1
Gd	0.0037	65.3	67.1	61.8
Cr	2.3825	65.5	60.1	73.7
Ag	0.1411	65.9	66.9	63.9
Zn	8.7774	66.4	67.6	64.7
Fe	28.2132	66.7	66.8	66.6
La	0.0376	67.6	67.3	68.2
Nd	0.0150	67.6	67.6	67.6

Elements	Baseline Concentration (ng m ⁻³)	% Concentrations Accounted by Episodes		
		Annual	Summer	Winter
Tb	0.0004	68.3	68.0	68.9
Dy	0.0024	68.9	69.3	68.1
Eu	0.0047	69.1	69.1	69.1
Pr	0.0036	69.5	70.4	67.9
Rb	0.0940	69.7	71.1	65.6
Er	0.0011	70.8	69.3	74.3
Yb	0.0009	72.0	73.3	69.5
Y	0.0075	72.2	72.7	71.0
Bi	0.0038	72.9	77.2	65.3
Be	0.0047	73.2	75.5	69.7
Ti	0.9404	76.3	77.0	74.9
Lu	0.0002	78.6	79.5	76.7
Hf	0.0038	80.4	81.1	78.7
Tm	0.0001	81.0	81.2	80.7
Co	0.1411	81.4	84.6	76.2
Zr	0.1411	83.1	83.3	82.6

Percent contributions of episodes on annual average concentrations of elements is also shown in Figure 4.25. Contribution of episodes vary between 30% (Ni) and 80% (Hf, Tm, Co and Zr). On the average 62% of measured concentrations of elements are due to episodes. This large episode contribution to elements suggest that with appropriate actions taken at source areas at a regional basis, current average element concentrations at Eastern Black Sea basin can be reduced by approximately 60%. The Table 4.13 also demonstrates that crustal elements are more episodic than anthropogenic elements. Contribution of episodes to crustal and anthropogenic elements are $66 \pm 11\%$ and $57 \pm 8\%$, respectively. Higher episodic contribution to crustal elements is not surprising. Episodes in concentrations of all elements are due to variations in air mass motions, as discussed in previous paragraphs. This includes both anthropogenic and crustal elements. However, variability of crustal elements also depends on variations in local wind speed and even to variability in wind speed at source areas (deserts in the Middle East, Arabic Peninsula and Africa). Since there are more factors affecting episodes in crustal particles, higher episodic contribution to concentrations of lithophilic elements, which are associated with those particles, should be expected.

Baseline concentrations were also calculated for Eastern Mediterranean (Öztürk et al., 2012) and Central Black Sea (Karakaş et al., 2004), using the same methodology. Baseline concentrations estimated in these stations are compared with baseline concentrations in this study in Figure 4.26. It can be seen from the figure that for most of the elements difference between baseline concentrations of elements are not as variable as their average concentrations. However, there are significant differences for some of the elements. For example; concentrations of Na and Mg at Torul is an order of magnitude smaller than baseline concentrations of these elements at Amasra and Antalya stations. Station at Amasra and Antalya are on the coastline (the one in Antalya is 0 m from the sea and station at Amasra is 3 km from the coast), but station at Torul is approximately 75 km from Black Sea coast and there are mountains between Torul and the coast, which are 2200 m high (altitude of the Torul station is approximately 1100 m). Because of all these distances and altitudes, the station at Torul is not affected from sea salt as much as stations at Antalya and Amasra. Since Na and Mg are major components of sea salt aerosol, which obviously make up the baseline levels of these elements at Antalya and Amasra, their lower concentrations at Torul station should be expected.

Major crustal elements like Al, Fe, except for Ca, are not different in all three stations. Baseline line concentration of Ca is high at Mediterranean station due to highly alkaline nature of the soil in the Eastern Mediterranean region (Lizarazo et al., 2005; Uz and Tavalı, 2014). Baseline concentrations of some of the minor and trace elements, such as changes from one station to another, because although major element composition of soil do not change much, trace element composition is variable.

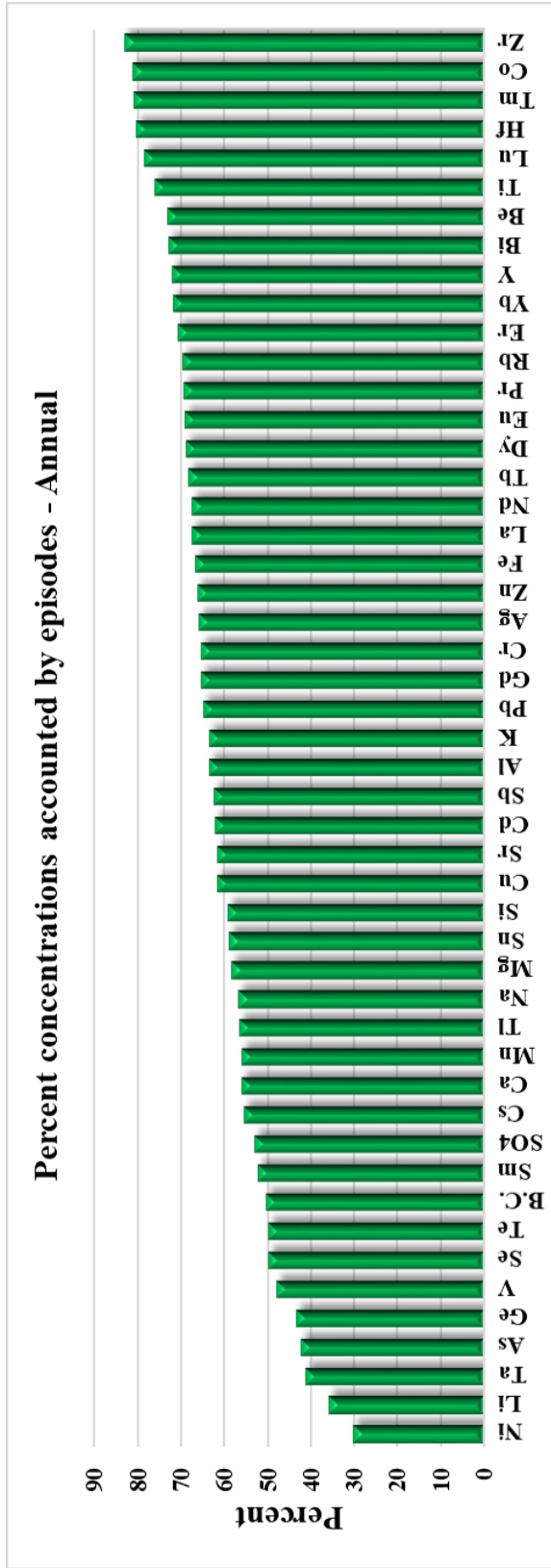


Figure 4.25 Percent concentrations accounted by episodes annually

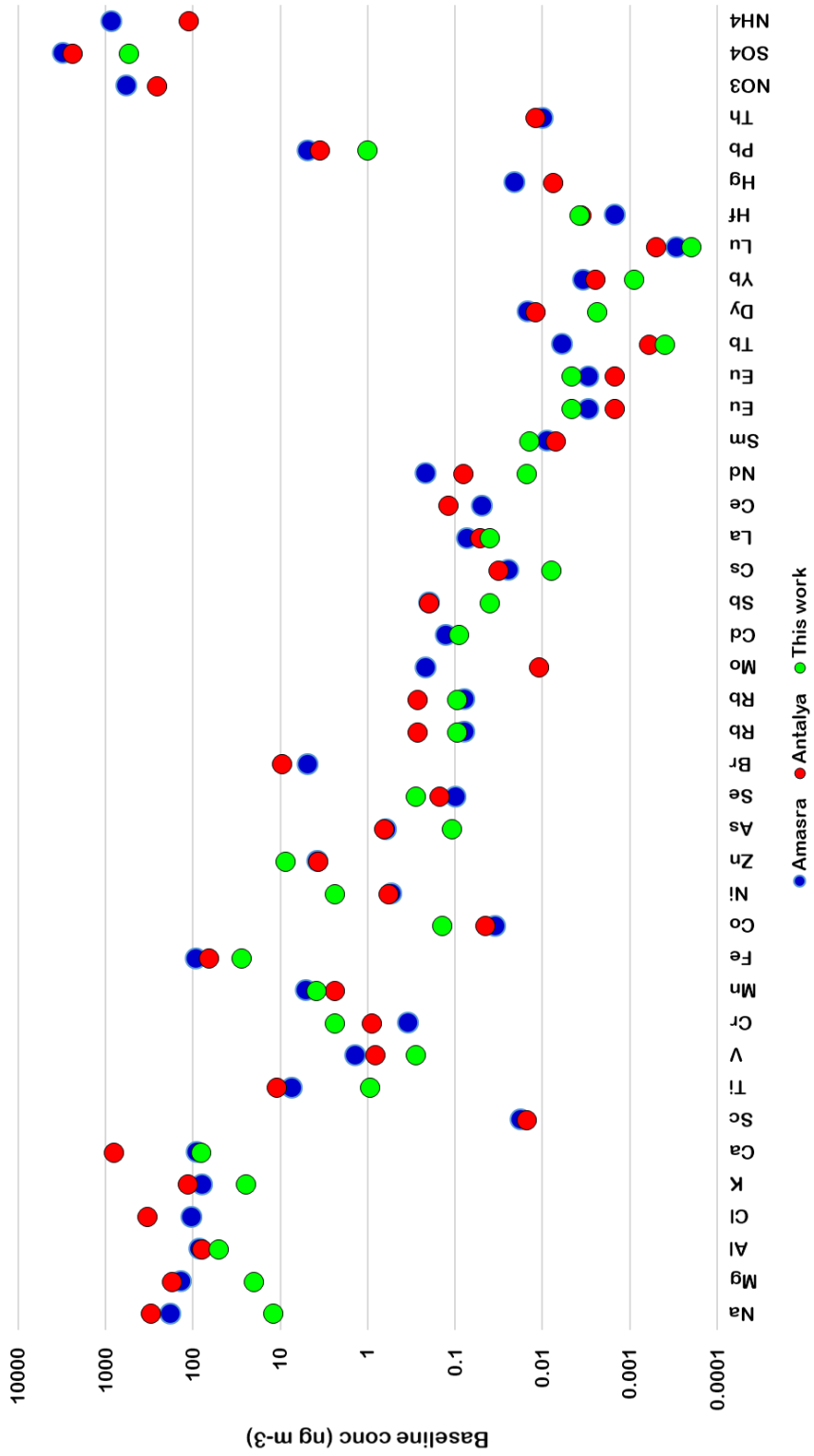


Figure 4.26 Baseline concentrations of elements Amasra, Antalya and Torul stations

Baseline concentrations of anthropogenic elements do not show similarity between stations that is observed in crustal elements. Baseline concentrations of anthropogenic elements are variable. Some of the anthropogenic elements, like Sb, Pb, Ti, V and SO_4^{2-} have lower baseline concentrations at Torul station. Concentrations of Zn, Ni and Cr are higher at Torul; and concentrations of Mn, Se and Cd have similar concentrations at all three stations. Lower concentrations of Pb and SO_4^{2-} at Torul relative to baseline concentrations of these elements at Amasra and Antalya is due to different times in which data sets are generated. Samples at Antalya and Amasra were collected between 1990 and 2000, before catalytic converters were installed to cars in this part of the world, but Torul data were generated 3 – 4 years ago, when most of the cars were equipped with catalytic converters and were using unleaded gasoline. This can explain lower Pb baseline concentration. Baseline concentration of SO_4^{2-} is lower at Torul due to regional scale decrease in SO_4^{2-} concentrations which was stemmed from reductions in SO_2 emissions by the actions taken at source regions (Berglen et al., 2007). Variability in baseline concentrations of other anthropogenic elements can be due to different sources, or source regions affecting Eastern Mediterranean and different parts of the Black sea region.

4.5.2 Long Term Variations

Long term variations in concentrations of elements, at rural areas, are due to seasonal variations in transport patterns in solar activity, in wet scavenging efficiency. Since most of the elements measured in this work are non-reactive, seasonal variation in wet scavenging efficiency is probably the most important parameter affecting seasonal variations in concentrations of elements. If an element is transported from distant sources its concentration is expected to be lower in winter due to more effective wet scavenging of particles with which that element is associated with.

Please note that, when more effective wet scavenging is mentioned, it doesn't mean scavenging with rain at the station site. Air masses during their transport picks up anthropogenic particles from particle source areas, which they cross. During their travel, they passes through several rain event. At each rain event particles they carry

is washed out, and then they pick up new particles from other source areas. These newly acquired particles may also be washed up in the next rain event. This process continues and whatever left in the air mass when it reaches to the station is sampled. This mechanism is more effective in winter, because air mass passes through more rain events. Wet scavenging of particles is not effective in summer, because rain is scarce. Since particles transported from distant sources will be scavenged more effectively by rain events, their concentrations are expected to be smaller in winter and higher in summer. On the other hand, particles that are emitted from local sources will not be wet scavenged as effectively, because they will arrive to Torul at a shorter time. Seasonal variations in their concentrations will not be determined by seasonal variation in wet scavenging efficiency.

The year is divided into two seasons as summer and winter. Division of the year into two seasons is based on rainfall amount. In the Eastern Black Sea region approximately 60-70% of annual rainfall is recorded in winter period. Since wet scavenging accounts for a significant fraction of variations in concentrations of elements, division of the year as wet and dry periods was reasonable. Summer is the period between May and October, and winter is the rest of the year.

Summer and winter average and median concentrations of elements are given in Table 4.14 and Table 4.15 for fine and coarse fractions, respectively. Summer-to-winter concentration ratios of elements in fine and coarse fractions of elements are given in Figure 4.27. For most of the elements the ratio is > 1.0 indicating that, with few exceptions concentrations of element groups are higher in summer seasons, not necessarily for the same reason.

Table 4.14 Summer and winter concentrations of elements in fine fraction
(concentrations are in ng m⁻³)

	Fine Summer	Fine Winter
	AVG ± σ (Median)	AVG ± σ (Median)
Mass (μg m⁻³)	12.54 ± 28.05 (8.16)	7.98 ± 7.31 (6.1)
B.C.	300.4 ± 822.3 (214.9)	190.7 ± 166.3 (159.3)
Li	0.841 ± 4.766 (0.318)	0.192 ± 0.187 (0.12)
Be	0.033 ± 0.053 (0.018)	0.024 ± 0.022 (0.019)
Na	32.49 ± 42.36 (28.57)	26.8 ± 27.72 (18.87)
Mg	69.76 ± 158.67 (38.86)	68.12 ± 93.06 (40.51)
Al	181.3 ± 386.1 (119.4)	174.4 ± 265.5 (65.5)
Si	448.2 ± 920.6 (308.4)	402.7 ± 604.1 (186.9)
SO₄²⁻	1755.7 ± 3903.8 (1273.6)	940.2 ± 760.3 (724.5)
K	93.78 ± 169.76 (74.62)	83.6 ± 85.41 (58.91)
Ca	246.8 ± 482.3 (158.6)	340.2 ± 625.9 (142.5)
Ti	8.3 ± 8.47 (5.88)	9.52 ± 15.43 (3.33)
V	0.657 ± 1.591 (0.406)	0.574 ± 2.025 (0.22)
Cr	9.27 ± 10.88 (5.53)	13.84 ± 13.72 (10.82)
Mn	12.25 ± 16.42 (8.92)	11.32 ± 15.57 (5.68)
Fe	168.5 ± 286.2 (82.7)	178 ± 295.2 (84.4)
Co	2.96 ± 2.73 (2.07)	2.56 ± 2.99 (0.76)
Ni	3.89 ± 18.06 (2.02)	3.1 ± 3.59 (1.75)
Cu	3.95 ± 6.51 (1.54)	4.54 ± 9.88 (1.84)
Zn	29.26 ± 25.47 (23.56)	32.05 ± 20.99 (28.92)
Ge	0.0299 ± 0.1195 (0.0174)	0.0195 ± 0.0183 (0.0142)
As	0.2231 ± 0.4307 (0.179)	0.2327 ± 0.1932 (0.1963)
Se	0.5613 ± 0.3644 (0.5139)	0.458 ± 0.3053 (0.4179)
Rb	0.8356 ± 1.5661 (0.1749)	0.3811 ± 0.7539 (0.0791)
Sr	4.31 ± 9.18 (1.33)	2.28 ± 4.51 (1.05)
Y	0.0598 ± 0.0798 (0.0305)	0.0613 ± 0.0962 (0.0183)
Zr	2.48 ± 2.78 (2)	1.58 ± 1.81 (0.85)
Ag	0.6 ± 1.094 (0.358)	0.512 ± 0.735 (0.262)
Cd	0.622 ± 1.178 (0.21)	0.405 ± 0.975 (0.105)
Sn	0.571 ± 0.807 (0.247)	0.762 ± 1.702 (0.233)
Sb	0.143 ± 0.267 (0.105)	0.115 ± 0.129 (0.086)
Te	0.057 ± 0.083 (0.046)	0.046 ± 0.03 (0.041)
Cs	0.029 ± 0.047 (0.018)	0.015 ± 0.017 (0.011)

	Fine Summer	Fine Winter
	AVG ± σ (Median)	AVG ± σ (Median)
La	0.148 ± 0.253 (0.077)	0.156 ± 0.193 (0.071)
Pr	0.023 ± 0.034 (0.011)	0.022 ± 0.034 (0.008)
Nd	0.083 ± 0.117 (0.046)	0.073 ± 0.119 (0.028)
Sm	0.062 ± 0.123 (0.022)	0.038 ± 0.08 (0.013)
Eu	0.03 ± 0.054 (0.014)	0.02 ± 0.039 (0.008)
Gd	0.0184 ± 0.0254 (0.0098)	0.0167 ± 0.0253 (0.007)
Tb	0.0022 ± 0.0032 (0.0014)	0.0022 ± 0.003 (0.0011)
Dy	0.0131 ± 0.0205 (0.0075)	0.0126 ± 0.0196 (0.0046)
Er	0.0074 ± 0.0112 (0.0037)	0.0087 ± 0.0109 (0.0046)
Tm	0.0011 ± 0.0012 (0.0007)	0.0011 ± 0.0014 (0.0006)
Yb	0.0061 ± 0.0084 (0.0034)	0.0065 ± 0.0092 (0.0034)
Lu	0.0013 ± 0.0017 (0.0007)	0.0012 ± 0.0014 (0.0006)
Hf	0.0539 ± 0.0634 (0.0286)	0.0451 ± 0.0462 (0.0299)
Ta	0.0148 ± 0.05 (0.0076)	0.0102 ± 0.0099 (0.008)
Tl	0.0118 ± 0.0232 (0.0082)	0.0088 ± 0.0084 (0.006)
Pb	3.46 ± 2.53 (2.8)	6.09 ± 9.53 (3.03)
Bi	0.025 ± 0.0373 (0.0183)	0.0187 ± 0.0179 (0.0152)

Table 4.15 Summer and winter concentrations of elements in coarse fraction.
(concentrations are in ng m⁻³)

	Coarse Summer	Coarse Winter
	AVG ± STD (Median)	AVG ± STD (Median)
Mass (µg m⁻³)	10.09 ± 22.51 (6.13)	9.33 ± 13.22 (5.69)
B.C.	94.6 ± 57.6 (90.5)	141.6 ± 197.4 (67)
Li	0.497 ± 0.845 (0.248)	0.805 ± 1.424 (0.267)
Be	0.024 ± 0.019 (0.019)	0.029 ± 0.023 (0.021)
Na	61.1 ± 44.08 (48.04)	91.17 ± 181.98 (12.12)
Mg	93.06 ± 89.87 (62.78)	431.4 ± 912.73 (53.87)
Al	262.1 ± 214.4 (194.2)	1220.3 ± 2373.1 (214.9)
Si	664 ± 544.9 (488.9)	3942.9 ± 8577.2 (493.8)
SO₄²⁻	574.4 ± 517.5 (379.6)	538.1 ± 591.8 (333.5)
K	107.01 ± 65.8 (85.93)	199.39 ± 374.53 (71.33)
Ca	599.2 ± 451.5 (499.7)	1202.6 ± 2679.5 (403.2)
Ti	19.55 ± 17.2 (12.45)	14.82 ± 17.81 (6.92)
V	0.953 ± 1.238 (0.526)	0.824 ± 1.386 (0.368)

	Coarse Summer	Coarse Winter
	AVG ± STD (Median)	AVG ± STD (Median)
Cr	12.8 ± 12.48 (7.82)	8.06 ± 12.18 (4.57)
Mn	12.04 ± 9.38 (8.8)	46.03 ± 159.77 (8.21)
Fe	419.8 ± 520.4 (203)	282.5 ± 462.1 (129.3)
Co	5.14 ± 10.74 (1.03)	6.39 ± 8.7 (4.99)
Ni	0.9 ± 0.63 (0.69)	6.57 ± 6.48 (2.95)
Cu	9.79 ± 19.57 (2.15)	4.48 ± 5.76 (1.88)
Zn	45.91 ± 33.05 (42.06)	44.51 ± 31.78 (43.72)
Ge	0.0167 ± 0.0158 (0.0118)	0.0172 ± 0.0171 (0.0121)
As	0.1465 ± 0.0823 (0.1448)	0.3794 ± 0.4006 (0.1597)
Se	0.5148 ± 0.3112 (0.4465)	0.5444 ± 0.7216 (0.3792)
Rb	0.2807 ± 0.2366 (0.2388)	0.4008 ± 0.5331 (0.3198)
Sr	2.57 ± 2.07 (2.35)	4.34 ± 9.26 (1.75)
Y	0.0894 ± 0.0727 (0.0694)	0.1025 ± 0.1726 (0.0519)
Zr	5.77 ± 6.5 (2.87)	5.72 ± 6.9 (3.09)
Ag	0.603 ± 1.771 (0.137)	0.68 ± 1.704 (0.103)
Cd	0.543 ± 1.449 (0.101)	0.518 ± 0.869 (0.157)
Sn	2.062 ± 3.447 (0.6)	1.602 ± 3.317 (0.651)
Sb	0.194 ± 0.259 (0.082)	0.128 ± 0.255 (0.042)
Te	0.041 ± 0.024 (0.037)	0.042 ± 0.031 (0.04)
Cs	0.025 ± 0.015 (0.022)	0.051 ± 0.184 (0.015)
La	0.188 ± 0.161 (0.151)	0.239 ± 0.346 (0.142)
Pr	0.029 ± 0.024 (0.019)	0.039 ± 0.066 (0.014)
Nd	0.111 ± 0.092 (0.072)	0.14 ± 0.24 (0.059)
Sm	0.027 ± 0.022 (0.019)	0.041 ± 0.06 (0.018)
Eu	0.024 ± 0.038 (0.008)	0.033 ± 0.043 (0.018)
Gd	0.0252 ± 0.0208 (0.0202)	0.0305 ± 0.0512 (0.0146)
Tb	0.0034 ± 0.0028 (0.0026)	0.0038 ± 0.0062 (0.0018)
Dy	0.0192 ± 0.0158 (0.0147)	0.0205 ± 0.0367 (0.0087)
Er	0.0098 ± 0.0075 (0.008)	0.0122 ± 0.0192 (0.0056)
Tm	0.0015 ± 0.0011 (0.0013)	0.0019 ± 0.0026 (0.0011)
Yb	0.0073 ± 0.006 (0.006)	0.011 ± 0.0168 (0.0045)
Lu	0.0016 ± 0.001 (0.0016)	0.0019 ± 0.0025 (0.0009)
Hf	0.1068 ± 0.1466 (0.0318)	0.1427 ± 0.1643 (0.0823)
Ta	0.0193 ± 0.0311 (0.0079)	0.0189 ± 0.0322 (0.0079)
Tl	0.0082 ± 0.0074 (0.0059)	0.0069 ± 0.0083 (0.0034)
Pb	2.72 ± 1.74 (2.12)	11 ± 13.39 (5.2)
Bi	0.0366 ± 0.0374 (0.0196)	0.0338 ± 0.0347 (0.0242)

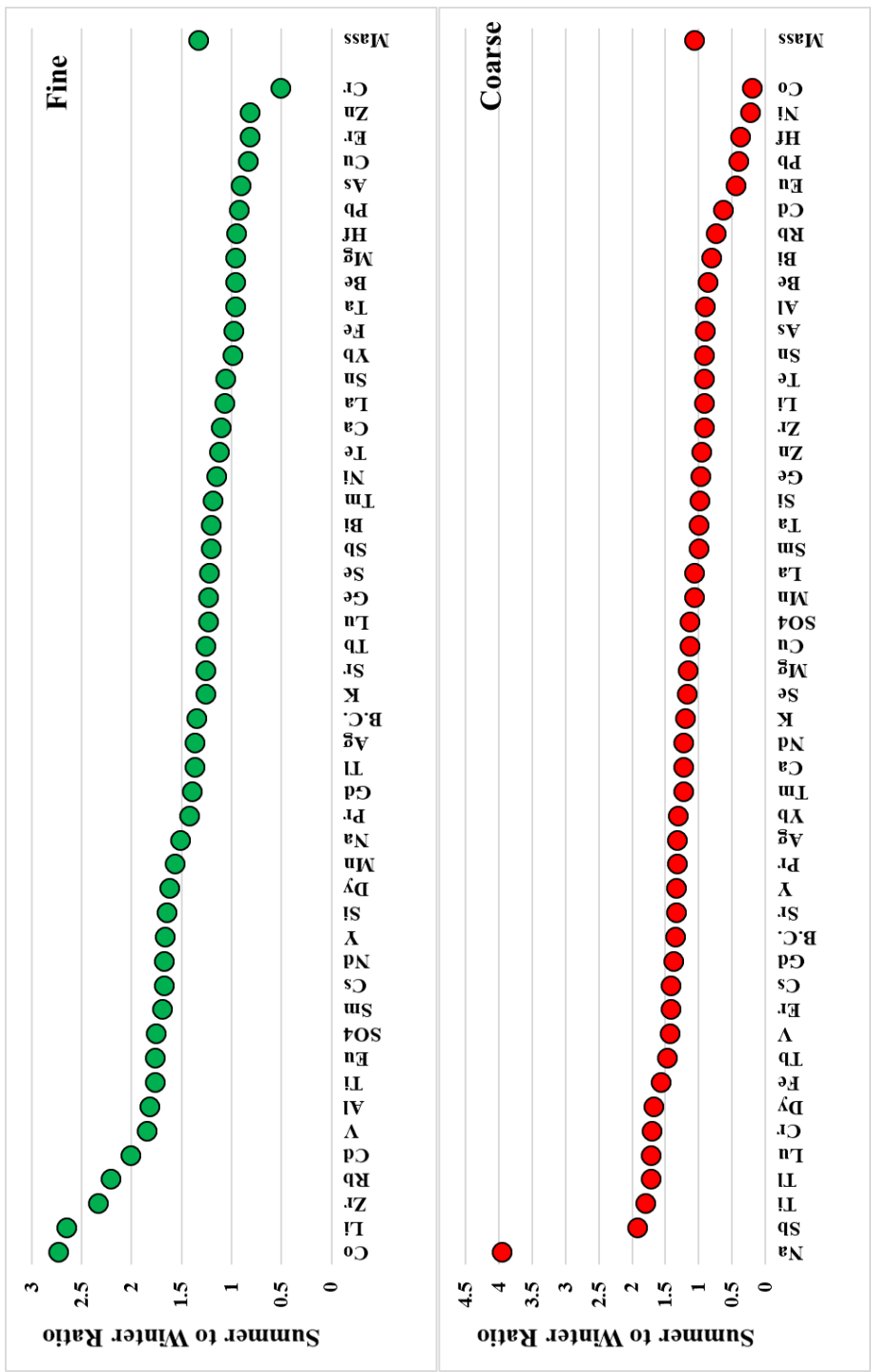


Figure 4.27 Summer-to-winter median ratios of elements in fine and coarse fractions

Monthly median concentrations of selected crustal elements in fine and coarse fractions are depicted in Figure 4.28. Concentrations of these elements and other crustal elements that are not shown in Figure 4.28 are also higher in summer season. Higher concentrations of crustal elements in summer season is not unique for this work, but observed in most studies in the Eastern Mediterranean (Koçak et al., 2007a; Mamane et al., 2008; Samara et al., 2005). Crustal particles can reach to the sampling point either after a long range transport from desert areas in Middle East, Arabic Peninsula and Sahara, or they can be resuspended from local soil by wind action. Both of these mechanism favors higher concentrations in summer. Higher concentrations of particles transported from distant sources are expected in summer season due to more effective wet scavenging of particles during winter, as discussed previously. Concentrations of particles resuspended from local soil surfaces are also expected to be higher in summer, because in summer soil is dry and resuspension occurs at relatively low wind speeds. However, in winter, soil is mud or ice covered, which makes resuspension more difficult.

Anthropogenic elements depicted two different seasonal variation patterns, which are shown in Figure 4.29 and Figure 4.30. Species like Mn, K, V, Ti, Sb Cd, SO_4^{2-} and B.C. show well – defined monthly variation patterns with higher concentrations in summer months. However, elements, such as Sn, Ag, Se, Zn, Ge, Cu do not show a very clear monthly variation. As pointed earlier in this section, these different monthly patterns for different element can be explained different distances between their sources and receptor. Elements that have high concentrations in summer season are probably transported from distant source areas and they are scavenged more effectively during winter, with more frequent encounter with rain during their several-days-long transport. The second group elements on the other hand are probably emitted at a closer distance to Torul and thus are not scavenged as effectively during their shorter travel to station in winter season. Short distance to station refers to sources in Ukraine, Georgia and Eastern Turkey. Long distance, on the other hand, refers to sources in Balkan countries and further away.

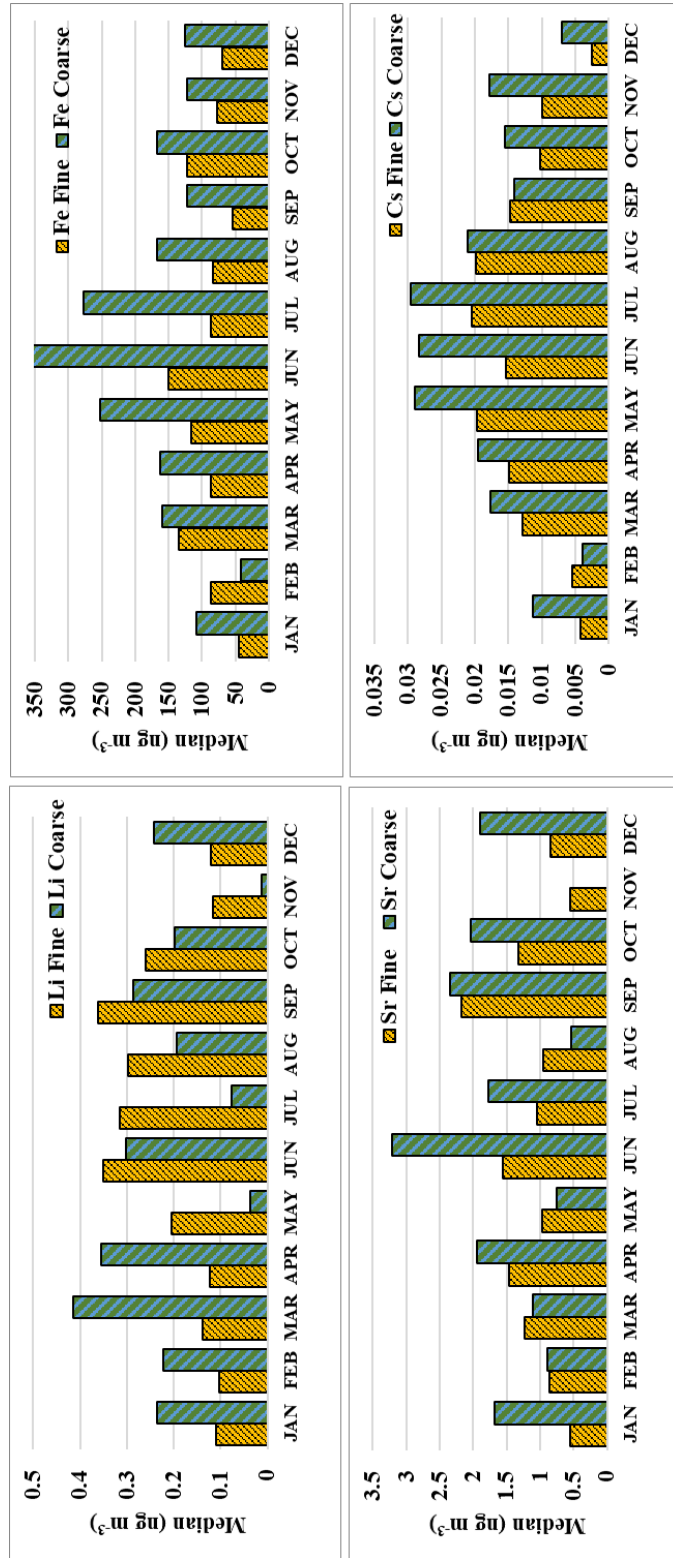


Figure 4.28 Monthly variation in concentrations of selected crustal elements at Eastern Black Sea

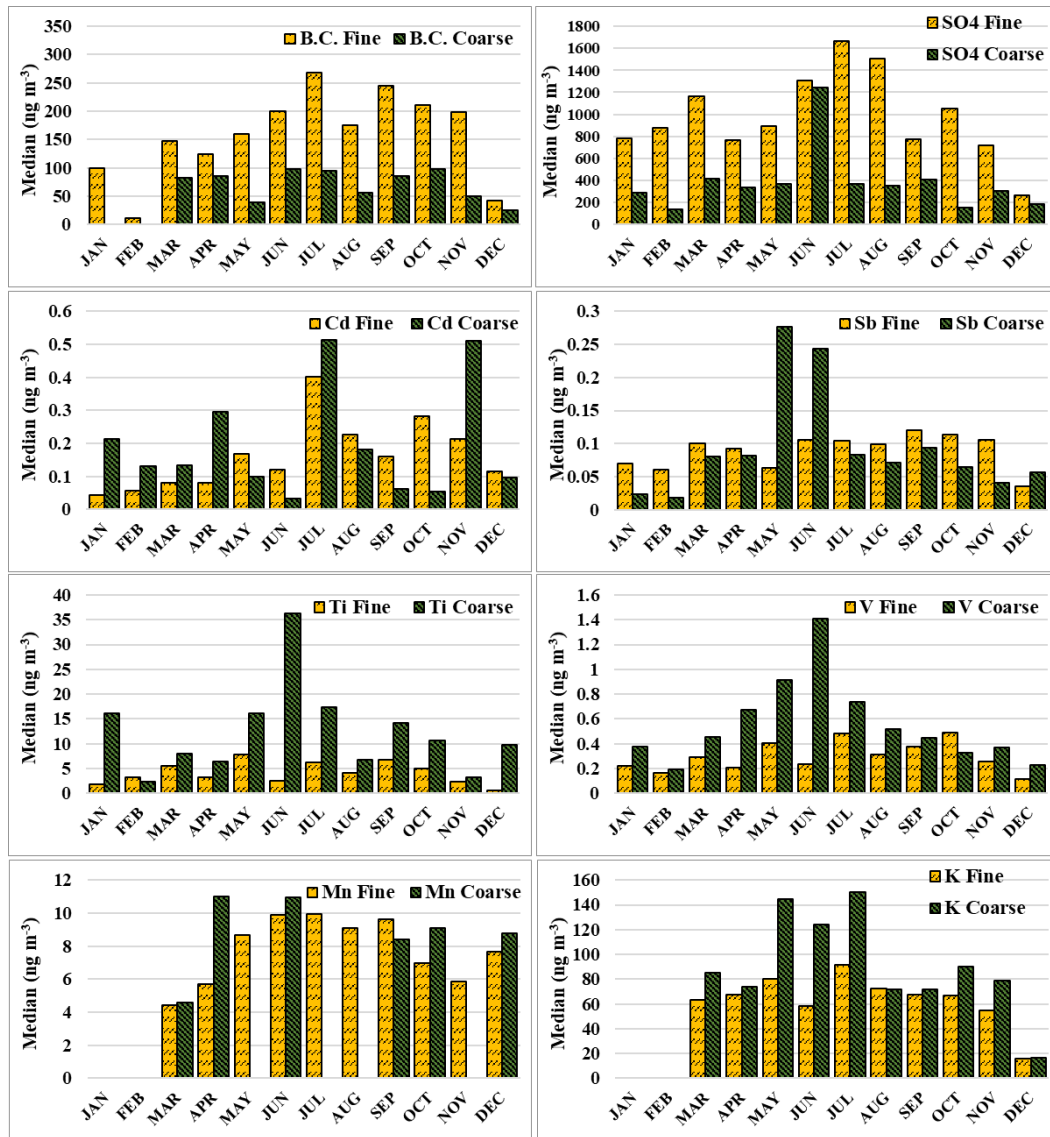


Figure 4.29 Anthropogenic elements with higher concentrations in summer

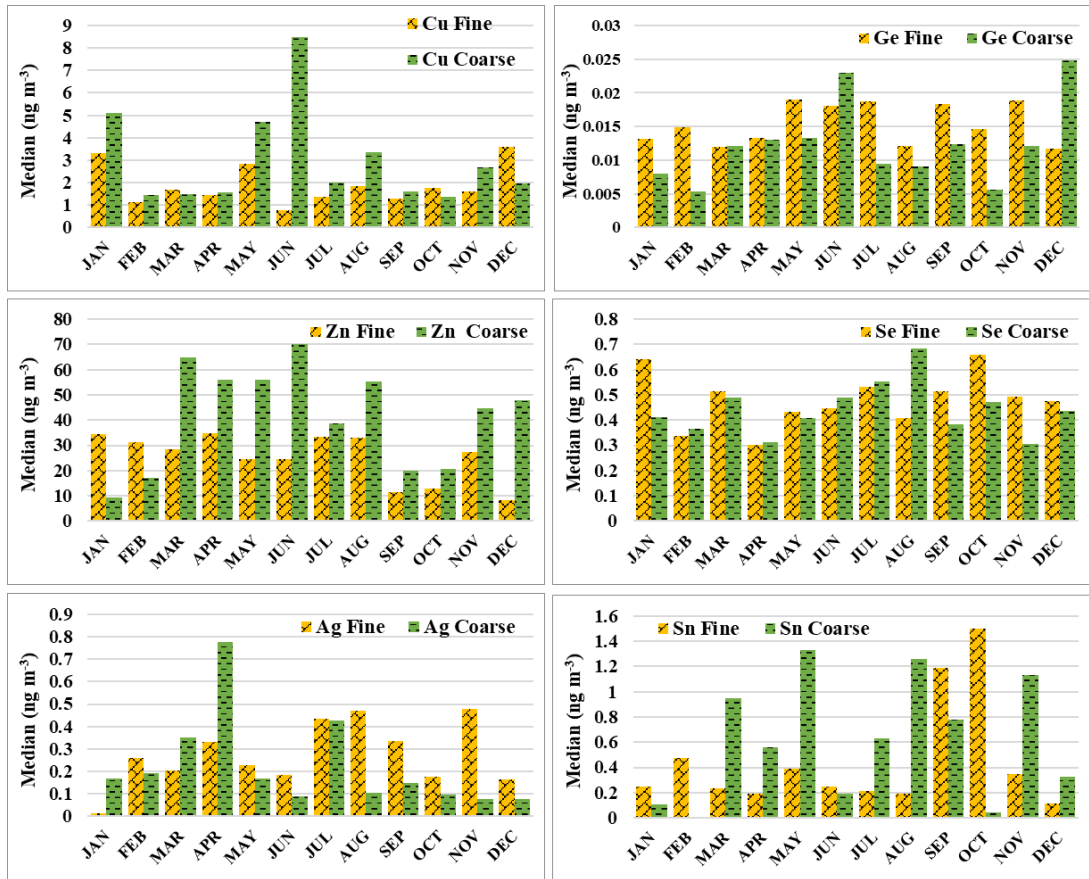


Figure 4.30 Anthropogenic elements, which do not show a well-defined seasonal variation

4.6 Source Apportionment

4.6.1 Enrichment Factor

Calculation of EF_c values of elements or preparing $EF_c - Al$ diagrams are first steps in source apportionment studies. The question that is answered by EF_c calculations is “how much is the contribution of crustal material on measured concentrations of elements”. This is an important question, because crustal material is a ubiquitous component of aerosol population in most parts of the world. Enrichment factors is in use since 70s (; Duce et al., 1975; Zoller et al., 1974), but it did not lose its charm due to its simplicity and usefulness.

Enrichment factor is a double normalization technique, which is given by the following equation:

$$EF_c = \frac{\left(\frac{C_x}{C_{Al}}\right)_{sample}}{\left(\frac{C_x}{C_{Al}}\right)_{soil}} \quad \text{Equation 4.1}$$

Where, $(C_x/C_{Al})_{sample}$ is the ratios of concentration of the test element to Al concentration in sample and $(C_x/C_{Al})_{soil}$ is the corresponding ratio in average crustal material. There are two important points to highlight in EF_c calculations. (1) Al is used as marker (tracer) for crustal material, because it does not have any source other than soil (it is emitted from Al smelters, but the effect is very local) and it can be easily measured by most analytical techniques. In principle, other lithophilic elements like Fe, Sc, Co can also be used as crustal marker, when Al data is not available. (2) Global soil compilations are used to compute $(C_x/C_{Al})_{soil}$ ratio. There are various compilations of crustal composition (Mason and Moore, 1966; Mason and Moore, 1982; Vinogradov 1959; Taylor 1964; Turekian and Wedepohl, 1961). Among these, Mason (1966) is the most frequently used compilation. The main source of uncertainty in EF_c is the potential difference between global compilations and actual soil affecting the

receptor. To avoid this problem, EF_c values < 10 are not considered as significant enrichment.

As the formula given above implies, values of EF_c close to unity indicates that there is a strong contribution of crustal material on measured concentrations of that particular element. Values of $EF_c > 10$, on the other hand indicates that contribution of crustal material is limited and there other sources contributing to measured concentration of that element. Please note that $EF_c > 10$ indicates the contribution of a non-crustal source, but that source is not necessarily anthropogenic. For example, in most data sets Na has EF_c values varying between 30 – 50, which is due to sea salt contribution to concentrations of Na and not due to presence of an anthropogenic source.

Enrichments of elements in PM_{10} and $PM_{2.5}$ samples are given in Figure 4.31. Elements with crustal sources, from Na to Li in Figure 4.31 have all $EF_{cs} < 10$. These elements are considered as non-enriched and their concentrations at Torul and Eastern Black Sea region is accounted by soil particles in the atmosphere. Remaining elements, from Ni, all the way to Se have enrichment factors varying between 20 for Ni and 7000 for Se. Concentrations of all of these elements in the second group are contributed by non-crustal sources, most of which is probably anthropogenic.

Another point that is clearly visible in the figure is higher enrichments of elements in fine fraction ($PM_{2.5}$). There is not a significant difference between enrichments of crustal elements (elements with $EF_c < 10$) in coarse and fine fractions. However, elements with $EF_c > 10$ are all more enriched in $PM_{2.5}$ fraction. Please note that soil does not contribute much to concentrations of these elements, which means that their concentrations are independent of concentration of crustal material in samples. Their higher enrichment in $PM_{2.5}$ fraction is due to variation in Al concentrations, but not due to variation in their own concentration. Dust particles with which Al is associated with are coarse. Their mass median diameter in the Mediterranean region is found to be $3.6 \mu\text{m}$ (Kuloğlu and Tuncel, 2005). Because of such coarse – fine partitioning, Al concentration is high in PM_{10} fraction, but low in $PM_{2.5}$ fraction, which results in higher enrichments of anthropogenic elements in $PM_{2.5}$ fraction.

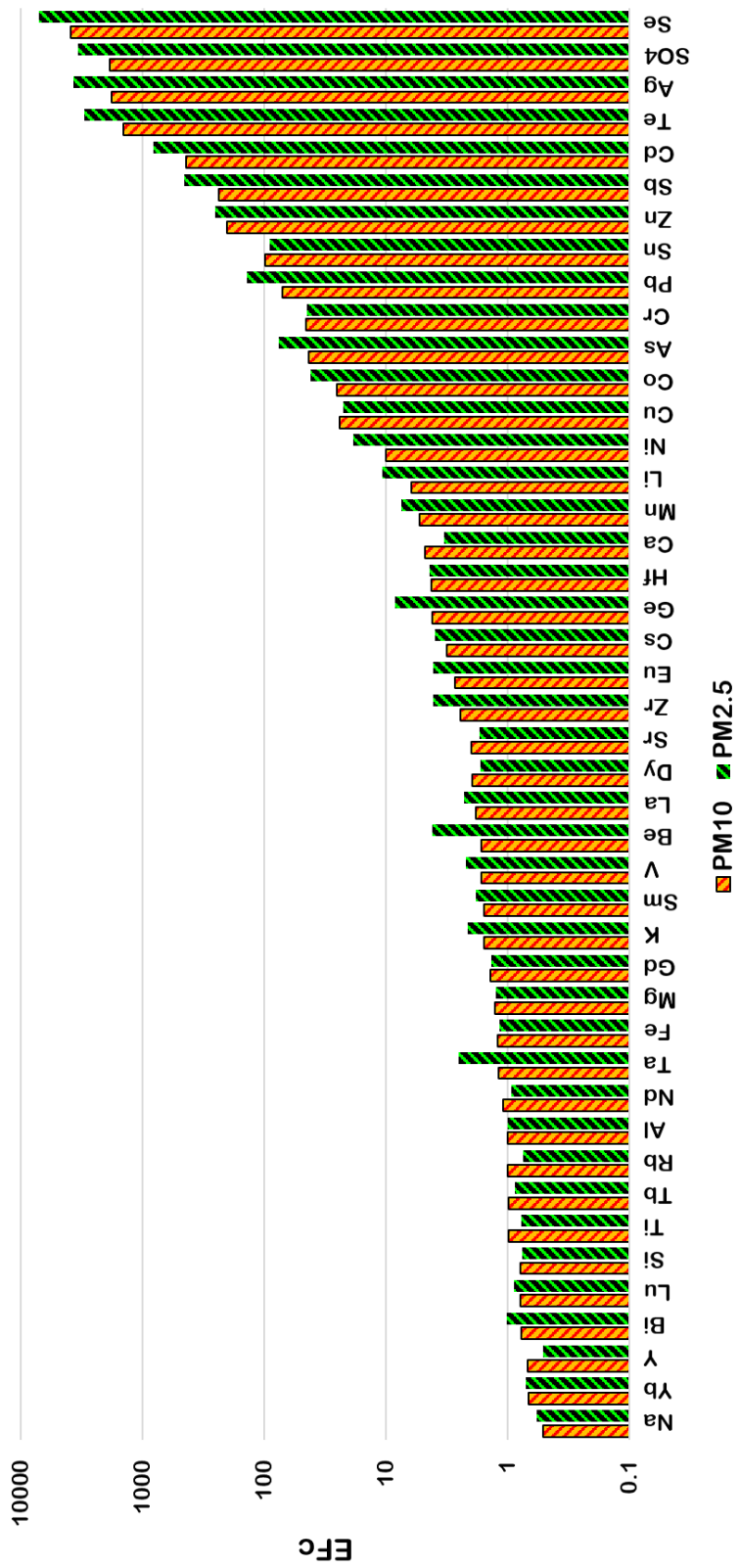


Figure 4.31 Crustal enrichment factors of elements in PM₁₀ and PM_{2.5} fractions

Soil-related elements do not show the similar pattern of higher enrichment in fine fraction because, unlike pollution-derived elements, their concentrations go up and down together with Al concentration. Elements like V, Mn, Cr, Ni, and K have moderate EF_c values, because although their major sources are anthropogenic (residual oil combustion for V and Ni, iron and steel industry for Cr and Mn) their concentrations in lithosphere is high and thus dust contribution to their concentrations is significant.

It should be noted that more or less similar enrichment pattern is also observed in very remote locations, such as islands in the middle of ocean (Arimoto et al., 1987; Parrington and Zoller, 1984), Arctic (Halter et al., 1985; Smirnov et al., 1998) and Antarctic (Tuncel et al., 1989). Although enrichment of calcophilic elements in urban and rural areas is due to anthropogenic emissions, the same elements are enriched in remote aerosol due to high-temperature natural sources, particularly volcanism.

Since soil particles in atmosphere is an abundant component of atmospheric aerosol, it contributes to measured concentrations of most elements. For lithophilic elements crustal material accounts for almost 100% of their concentrations. For remaining elements, soil contribution changes. How much crustal material affects concentrations of elements can be best understood using “ $EF_c - Al$ ” diagrams, where crustal enrichment factors of elements are plotted against Al concentration.

Since concentrations of lithophilic elements, for which crustal material is the only source, follow Al concentrations, their EF_c s do not change with increasing Al concentration. Some examples of this pattern is shown in Figure 4.32 for Si, Fe and Ca. There are two important points in Figure 4.32. At very low Al concentrations ($C_{Al} < 10 - 20 \text{ ng m}^{-3}$), $EF_{c, Fe}$ decrease with increasing Al concentration, which is typical pattern for elements that has non-crustal sources. However, At $C_{Al} > 10 - 20 \text{ ng m}^{-3}$, $EF_{c, Fe}$ does not change with Al concentration any more, which is a typical pattern for lithophilic elements. Main source of Fe in atmosphere is crustal aerosol; however Fe is also emitted from iron and steel industry. Generally, contribution of soil particles on aerosol Fe concentration is so high that, its anthropogenic source is masked. The figure demonstrate that anthropogenic Fe becomes visible only when Al concentration (dust

concentration) is very low ($< 10 - 20 \text{ ng m}^{-3}$). The second point in the figure, worth noting is that non unity EF_c for Ca. Enrichment factors for Ca does not change with increasing Al concentration, as expected from a lithophilic element. However, that line defined by $EF_c \text{ Ca}$ is not on $EF_c = 1.0$ which is expected from crustal elements. EF_c vs Al lines for Si and Fe are approximately on $EF_c = 1.0$ line, but that of Ca is approximately on line $EF_c = 5$. This deviation from standard behavior is due to difference between Ca concentration in actual dust particles intercepted at Torul station and Ca concentration in Masons (1964) global soil compilation. This is not surprising, because calcareous nature of soil in Eastern Mediterranean basin is well documented (Güllü et al., 1998; Öztürk et al., 2012).

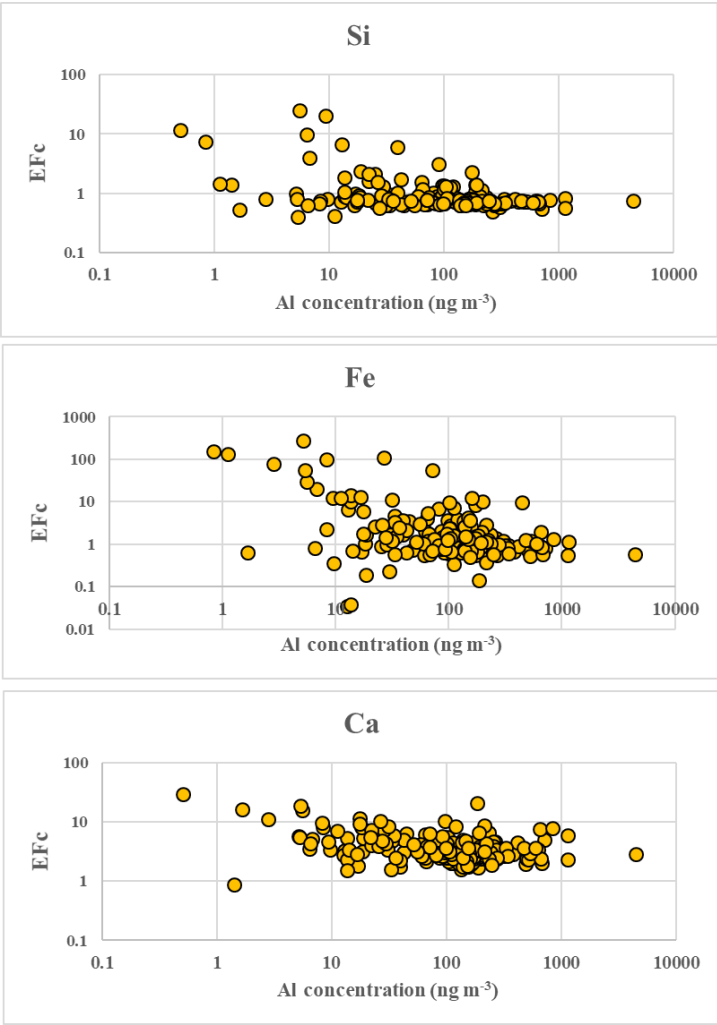


Figure 4.32 EF_c -Al diagram for crustal elements

Concentrations of elements with anthropogenic sources are independent of Al concentration. Thus their EF_c s decrease with increasing Al concentration. This pattern is depicted in Figure 4.33 for SO_4^{2-} , Cd, Zn, and As. For all these elements contribution of crustal material is negligible, because their concentrations continue to decrease with Al concentration even at very high Al levels. Most of the calcophilic elements measured in this work depicted very similar behavior with SO_4^{2-} , Cd, Zn, and As.

A third group of elements including Cr, Ni, K, Mg, Ti, Na and Mn depicted different pattern in their EF_c vs Al concentration plots. These are separated as a group, because although crustal aerosol have significant contribution to their atmospheric concentrations (because their concentration in Earth's crust is high), but they also have non-crustal sources. Plots of EF_c vs Al for these elements are given in Figure 4.34. The general pattern for these elements is a decrease in their EF_c s with increasing Al concentration up to a threshold Al concentration and following crustal pattern after that threshold Al level. Threshold Al concentration, beyond which these elements show crustal pattern changes from one element to another depending on the magnitude of crustal contribution to their atmospheric levels.

As can be seen from the Figure 4.34, the patterns are different for different elements in this group. The Plot for Cr shows that there is very little crustal component in Cr levels measured at Torul. Obviously most of the measured Cr is anthropogenic. In an earlier aerosol study in the Black Sea, Hacısalıhoğlu et al. (1992) measured high Cr and Mn concentrations and attributed it to transport of particles from metallurgical industries in Russia. Interestingly, Mn and Ni also depicts entirely anthropogenic pattern in Figure 4.34.

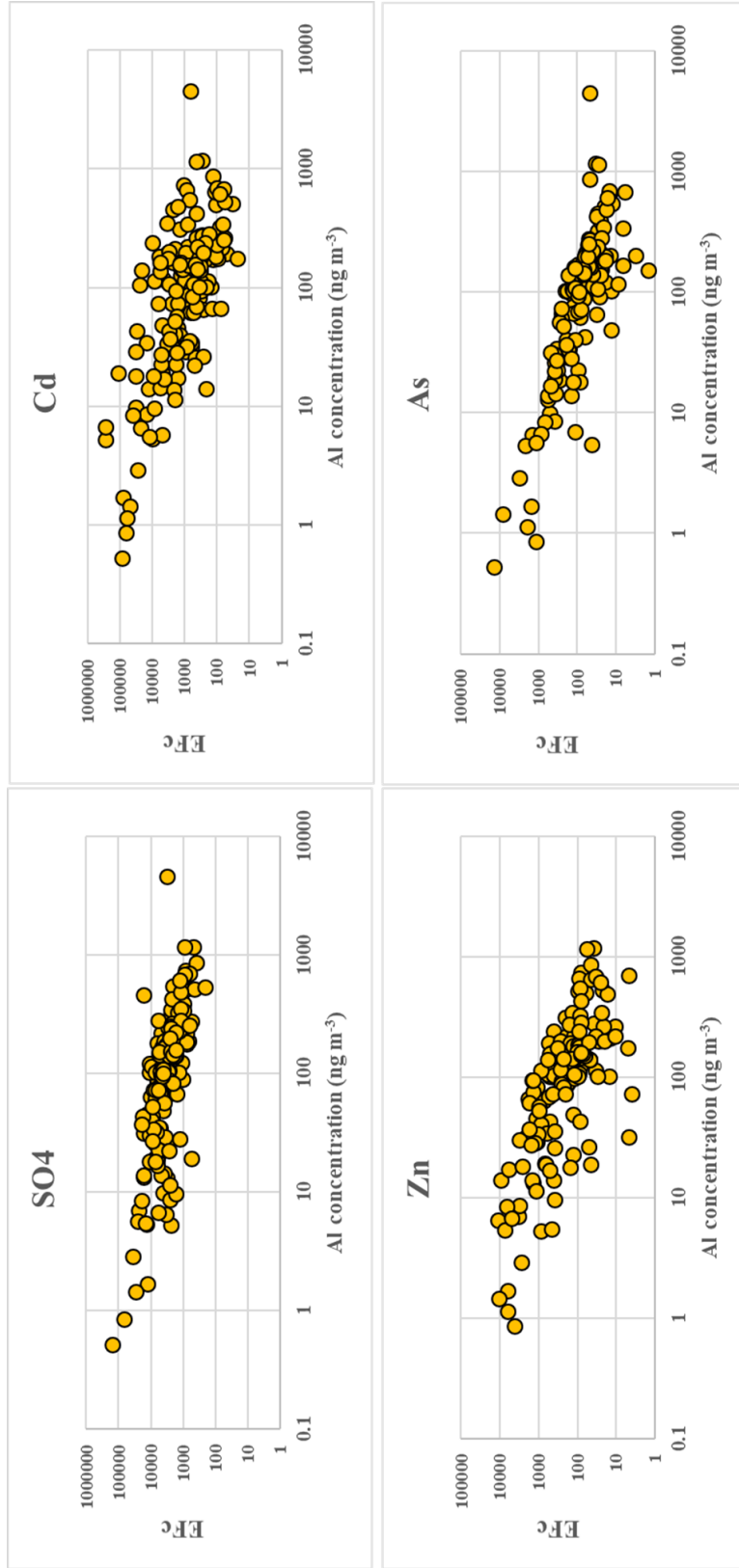


Figure 4.33 EF_c -Al diagram of anthropogenic elements

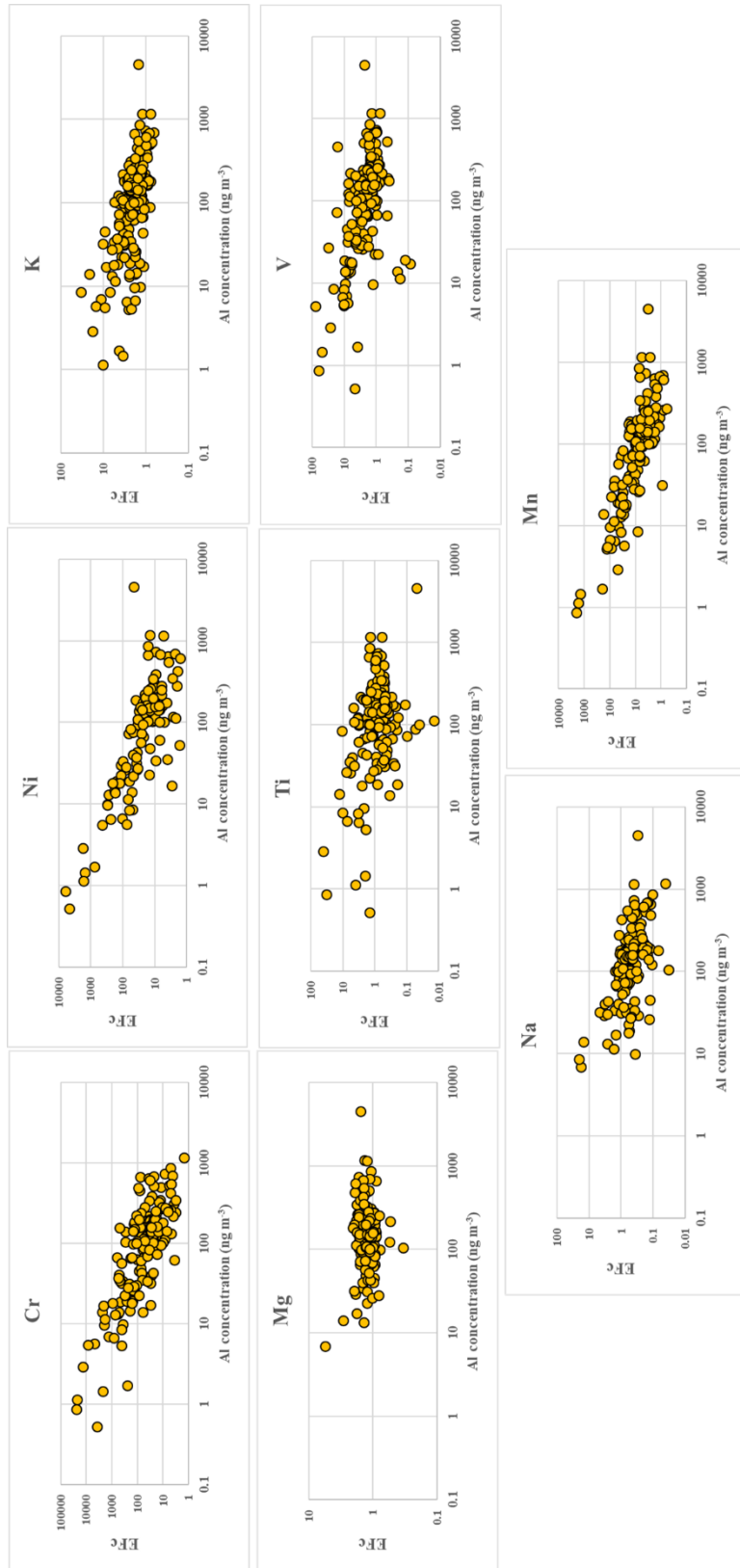


Figure 4.34 EF_c -Al diagram of elements with mixed origin

The $EF_c - Al$ diagrams for Na and Mg depict a crustal pattern except for low Al concentrations. At receptors not too far from sea, these elements show a non-crustal pattern due to significant sea salt contribution to their concentrations. However at Torul Na and Mg are mostly crustal due to 75 km distance to Black Sea coast and high mountains in between. Vanadium and K have non-crustal pattern at Al concentration $< 100 \text{ ng m}^{-3}$ and have typical crustal pattern at higher Al concentrations. This behavior in their $EF_c - Al$ diagrams is due to residual oil combustion source for V (Peltier et al., 2010) and biomass burning source for K (Lee et al., 2016; Urban et al., 2012).

4.6.2 Contribution of Forest Fires

Particles emitted from forest fires are important component of atmospheric particles in certain places where forest fires are common. For example boreal forest fires in Canada is shown to be transported all the way to Europe and affect aerosol composition in rural locations (Chen et al., 2009; Hyer et al., 2007; Strode et al., 2012). Turkey is situated in a geography where forest fires are very common, due to very dry summer season. Forest fires are frequent not only in Turkey, but also at other Balkan countries, such as Bulgaria, Romania and Western Parts of Ukraine. With such geographical distribution of forest fires we can expect that the particles emitted from forest fires can be an important component of Eastern Black Sea aerosol and can affect its chemical composition. Tokgöz (2013) detected such effect of forest fire particles. In this part of the manuscript, the efforts are to detect particles emitted from forest fires and their impact on chemical composition of aerosol population in the Eastern Black Sea is discussed.

Particles emitted from forest fires are generally carbonaceous in nature. Since particle-bound organics are not measured in this work, we are very limited in forest fire markers that can be used to differentiate between forest fire particles from others. The only inorganic species that is being used as a marker for particles emitted from forest fires is potassium. Potassium is used to identify forest-fire related particles in number of studies (Pio et al., 2007; Poirot et al., 2004; Quennehen et al., 2012).

In this study, K was used as a marker of biogenic emissions. In the first step, the days with K concentration above average were selected. Please note that since K data in data set is lognormally distributed average concentration corresponds to highest 30 – 40% of the data. Emissions from forest fires is not the main K source in the atmosphere. Potassium is a crustal element and most of the K measured in air comes from soil particles. Because of this, enrichment factor of K was used instead of its concentration to identify days in which samples were affected from forest fire emissions. Time series plots of both K concentration and its crustal enrichment factor are depicted in Figure 4.35.

Seven days with EFC of K is > 10 were identified. These were; November 24, 2011, November 29 and 30, 2011, August 27, 2011 and December 3, 4, 5, 2012. In all of these days EFC value of K was > 10 , which indicates contribution of non-crustal sources to measured K concentrations. To ensure that excess K in those days come from forest fires, we calculated back trajectories in those seven days and compiled geographic locations of every single forest fire in those days and five days backwards in time (because trajectories were calculated five days backwards in time). Forest fire data were downloaded from MODIS Aqua and Terra satellites, which detect and show forest fires in whole world, every day. Trajectories along with the locations of the forest fires during K episode days are depicted in Figure 4.36.

It is very clear from the figure that the region in which Torul station is located is surrounded by forest fires in more or less all directions. From trajectories, it can be seen that Eastern Black Sea is affected from fires in Ukraine, Russia and eastern parts of Turkey. This generalization has to be made with caution, because forest fire signature were detected in only seven days out of approximately 350 days. Conclusion that bases on better statistics with longer term sampling would be more reliable.

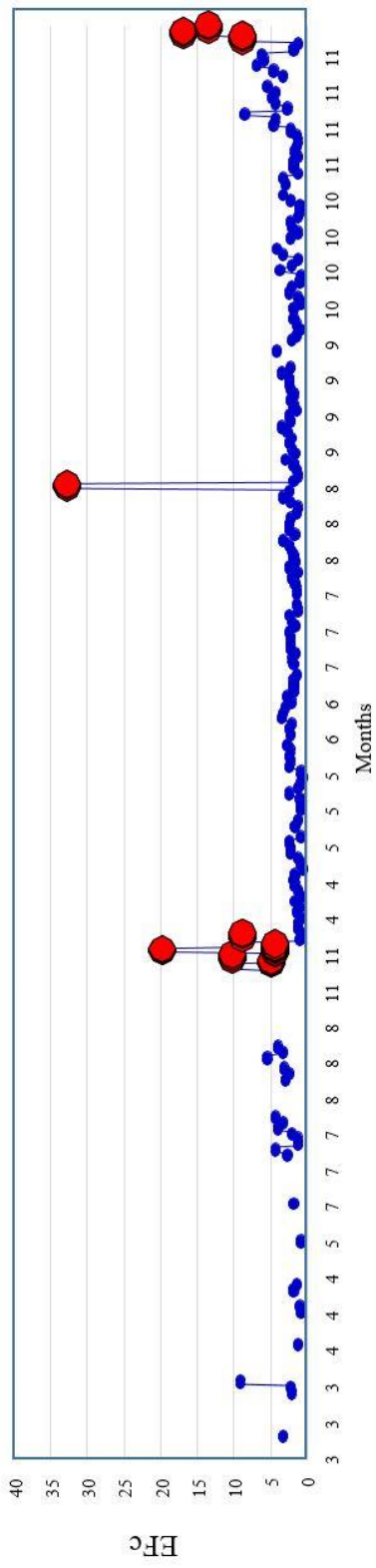
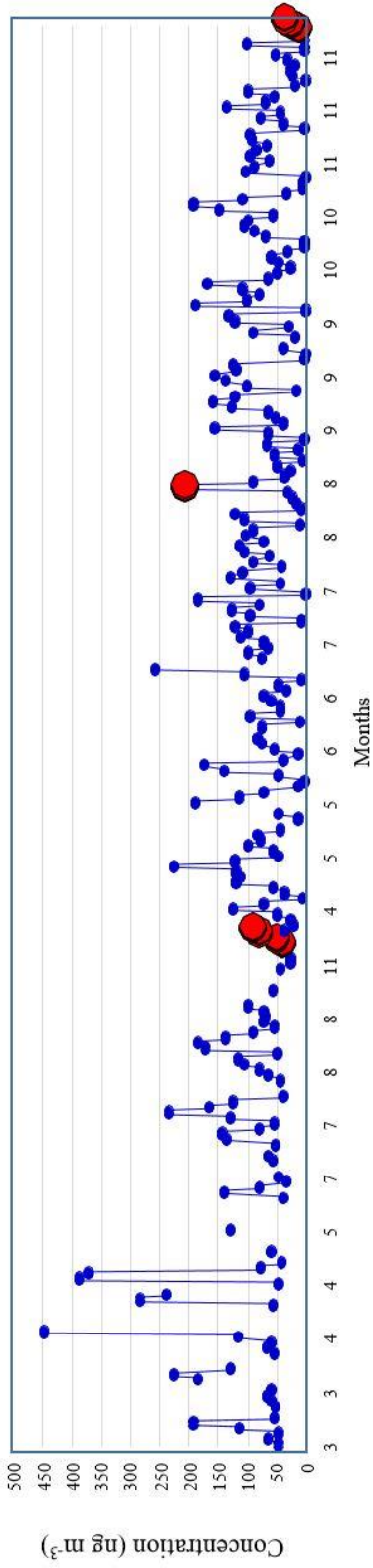


Figure 4.35 Time series plots of K concentration and enrichment factor

Average concentrations of K in PM_{2.5} fraction is $91 \pm 142 \text{ ng m}^{-3}$ and average EFC for K is 2.94, which is a typical enrichment factor for crustal elements. When these averages were calculated excluding forest fire days, average K concentration becomes $90 \pm 143 \text{ ng m}^{-3}$ and average EFC became 2.1. Obviously, forest fires does not significantly affect mean K concentration at Eastern Black Sea region. However, forest fires accounted for 18% increase in K enrichment factor (EFC). In the data set as will be discussed in coming sections EFC of K was 2.94. Enrichment factor decreased to 2.40 when it is calculated excluding forest fire days. Average K concentration is not affected significantly from forest fires, not only because there were only seven forest fire days during the sampling period, but also K concentrations in those fire days was not the highest K concentrations in data set. Potassium is a major component in the aluminosilicate structure of soil. Most of the high K concentrations in data set corresponds to dust episodes with high concentrations of other lithophilic elements as well.

Contribution of fires to PM_{2.5} mass concentrations was also investigated. There were no statistically significant difference between PM_{2.5} concentrations calculated with and without forest fire days. Obviously, forest fires does not affect composition of Eastern Mediterranean aerosol significantly.

Other elements that may have significantly different concentrations during forest fire days were also investigated. For this, ratios of concentrations and enrichment factors of elements calculated for days, which were identified as forest fire days, based on K data, is compared with their concentrations and enrichment factors calculated for the remainder of the sampling period. The ratios are depicted in Figure 4.37. For most of the element that are measured in this study, concentrations during forest fire days are lower than corresponding concentrations measured in non-fire period (concentration ratios <1). However, few elements depicted higher concentrations and enrichment factors during forest fire days with statistically significance better than 95%. The highest ratio was found by Cr, which is followed by Sn and Na. These three elements have factors of 2.6, 2.3, and 1.8 higher concentrations during forest fire days. There are few more elements, like Cu, Zn, Se, Ta and Bi that have 10% - 50% higher

concentrations during fire days. These elements can be used as tracers of forest fire emission. However, it should also be noted that during entire sampling period, station is impacted from forest fires in only seven days. Concentrations of these elements are high either they are mobilized from biota or soil, or both by forest fires, or air masses that brings forest fire emissions, by coincidence passes over anthropogenic emission areas and picks up these elements. It is difficult to differentiate between two mechanisms with only seven samples. This issue will be clarify in the future studies when more samples that arte affected from forest fire emissions will be collected.

Contribution of fires to $PM_{2.5}$ mass concentrations was investigated. There were no statistically significant difference between $PM_{2.5}$ concentrations calculated with and without forest fire days. All these suggest that, forest fires does not affect composition and $PM_{2.5}$ mass concentrations of Eastern Mediterranean aerosol population significantly.

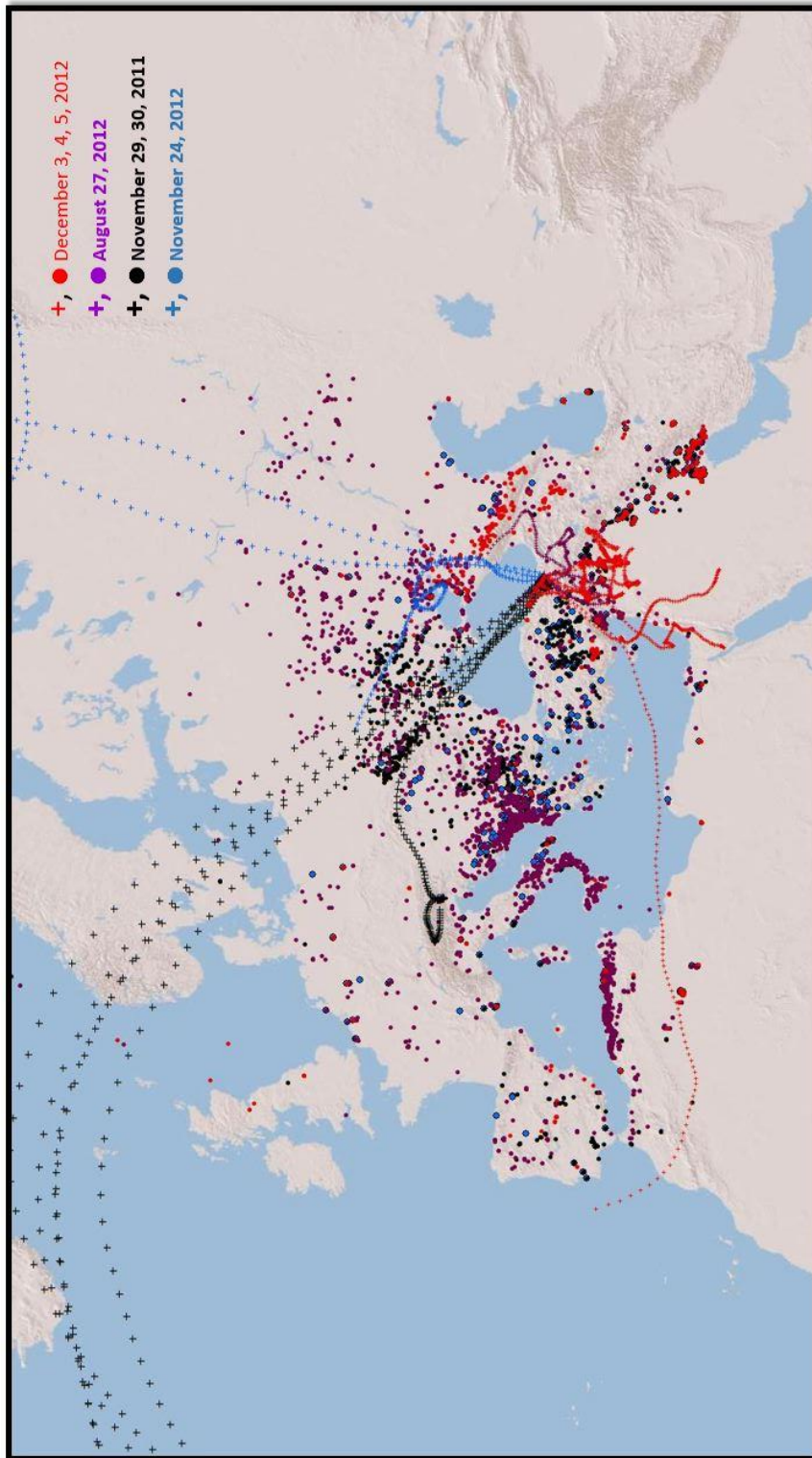


Figure 4.36 Trajectories and locations of forest fires during K episode days

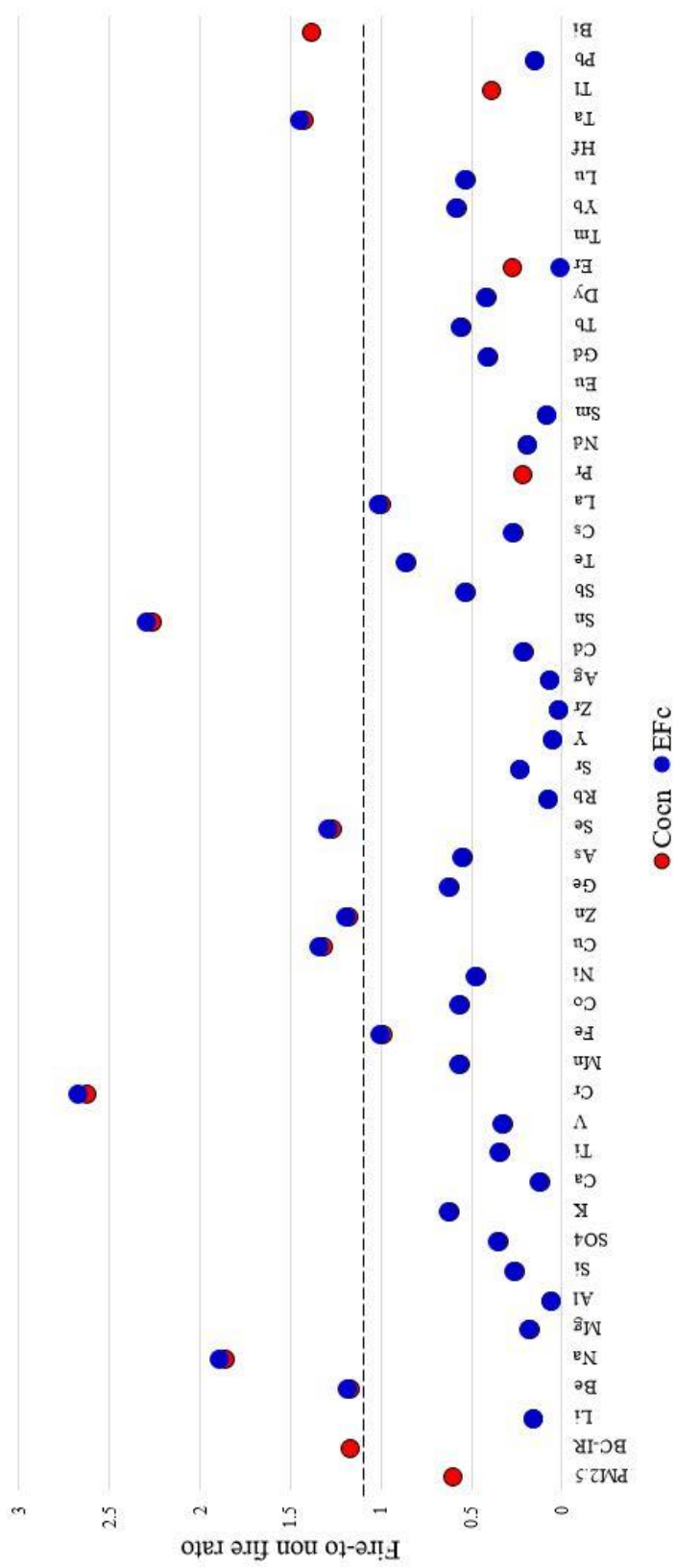


Figure 4.37 Fire day – to – non fire day ratios of concentrations and enrichment factors of elements

4.6.3 Dust Transport to the Eastern Black Sea Region

Mineral dust associated with dust intrusions may be another factor causing episodic changes in crustal species. To identify a mineral dust episodes, the days with Al and Si concentrations > Average were selected. Please note that these elements have right-skewed Frequency distributions. In right-skewed distributions, average corresponds the highest 30% - 40% of data.

Having high Al and Si concentrations in a sample does not necessarily means that it is impacted by desert dust. Crustal material resuspended from local soil or transported from non-desert regions may also result in high Al and Si concentration in that sample. Because of this desert source for observed high Al and Si must be confirmed by other means as well. Five different tools for confirmation were used:

- Dream model output
- OMI Aerosol index (AI)
- Modis Aerosol optical depth (AOD)
- Back trajectories
- Satellite pictures

Dream is a dust forecast model operated by Barcelona Super Computing Center. The model provides dust forecasts for a region including Turkey. Since dust sources in Africa and Middle East are input to the model. Dream Dust forecasts at Torul station were be used as confirmation of presence of dust at sampling site. Dream model is widely used for similar purposes (Balis. 2012; Gerasopoulos et al., 2009; Shaw, 2008). Dream model outputs for selected dust days at Torul station is given in Figure 4.38.

Aerosol Optical Depth (AOD) (or Aerosol Optical Thickness) indicates the level at which particles in the air (aerosols) prevent light from traveling through the atmosphere. AOD is widely used for dust events (Lemmon et al., 2015; Mehta et al., 2018) MODIS AOD satellite images for selected dust days at Torul station is given in Figure 4.39.

The Aerosol Index (AI) layer indicates the presence of ultraviolet (UV)-absorbing particles in the air (aerosols) such as desert dust and soot particles in the atmosphere. The Aerosol Index layer is useful for identifying and tracking the long-range transport of volcanic ash from volcanic eruptions, smoke from wildfires or biomass burning events and dust from desert dust storms, even tracking over clouds and areas of snow and ice. AI is widely used for dust events (Deroubaix et al., 2013; Dey et al., 2004) OMI AI satellite images for selected dust days at Torul station is given in Figure 4.40.

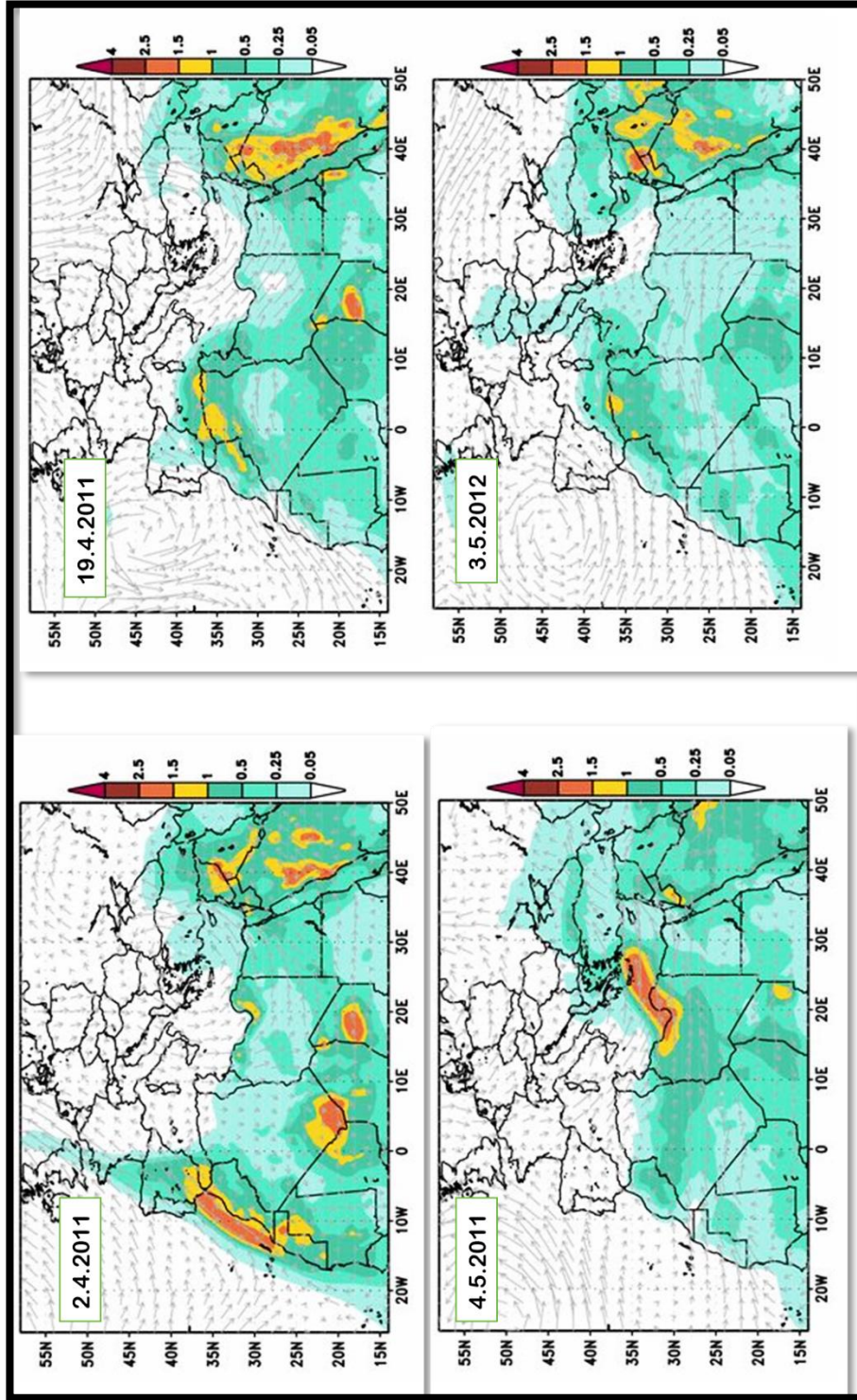


Figure 4.38 Dream model outputs for selected dust days at Torul station

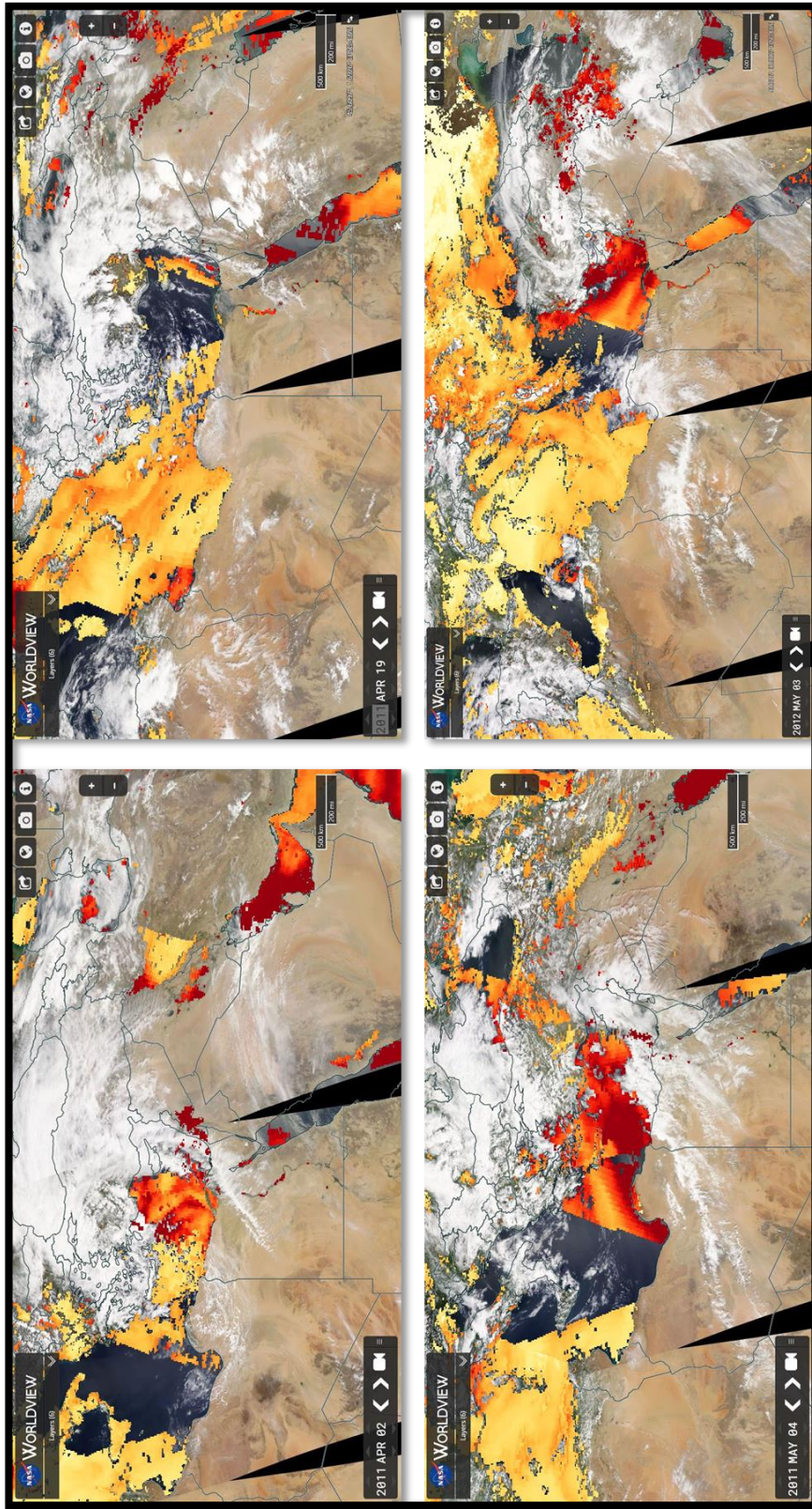


Figure 4.39 Modis optical depth satellite images for selected dust days at Torul station

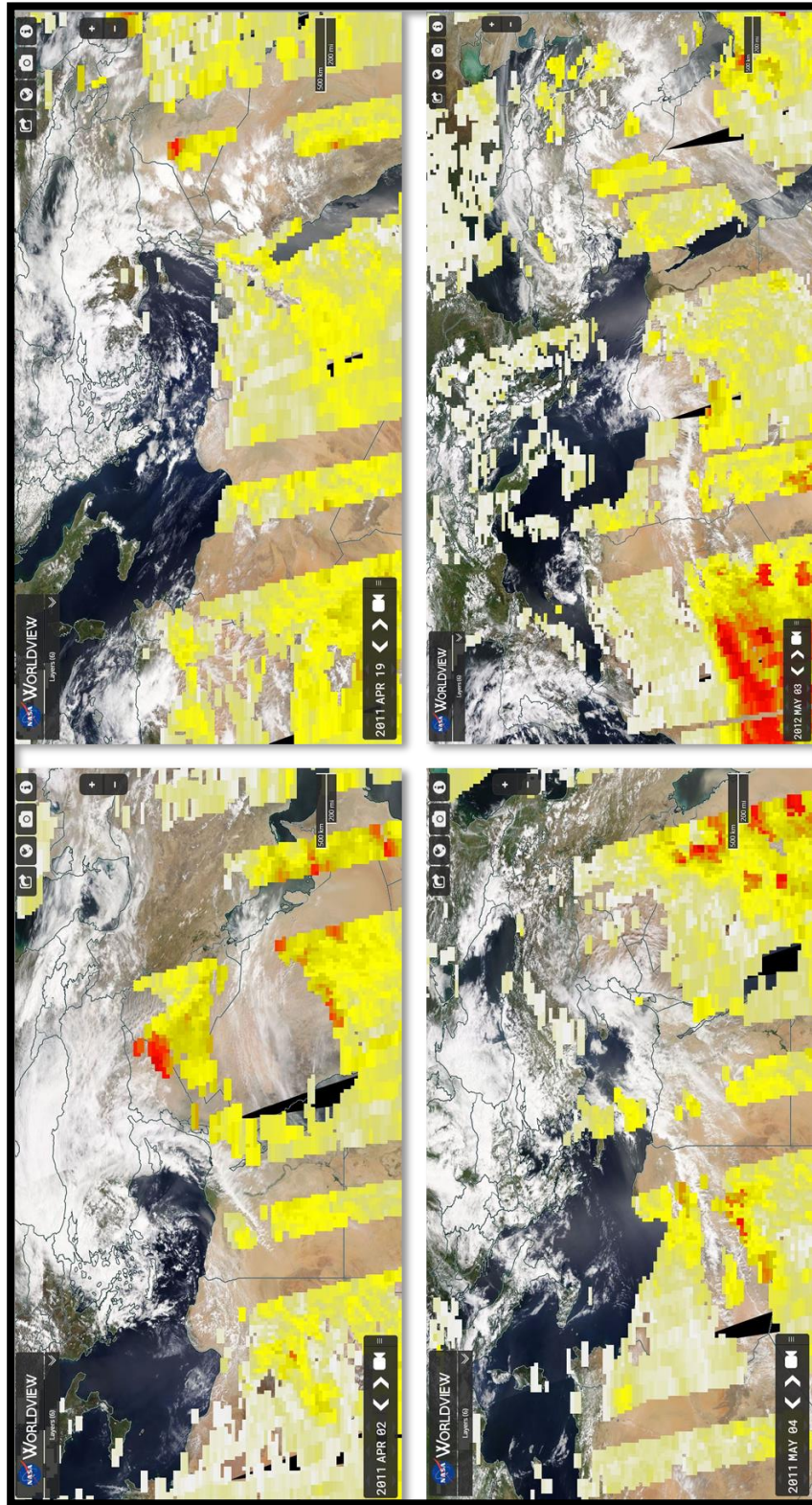


Figure 4.40 OMI Aerosol Index satellite images for selected dust days at Torul station

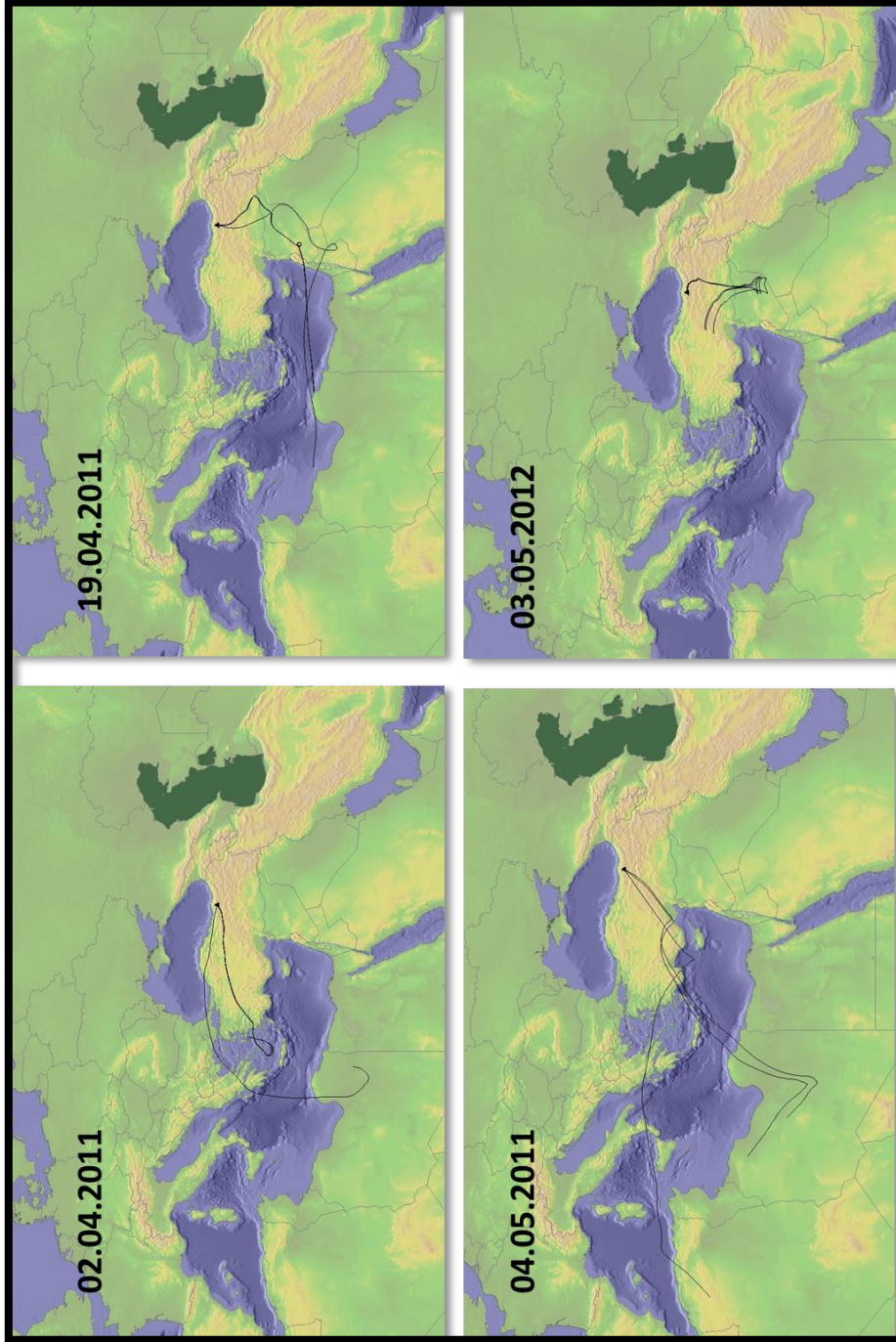


Figure 4.41 Back trajectories for selected dust days at Torul station

Based on the procedure described in previous paragraphs, 28 samples (days) were identified as dust days in the data set. April, May and July were the months with most frequent dust intrusion to Torul (see Figure 4.42). These three months accounted for 21 out of 28 dust days identified in approximately one-year-long study period (72% of dust days). Another interesting point worth noting is that Torul station is affected most from Dust transport from Middle East and Arabic Peninsula, but not much from Sahara. Only three dust days were due to dust transported from Sahara. On the other hand, 21 dust events were due to dust transported from Middle East and Arabic deserts. There were also four days in which dust appears to be transported from both Africa and Middle East. This information is fairly useful in terms of dust dynamics in the Black sea region. Please note that there are plenty of information available about dynamics of Saharan Dust in both Eastern and Western Mediterranean regions. However, information on dust dynamics in Black Sea region, particularly in the Eastern Black Sea region is scarce. We know that Saharan dust transport is most frequent in April and May (Athanasopoulou et al., 2016; Cuspilici et al., 2017; Duchi et al., 2016; Marineu et al., 2017), but similar information is not available for the Black Sea. Consequently, transport frequency information discussed in previous paragraphs is quite novel for this part of the world.

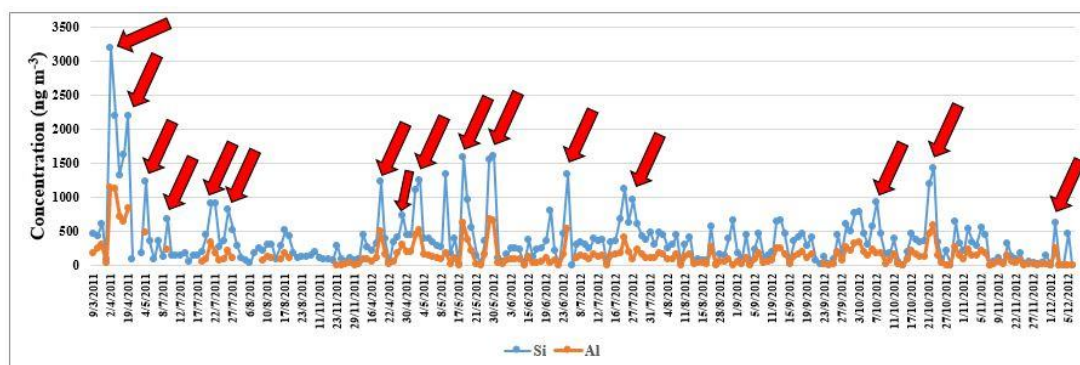


Figure 4.42 Selected Dust episode days along with Al and Si time series

Dust and non-dust concentrations of measured elements in PM_{2.5} fraction are given in Figure 4.43(a) along with dust-to-non-dust concentration ratio. The ratio varies between 5.8 Y and Pr and 0.4 for Co. Liphilic elements have the highest dust-to-non dust ratios as expected. Contribution of dust intrusion to concentrations of

elements at Torul station was also estimated by calculating mean and median concentrations of elements in all samples and excluding dust days. The difference would naturally show the contribution of dust intrusion to Torul station on concentrations of elements.

The comparison, which is shown in Figure 4.43, demonstrate that approximately 5% of PM_{2.5} mass at Torul station is accounted for by desert dust.

Average contribution of dust to lithophilic elements is 13%. For individual lithophiles, dust contribution to their concentrations vary between 30% for Er and Rb and 4% for Co and Yb. Contribution of dust to concentrations of chalcophilic elements is, on the average, 3%. This computation demonstrate that dust reaching to Torul have significant contribution on concentrations of lithophilic elements. It also has non-negligible contribution to PM_{2.5} mass (5%).

Differences in chemical compositions of dust originating from Sahara and Middle East was also attempted to identify. Please note that dust from Middle East also includes dust from Arabic Peninsula, because they are in the same transport direction relative to sampling station at Torul. Median concentrations of elements in days that were identified as Middle Eastern and Saharan Dust days are shown in Figure 4.43(b) along with concentration ratios of elements in these two data subsets. Please note that conclusions reached for individual elements are prone to high uncertainties, because there is very few samples that are affected from Saharan Dust. However, conclusions those bases on groups of element should be more realistic. The largest difference is observed for Co. Middle East-to-Saharan ratio for Co is 15, which is much higher than corresponding ratio found for other elements (the second highest ratio is 2.5). However, this ratio is not reliable, because there is only one Co datum in Saharan data subset and Co concentrations in Middle East data subset is highly variable.

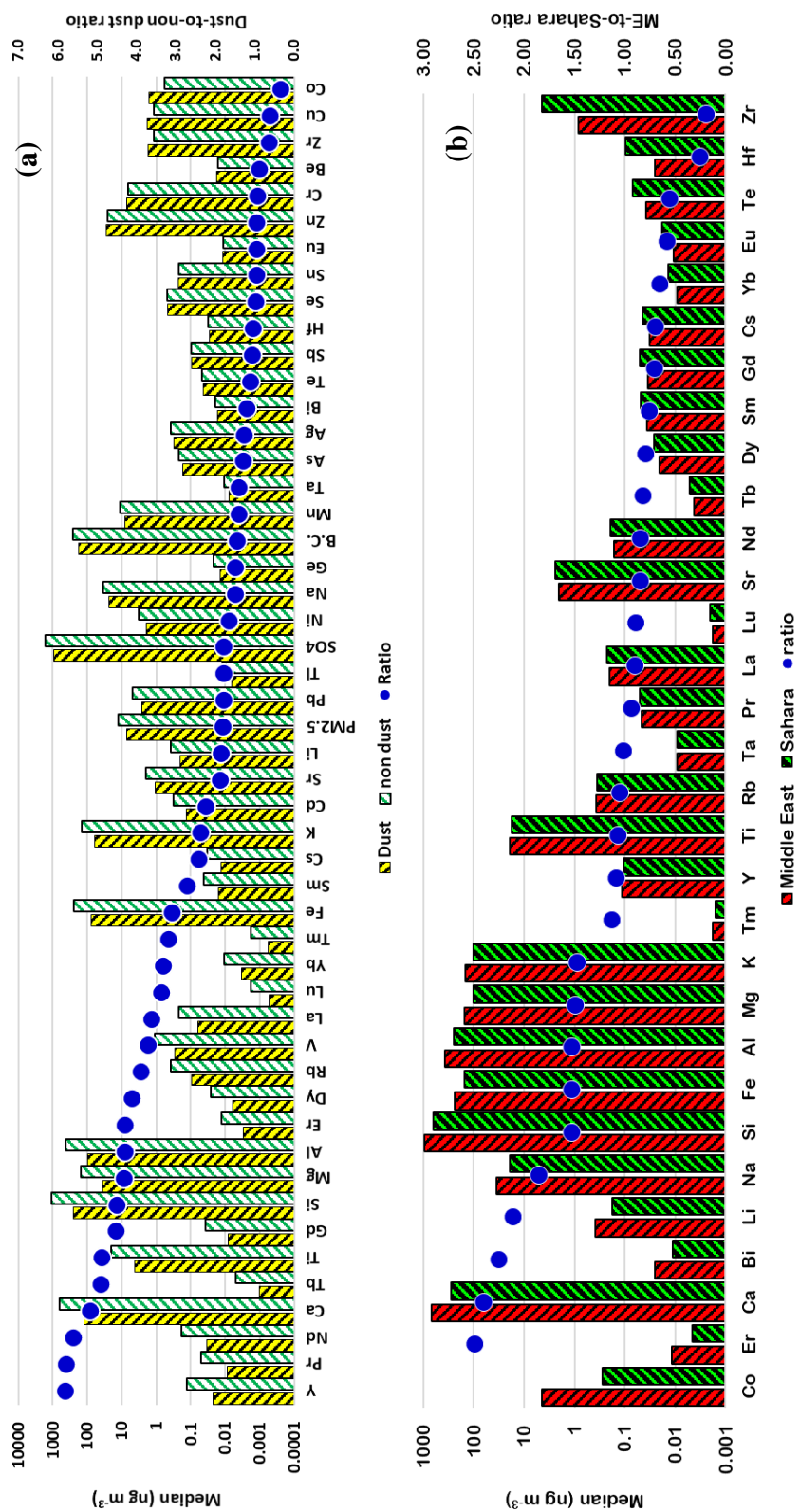


Figure 4.43 Comparison of (a) dust and non-dust days, (b) trace element composition of dust arriving from Middle East + Arabic Peninsula and Sahara

In general, concentrations of major lithophilic elements, like Ca, Li, Si, Fe, Al Na, M, K have higher concentrations in Middle East dust, whereas concentrations of trace lithophilic elements, particularly, rare earth elements have higher concentrations in Saharan Dust. As pointed before, uncertainty in these conclusions is high due to very small data subset from Sahara, but if these differences stands when Saharan Dust profile that will be generated in stations on the Mediterranean coast where Saharan Dust incursions is more frequent, then it will provide a good opportunity to differentiate between dust originating from these two different source regions.

4.6.4 Positive Matrix Factorization and Potential Source Contribution Function

Positive Matrix Factorization (PMF) was used in this study to identify the sources of particulate matter and to determine their contributions to total PM_{2.5} mass. PMF was applied to PM_{2.5} fraction of the data set. The details of the PMF were discussed previously in Section 3.4.1. Determining the optimum number of factors (source types) is the most challenging part of the PMF analysis. As discussed in Section 3.4.1, different performance criteria used in PMF to have a feasible solution. The most important performance indicator in PMF is the objective function Q. The aim in PMF analysis is to minimize Q by adjusting various parameters, such as F-peak, scaled residuals etc. The steps followed in the PMF analysis are discussed in following paragraphs.

PMF model requires two input files, species concentrations file and uncertainty file which contains uncertainties assigned to each data point. As stated in Section 2.8, receptor models do not accept missing data point in concentrations of species. The missing data points in concentrations of species and the values below method detection limit (BDL) were dealt with the methodology described by Reff et al. (2007). In this methodology, the missing data points of a species are replaced with the geometric mean of the specie, while BDL vales are replaced with half of the method detection limit. The uncertainties assigned to missing data points and BDL values are 4 times the geometric mean and 5/6 of the method detection limit, respectively. Norris (2014)

recommended to exclude this species having BDL values is higher than 95% of samples. No specie in the data was excluded due to high 95% BDL values.

The next step in PMF analysis is to assigning categories to the species according to their S/N (signal-to-noise) ratios. There different categories are defined in PMF analysis. These categories are “Bad”, “Weak” and “Strong”. “Bad” removes the specie from the analysis and not included in the further analysis. “Weak” category multiplies the uncertainties associated to these species in the model by three. “Strong” category uses the uncertainties as they are provided. Norris (2014) recommended to categorize the species as “Bad” if the S/N ratio is less than 0.5; “Weak” if the S/N ratio is greater than 0.5 but less than 1; and “Strong” if the S/N ratio is greater than 1. After various base runs and trial and errors in the PMF analysis, the categories assigned to species in data set is provided in Table 4.16. Important source tracers were assigned as “Strong” even though their ratios were less than 1 (for example; Ca, Si, Na, Al, Cd). Some species Co, Sr, Zr, Er, Tm and Ta were assigned as “Bad” in accordance with the S/N recommendation by Norris. (2014).

Table 4.16 Categories assigned to species

Species	Category	S/N	Species	Category	S/N
PM_{2.5}	Weak	8.58	Y	Weak	0.52
B.C.	Strong	4.98	Zr	Bad	0.31
Li	Weak	0.64	Ag	Strong	1.21
Be	Weak	0.05	Cd	Strong	0.72
Na	Weak	0.94	Sn	Weak	0.08
Mg	Strong	0.97	Sb	Strong	3.55
Al	Strong	0.45	Te	Strong	1.93
Si	Strong	0.64	Cs	Strong	2.81
SO₄	Strong	8.74	La	Strong	1.23
K	Strong	3.44	Pr	Strong	1.25
Ca	Strong	0.65	Nd	Strong	1.27
Ti	Strong	0.79	Sm	Strong	1.6
V	Strong	0.84	Eu	Strong	1.1
Cr	Strong	1.68	Gd	Strong	1.94

Species	Category	S/N	Species	Category	S/N
Mn	Weak	0.59	Tb	Weak	0.69
Fe	Strong	8.27	Dy	Weak	0.59
Co	Bad	0.19	Er	Bad	0.37
Ni	Weak	0.48	Tm	Bad	0.28
Cu	Weak	0.45	Yb	Weak	0.51
Zn	Weak	0.48	Lu	Weak	0.51
Ge	Strong	1.71	Hf	Weak	0.68
As	Weak	0.01	Ta	Bad	0.47
Se	Weak	0.17	Tl	Strong	1.9
Rb	Weak	0.57	Pb	Weak	0.03
Sr	Bad	0.23	Bi	Strong	1.24

As stated before, determining the optimum number of factors (source types) is the most challenging part of the PMF analysis. Starting from 3 factors to 9 factors were calculated and examined. Selection of the optimum number of factors was based on the PMF performance criteria described in Section 3.4.1. Once the categories were assigned to species the next step was the comparison of the closeness of $Q(\text{robust})$, $Q(\text{trues})$ values calculated by the PMF model and $Q(\text{theoretical})$ for each number of factors (see section 3.4.1 for definitions of Q values). The closeness of the Q values was not the only criteria used during the PMF runs for different number of factor. Scaled residuals, observed and predicted concentrations of species and correlations between factor contributions were also examined in each PMF run (see Section 3.4.1 for details of details of performance criteria used in PMF).

The stability of the PMF factors were tested with the bootstrapping tool of the PMF model. Bootstrapping tool in PMF generates a new data set from the provided data set to the PMF by selecting non-overlapping blocks of samples (Norris 2014). This data is called bootstrap data. PMF generates bootstrap factors from bootstrap data and assigns these bootstrap factors to the base factors based on the linear correlation between the factor contributions. In this study, the number of iterations used in bootstrapping tool was 100 and 0.6 was used a threshold value for assigning bootstrap factor to base run factor. The result of bootstrap run for the optimum number of factor

is given Table 4.17. As seen in Table 4.17, only a few of 100 bootstrap factors were not mapped to the base solution, which indicates a stable solution.

Table 4.17 Bootstrap factors mapped to base factors

Factor 1	Factor 2	Factor 3	Factor 4	Factor 5	Factor 6	Factor 7	Unmapped
94	0	5	0	0	0	0	1
1	97	0	0	0	0	0	2
0	0	100	0	0	0	0	0
0	0	1	99	0	0	0	0
2	0	9	0	81	0	2	6
3	0	5	0	0	85	1	5
0	0	1	0	1	0	98	0

Based on discussion above optimum number of factors were determined as seven in this study. An extra 10% modeling was used in the model runs. PMF calculated Q(robust) and Q(trues) values as 5422.17 and 5421.54. The Q(theoretical) was 6161 for a seven factor solution. Residuals were in the range of -3 to +3 for almost all of the species and some selected species is given in Figure 4.44. Observed to predicted plots of some representative species are given in Figure 4.45 and for PM_{2.5} mass Figure 4.46. The minimum values for Q(robust) and Q(true) were obtained at F-peak = -0.5.

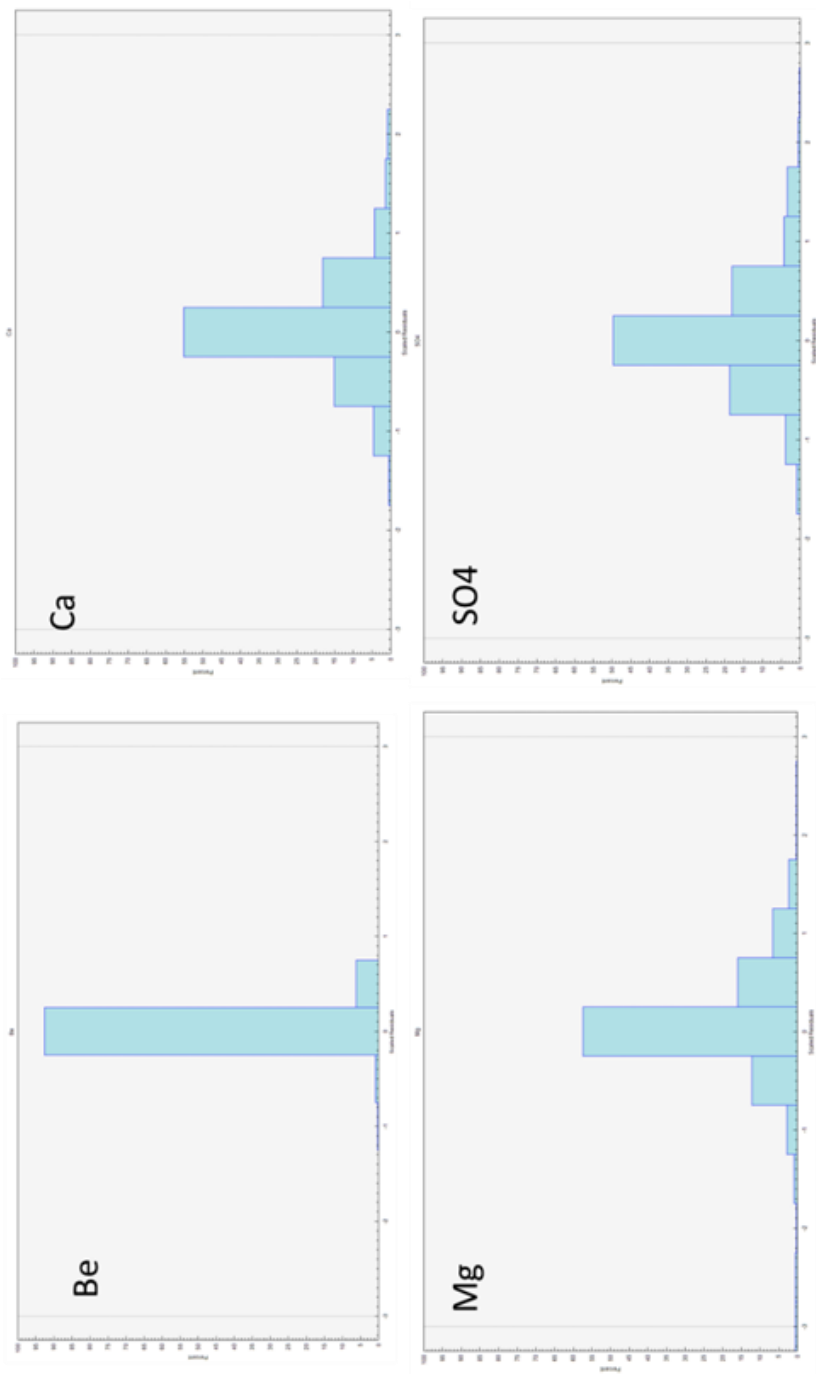


Figure 4.44 Scaled residuals of some selected elements

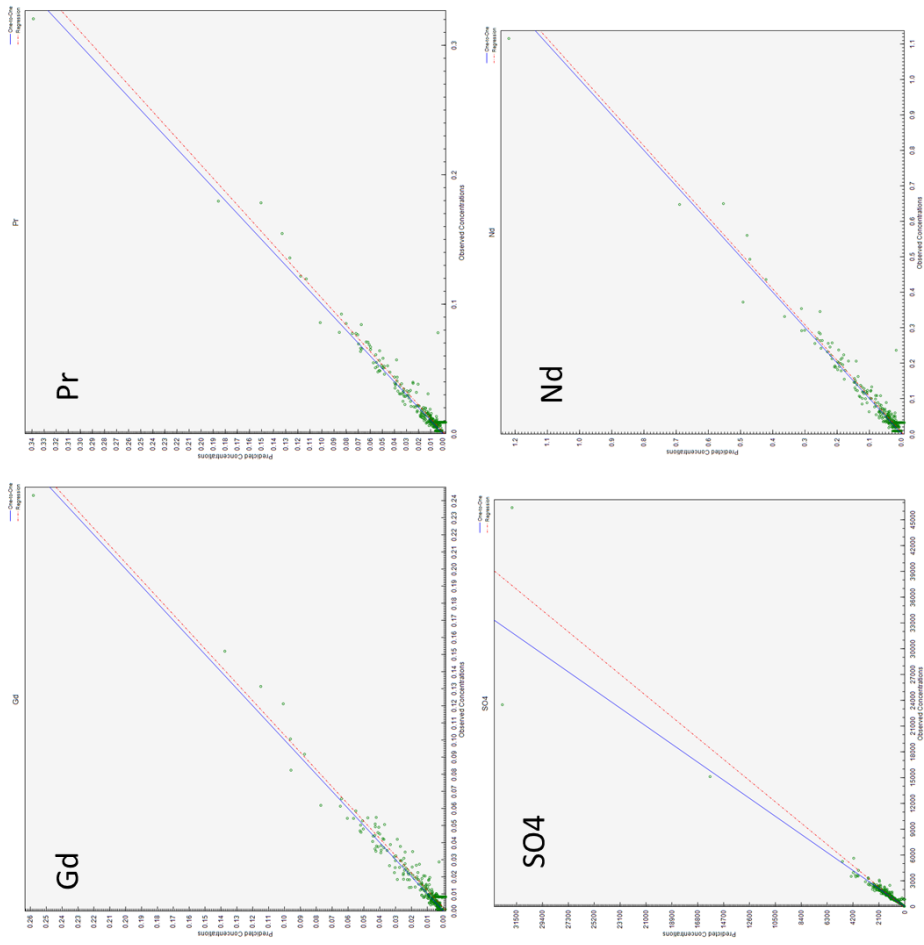


Figure 4.45 Observed and predicted concentrations of selected species

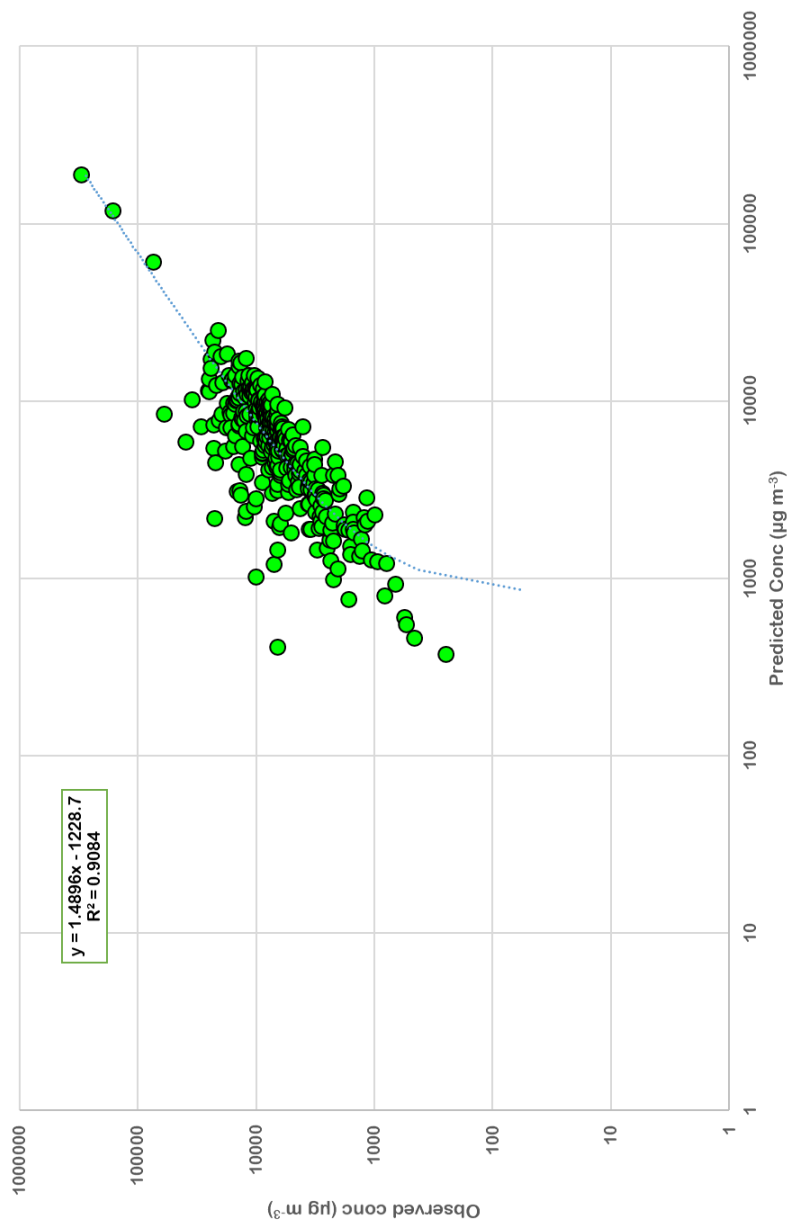


Figure 4.46 Observed and predicted concentrations of PM_{2.5} mass

Factor 1

Factor 1 loadings, percentages of element concentrations accounted for by factor1, Seasonal variation in factor 1 scores and crustal enrichment factors of elements in Factor one (calculated using factor 1 loadings) are given in Figure 4.47. Factor 1 accounts for >80% of Sb, >40% of Na, >20% of Cu, K, Cu, As, Sn, Tl and Pb concentrations. The factor does not account for significant fractions of lithophilic elements. This is an anthropogenic factor also indicated by high enrichments of most anthropogenic elements. Factor 1 scores are only slightly higher during summer season, suggesting source regions that are not in the immediate vicinity of the station, but also not too far (such as Balkans and Europe) as well. Back trajectories calculated for the days corresponding to highest 30% of factor 1 scores are given in Figure 4.48. Back trajectories suggest three source areas over which they are concentrated. One of these potential source areas for factor 1 is located to the east of sampling location. There is a group of trajectories arriving from that sector. The second potential source area is the Eastern part of Turkey Potential Source Contribution Function distributions confirm this conclusion.

The PSCF map for factor 1 which was prepared by interpolating PSCF values in each grid is depicted in Figure 4.49 for Factor 1. Potential source contribution function will not be discussed here as a method, because it was explained in detail in Section 3.4.3. Factor scores (G-scores) were used in PSCF calculations and trajectories that correspond to highest 30% of the scores were adopted as “polluted” trajectories. Source areas for factor 1 are located to the east of Turkey. Including Northern Iran, Coasts of the Caspian Sea, both in Kazakhstan side, Russian and Azerbaijan coasts. In addition to these central areas of Ukraine, eastern parts of Turkey and Iraq are the other source areas that contributes to factor 1. Percent contribution of each factor to $PM_{2.5}$ mass concentration at the station is given in Figure 4.50. As can be seen from the figure Factor 1 accounts for approximately 17% of $PM_{2.5}$ mass at Eastern Black Sea, which is the second highest contributing factor to fine aerosol mass in this region.

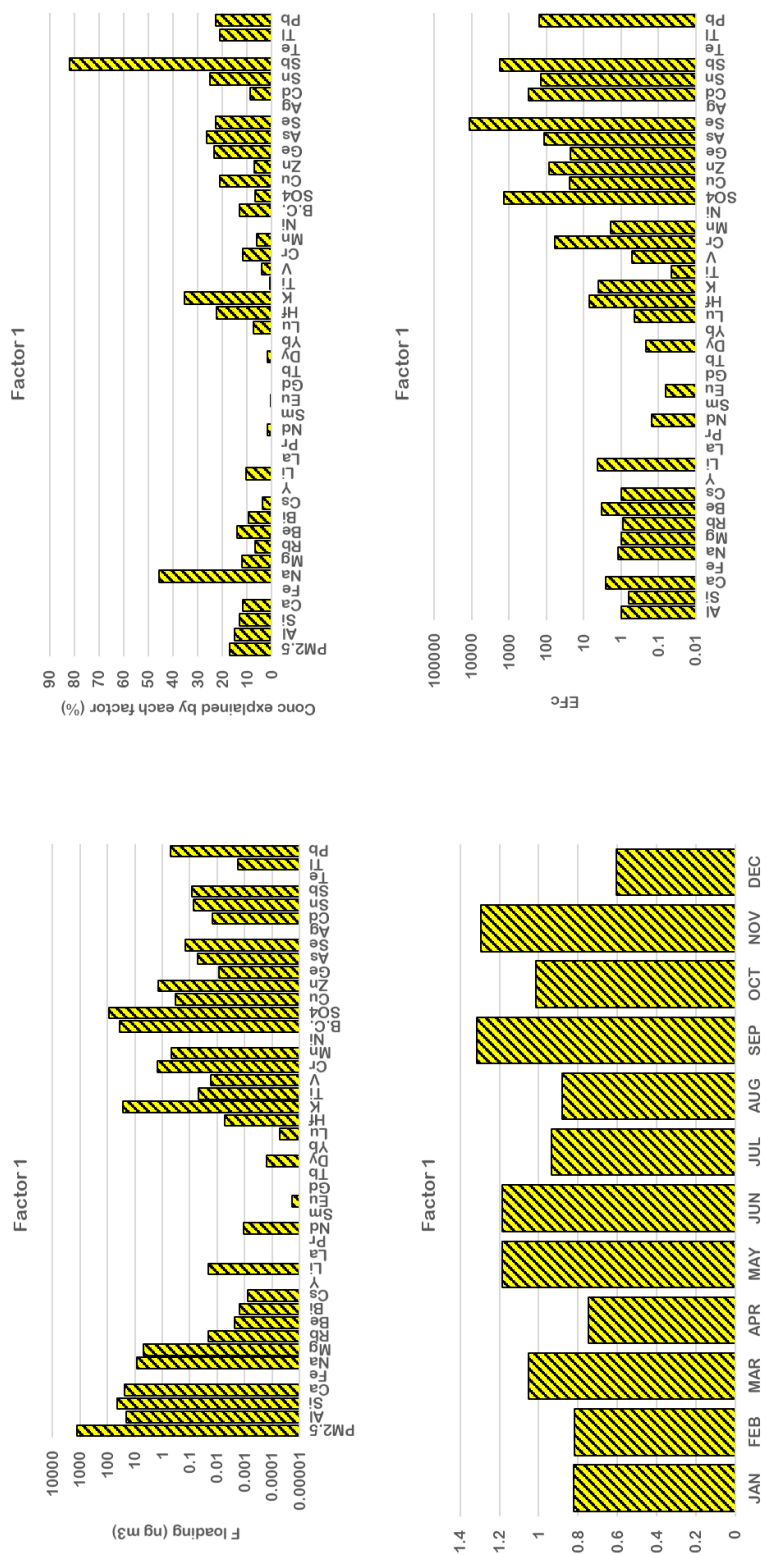


Figure 4.47 Diagnostic figures for factor 1, which includes Factor loadings, fractions of elemental concentrations explained, Seasonal variation in factor scores and crustal enrichment factors of elements

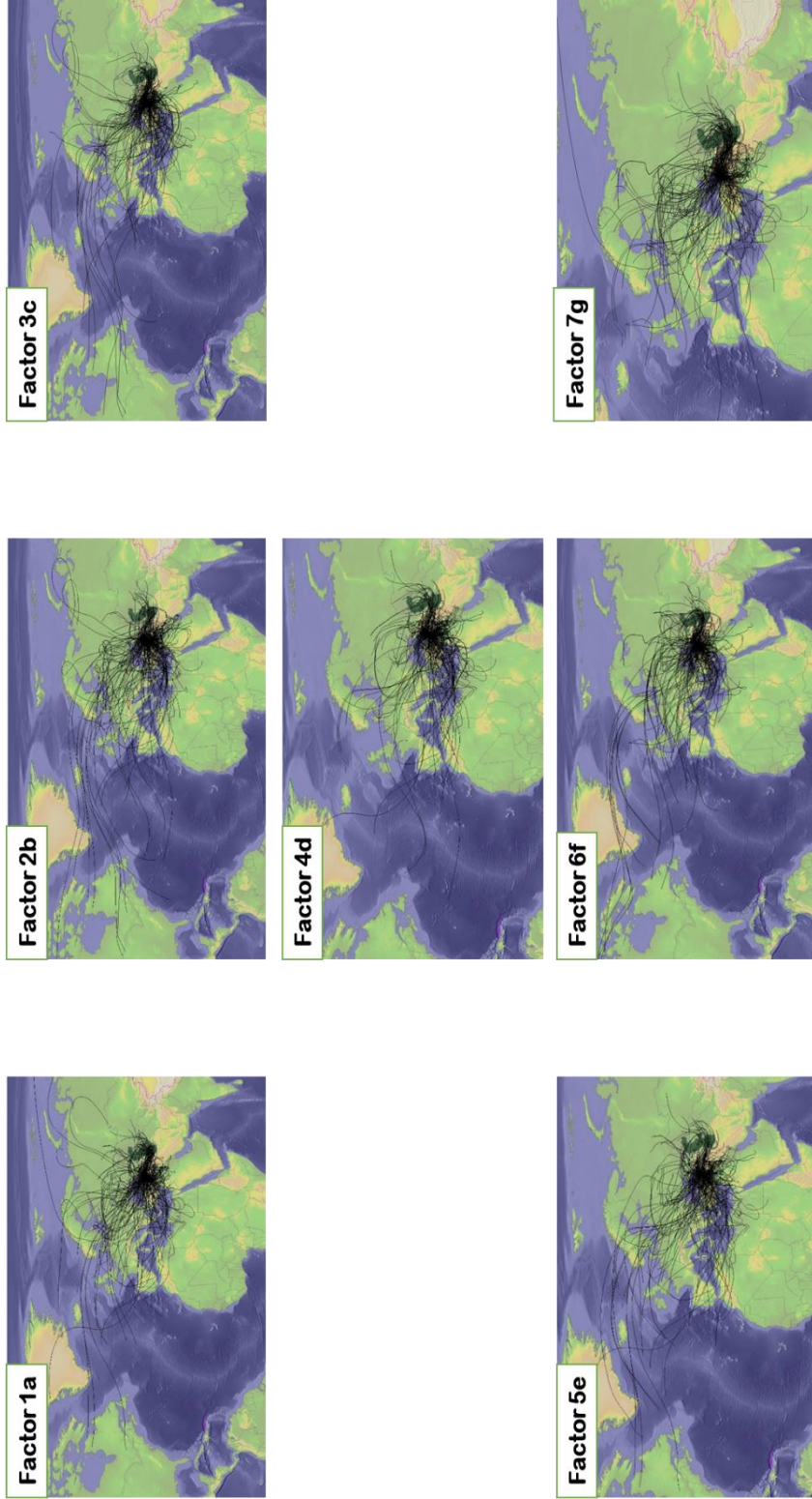


Figure 4.48 Trajectories corresponding to highest 30% of g-scores of each factor

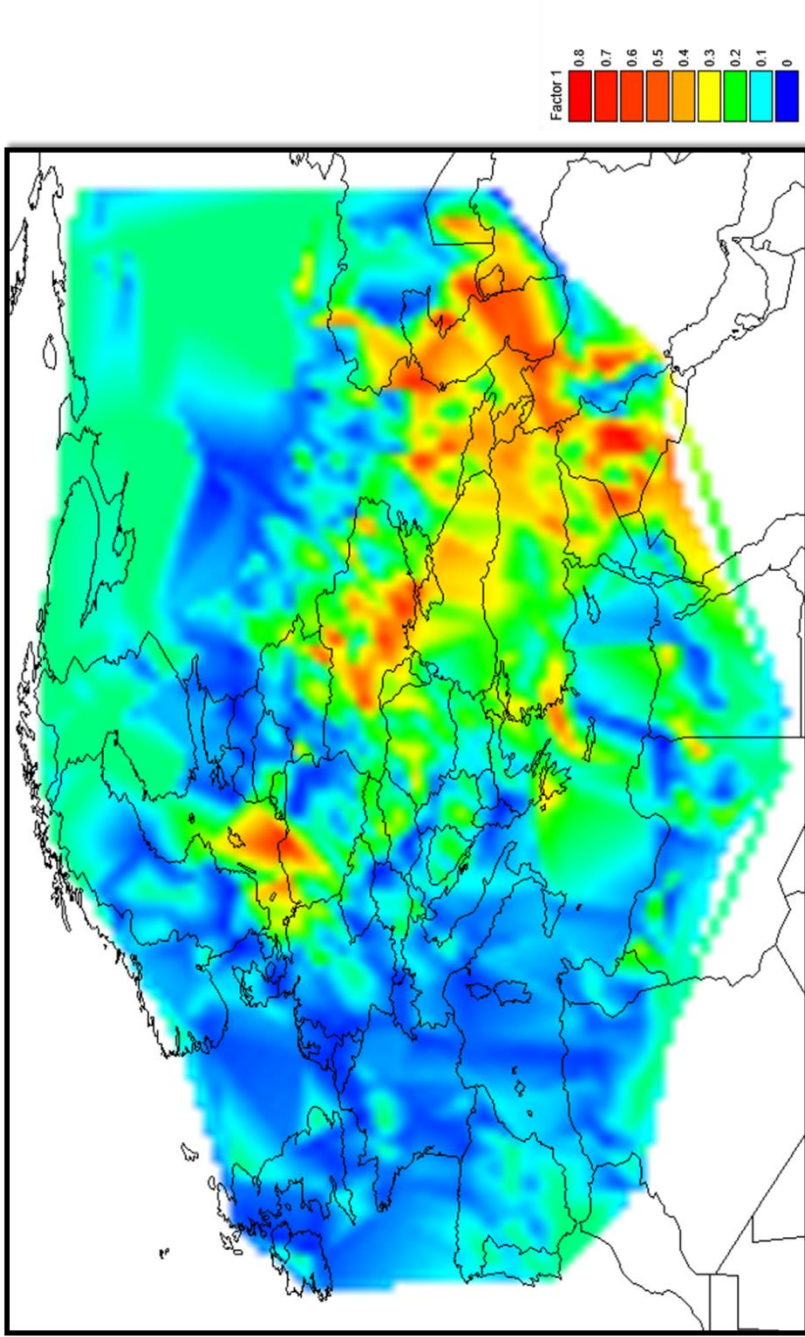


Figure 4.49 Distribution of PSCF values computed using trajectories that correspond to highest 30% of factor 1 scores as “polluted” trajectories

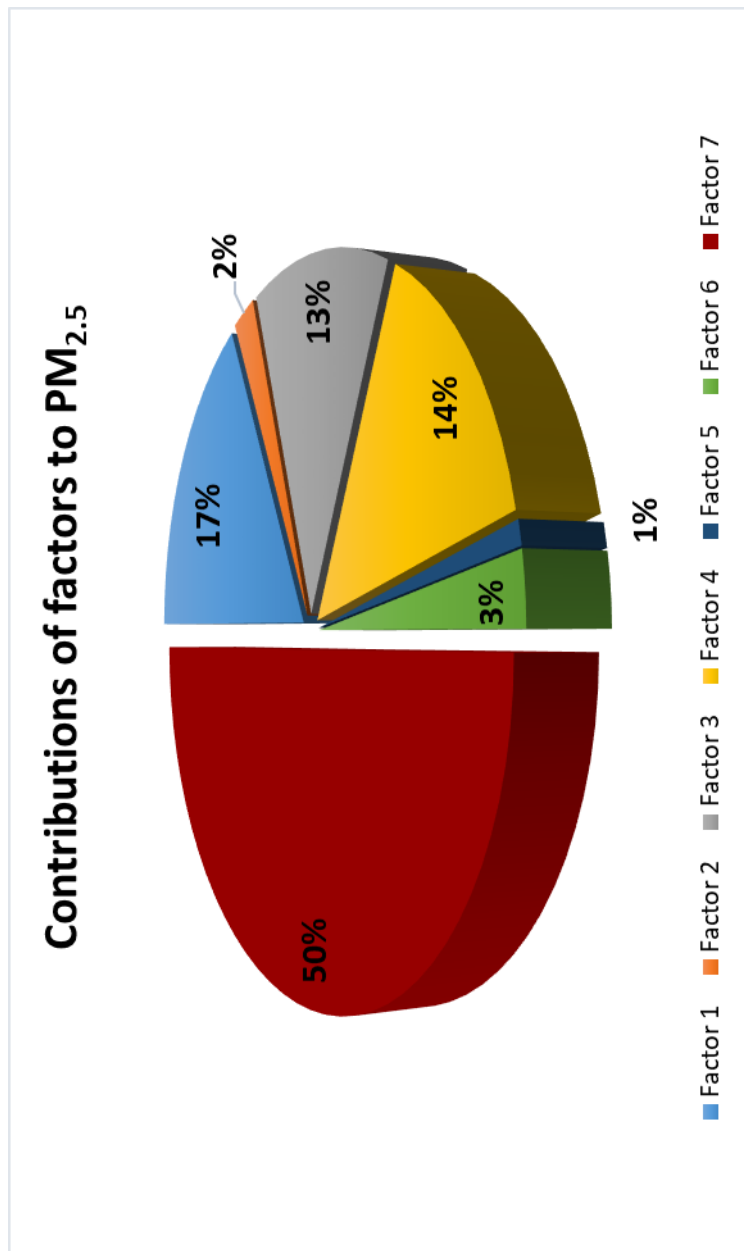


Figure 4.50 Contribution of each factor to PM_{2.5} mass at Eastern Black Sea

Factor 2

Diagnostic figures for factor 2 are given in Figure 4.51. Chromium is the marker element for factor 2. Approximately 85% of measured Cr concentration is accounted for by this factor. In addition to Cr, Factor 2 also explains approximately 20% of Cu, Sn, Te, Pb, 30% of Be and 40% of Fe concentrations. This is obviously an anthropogenic factor, which is also confirmed in Figure 4.51 where EFcs of elements are plotted. As can be seen from the figure, all elements with known anthropogenic sources are enriched.

There is a well-defined seasonal pattern with lower scores in summer and higher scores in winter months. This is an indication of local sources. Most of the elements that reach to the station as a result of long range transport are expected to have higher concentrations in summer, because temporal variation in their concentrations are determined by wet scavenging during long range transport, which is more effective in winter. Factor scores that are higher in winter implies that particles associated with this factor do not travel too long in atmosphere and thus are not wet scavenged as effectively as particles coming from distant sources. Distant sources refer to sources at Balkans, Western Parts of Turkey and further away. Local sources means sources in Eastern Turkey, Caspian Sea region, Iran, Iraq, Syria.

Please note that Fe and Be are also moderately enriched in factor 2. For other lithophilic elements EFcs are about unity. Factor 2 is identified as iron and steel factor due to enrichments of Fe, Cr and Mn in this factor. Most of the pollution-derived elements including SO_4^{2-} are also enriched in factor 2, suggesting that factor is not a pure steel factor, but also include particles from combustion sources. Contribution of Factor 2 to $\text{PM}_{2.5}$ mass is 2% showing that it is a minor component in Eastern Black Sea aerosol.

Back trajectories associated with this factor, which are given Figure 4.48b and distribution of PSCF values associated with this factor, which is given in Figure 4.52. Figure 4.48b confirms local nature of Factor 2, because most of the trajectories are short and spends most of their time in Eastern Turkey. PSCF values associated with

this factor, which is given in Figure 4.52, demonstrate that the area to the north of the Persian Gulf and Western Iran are potential source regions contributing this component of aerosol population at Eastern.

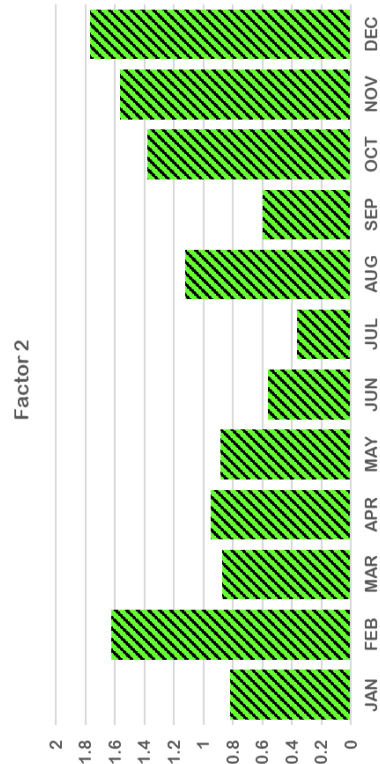
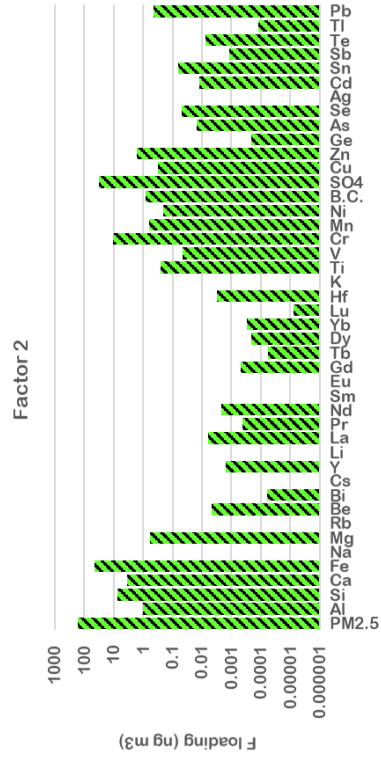
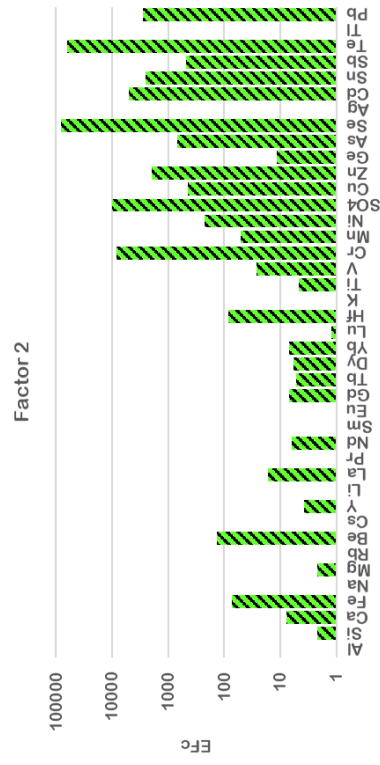
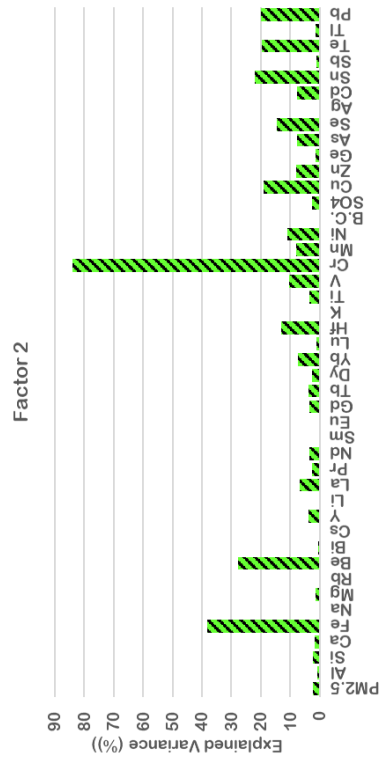


Figure 4.51 Diagnostic figures for factor 2, which includes Factor loadings, fractions of elemental concentrations explained, Seasonal variation in factor scores and crustal enrichment factors of elements

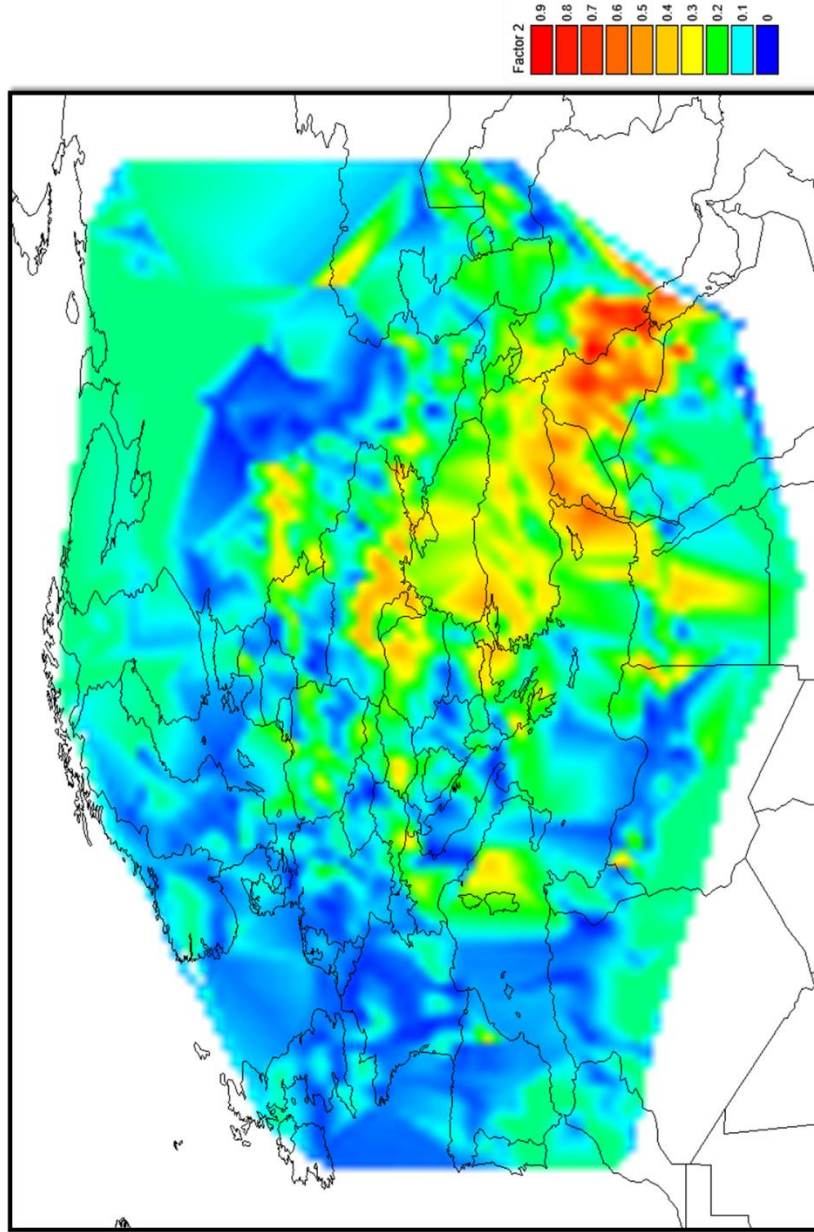


Figure 4.52 Distribution of PSCF values computed using trajectories that correspond to highest 30% of factor 2 scores as “polluted” trajectories

Factor 3

Diagnostic figures for factor 3 are given in Figure 4.53. Factor 3 is also a pollution factor. It accounts for approximately 80% of BC, 70% of Ag, 50% of Ni and 30% Mn, Cu, As, Te concentrations. Most of the chalcophilic elements are enriched in Factor 3. Factor 3 scores are higher in summer suggesting that sources contributing to this factor are not in the immediate vicinity of the station.

Trajectories corresponding to highest 30% of factor 3 scores are given in Figure 4.48c. Back trajectories representing factor 3 are not very different from those corresponding to highest factor 2 scores. There is an eastern component which brings pollution from Armenia, Azerbaijan, Georgia and from east coast of Caspian Sea, which is part of Turkmenistan. The other component is the NW sector, which can be seen by high intensity of back trajectories in NW direction. These trajectories makes Ukraine a potential source area for aerosol component represented by factor 3. The third component is Turkey, particularly eastern parts of the country.

Distribution of PSCF values computed for Factor 3 is shown in Figure 4.54. Potential source contribution calculations confirmed the conclusions based on trajectories in the previous paragraph. Potential source areas for factor 3 component are Turkmenistan, Azerbaijan, Armenia and Georgia, part of Russia between Ukraine and Caspian Sea at the East of the sampling point, central and Eastern Parts of Ukraine, Most of Turkey, Eastern Parts of Greece. There are also some contribution from the African Coast and in Syria.

Marker species for factor 3 are BC and Ag. Main sources of BC in atmosphere are biomass burning (Bond et al., 2004; Chan et al., 2017), traffic (particularly diesel traffic) (Kimbrough et al., 2018; Krecl et al.; 2017) and coal combustion (Li et al.; 2016; Wang et al., 2016). Silver in atmosphere can be due to mining activities (Lecerda et al., 1997; World Health Organization, 2002), coal combustion for space heating (Renville et al., 2010; Waheed et al., 2011; Duan et al., 2012), Iron and steel industry (Vlastelic et al., 2014), Automobile exhaust (Vlastelic et al., 2014). Factor 3 is

identified as urban pollution factor due to (1) elements which's concentrations are highly contributed by factor 3 have significant urban sources, and (2) distribution of PSCF values, which were calculated using trajectories corresponding to high factor 3 scores have high values at populated cities in the region, including Ankara, Turkey (Population 5500000), Izmir Turkey (population 4300000), Athens Greece (population 660000), Cairo, Egypt (population 9500000), Urban pollution factor accounts for 13% of PM_{2.5} mass concentration.

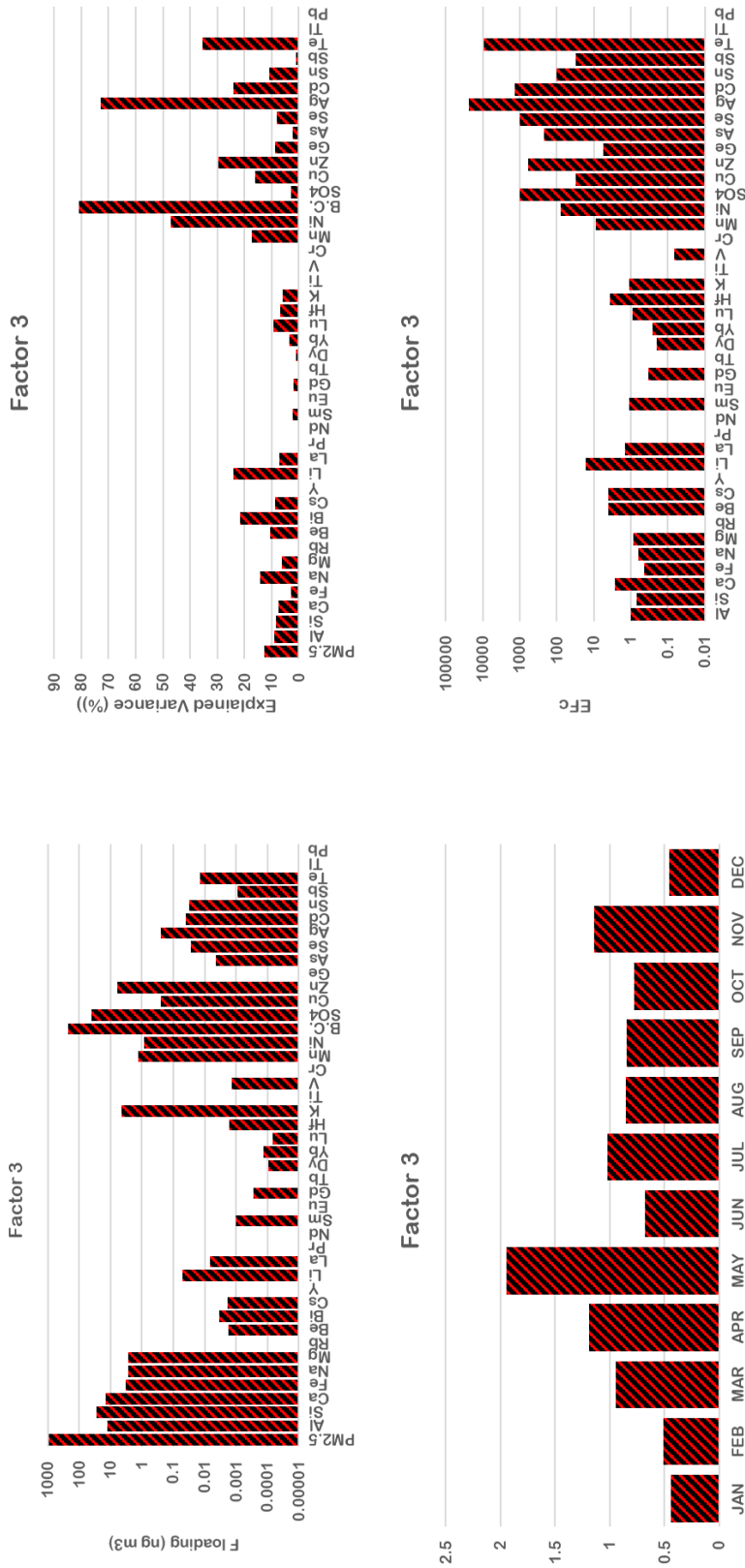


Figure 4.53 Diagnostic figures for factor 3, which includes Factor loadings, fractions of elemental concentrations explained, Seasonal variation in factor scores and crustal enrichment factors of elements

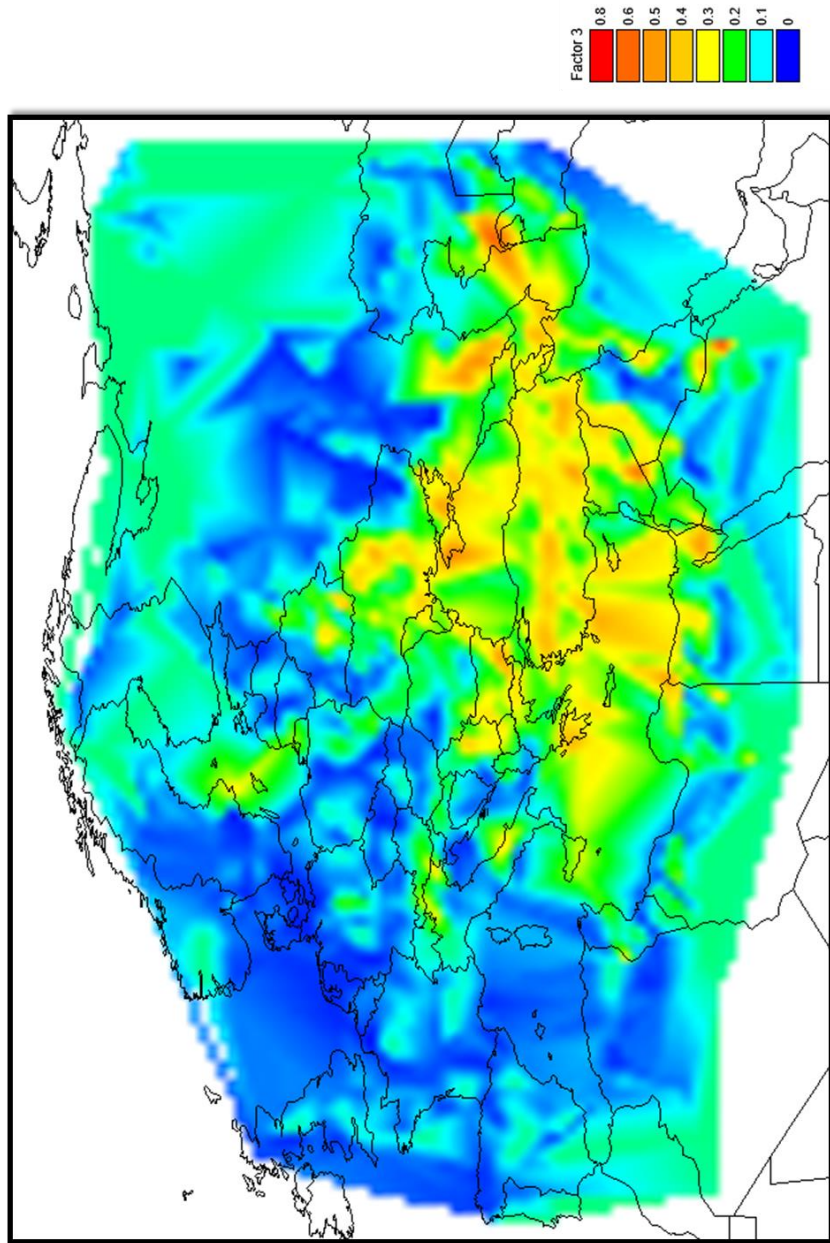


Figure 4.54 Distribution of PSCF values computed using trajectories that correspond to highest 30% of factor 3 scores as “polluted” trajectories

Factor 4

Diagnostic figures for factor 4 are given in Figure 4.55. Factor 4 is a typical crustal factor. It accounts 70 – 80% of concentrations of most lithophiles. Factor 4 scores are higher during summer, which is expected, because soil resuspension is enhanced during summer due to dry surface soil. Calcophiles are slightly-to-moderately enriched (EFcs vary between 10 and > 100). This is also not surprising, because crustal particles transported to sampling location are frequently mixed with anthropogenic particles. Trajectories associated with highest 30% of factor 4 scores and distribution of PSCF values in the study area are given in Figure 4.48d and Figure 4.56, respectively. Both trajectories and PSCF distribution map clearly demonstrate that source of this crustal component is at eastern Turkey and Middle East. This is the first time we were able to isolate dust originating from Source areas in the Middle East. Contribution of Crustal factor to PM_{2.5} mass concentration is 14%.

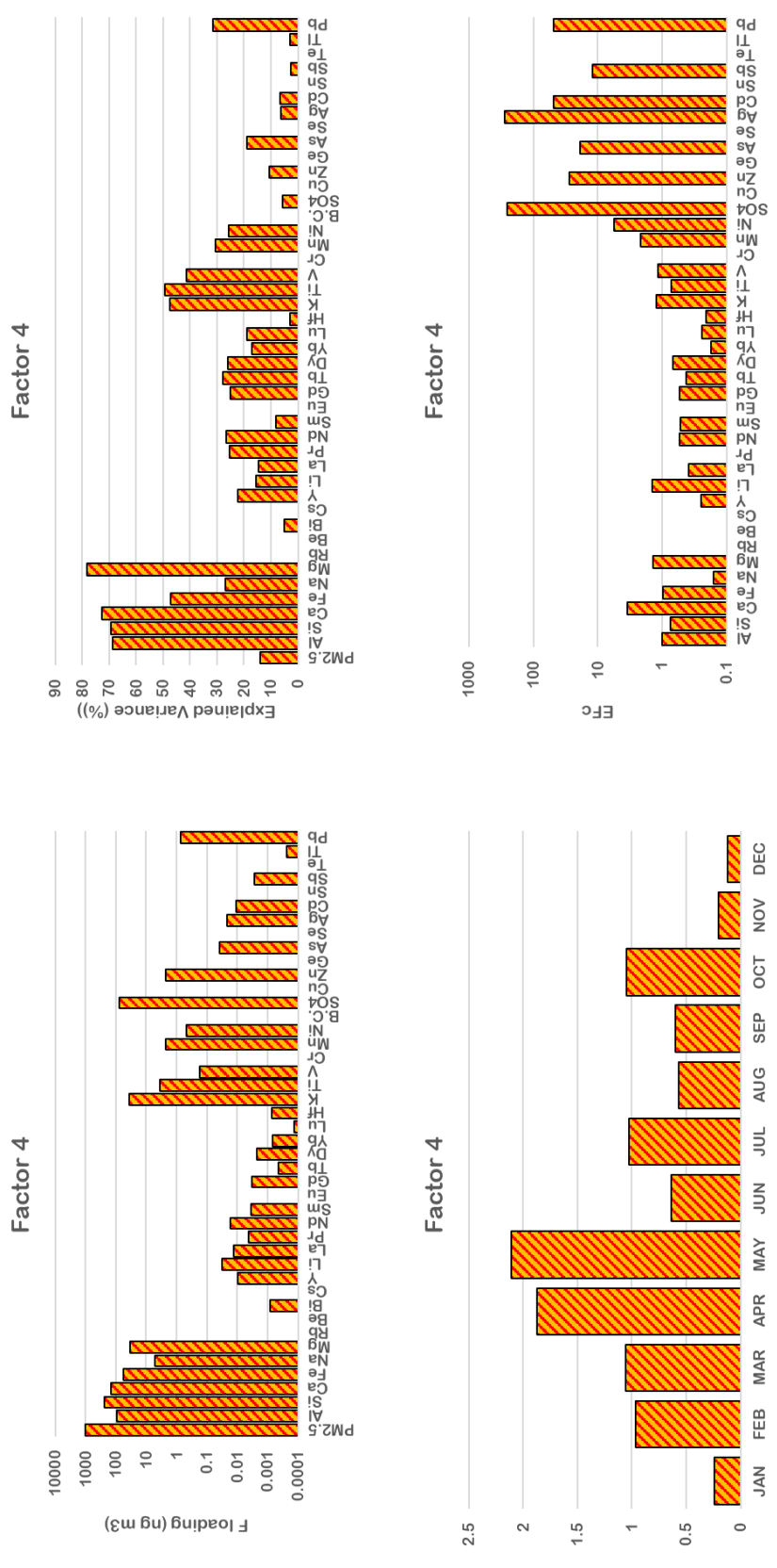


Figure 4.55 Diagnostic figures for factor 4, which includes Factor loadings, fractions of elemental concentrations explained, Seasonal variation in factor scores and crustal enrichment factors of elements

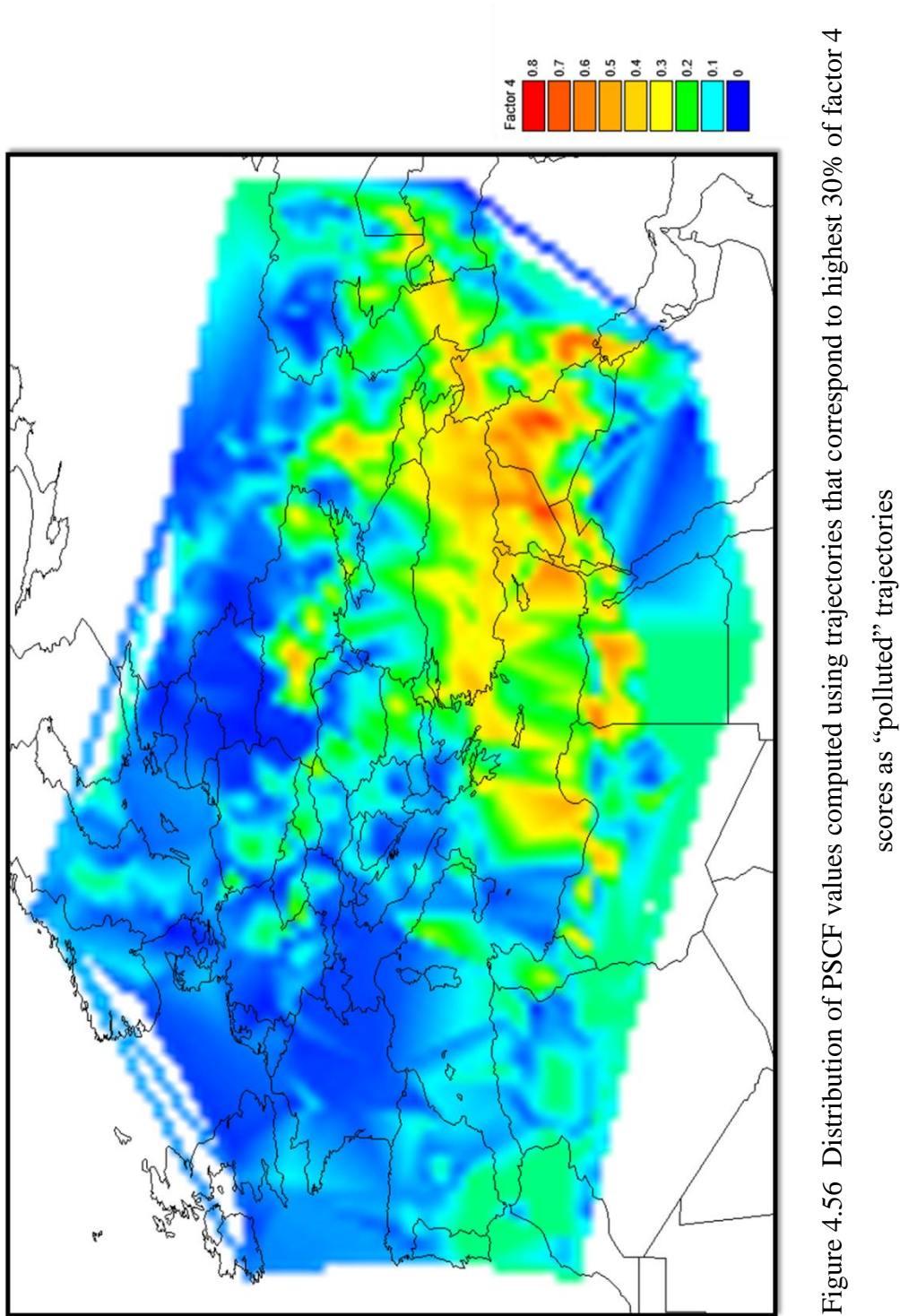


Figure 4.56 Distribution of PSCF values computed using trajectories that correspond to highest 30% of factor 4 scores as “polluted” trajectories

Factor 5

Diagnostic figures for factor 5 are given in Figure 4.57. Factor 5 is another crustal factor. It is an interesting factor. It accounts 50 to 60% of concentrations of rare earth elements. None of the elements are significantly enriched, which is a clear indication of crustal component in aerosol population. Higher factor scores in winter also confirms that factor 5 is a crustal factor, as discussed in previous paragraphs for Factor 4.

Back trajectories corresponding to high factor 5 scores are depicted in Figure 4.48e and distribution of PSCF values calculated using back trajectories corresponding to high factor 5 scores as polluted trajectories is given in Figure 4.58. Back trajectories and distribution of PSCF values, particularly the PSCF map suggests that source areas are not as specific as source areas for factor 4 crustal material. Source areas for Factor 5 dust is at west of Turkey Parts of North Africa, West of Ukraine, North of Caspian Sea. Although there are some source areas in Iraq and Syria, they are not as dominating as they are for factor 4 dust. It is believed that factor 5 represents a second crustal component (Crust II) in Eastern Black Sea aerosol population with different mineralogy than Factor 4 crustal material. This is not surprising, because major element composition of crustal material does not change much from one place to another, but minor element composition do change. That is why rare earth elements are used to differentiate between different soil types (Daud and Mohamed, 2016; Moreno et al 2010; Yokoo et al., 2004; Güllü 1996; Tuncel et al., 1989). Contribution of Crust II factor on $PM_{2.5}$ mass concentration is 1%, indicating that Crust II is not a significant component of Eastern Black Sea aerosol population.

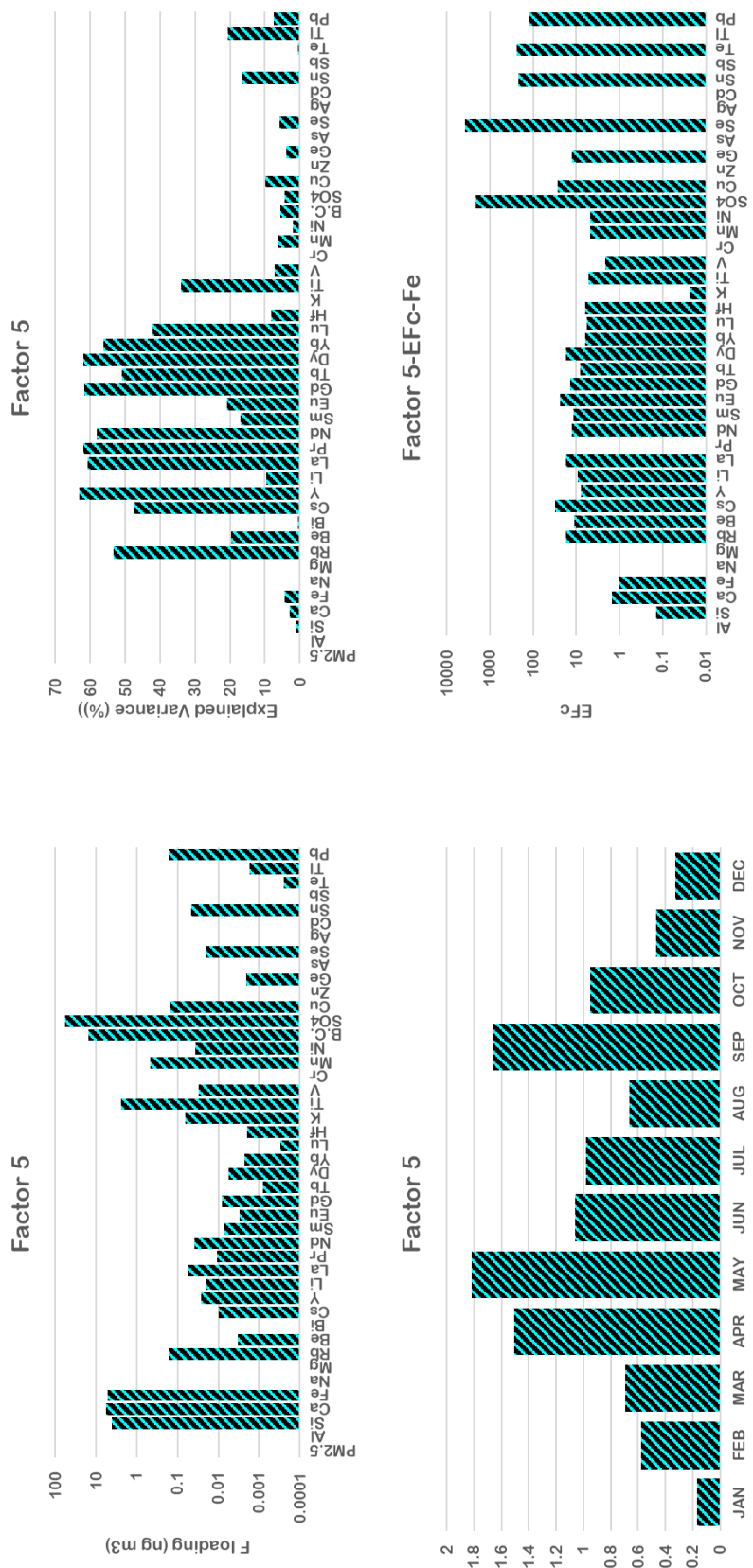


Figure 4.57 Diagnostic figures for factor 5, which includes Factor loadings, fractions of elemental concentrations explained, Seasonal variation in factor scores and crustal enrichment factors of elements

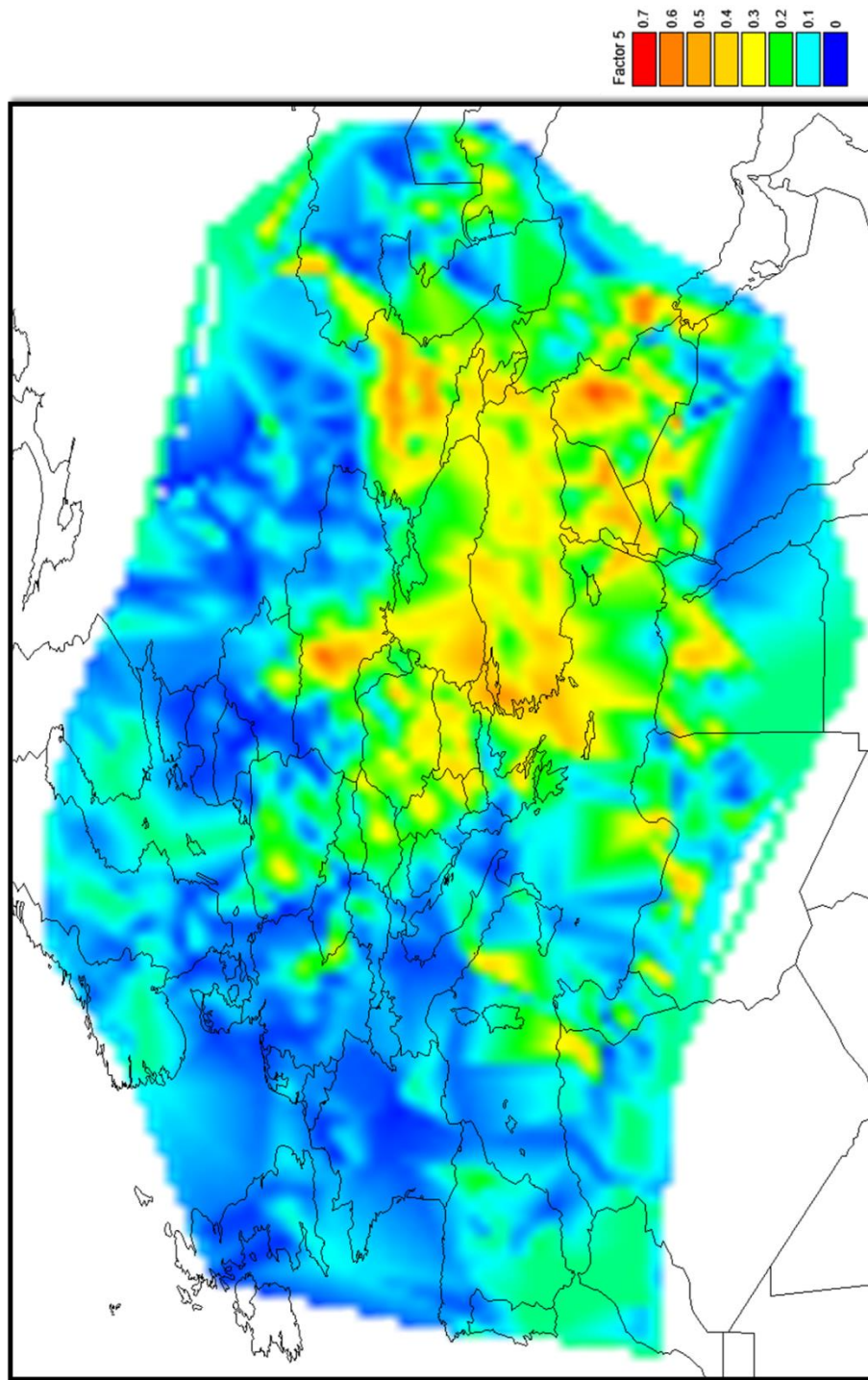


Figure 4.58 Distribution of PSCF values computed using trajectories that correspond to highest 30% of factor 5 scores as “polluted” trajectories

Factor 6

Diagnostic figures for factor 6 are given in Figure 4.59. Factor 6 accounts for 70 – 80% of concentrations of Sm and Eu. It also accounts for 10-to-20% of chalcophile concentrations. Most of the pollution-derived elements are enriched, indicating that it is an anthropogenic factor. Factor scores are higher during summer season as in most of the other factors except for Factor 2. Back trajectories associated with this factor, which are given Figure 4.48f and distribution of PSCF values associated with this factor, which is given in Figure 4.60, demonstrate that Mediterranean area, particularly, cost of Israel, Mediterranean coast of Turkey, Balkan countries, central parts of Ukraine and countries around the Caspian Sea, such as Azerbaijan, Armenia, Georgia and Turkmenistan are potential source regions contributing this component of aerosol population at Eastern Black Sea region. This factor was identified as oil processing factor due to enrichment of Sm and Eu. Olmez and Gordon (1985) demonstrated that emissions from oil combustion and refineries are highly enriched with rare earth elements due to zeolite catalysts used during refining of crude oil in refineries. Authors believe that these emissions can alter rare earth composition of aerosol in the regional scale due to very low concentrations of this element group in atmospheric aerosol. Oil refining is widespread in the region where 47% of world petroleum is produced (EIA. 2016). Locations of major refineries in the region are marked on PSCF map. There is a close relation between high potential source areas for factor 6 and distribution of refineries in the region, confirming that factor 6 is a petroleum processing factor. Factor 6 is a minor component of aerosol population accounting for 3% of PM_{2.5} mass.

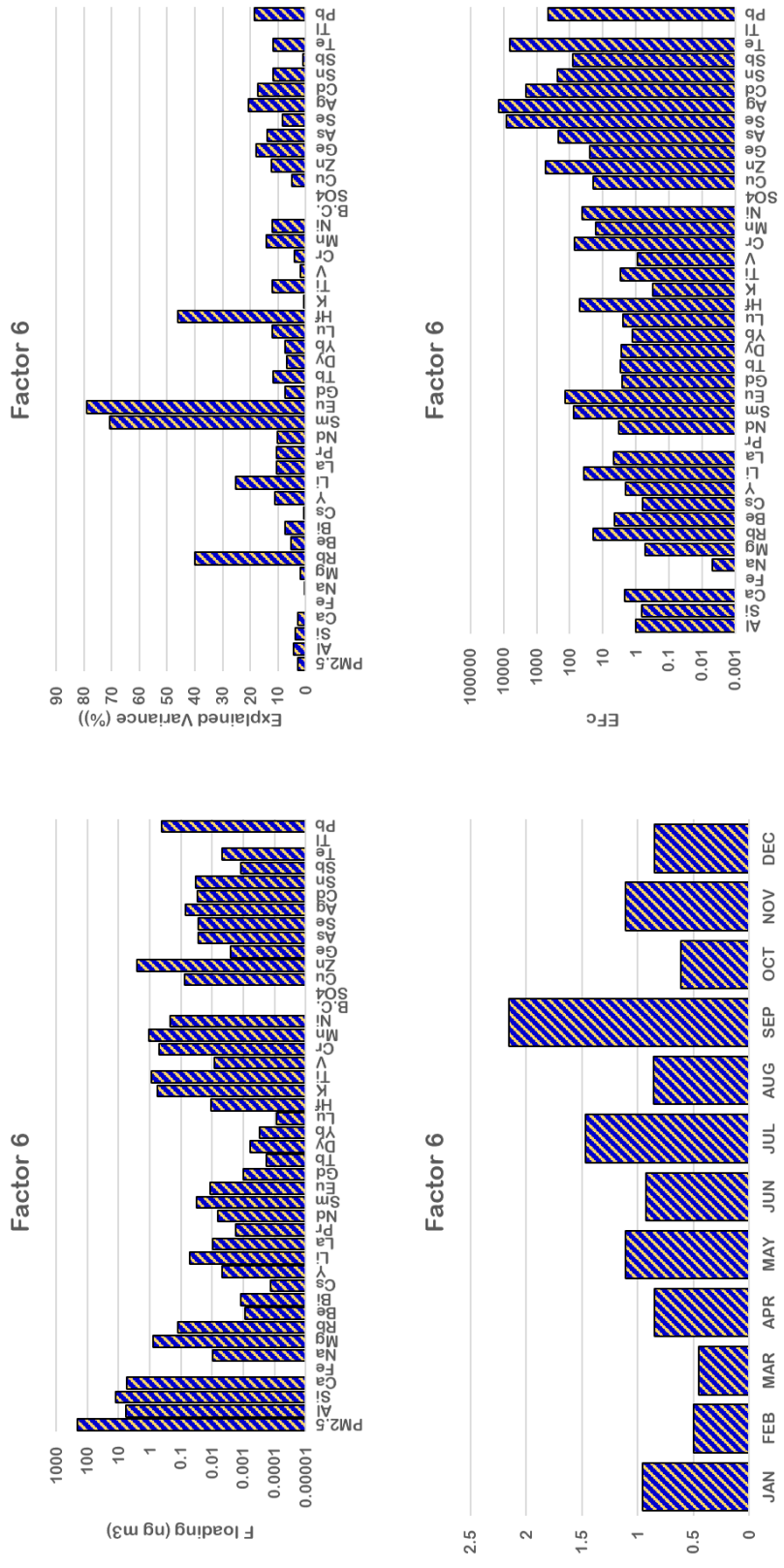


Figure 4.59 Diagnostic figures for factor 6, which includes Factor loadings, fractions of elemental concentrations explained, Seasonal variation in factor scores and crustal enrichment factors of elements

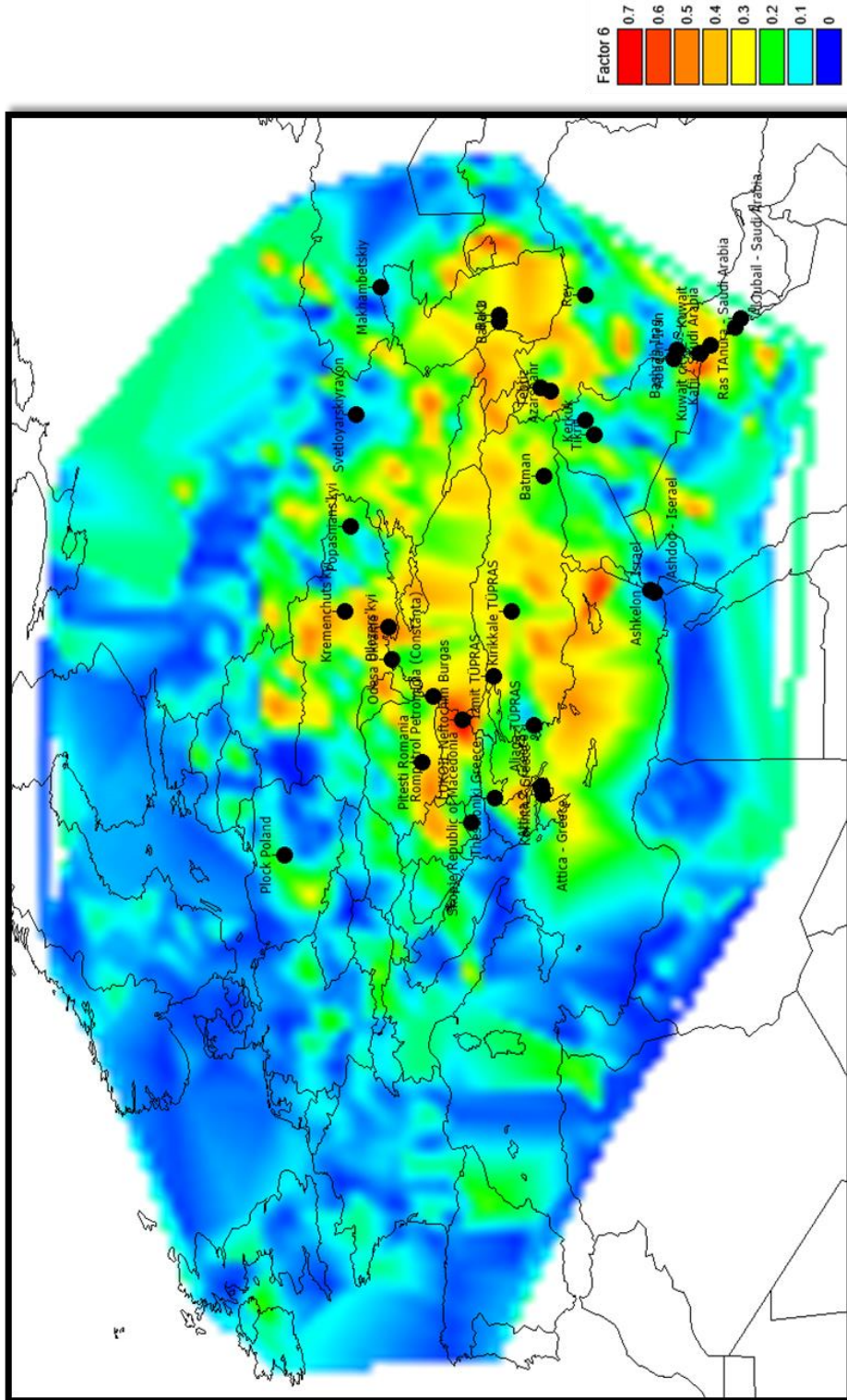


Figure 4.60 Distribution of PSCF values computed using trajectories that correspond to highest 30% of factor 6 scores as “polluted” trajectories. Locations of Refineries in the region are marked on the map

Factor 7

Diagnostic figures for Factor 7 are given in Figure 4.61. Factor 7 is an interesting factor. It accounts for approximately 80% of SO_4^{2-} concentration. It also accounts for 30 - 50% of Cu, Zn, Ge, As, Se, Cd, Te and Tl concentrations. All elements with known anthropogenic elements are highly enriched in Factor 7. Factor scores are higher in summer, which is typical for long-range transported particles.

High contribution of factor 7 to SO_4^{2-} , As, Se, Ge and Tl concentration, which are well documented markers of coal combustion suggests that factor is related with coal combustion and thus identified as power plant factor.

Back trajectories corresponding to days with high factor 7 scores and distribution of PSCF values for factor 7 are given in Figure 4.48g and Figure 4.62, respectively. There is high density of back trajectories in East, NW and South sectors. It is interesting to note that there is not much trajectories extending to west sector, which includes industrialized parts of Turkey. This is confirmed by PSCF distribution map. Main potential source areas for factor 7 are located to the east of station, at Northern parts of Iran, Azerbaijan, Georgia and East bank of Caspian Sea and to the Northeast of the station at Ukraine. The factor does not have any contribution from west sector where power stations at least in Turkey are located. Please note that contribution of a source area to a receptor does not only depends on emission strength at the source, but also depends on frequency of air mass transport from that source area. Obviously source areas to the east of the station and at Ukraine dominates due to their close proximity to the sampling point.

Factor 7 accounts for 50% of $\text{PM}_{2.5}$ mass concentration, indicating that potential source areas associated with this factor has determining effect on fine particle concentrations at Eastern Black Sea. One reason for high contribution of factor 7 to fine particle mass is the occurrence of SO_4^{2-} in this factor. Sulphate is the most abundant component in inorganic particle mass and one of the most important contributors (with organic fraction) to fine fraction particle mass. It accounts for approximately 60% inorganic

mass and approximately 20% of PM_{2.5} mass. The second reason is the close proximity of source areas to the station. Higher factor scores in summer suggests that particles associated with this factor comes from distant sources. Please note that this statement is true only if emissions are the same in summer and winter, which is generally the case in regional scale. However, SO₄²⁻ is a secondary specie produced by photochemical oxidation of SO₂ in atmosphere. This oxidation is enhanced in summer due to higher solar flux. That is why higher SO₄²⁻ concentrations in summer season are measured in most studies (Öztürk 2009; Tokgöz, 2013) Since SO₄²⁻ has dominating influence on factor 7, higher factor 7 scores in summer season may not indicate distant sources and may be due to faster oxidation of SO₂ to SO₄²⁻ in summer season.

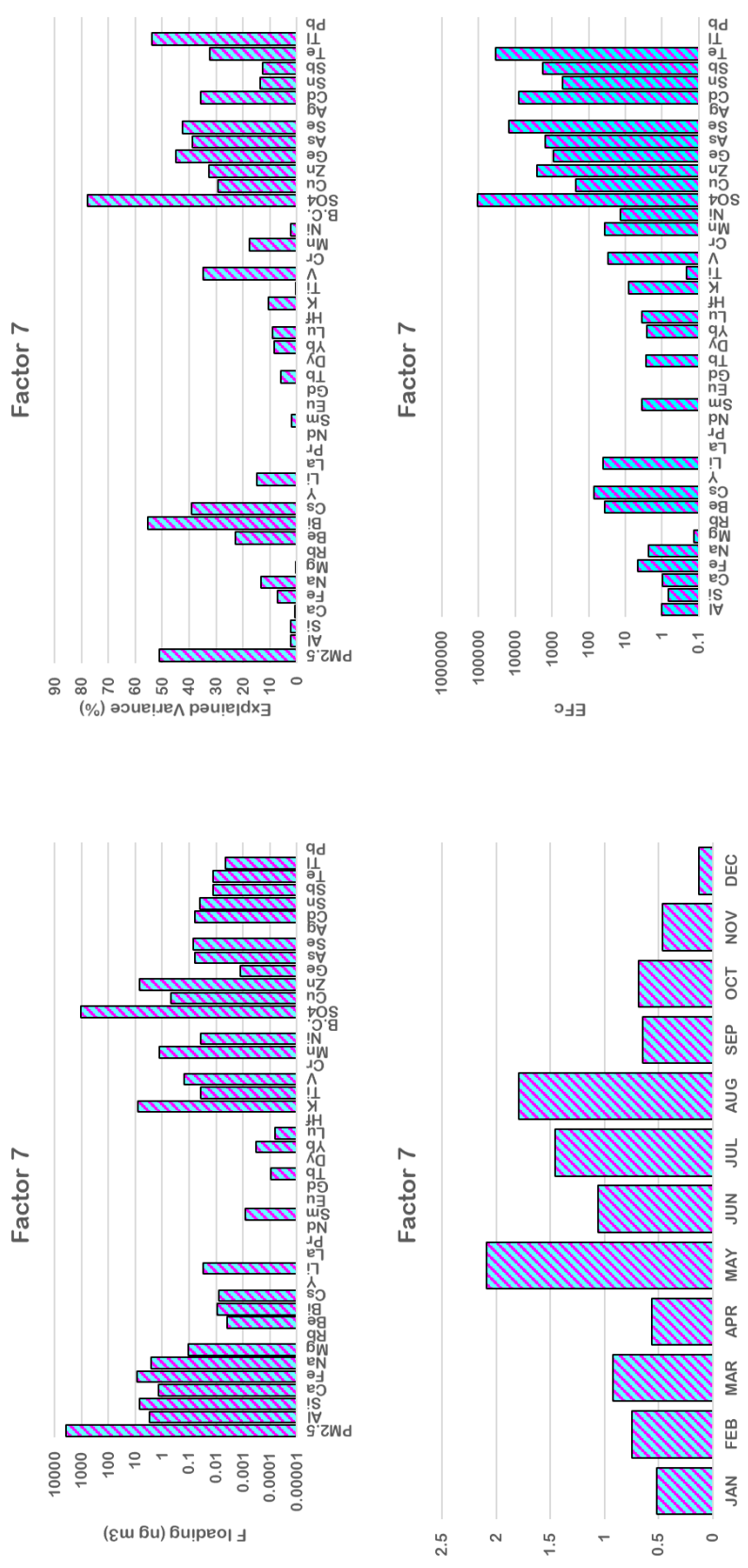


Figure 4.61 Diagnostic figures for factor 7, which includes Factor loadings, fractions of elemental concentrations explained, Seasonal variation in factor scores and crustal enrichment factors of elements

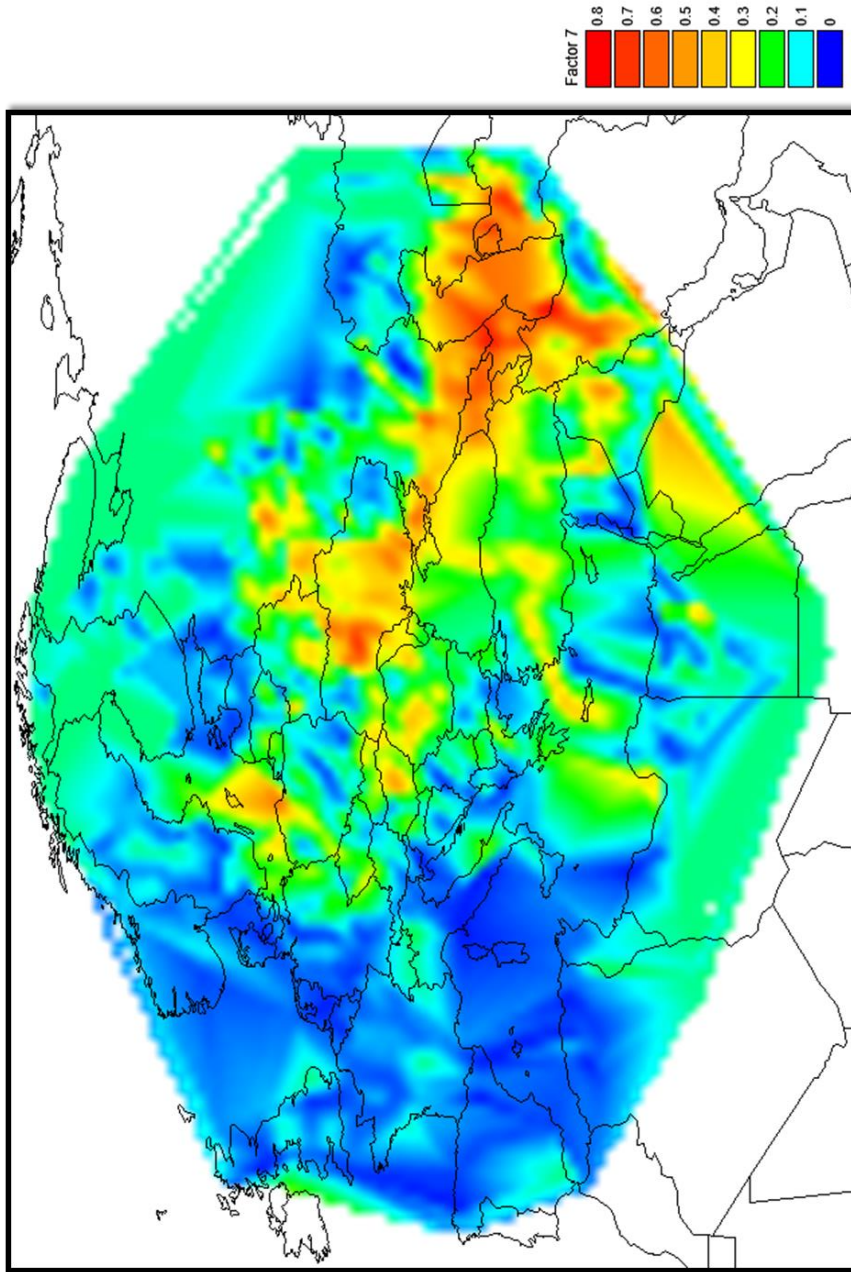


Figure 4.62 Distribution of PSCF values computed using trajectories that correspond to highest 30% of factor 7 scores as “polluted” trajectories

CHAPTER 5

CONCLUSIONS AND RECOMMENDATIONS

Generation of a comprehensive data set reflecting chemical composition of atmosphere at Eastern Black Sea region is important, because this is the first data set since 1990s in the region. The literature associated with temporal coverage of trace element concentrations of Eastern Black Sea atmosphere is very limited. There are available studies in the Black Sea region, but the studies were conducted on the Central or Western Black Sea and the composition of PM at different parts of the Black Sea region are not same.

Daily size distributed PM samples collected using a SFU on the Eastern Black Sea region of Turkey were analyzed with ICP-MS, ED-XRF and Aethalometer to provide a multi-specie data set. Mean concentrations of trace elements in the fine fraction varied between 0.0011 ng m⁻³ for Tm and 1382.42 ng m⁻³ for SO₄²⁻, while mean concentrations in the coarse fraction varied between 0.0017 ng m⁻³ for Tm and 1441.5 ng m⁻³ for Si. The comparison of the measured concentrations of trace element with the studies conducted in Mediterranean basin and other parts of the Turkey showed that the concentration of species originate from iron and steel plants such as Cr, Mn, Ni and Zn are higher than those measured levels at Mediterranean Basin. This indicates a remarkable influence of anthropogenic species at the region.

Back trajectories were classified into eight clusters depending on their direction and speed. Each of these groups represented main atmospheric transport pattern of air masses arriving the region. Relation between chemical composition of aerosols and clusters were investigated to establish a source-receptor relation. Cluster 1 and 6 together represented slowest moving back trajectories and expected to transport pollutants to the station from the nearby sources. Cluster 5 back trajectories covered region over Africa. Back trajectories of Cluster 4 showed movement air masses from east direction. The remaining clusters 2, 3, 7 and 8 were consisted of back trajectories

arriving from West and Northwest directions. Variation of concentrations of species among the clusters showed that: Cluster 5 and Cluster 1 carried crustal species; anthropogenic composition of Cluster 3, Cluster 4, and Cluster 8 were higher than others.

Species concentrations were not directly related with local wind speed and temperature. Local rain events were not effective on majority of the species. They were effective only on Na, SO₄²⁻, V, Sn, Sb, Lu, and Tl. This confirmed long-range transport nature of the species.

Temporal variations of species were investigated in two different temporal time-scales as short term (episodic) and long term (seasonal). Episodic nature of trace elements were investigated in the short term variations. Contribution of episodes to crustal and anthropogenic species were $66 \pm 11\%$ and $57 \pm 8\%$ and, respectively. Variations in air mass motions were identified as major factor determining episodic contributions. Species showed well-defined seasonal variations. Most of crustal and anthropogenic species had their maxima in the summer season. Seasonal differences of species were mostly controlled by proximity sources and rain events occurred on the ways of pollutants during their long-range transport to the station.

The influence of forest fires on aerosol composition at Eastern Black Sea was identified by satellite forest fire data, back trajectories and using K as tracer for forest fire emissions. Seven forest fire days were identified. These forest fires were mostly located Ukraine, Russia, and eastern parts of Turkey. Forest fires did not significantly affect mean K concentration at Eastern Black Sea region. However, forest fires accounted for 18% increase in K enrichment factor.

Mineral dust tracers (Al and Si), air mass back trajectories, satellite images and mineral dust forecast models were used to identify PM samples affected from dust transports from different deserts. Twenty-eight dust events were identified with this approach. It was concluded that Eastern Black Sea region is affected most from dust transport from Middle East and Arabic Peninsula, but not much from Sahara. Average contribution

of dust to lithophilic elements was 13% and approximately 5% of PM_{2.5} mass at the station was accounted by desert dust. Concentrations of major lithophilic elements, like Ca, Li, Si, Fe, Al Na, M, K had higher concentrations in Middle East dust, whereas concentrations of trace lithophilic elements, particularly, rare earth elements had higher concentrations in Saharan Dust.

Source apportionment of PM was carried out by PMF model. PMF resolved PM sampled at the station into seven components. These components include (1) Anthropogenic emission which accounted for 17% of PM_{2.5} mass and accounted for >80% of Sb, >40% of Se, >20% of Na, Cu, K, Cu, As, Sn, Tl and Pb concentrations; (2) iron and steel plant emissions which accounted 2% of PM_{2.5} mass and accounted for 85% Cr, 40% for Fe and 20% of Cu, Sn, Te, Pb, 30%; (3) urban pollution emissions which accounted 13% of PM_{2.5} mass and accounted for approximately 80% of BC, 70% of Ag, 50% of Ni and 30% Mn, Cu, As, Te concentrations; (4) Crustal emissions which accounted 14% of PM_{2.5} mass and accounted for 70 – 80% of concentrations of most lithophiles; (5) Another crustal emissions which accounted 1% of PM_{2.5} mass and accounted for 50 to 60% of concentrations of rare earth elements; (6) Oil processing emissions which accounted 3% of PM_{2.5} mass and accounted for 70 – 80% of concentrations of Sm and Eu and 10-to-20% of chalcophile concentrations; (7) Power plant emissions which accounted 50% of PM_{2.5} mass and accounted for 80% of SO₄²⁻ concentration and 30 - 50% of Cu, Zn, Ge, As, Se, Cd, Te and Tl concentrations.

Potential source regions for sources resolved by PMF were identified using weighted potential source contribution function (PSCF) analysis. Middle East was an obvious source region for factor 4, which accounted for lithophiles, whereas for factor 5 west of Turkey, parts of North Africa, west of Ukraine, north of Caspian Sea were highlighted as source regions. For most of the anthropogenic nature factors source regions were highlighted as countries to the east of Turkey. Countries around the Caspian Sea were source regions for anthropogenic elements. For factor 6, which accounted for oil processing emissions, countries surrounding Turkey, from Balkan countries to all the way to Caspian Sea countries, were highlighted as source regions. Relatively local source regions concluded as Caspian Sea region, Iran, Iraq, Syria in PSCF approach.

Air pollution is a complex environmental problem. In order to solve air pollution problems and determine strategies, both the scientific community and the relevant authority have focused on monitoring and analyzing the atmospheric pollutant concentrations. Authorities put air quality limits to prevent or reduce the harmful effects of air pollution on the environment and human health. The delineation of contribution of local sources and distant sources is a crucial step in forming balanced and cost effective strategies for dealing complex air pollution problem in a region. Pollution in rural areas are predominantly caused by long range transport as local sources are scarce or non-exist. This study provided invaluable information on source types affecting the aerosol population in the Eastern Black Sea Region, contribution of these to the measured levels of pollutants and locations of these sources to the policy makers. The results of the showed that the PM_{10} limit value was exceeded 10 times during sampling period. It is suggested that with appropriate actions taken at source areas at a regional basis, current average element concentrations at Eastern Black Sea basin can be reduced by approximately 60%.

This study indicated that Eastern Black Sea region is influenced from long range and regionally transported PM. The outcomes of the study was interesting at some points; for example when dust transport to Turkey is mentioned transport from Saharan comes to mind first. But, the source apportionment of PM showed that Middle East is a significant source region for dust transport. Another example is the anthropogenic content transported from the countries east of Turkey. Various studies have shown that Balkan countries, Ukraine and Russia were important source regions for anthropogenic content of PM for Turkey. All these outcomes were based on a one year-long sampling. Therefore, continuous measurements of aerosol in this region can be performed to have statistically more confidential answers.

Number of parameters measured can be increased to increase the resolution of the PMF model, major ions may be included to data set. Thus, the common tracers for specific sources could be more helpful to determine the source types. Each receptor model has its physical assumptions. Therefore, each model has advantages and physical limitations compared to other receptor models. In this study, PMF model was used to

apportion sources affecting Eastern Black Sea atmosphere. Using different receptor models (e.g., UNMIX, ME and PMF) together in a comparative manner may give more statistically confidential results to the sources types affecting the Eastern Black Sea region.

REFERENCES

- Abdalmogith, S. S., Harrison, R. M. (2005). The use of trajectory cluster analysis to examine the long-range transport of secondary inorganic aerosol in the UK. *Atmospheric Environment*, 39(35), 6686-6695.
- Abdolahnejad, A., Jafari, N., Mohammadi, A., Miri, M., Hajizadeh, Y., Nikoonahad, A. (2017). Cardiovascular, respiratory, and total mortality ascribed to PM10 and PM2.5 exposure in Isfahan, Iran. *Journal of education and health promotion*, 6.
- Alagha, O., Tuncel, G. (2003). Evaluation of air quality over the Black Sea: Major ionic composition of rainwater. *Water, Air and Soil Pollution: Focus*, 3(5-6), 89-98.
- Al-Eshaikh, M. A., Kadachi, A. (2011). Elemental analysis of steel products using X-ray fluorescence (XRF) technique. *Journal of King Saud University-Engineering Sciences*, 23(2), 75-79.
- Almeida, S. M., Pio, C. A., Freitas, M. C., Reis, M. A., Trancoso, M. A. (2005). Source apportionment of fine and coarse particulate matter in a sub-urban area at the Western European Coast. *Atmospheric Environment*, 39(17), 3127-3138.
- Al-Momani, I. F., Daradkeh, A. S., Haj-Hussein, A. T., Yousef, Y. A., Jaradat, Q. M., Momani, K. A. (2005). Trace elements in daily collected aerosols in Al-Hashimya, central Jordan. *Atmospheric Research*, 73(1-2), 87-100.
- Anderson, J. O., Thundiyil, J. G., Stolbach, A. (2012). Clearing the air: a review of the effects of particulate matter air pollution on human health. *Journal of Medical Toxicology*, 8(2), 166-175.
- AQEG. (2005). *Particulate Matter in the UK: Summary*. Defra. London.
- Arimoto, R., Duce, R. A., Ray, B. J., Hewitt, A. D., Williams, J. (1987). Trace elements in the atmosphere of American Samoa: concentrations and deposition to the

- tropical South Pacific. *Journal of Geophysical Research: Atmospheres*, 92(D7), 8465-8479.
- Artaxo, P., Fernandes, E. T., Martins, J. V., Yamasoe, M. A., Hobbs, P. V., Maenhaut, W., Longo, K. M., Castanho, A. (1998). Large-scale aerosol source apportionment in Amazonia. *Journal of Geophysical Research: Atmospheres*, 103(D24), 31837-31847.
- Artaxo, P., Oyola, P., Martinez, R. (1999). Aerosol composition and source apportionment in Santiago de Chile. *Nuclear Instruments and Methods in Physics Research Section B: Beam Interactions with Materials and Atoms*, 150(1-4), 409-416.
- Ashbaugh, L. L., Malm, W. C., Sadeh, W. Z. (1985). A residence time probability analysis of sulfur concentrations at Grand Canyon National Park. *Atmospheric Environment* (1967), 19(8), 1263-1270.
- Athanasopoulou, E., Protonotariou, A., Papangelis, G., Tombrou, M., Mihalopoulos, N., Gerasopoulos, E. (2016). Long-range transport of Saharan dust and chemical transformations over the Eastern Mediterranean. *Atmospheric Environment*, 140, 592-604.
- Balis, D. (2012). Geometrical characteristics of desert dust layers over Thessaloniki estimated with backscatter/Raman lidar and the BSC/DREAM model. *Remote sensing letters*, 3(4), 353-362.
- Balis, D. S., Amiridis, V., Zerefos, C., Gerasopoulos, E., Andreae, M., Zanis, P., Kazantzidis, A., Kazadzis, S., Papayannis, A. (2003). Raman lidar and sunphotometric measurements of aerosol optical properties over Thessaloniki, Greece during a biomass burning episode. *Atmospheric Environment*, 37(32), 4529-4538.
- Barbaro, E., Zangrando, R., Kirchgeorg, T., Bazzano, A., Illuminati, S., Annibaldi, A., Rella, S., Truzzi, C., Grotti, M., Ceccarini, A., Malitesta, C. (2016). An integrated study of the chemical composition of Antarctic aerosol to investigate natural and anthropogenic sources. *Environmental Chemistry*, 13(5), 867-876.
- Bari, M. A., Baumbach, G., Sarachage-Ruiz, L., Kleanthous, S. (2009). Identification of PM 10 sources in a Mediterranean island. *Water, Air, & Soil Pollution: Focus*, 9(1-2), 39-53.

- Barnaba, F., Gobbi, G. P. (2004). Aerosol seasonal variability over the Mediterranean region and relative impact of maritime, continental and Saharan dust particles over the basin from MODIS data in the year 2001. *Atmospheric Chemistry and Physics*, 4(9/10), 2367-2391.
- Bennet, C., Jonsson, P., Selin Lindgren, E. (2005). Concentrations and sources of trace elements in particulate air pollution, Dar es Salaam, Tanzania, studied by EDXRF. *X-Ray Spectrometry*, 34(1), 1-6.
- Berglen, T. F., Myhre, G., Isaksen, I. S., Vestreng, V., Smith, S. J. (2007). Sulphate trends in Europe: are we able to model the recent observed decrease?. *Tellus B*, 59(4), 773-786.
- Birmili, W., Heinke, K., Pitz, M., Matschullat, J., Wiedensohler, A., Cyrys, J., Wichmann, H. E., Peters, A. (2010). Particle number size distributions in urban air before and after volatilisation. *Atmospheric Chemistry and Physics*, 10(10), 4643-4660.
- Bond, T. C., Streets, D. G., Yarber, K. F., Nelson, S. M., Woo, J. H., Klimont, Z. (2004). A technology-based global inventory of black and organic carbon emissions from combustion. *Journal of Geophysical Research: Atmospheres*, 109(D14).
- Brankov, E., Henry, R. F., Civerolo, K. L., Hao, W., Rao, S. T., Misra, P. K., Bloxam, R., Reid, N. (2003). Assessing the effects of transboundary ozone pollution between Ontario, Canada and New York, USA. *Environmental Pollution*, 123(3), 403-411.
- Brankov, E., Rao, S. T., Porter, P. S. (1998). A trajectory-clustering-correlation methodology for examining the long-range transport of air pollutants. *Atmospheric Environment*, 32(9), 1525-1534.
- Braziewicz, J., Kownacka, L., Majewska, U., Korman, A. (2004). Elemental concentrations in tropospheric and lower stratospheric air in a Northeastern region of Poland. *Atmospheric environment*, 38(13), 1989-1996.
- Brook, J. R., Lillyman, C. D., Shepherd, M. F., Mamedov, A. (2002). Regional transport and urban contributions to fine particle concentrations in southeastern Canada. *Journal of the Air & Waste Management Association*, 52(7), 855-866.

- Buseck, P. R., POsfai, M. (1999). Airborne minerals and related aerosol particles: Effects on climate and the environment. *Proceedings of the National Academy of Sciences*, 96(7), 3372-3379.
- Cabello, M., Orza, J. A. G., Barrero, M. A., Gordo, E., Berasaluce, A., Cantón, L., Dueñas, C., Fernández, M.C., Pérez, M. (2012). Spatial and temporal variation of the impact of an extreme Saharan dust event. *Journal of Geophysical Research: Atmospheres*, 117(D11).
- Çelik, İ. (2014). *Source Apportionment of Trace Elements in Ankara*. MSc Thesis, Middle East Technical University, Ankara
- Cetin, B., Yatkin, S., Bayram, A., Odabasi, M. (2007). Ambient concentrations and source apportionment of PCBs and trace elements around an industrial area in Izmir, Turkey. *Chemosphere*, 69(8), 1267-1277.
- Chan, K. L. (2017). Biomass burning sources and their contributions to the local air quality in Hong Kong. *Science of the Total Environment*, 596, 212-221.
- Charlson, R. J., Schwartz, S. E., Hales, J. M., Cess, R. D., Coakley, J. J., Hansen, J. E., Hofmann, D. J. (1992). Climate forcing by anthropogenic aerosols. *Science*, 255(5043), 423-430.
- Chen, Y., Li, Q., Randerson, J. T., Lyons, E. A., Kahn, R. A., Nelson, D. L., Diner, D. J. (2009). The sensitivity of CO and aerosol transport to the temporal and vertical distribution of North American boreal fire emissions. *Atmospheric Chemistry and Physics*, 9(17), 6559-6580.
- Cheng, Z., Wang, S., Jiang, J., Fu, Q., Chen, C., Xu, B., Yu, J., Fu, X., Hao, J. (2013). Long-term trend of haze pollution and impact of particulate matter in the Yangtze River Delta, China. *Environmental pollution*, 182, 101-110.
- Cuspilici, A., Monforte, P., Ragusa, M. A. (2017). Study of Saharan dust influence on PM10 measures in Sicily from 2013 to 2015. *Ecological Indicators*, 76, 297-303.
- Daud, Z., Mohamed, C. A. R. (2016). A short review of the distribution and behavior of rare earth elements in the Southern South China Sea. *Pollution Research*, 35(2), 235-246.

- DeCarlo, P. F., Slowik, J. G., Worsnop, D. R., Davidovits, P., Jimenez, J. L. (2004). Particle morphology and density characterization by combined mobility and aerodynamic diameter measurements. Part 1: Theory. *Aerosol Science and Technology*, 38(12), 1185-1205.
- Deroubaix, A., Martiny, N., Chiapello, I., Marticoréna, B. (2013). Suitability of OMI aerosol index to reflect mineral dust surface conditions: Preliminary application for studying the link with meningitis epidemics in the Sahel. *Remote sensing of environment*, 133, 116-127.
- Dey, S., Tripathi, S. N., Singh, R. P., Holben, B. N. (2004). Influence of dust storms on the aerosol optical properties over the Indo-Gangetic basin. *Journal of Geophysical Research: Atmospheres*, 109(D20).
- Dogan, G., Gullu, G., Karakas, D., Tuncel, G. (2010). Comparison of Source Regions Affecting SO₄²⁻ and NO₃⁻ Concentrations at the Eastern Mediterranean and Black Sea Atmospheres. *Current Analytical Chemistry*, 6(1), 66-71.
- Dorling, S. R., Davies, T. D., Pierce, C. E. (1992). Cluster analysis: A technique for estimating the synoptic meteorological controls on air and precipitation chemistry—Method and applications. *Atmospheric Environment. Part A. General Topics*, 26(14), 2575-2581.
- Draxler, R. R., Hess, G. D. (1998). An overview of the HYSPLIT_4 modelling system for trajectories. *Australian meteorological magazine*, 47(4), 295-308.
- Duce, R. A., Hoffman, G. L., Zoller, W. H. (1975). Atmospheric trace metals at remote northern and southern hemisphere sites: pollution or natural?. *Science*, 187(4171), 59-61.
- Duchi, R., Cristofanelli, P., Landi, T. C., Arduini, J., Bonafe, U., Bourcier, L., Busetto, M., Calzolari, F., Marinoni, A., Putero, D., Bonasoni, P. (2016). Long-term (2002–2012) investigation of Saharan dust transport events at Mt. Cimone GAW global station, Italy (2165 m asl). *Elem Sci Anth*, 4.
- Dzubay, T. G., Stevens, R. K., Haagenson, P. L. (1984). Composition and origins of aerosol at a forested mountain in Soviet Georgia. *Environmental science & technology*, 18(11), 873-883.

- EIA. (2016). The U.S. Energy Information Administration. Retrieved from <https://www.eia.gov/beta> (March 12, 2018)
- El-Agha, O. (2000). *Chemical Composition of Precipitation in Black Sea Region*. PhD Thesis, Middle East Technical University, Ankara
- Energy Information Administration. (1999). Natural Gas 1998 Issues and Trends. Retrieved from https://www.eia.gov/oil_gas/natural_gas/analysis_publications/natural_gas_1998_issues_and_trends/it98.html (June 01, 2017)
- Eneroth, K., Kjellström, E., Holmén, K. (2003). A trajectory climatology for Svalbard; investigating how atmospheric flow patterns influence observed tracer concentrations. *Physics and Chemistry of the Earth, Parts A/B/C*, 28(28-32), 1191-1203.
- Esteve, A. R., Estellés, V., Utrillas, M. P., Martínez-Lozano, J. A. (2012). In-situ integrating nephelometer measurements of the scattering properties of atmospheric aerosols at an urban coastal site in western Mediterranean. *Atmospheric environment*, 47, 43-50.
- European Commission. (1997). Ambient air pollution by particulate matter. Retrieved from http://ec.europa.eu/environment/air/pdf/pp_pm.pdf (September 23, 2017)
- European Commission. (2017). Air Quality Standards. Retrieved from <http://ec.europa.eu/environment/air/quality/standards.htm> (March 2, 2018)
- Fast, J. D., Berkowitz, C. M. (1997). Evaluation of back trajectories associated with ozone transport during the 1993 North Atlantic Regional Experiment. *Atmospheric Environment*, 31(6), 825-837.
- Fenger, J. (1999). Urban air quality. *Atmospheric environment*, 33(29), 4877-4900.
- Forster, C., Wandler, U., Wotawa, G., James, P., Mattis, I., Althausen, D., Simmonds, P., O'Doherty, S., Jennings, S.G., Kleefeld, C., Schneider, J. (2001). Transport of boreal forest fire emissions from Canada to Europe. *Journal of Geophysical Research: Atmospheres*, 106(D19), 22887-22906.

- Fotiadi, A., Hatzianastassiou, N., Drakakis, E., Matsoukas, C., Pavlakis, K. G., Hatzidimitriou, D., Gerasopoulos, E., Mihalopoulos, N., Vardavas, I. (2006). Aerosol physical and optical properties in the Eastern Mediterranean Basin, Crete, from Aerosol Robotic Network data. *Atmospheric Chemistry and Physics*, 6(12), 5399-5413.
- Franzi, L. M., Bratt, J. M., Williams, K. M., Last, J. A. (2011). Why is particulate matter produced by wildfires toxic to lung macrophages?. *Toxicology and applied pharmacology*, 257(2), 182-188.
- Fuzzi, S., Baltensperger, U., Carslaw, K., Decesari, S., Denier Van Der Gon, H., Facchini, M. C., Fowler, D., Koren, I., Langford, B., Lohmann, U., Nemitz, E. (2015). Particulate matter, air quality and climate: lessons learned and future needs. *Atmospheric chemistry and physics*, 15(14), 8217-8299.
- Galindo, N., Yubero, E., Nicolás, J. F., Crespo, J., Varea, M., Gil-Moltó, J. (2017). Regional and long-range transport of aerosols at Mt. Aitana, Southeastern Spain. *Science of the Total Environment*, 584, 723-730.
- Gálvez, O. (2007). Synoptic-scale transport of ozone into Southern Ontario. *Atmospheric Environment*, 41(38), 8579-8595.
- Gatari, M., Wagner, A., Boman, J. (2005). Elemental composition of tropospheric aerosols in Hanoi, Vietnam and Nairobi, Kenya. *Science of the Total Environment*, 341(1-3), 241-249.
- Gerasopoulos, E., Kokkalis, P., Amiridis, V., Liakakou, E., Perez, C., Haustein, K., Eleftheratos, K., Andreae, M.O., Andreae, T.W., Zerefos, C. S. (2009, July). Dust specific extinction cross-sections over the Eastern Mediterranean using the BSC-DREAM model and sun photometer data: the case of urban environments. In *Annales Geophysicae* (Vol. 27, No. 7, pp. 2903-2912). Copernicus GmbH.
- Gerasopoulos, E., Kouvarakis, G., Babasakalis, P., Vrekoussis, M., Putaud, J. P., Mihalopoulos, N. (2006). Origin and variability of particulate matter (PM10) mass concentrations over the Eastern Mediterranean. *Atmospheric Environment*, 40(25), 4679-4690.
- Gerasopoulos, E., Kouvarakis, G., Vrekoussis, M., Kanakidou, M., Mihalopoulos, N. (2005). Ozone variability in the marine boundary layer of the eastern

- Mediterranean based on 7-year observations. *Journal of Geophysical Research: Atmospheres*, 110(D15).
- Gertler, A. W. (2005). Diesel vs. gasoline emissions: Does PM from diesel or gasoline vehicles dominate in the US?. *Atmospheric Environment*, 39(13), 2349-2355.
- Gildemeister, A. E., Hopke, P. K., Kim, E. (2007). Sources of fine urban particulate matter in Detroit, MI. *Chemosphere*, 69(7), 1064-1074.
- Gordon, G. E. (1988). Receptor models. *Environmental science & technology*, 22(10), 1132-1142.
- Grythe, H., Ström, J., Krejci, R., Quinn, P., Stohl, A. (2014). A review of sea-spray aerosol source functions using a large global set of sea salt aerosol concentration measurements. *Atmospheric Chemistry and Physics*, 14(3), 1277.
- Gülen, G. (1989) *Sources of Atmospheric Aerosols in the Eastern Mediterranean Basin*. PhD Thesis, Middle East Technical University, Ankara
- Güllü, G. H., Ölmez, İ., Tuncel, G. (2000). Temporal variability of atmospheric trace element concentrations over the eastern Mediterranean Sea. *Spectrochimica Acta Part B: Atomic Spectroscopy*, 55(7), 1135-1150.
- Güllü, G. H., Ölmez, I., Aygün, S., Tuncel, G. (1998). Atmospheric trace element concentrations over the eastern Mediterranean Sea: Factors affecting temporal variability. *Journal of Geophysical Research: Atmospheres*, 103(D17), 21943-21954.
- Hacisalihoglu, G., Eliyakut, F., Ölmez, I., Balkas, T. I., Tuncel, G. (1992). Chemical composition of particles in the Black Sea atmosphere. *Atmospheric Environment. Part A. General Topics*, 26(17), 3207-3218.
- Halter, B. C., Harris, J. M., Rahn, K. A. (1985). A study of winter variability in carbon dioxide and Arctic haze aerosols at Barrow, Alaska. *Atmospheric Environment (1967)*, 19(12), 2033-2037.
- Harris, J. M., Kahl, J. D. (1990). A descriptive atmospheric transport climatology for the Mauna Loa Observatory, using clustered trajectories. *Journal of Geophysical Research: Atmospheres*, 95(D9), 13651-13667.

- Haywood, J., Boucher, O. (2000). Estimates of the direct and indirect radiative forcing due to tropospheric aerosols: A review. *Reviews of geophysics*, 38(4), 513-543.
- Herut, B., Nimmo, M., Medway, A., Chester, R., Krom, M. D. (2001). Dry atmospheric inputs of trace metals at the Mediterranean coast of Israel (SE Mediterranean): sources and fluxes. *Atmospheric Environment*, 35(4), 803-813.
- Hinds, W. C. (2012). *Aerosol technology: properties, behavior, and measurement of airborne particles*. John Wiley & Sons.
- Hopke, P. K. (2016). Review of receptor modeling methods for source apportionment. *Journal of the Air & Waste Management Association*, 66(3), 237-259.
- Hopke, P. K., Le Li, C., Ciszek, W., Landsberger, S. (1995). The use of bootstrapping to estimate conditional probability fields for source locations of airborne pollutants. *Chemometrics and Intelligent Laboratory Systems*, 30(1), 69-79.
- Hopke, P. K., Xie, Y., Raunemaa, T., Biegalski, S., Landsberger, S., Maenhaut, W., Artaxo, P., Cohen, D. (1997). Characterization of the Gent stacked filter unit PM10 sampler. *Aerosol Science and Technology*, 27(6), 726-735.
- Houghton, J. T., Ding, Y. D. J. G., Griggs, D. J., Noguera, M., van der Linden, P. J., Dai, X., Johnson, C. A. (2001). *Climate change 2001: the scientific basis*. The Press Syndicate of the University of Cambridge.
- Huang, J. J., Löwemark, L., Chang, Q., Lin, T. Y., Chen, H. F., Song, S. R., Wei, K. Y. (2016). Choosing optimal exposure times for XRF core-scanning: Suggestions based on the analysis of geological reference materials. *Geochemistry, Geophysics, Geosystems*, 17(4), 1558-1566.
- Hung-Lung, C., Yao-Sheng, H. (2009). Particulate matter emissions from on-road vehicles in a freeway tunnel study. *Atmospheric Environment*, 43(26), 4014-4022.
- Husain, L., Parekh, P. P., Halstead, J. A., Dutkiewicz, V. A. (1982). Sources of aerosol sulfate and trace elements of Whiteface Mountain, New York. Presented at the 75th Annual Meeting of the Air Pollution Control Association, New Orleans, LA.

- Hyer, E. J., Kasischke, E. S., Allen, D. J. (2007). Effects of source temporal resolution on transport simulations of boreal fire emissions. *Journal of Geophysical Research: Atmospheres*, 112(D1).
- Ichoku, C., Andreae, M. O., Andreae, T. W., Meixner, F. X., Schebeske, G., Formenti, P., Maenhaut, W., Cafmeyer, J., Ptasinski, J., Karnieli, A., Orlovsky, L. (1999). Interrelationships between aerosol characteristics and light scattering during late winter in an Eastern Mediterranean arid environment. *Journal of Geophysical Research: Atmospheres*, 104(D20), 24371-24393.
- Jacob, D. J. (2000). Heterogeneous chemistry and tropospheric ozone. *Atmospheric Environment*, 34(12-14), 2131-2159.
- Jimoda, L. A. (2012). Effects of particulate matter on human health, the ecosystem, climate and materials: a review. *Facta universitatis-series: Working and Living Environmental Protection*, 9(1), 27-44.
- Jones, A. M., Yin, J., Harrison, R. M. (2008). The weekday–weekend difference and the estimation of the non-vehicle contributions to the urban increment of airborne particulate matter. *Atmospheric Environment*, 42(19), 4467-4479.
- Kalivitis, N., Gerasopoulos, E., Vrekoussis, M., Kouvarakis, G., Kubilay, N., Hatzianastassiou, N., Vardavas, I., Mihalopoulos, N. (2007). Dust transport over the eastern Mediterranean derived from Total Ozone Mapping Spectrometer, Aerosol Robotic Network, and surface measurements. *Journal of Geophysical Research: Atmospheres*, 112(D3).
- Kalivitis, N., Kerminen, V. M., Kouvarakis, G., Stavroulas, I., Bougiatioti, A., Nenes, A., Manninen, H.E., Petäjä, T., Kulmala, M., Mihalopoulos, N. (2015). Atmospheric new particle formation as a source of CCN in the eastern Mediterranean marine boundary layer. *Atmospheric Chemistry and Physics*, 15(16), 9203-9215.
- Karakas, D., Olmez, I., Tosun, S., Tuncel, G. (2004). Trace element composition of Black Sea aerosols. *Journal of Radioanalytical and Nuclear Chemistry*, 159(2), 187-192.
- Karanasiou, A. A., Siskos, P. A., Eleftheriadis, K. (2009). Assessment of source apportionment by Positive Matrix Factorization analysis on fine and coarse urban aerosol size fractions. *Atmospheric Environment*, 43(21), 3385-3395.

- Karanasiou, A., Moreno, N., Moreno, T., Viana, M., De Leeuw, F., Querol, X. (2012). Health effects from Sahara dust episodes in Europe: literature review and research gaps. *Environment international*, 47, 107-114.
- Katsoulis, B. D. (1999). The potential for long-range transport of air-pollutants into Greece: a climatological analysis. *Science of the total environment*, 231(2-3), 101-113.
- Keeler, G. J., Spengler, J. D., Koutrakis, P., Allen, G. A., Raizenne, M., Stern, B. (1990). Transported acid aerosols measured in southern Ontario. *Atmospheric Environment. Part A. General Topics*, 24(12), 2935-2950.
- Kerminen, V. M., Paramonov, M., Anttila, T., Riipinen, I., Fountoukis, C., Korhonen, H., Asmi, E., Laakso, L., Lihavainen, H., Swietlicki, E., Svenningsson, B. (2012). Cloud condensation nuclei production associated with atmospheric nucleation: a synthesis based on existing literature and new results. *Atmospheric Chemistry and Physics*, 12(24), 12037-12059.
- Khan, A. J., Li, J., Dutkiewicz, V. A., Husain, L. (2010). Elemental carbon and sulfate aerosols over a rural mountain site in the northeastern United States: Regional emissions and implications for climate change. *Atmospheric Environment*, 44(19), 2364-2371.
- Kim, E., Hopke, P. K., Edgerton, E. S. (2003). Source identification of Atlanta aerosol by positive matrix factorization. *Journal of the Air & Waste Management Association*, 53(6), 731-739.
- Kim, K. H., Kabir, E., Kabir, S. (2015). A review on the human health impact of airborne particulate matter. *Environment international*, 74, 136-143.
- Kimbrough, S., Hanley, T., Hagler, G., Baldauf, R., Snyder, M., Brantley, H. (2018). Influential factors affecting black carbon trends at four sites of differing distance from a major highway in Las Vegas. *Air Quality, Atmosphere & Health*, 11(2), 181-196.
- Koçak, M., Mihalopoulos, N., Kubilay, N. (2007a). Chemical composition of the fine and coarse fraction of aerosols in the northeastern Mediterranean. *Atmospheric Environment*, 41(34), 7351-7368.

- Koçak, M., Mihalopoulos, N., Kubilay, N. (2007b). Contributions of natural sources to high PM₁₀ and PM_{2.5}. 5 events in the eastern Mediterranean. *Atmospheric Environment*, 41(18), 3806-3818.
- Koçak, M., Nimmo, M., Kubilay, N., Herut, B. (2004). Spatio-temporal aerosol trace metal concentrations and sources in the Levantine Basin of the Eastern Mediterranean. *Atmospheric Environment*, 38(14), 2133-2144.
- Koulouri, E., Saarikoski, S., Theodosi, C., Markaki, Z., Gerasopoulos, E., Kouvarakis, G., Mäkelä, T., Hillamo, R., Mihalopoulos, N. (2008). Chemical composition and sources of fine and coarse aerosol particles in the Eastern Mediterranean. *Atmospheric Environment*, 42(26), 6542-6550.
- Krecl, P., Johansson, C., Targino, A. C., Ström, J., Burman, L. (2017). Trends in black carbon and size-resolved particle number concentrations and vehicle emission factors under real-world conditions. *Atmospheric Environment*, 165, 155-168.
- Kubilay, N., Yemenicioglu, S., Saydam, A. C. (1995). Airborne material collections and their chemical composition over the Black Sea. *Marine Pollution Bulletin*, 30(7), 475-483.
- Kulkarni, P., Chellam, S., Flanagan, J. B., Jayanty, R. K. M. (2007). Microwave digestion—ICP-MS for elemental analysis in ambient airborne fine particulate matter: rare earth elements and validation using a filter borne fine particle certified reference material. *Analytica chimica acta*, 599(2), 170-176.
- Kuloglu, E., Tuncel, G. (2005). Size distribution of trace elements and major ions in the eastern Mediterranean atmosphere. *Water, air, and soil pollution*, 167(1-4), 221-241.
- Kuntasal, O. Ö. (2005). *Temporal variations and sources of organic pollutants in two urban atmospheres*. PhD Thesis, Middle East Technical University, Ankara
- Künzli, N., Kaiser, R., Medina, S., Studnicka, M., Chanel, O., Filliger, P., Herry, M., Horak Jr, F., Puybonnieux-Textier, V., Quénel, P., Schneider, J. (2000). Public-health impact of outdoor and traffic-related air pollution: a European assessment. *The Lancet*, 356(9232), 795-801.

- Kyrkilis, G., Chaloulakou, A., Kassomenos, P. A. (2007). Development of an aggregate Air Quality Index for an urban Mediterranean agglomeration: Relation to potential health effects. *Environment International*, 33(5), 670-676.
- Lacerda, L. D. (1997). Global mercury emissions from gold and silver mining. *Water, Air, and Soil Pollution*, 97(3-4), 209-221.
- Langmann, B. (2013). Volcanic ash versus mineral dust: atmospheric processing and environmental and climate impacts. *ISRN Atmospheric Sciences*, 2013.
- Laskin, D. (2006). The great London smog. *Weatherwise*, 59(6), 42-45.
- Lee, A. K., Willis, M. D., Healy, R. M., Wang, J. M., Jeong, C. H., Wenger, J. C., Evans, G.J., Abbatt, J. P. (2016). Single-particle characterization of biomass burning organic aerosol (BBOA): evidence for non-uniform mixing of high molecular weight organics and potassium. *Atmospheric Chemistry and Physics*, 16(9), 5561-5572.
- Lee, J. H., Hopke, P. K. (2006). Apportioning sources of PM_{2.5} in St. Louis, MO using speciation trends network data. *Atmospheric Environment*, 40, 360-377.
- Lelieveld, J., Berresheim, H., Borrmann, S., Crutzen, P. J., Dentener, F. J., Fischer, H., Feichter, J., Flatau, P.J., Heland, J., Holzinger, R., Korrman, R. (2002). Global air pollution crossroads over the Mediterranean. *Science*, 298(5594), 794-799.
- Lemmon, M. T., Wolff, M. J., Bell III, J. F., Smith, M. D., Cantor, B. A., Smith, P. H. (2015). Dust aerosol, clouds, and the atmospheric optical depth record over 5 Mars years of the Mars Exploration Rover mission. *Icarus*, 251, 96-111.
- Li, Q., Li, X., Jiang, J., Duan, L., Ge, S., Zhang, Q., Deng, J., Wang, S., Hao, J. (2016). Semi-coke briquettes: towards reducing emissions of primary PM_{2.5}, particulate carbon, and carbon monoxide from household coal combustion in China. *Scientific reports*, 6, 19306.
- Liu, W., Hopke, P. K., VanCuren, R. A. (2003). Origins of fine aerosol mass in the western United States using positive matrix factorization. *Journal of Geophysical Research: Atmospheres*, 108(D23).

- Lizarazo, L. M., Jordá, J. D., Juárez, M., Sánchez-Andreu, J. (2005). Effect of humic amendments on inorganic N, dehydrogenase and alkaline phosphatase activities of a Mediterranean soil. *Biology and fertility of soils*, 42(2), 172-177.
- Lopes, F., Appoloni, C. R., Nascimento, V. F., Melquiades, F. L., Almeida, L. C. (2006). Chemical characterization of particulate matter suspended in the atmosphere by energy dispersive X-ray fluorescence (EDXRF). *Journal of radioanalytical and nuclear chemistry*, 270(1), 43-46.
- Lu, H. C., Fang, G. C. (2002). Estimating the frequency distributions of PM10 and PM2.5 by the statistics of wind speed at Sha-Lu, Taiwan. *Science of the total environment*, 298(1-3), 119-130.
- Lupu, A., Maenhaut, W. (2002). Application and comparison of two statistical trajectory techniques for identification of source regions of atmospheric aerosol species. *Atmospheric Environment*, 36(36-37), 5607-5618.
- Ma, C. J., Kim, K. H. (2014). Preliminary Study on the Cloud Condensation Nuclei (CCN) Activation of Soot Particles by a Laboratory-scale Model Experiments. *Asian Journal of Atmospheric Environment (AJAE)*, 8(4).
- Mallet, M., Gomes, L., Solmon, F., Sellegri, K., Pont, V., Roger, J. C., Missamou, T., Piazzola, J. (2011). Calculation of key optical properties of the main anthropogenic aerosols over the Western French coastal Mediterranean Sea. *Atmospheric research*, 101(1-2), 396-411.
- Malm, W. C. (1999). Introduction to Visibility. Fort Collins, CO: Cooperative Institute for Research in the Atmosphere. Retrieved from <https://www.epa.gov/sites/production/files/2015-05/documents/introvis.pdf> (February 27, 2018)
- Mamane, Y., Perrino, C., Yossef, O., Catrambone, M. (2008). Source characterization of fine and coarse particles at the East Mediterranean coast. *Atmospheric Environment*, 42(24), 6114-6130.
- Mantas, E., Remoundaki, E., Halari, I., Kassomenos, P., Theodosi, C., Hatzikioseyan, A., Mihalopoulos, N. (2014). Mass closure and source apportionment of PM2.5 by Positive Matrix Factorization analysis in urban Mediterranean environment. *Atmospheric environment*, 94, 154-163.

- Marinou, E., Amiridis, V., Binietoglou, I., Tsikerdekis, A., Solomos, S., Proestakis, E., Konsta, D., Papagiannopoulos, N., Tsekeri, A., Vlastou, G., Zanis, P. (2017). Three-dimensional evolution of Saharan dust transport towards Europe based on a 9-year EARLINET-optimized CALIPSO dataset. *Atmospheric Chemistry and Physics*, 17(9), 5893.
- Mason, B., Moore, C. B. (1966). *Principles of Geochemistry*. John Willey and Sons. INC. New York. ISBN, 0471-57521.
- Mason, B., Moore, C. B. (1982). *Principles of Geochemistry forth edition*. John Willey and Sons. INC. New York.
- Mathys, P., Oetterli, C., Stern, W. B., Oglesby, L., Hazenkamp-von Arx, M. E., Kuenzli, N. (2002). Elemental analysis of PM_{2.5} samples collected in the framework of the ECRHS II study: description of methods.
- Mayer, H. (1999). Air pollution in cities. *Atmospheric environment*, 33(24-25), 4029-4037.
- Mehta, M., Sharma, V. Doley, G. J. (2018). Aerosol Optical Depth Variation During a Recent Dust Event in North India. In *Environmental Pollution* (pp. 567-571). Springer, Singapore.
- Merikanto, J., Spracklen, D. V., Mann, G. W., Pickering, S. J., Carslaw, K. S. (2009). Impact of nucleation on global CCN. *Atmospheric Chemistry and Physics*, 9(21), 8601-8616.
- Miller, P. J., Van Atten, C. (2005). North American power plant emissions. Retrieved from https://www.etde.org/etdeweb/details_open.jsp?osti_id=20572912 (October 4, 2017)
- Mitsakou, C., Kallos, G., Papantoniou, N., Spyrou, C., Solomos, S., Astitha, M., Housiadas, C. (2008). Saharan dust levels in Greece and received inhalation doses. *Atmospheric Chemistry and Physics*, 8(23), 7181-7192.
- Mitsakou, C., Kallos, G., Papantoniou, N., Spyrou, C., Solomos, S., Astitha, M., Housiadas, C. (2008). Saharan dust levels in Greece and received inhalation doses. *Atmospheric Chemistry and Physics*, 8(23), 7181-7192.

- Molteni, F., Buizza, R., Palmer, T. N., Petroliagis, T. (1996). The ECMWF ensemble prediction system: Methodology and validation. *Quarterly journal of the royal meteorological society*, 122(529), 73-119.
- Montaser, A. (Ed.). (1998). *Inductively coupled plasma mass spectrometry*. John Wiley & Sons.
- Moody, J. L., Keene, W. C., Cooper, O. R., Voss, K. J., Aryal, R., Eckhardt, S., Holben, B., Maben, J. R., Izaguirre, M. A., Galloway, J. N. (2014). Flow climatology for physicochemical properties of dichotomous aerosol over the western North Atlantic Ocean at Bermuda. *Atmospheric Chemistry and Physics*, 14(2), 691-717.
- Morawska, L., Zhang, J. J. (2002). Combustion sources of particles. 1. Health relevance and source signatures. *Chemosphere*, 49(9), 1045-1058.
- Moreno, T., Querol, X., Alastuey, A., de la Rosa, J., de la Campa, A. M. S., Minguillón, M., Pandolfi, M., González-Castanedo, Y., Monfort, E., Gibbons, W. (2010). Variations in vanadium, nickel and lanthanoid element concentrations in urban air. *Science of the Total Environment*, 408(20), 4569-4579.
- Müller, D., Mattis, I., Wandinger, U., Ansmann, A., Althausen, D., Stohl, A. (2005). Raman lidar observations of aged Siberian and Canadian forest fire smoke in the free troposphere over Germany in 2003: Microphysical particle characterization. *Journal of Geophysical Research: Atmospheres*, 110(D17).
- Munzur, B. (2008). *Chemical Composition of Atmospheric Particles in the Aegean Region*. MSc Thesis, Middle East Technical University, Ankara
- National Institute of Standards & Technology. (2011). Certificate of Analysis Standard Reference Material 2783
- National Research Council. (1980). *Controlling airborne particles*. National Academies.
- National Research Council. (2010). *Global sources of local pollution: An assessment of long-range transport of key air pollutants to and from the United States*. National Academies Press.

- Nemery, B., Hoet, P. H., Nemmar, A. (2001). The Meuse Valley fog of 1930: an air pollution disaster. *The lancet*, 357(9257), 704-708.
- Norris, G. (2014). EPA Positive Matrix Factorization (PMF) 5.0 Fundamentals & User Guide, US. Environmental Protection Agency.
- O'dowd, C. D., Facchini, M. C., Cavalli, F., Ceburnis, D., Mircea, M., Decesari, S., Fuzzi, S., Yoon, Y.J., Putaud, J. P. (2004). Biogenically driven organic contribution to marine aerosol. *Nature*, 431(7009), 676.
- Olmez, I., Gordon, G. E. (1985). Rare earths: atmospheric signatures for oil-fired power plants and refineries. *Science*, 229(4717), 966-968.
- Omidvarborna, H., Kumar, A., Kim, D. S. (2014). Characterization of particulate matter emitted from transit buses fueled with B20 in idle modes. *Journal of Environmental Chemical Engineering*, 2(4), 2335-2342.
- Öztürk, F. (2009). *Investigation of Short And Long Term Trends In The Eastern Mediterranean Aerosol Composition*. PhD Thesis, Middle East Technical University, Ankara
- Öztürk, F., Zararsız, A., Dutkiewicz, V. A., Husain, L., Hopke, P. K., Tuncel, G. (2012). Temporal variations and sources of Eastern Mediterranean aerosols based on a 9-year observation. *Atmospheric environment*, 61, 463-475.
- Paatero, P., Tapper, U. (1993). Analysis of different modes of factor analysis as least squares fit problems. *Chemometrics and Intelligent Laboratory Systems*, 18(2), 183-194.
- Paatero, P., Tapper, U. (1994). Positive matrix factorization: A non-negative factor model with optimal utilization of error estimates of data values. *Environmetrics*, 5(2), 111-126.
- Pacyna, J. M., Pacyna, E. G. (2001). An assessment of global and regional emissions of trace metals to the atmosphere from anthropogenic sources worldwide. *Environmental Reviews*, 9(4), 269-298.

- Padoan, E., Malandrino, M., Giacomino, A., Grosa, M. M., Lollobrigida, F., Martini, S., Abollino, O. (2016). Spatial distribution and potential sources of trace elements in PM10 monitored in urban and rural sites of Piedmont Region. *Chemosphere*, 145, 495-507.
- Palmer, R. F., Royall, D. R. (2010). Missing data? Plan on it!. *Journal of the American Geriatrics Society*, 58(s2).
- Parrington, J. R., Zoller, W. H. (1984). Diurnal and longer-term temporal changes in the composition of atmospheric particles at Mauna Loa, Hawaii. *Journal of Geophysical Research: Atmospheres*, 89(D2), 2522-2534.
- Paschalidou, A. K., Kassomenos, P., Karanikola, P. (2015). Disaggregating the contribution of local dispersion and long-range transport to the high PM10 values measured in a Mediterranean urban environment. *Science of the Total Environment*, 527, 119-125.
- Passant, N. R., Peirce, M., Rudd, H. J., Scott, D. W., Marlowe, I., Watterson, J. D. (2002). UK particulate and heavy metal emissions from industrial processes. *Netcen, AEA Technology, Harwell, Oxfordshire, Report No AEAT-6270*, (2).
- Peltier, R. E., Lippmann, M. (2010). Residual oil combustion: 2. Distributions of airborne nickel and vanadium within New York City. *Journal of Exposure Science and Environmental Epidemiology*, 20(4), 342.
- Perraud, V., Bruns, E. A., Ezell, M. J., Johnson, S. N., Yu, Y., Alexander, M. L., Zelenyuk, A., Imre, D., Chang, W.L., Dabdub, D., Pankow, J. F. (2012). Nonequilibrium atmospheric secondary organic aerosol formation and growth. *Proceedings of the National Academy of Sciences*, 109(8), 2836-2841.
- Pervan, T. (1991). *Application of a Regional Air Pollution Transport Model*. MSc Thesis, Middle East Technical University, Ankara
- Pey, J., Alastuey, A., Querol, X. (2013). PM10 and PM2.5 sources at an insular location in the western Mediterranean by using source apportionment techniques. *Science of the total environment*, 456, 267-277.

- Pio, C. A., Alves, C. A., Oliveira, T., Afonso, J., Puxbaum, H., Kasper-Giebl, A., Preunkfert, S., Legrand, M., Gelencser, A. (2007). Composition and source apportionment of atmospheric aerosols in Portugal during the 2003 summer intense forest fire period. *Air Pollution XV.*, 1, 45-57.
- Plaisance, H., Galloo, J. C., Guillermo, R. (1997). Source identification and variation in the chemical composition of precipitation at two rural sites in France. *Science of the Total Environment*, 206(1), 79-93.
- Poirot, R. L., Husar, R. B. (2004, October). Chemical and physical characteristics of wood smoke in the northeastern US during July 2002 impacts from Quebec forest fires. *In A&WMA Specialty Conference on Regional and Global Perspectives on Haze: Causes, Consequences and Controversies, Asheville NC (USA)*.
- Quennehen, B., Schwarzenboeck, A., Matsuki, A., Burkhart, J. F., Stohl, A., Ancellet, G., Law, K. S. (2012). Anthropogenic and forest fire pollution aerosol transported to the Arctic: observations from the POLARCAT-France spring campaign. *Atmospheric Chemistry and Physics*, 12(14), 6437-6454.
- Querol, X., Alastuey, A., Pey, J., Cusack, M., Pérez, N., Mihalopoulos, N., Kubilay, N., Koçak, M. (2009). Variability in regional background aerosols within the Mediterranean. *Atmospheric Chemistry and Physics*, 9(14), 4575-4591.
- Querol, X., Pey, J., Pandolfi, M., Alastuey, A., Cusack, M., Pérez, N., Moreno, T., Viana, M., Mihalopoulos, N., Kallos, G., Kleanthous, S. (2009). African dust contributions to mean ambient PM10 mass-levels across the Mediterranean Basin. *Atmospheric Environment*, 43(28), 4266-4277.
- Radke, L. F., Hegg, D. A., Hobbs, P. V., Nance, J. D., Lyons, J. H., Laursen, K. K., Weiss, R.E., Riggan, P.J., Ward, D. E. (1991). Particulate and trace gas emissions from large biomass fires in North America. *Global biomass burning: Atmospheric, climatic, and biospheric implications*, 209-224.
- Reff, A., Eberly, S. I., Bhave, P. V. (2007). Receptor modeling of ambient particulate matter data using positive matrix factorization: review of existing methods. *Journal of the Air & Waste Management Association*, 57(2), 146-154.
- Remoundaki, E., Kassomenos, P., Mantas, E., Mihalopoulos, N., Tsezos, M. (2013). Composition and mass closure of PM2.5 in urban environment (Athens, Greece). *Aerosol Air Qual. Res.*, 13, 72-82.

- Resmi Gazete. (2008). Hava Kalitesi Değerlendirme ve Yönetimi Yönetmeliği. Retrieved from <http://www.mevzuat.gov.tr/Metin.Aspx?MevzuatKod=7.5.12188&MevzuatIliski=0&sourceXmlSearch> (March 2, 2018)
- Robert, M. A., VanBergen, S., Kleeman, M. J., Jakober, C. A. (2007). Size and composition distributions of particulate matter emissions: Part 1—Light-duty gasoline vehicles. *Journal of the Air & Waste Management Association*, 57(12), 1414-1428.
- Samara, C. (2005). Chemical mass balance source apportionment of TSP in a lignite-burning area of Western Macedonia, Greece. *Atmospheric Environment*, 39(34), 6430-6443.
- Schauer, J. J. (2003). Evaluation of elemental carbon as a marker for diesel particulate matter. *Journal of Exposure Science and Environmental Epidemiology*, 13(6), 443.
- Sciare, J., Cachier, H., Oikonomou, K., Ausset, P., Sarda-Esteve, R., Mihalopoulos, N. (2003). Characterization of carbonaceous aerosols during the MINOS campaign in Crete, July–August 2001: a multi-analytical approach. *Atmospheric Chemistry and Physics*, 3(5), 1743-1757.
- Seinfeld, J. H., Pandis, S. N. (2006). *Atmospheric chemistry and physics*. A Wiley-Inter Science Publication.
- Shaw, P. (2008). Application of aerosol speciation data as an in situ dust proxy for validation of the Dust Regional Atmospheric Model (DREAM). *Atmospheric Environment*, 42(31), 7304-7309.
- Sirois, A., Bottenheim, J. W. (1995). Use of backward trajectories to interpret the 5-year record of PAN and O₃ ambient air concentrations at Kejimikujik National Park, Nova Scotia. *Journal of Geophysical Research: Atmospheres*, 100(D2), 2867-2881.
- Smirnov, V. V., Radionov, V. F., Savchenko, A. V., Pronin, A. A., Kuusk, V. V. (1998). Variability in aerosol and air ion composition in the Arctic spring atmosphere. *Atmospheric Research*, 49(2), 163-176.

- Spurny, K. R. (Ed.). (1999). *Analytical Chemistry of Aerosols: Science and Technology*. CRC Press.
- Spyridaki, A., Lazaridis, M., Eleftheriadis, K., Smolik, J., Mihalopoulos, N., Aleksandropoulou, V. (2006). Modelling and evaluation of size-resolved aerosol characteristics in the Eastern Mediterranean during the SUB-AERO project. *Atmospheric Environment*, 40(32), 6261-6275.
- Statgraphics Centurion XVI. User Manual. (2010). StatPoint Technologies.
- Stein, A. F., Draxler, R. R., Rolph, G. D., Stunder, B. J., Cohen, M. D., Ngan, F. (2015). NOAA's HYSPLIT atmospheric transport and dispersion modeling system. *Bulletin of the American Meteorological Society*, 96(12), 2059-2077.
- Stohl, A., Eckhardt, S., Forster, C., James, P., Spichtinger, N. (2002). On the pathways and timescales of intercontinental air pollution transport. *Journal of Geophysical Research: Atmospheres*, 107(D23).
- Stohl, A., Wotawa, G., Seibert, P., Kromp-Kolb, H. (1995). Interpolation errors in wind fields as a function of spatial and temporal resolution and their impact on different types of kinematic trajectories. *Journal of Applied Meteorology*, 34(10), 2149-2165.
- Strode, S. A., Ott, L. E., Pawson, S., Bowyer, T. W. (2012). Emission and transport of cesium-137 from boreal biomass burning in the summer of 2010. *Journal of Geophysical Research: Atmospheres*, 117(D9).
- Subramoney, P., Karnae, S., Farooqui, Z., John, K., Gupta, A. K. (2013). Identification of PM_{2.5} sources affecting a semi-arid coastal region using a chemical mass balance model. *Aerosol and Air Quality Research*, 13(1), 60-71.
- Taylor, S. R. (1964). Abundance of chemical elements in the continental crust: a new table. *Geochimica et cosmochimica acta*, 28(8), 1273-1285.
- Thurston, G. D., Ito, K., Lall, R. (2011). A source apportionment of US fine particulate matter air pollution. *Atmospheric Environment*, 45(24), 3924-3936.

- Tokgöz, D. D. G. (2013). *Temporal Variation in Aerosol Composition at Northwestern Turkey*. PhD Thesis, Middle East Technical University, Ankara
- Trickl, T., Vogelmann, H., Flentje, H., Ries, L. (2015). Stratospheric ozone in boreal fire plumes—the 2013 smoke season over central Europe. *Atmospheric Chemistry and Physics*, 15(16), 9631-9649.
- Tuncel, G., Aras, N. K., Zoller, W. H. (1989). Temporal variations and sources of elements in the South Pole atmosphere: 1. Nonenriched and moderately enriched elements. *Journal of Geophysical Research: Atmospheres*, 94(D10), 13025-13038.
- Turekian, K. K., Wedepohl, K. H. (1961). Distribution of the elements in some major units of the earth's crust. *Geological Society of America Bulletin*, 72(2), 175-192.
- Türküm, A., Pekey, B., Pekey, H., Tuncel, G. (2008). Comparison of sources affecting chemical compositions of aerosol and rainwater at different locations in Turkey. *Atmospheric Research*, 89(4), 306-314.
- Twomey, S. (1991). Aerosols, clouds and radiation. *Atmospheric Environment. Part A. General Topics*, 25(11), 2435-2442.
- Urban, R. C., Lima-Souza, M., Caetano-Silva, L., Queiroz, M. E. C., Nogueira, R. F., Allen, A. G., Cardoso, A.A., Held, G., Campos, M. L. A. (2012). Use of levoglucosan, potassium, and water-soluble organic carbon to characterize the origins of biomass-burning aerosols. *Atmospheric environment*, 61, 562-569.
- Urbanski, S. P., Hao, W. M., Baker, S. (2008). Chemical composition of wildland fire emissions. *Developments in Environmental Science*, 8, 79-107.
- URL 1. Retrieved from <http://www.steelonthenet.com/maps.html> (February 25, 2018)
- US EPA. (1995). AP 42, Fifth Edition: Compilation of Air Pollutant Emission Factors. North Carolina. Retrieved from <https://www3.epa.gov/ttnchie1/ap42/ch01/final/c01s04.pdf> (June 17, 2017)
- US EPA. (2005). Environmental Protection Agency Air Toxics Division

- US EPA. (2015). National Emissions Inventory, version 2 Technical Support Document. Retrieved from https://www.epa.gov/sites/production/files/2015-10/documents/nei2011v2_tsd_14aug2015.pdf (September 22, 2017)
- US EPA. (2016a). Basic Information Particulate Matter. Retrieved from <https://www.epa.gov/pm-pollution/particulate-matter-pm-basics#PM> (March 10, 2018)
- US EPA. (2016b). Health and Environmental Effects of Particulate Matter (PM). Retrieved from <https://www.epa.gov/pm-pollution/health-and-environmental-effects-particulate-matter-pm> (January 15, 2018)
- US EPA. (2016c). Air Quality and Climate Change Research. Retrieved from <https://www.epa.gov/air-research/air-quality-and-climate-change-research> (June 4, 2017)
- US EPA. (2016d). National Ambient Air Quality Standards. Retrieved from <https://www.epa.gov/criteria-air-pollutants/naaqs-table> (March 2, 2018)
- US EPA. (2017a). Air Emission Sources. Retrieved from https://www3.epa.gov/cgi-bin/broker?polchoice=PM&_debug=0&_service=data&_program=dataprog.national_1.sas (March 10, 2018)
- US EPA. (2017b). Particulate matter (PM) Pollution. Retrieved from <https://www.epa.gov/pm-pollution> (November 2, 2017)
- US EPA. (2018). Criteria Air Pollutants. Retrieved from <https://www.epa.gov/criteria-air-pollutants> (March 10, 2018)
- US EPA.(2017c). Method Detection Limit - Frequent Questions. Retrieved from <https://www.epa.gov/cwa-methods/method-detection-limit-frequent-questions> (February 8, 2018)
- Uz, I., Tavali, I. E. (2014). Short-term effect of vermicompost application on biological properties of an alkaline soil with high lime content from Mediterranean region of Turkey. *The Scientific World Journal*, 2014.

- Vet, R., Ro, C. U. (2008). Contribution of Canada–United States transboundary transport to wet deposition of sulphur and nitrogen oxides—A mass balance approach. *Atmospheric Environment*, 42(10), 2518-2529.
- Viana, M., Kuhlbusch, T. A. J., Querol, X., Alastuey, A., Harrison, R. M., Hopke, P. K., Winiwarter, W., Vallius, M., Szidat, S., Prévôt, A.S.H., Hueglin, C. (2008). Source apportionment of particulate matter in Europe: a review of methods and results. *Journal of aerosol science*, 39(10), 827-849.
- Vinogradov, A. P. (1959). Geochemistry of rare and dispersed chemical elements in soils.
- Voiland, A. (2010). Aerosols: Tiny Particles, Big Impact. Retrieved from <https://earthobservatory.nasa.gov/Features/Aerosols/> (March 10, 2018)
- Wang, X., Jing, H., Dhungel, B., Wang, W. N., Kumfer, B. M., Axelbaum, R. L., Biswas, P. (2016). Characterization of organic and black carbon aerosol formation during coal combustion: An experimental study in a 1MW pilot scale coal combustor. *Fuel*, 180, 653-658.
- Wang, Y. Q., Zhang, X. Y., Draxler, R. R. (2009). TrajStat: GIS-based software that uses various trajectory statistical analysis methods to identify potential sources from long-term air pollution measurement data. *Environmental Modelling & Software*, 24(8), 938-939.
- Wang, Y., Zhuang, G., Zhang, X., Huang, K., Xu, C., Tang, A., Chen, J., An, Z. (2006). The ion chemistry, seasonal cycle, and sources of PM_{2.5} and TSP aerosol in Shanghai. *Atmospheric Environment*, 40(16), 2935-2952.
- Ward Jr, J. H. (1963). Hierarchical grouping to optimize an objective function. *Journal of the American statistical association*, 58(301), 236-244.
- Watson, J. G., Antony Chen, L. W., Chow, J. C., Doraiswamy, P., Lowenthal, D. H. (2008). Source apportionment: findings from the US supersites program. *Journal of the Air & Waste Management Association*, 58(2), 265-288.
- Westervelt, D. M., Pierce, J. R., Adams, P. J. (2014). Analysis of feedbacks between nucleation rate, survival probability and cloud condensation nuclei formation. *Atmospheric Chemistry and Physics*, 14(11), 5577-5597.

- Whitby, K. T. (1978). The physical characteristics of sulfur aerosols. In *Sulfur in the Atmosphere* (pp. 135-159).
- Whitby, K. T., Sverdrup, G. M. (1980). California aerosols-their physical and chemical characteristics. *Adv. Environ. Sci. Technol.:(United States)*, 9.
- World Health Organization. (2002). SILVER AND SILVER COMPOUNDS: ENVIRONMENTAL ASPECTS. Retrieved from <http://apps.who.int/iris/bitstream/10665/42553/1/9241530448.pdf> (March 12, 2018)"
- World Health Organization. (2003). Health Aspects of Air Pollution with Particulate Matter, Ozone and Nitrogen Dioxide. Retrieved from www.euro.who.int/__data/assets/pdf_file/0005/112199/E79097.pdf (March 10, 2018)
- World Health Organization. (2013). Health effects of particulate matter. Retrieved from http://www.euro.who.int/__data/assets/pdf_file/0006/189051/Health-effects-of-particulate-matter-final-Eng.pdf (March 10, 2018)
- Xie, Y. L., Hopke, P. K., Paatero, P., Barrie, L. A., Li, S. M. (1999). Identification of Source Nature and Seasonal Variations of Arctic Aerosol by positive matrix factorization. *Journal of the Atmospheric Sciences*, 56(2), 249-260.
- Yatin, M., Tuncel, S., Aras, N. K., Olmez, I., Aygun, S., Tuncel, G. (2000). Atmospheric trace elements in Ankara, Turkey: 1. Factors affecting chemical composition of fine particles. *Atmospheric Environment*, 34(8), 1305-1318.
- Yendra, R., Jemain, A. A., Zahari, M., Wan Zin, W. Z. (2013, April). Methods on handling missing rainfall data with Neyman-Scott rectangular pulse modeling. *In AIP Conference Proceedings* (Vol. 1522, No. 1, pp. 1213-1220). AIP.
- Yokoo, Y., Nakano, T., Nishikawa, M., Quan, H. (2004). Mineralogical variation of Sr-Nd isotopic and elemental compositions in loess and desert sand from the central Loess Plateau in China as a provenance tracer of wet and dry deposition in the northwestern Pacific. *Chemical Geology*, 204(1-2), 45-62.
- Zeng, Y., Hopke, P. K. (1989). A study of the sources of acid precipitation in Ontario, Canada. *Atmospheric Environment (1967)*, 23(7), 1499-1509.

- Zhang, C., Yao, Q., Sun, J. (2005). Characteristics of particulate matter from emissions of four typical coal-fired power plants in China. *Fuel Processing Technology*, 86(7), 757-768.
- Zhao, H., Che, H., Zhang, X., Ma, Y., Wang, Y., Wang, H., Wang, Y. (2013). Characteristics of visibility and particulate matter (PM) in an urban area of Northeast China. *Atmospheric Pollution Research*, 4(4), 427-434.
- Zhao, W., Hopke, P. K. (2006). Source investigation for ambient PM 2.5 in Indianapolis, IN. *Aerosol science and technology*, 40(10), 898-909.
- Zhu, Y., Hinds, W. C., Kim, S., Shen, S., Sioutas, C. (2002). Study of ultrafine particles near a major highway with heavy-duty diesel traffic. *Atmospheric environment*, 36(27), 4323-4335.
- Zoller, W. H., Gladney, E. S., Duce, R. A. (1974). Atmospheric concentrations and sources of trace metals at the South Pole. *Science*, 183(4121), 198-200.

CIRRICULUM VITAE

PERSONAL INFORMATION

Surname, Name: Balcılar, İlker

Nationality: Turkish (TC)

Date and Place of Birth: 1 January 1985, Kadirli

Marital Status: Married

Email: ibalcilar@hotmail.com

EDUCATION

Degree	Institution	Year of Graduation
BS	Ç.U., Environmental Engineering	2010

WORK EXPERIENCE

Year	Place	Enrollment
2016-2017	Desert Research Institute, USA	Visiting Researcher
2011-2018	METU, Environmental Engineering	Teaching Assistant
2010-Present	AU, Environmental Engineering	Teaching Assistant

FOREIGN LANGUAGES

English: Advanced

GRANTS AND AWARDS

TÜBİTAK- International Doctoral Research Fellowship Programme for PhD Students
Scholarship

PUBLICATIONS AND PROCEEDINGS

PEER-REVIEWED JOURNAL ARTICLES

Balcılar, İ., Zararsız, A., Kalaycı, Y., Doğan, G., Tuncel, G. (2014). Chemical composition of Eastern Black Sea aerosol—preliminary results. *Science of the Total Environment*, 488, 422-428.

Balcilar, I., Zararsiz, A., Kalayci, Y., Dogan, G., Tuncel, G. (2017). Similarities and Differences in Compositions of Eastern and Western Black Sea Aerosol. *Fresenius Environmental Bulletin*, 26(1), 301-309.

Balcilar, I., Zararsiz, A., Kalayci, Y., Dogan, G., Tuncel, G. (2018). Temporal Variations of Eastern Black Sea Aerosol. *Global NEST Journal*, 20(1), 115-121.

PUBLICATIONS IN INTERNATIONAL CONFERENCE PROCEEDINGS

İlker Balcılar, Abdullah Zararsız, Yakup Kalaycı, Güray Dogan, Gürdal Tuncel, 2012, Chemical composition of Eastern Black Sea Aerosol. Air Quality Management at Urban, Regional and Global Scales, 4th International Symposium and IUAPPA Regional Conference, Book of Proceedings, pp 302-310, Istanbul 10-13 September.

İlker Balcılar, Abdullah Zararsız, Yakup Kalaycı, Güray Dogan, Gürdal Tuncel, 2015, Sources Affecting The Chemical Composition Of Particles In The Eastern Black Sea Basin. The International Network of Environmental Forensics 2015. Book of Abstracts, pp 39, Victoria College, Toronto, Canada, 3-6 August 2015.

İlker Balcılar, Abdullah Zararsız, Yakup Kalaycı, Güray Dogan, Gürdal Tuncel, 2015, Similarities and differences in compositions of Eastern and Western Black Sea aerosol, 18th International Symposium on Environmental Pollution and its Impact on Life in the Mediterranean Region, Book of Abstracts, pp 124, Crete- Greece, 26-30 September 2015.

Ahmet Mustafa Tepe, Güray Doğan, İlker Balcılar, 2015, Comparison of influence of dust transport to PM10 concentrations in different cities located on Mediterranean coast of Turkey, 18th International Symposium on Environmental Pollution and its Impact on Life in the Mediterranean Region, Book of Abstracts, pp 136, Crete- Greece, 26-30 September 2015.

Deniz G. Tokgöz, İlker Balcılar, Güray Doğan, Ali İhsan İlhan, Tulay Balta, Gürdal Tuncel, 2016, Chemical composition of atmospheric aerosol at the western Black Sea atmosphere, 1st International Black Sea Congress on Environmental Sciences, Book of Abstracts, pp 27, Giresun-Turkey, August 31 - September 03, 2016.

İlker Balcılar, Abdullah Zararsız, Yakup Kalaycı, Güray Doğan, Gürdal Tuncel, 2016, Temporal variations of Eastern Black Sea aerosol, 1st International Black Sea Congress on Environmental Sciences, Full Paper Book, pp 9-20, Giresun-Turkey, August 31 - September 03, 2016.

Ahmet Mustafa Tepe, İlker Balcılar and Güray Doğan, 2016, Determination of elemental composition of winter season particulates in Antalya urban atmosphere, 1st International Black Sea Congress On Environmental Sciences, Full Paper Book, pp 914- 922, Giresun-Turkey, August 31 - September 03, 2016.

Ömer Ateş, İlker Balcılar and Gürdal Tuncel, 2016, Design and construction of a sampling system that can collect Pm10, Pm2.5 and Pm1 samples simultaneously from atmosphere, 1st International Black Sea Congress On Environmental Sciences, Book of Abstracts, pp 153, Giresun-Turkey, August 31 - September 03, 2016.

İlker Balcılar, Abdullah Zararsız, Yakup Kalaycı, Güray Doğan, Gürdal Tuncel, 2017, The Use of Back Trajectory Cluster Analysis with PM2.5 Composition at the Eastern Black Sea of Turkey, 8th Atmospheric Sciences Symposium, 01 – 04 November 2017 Istanbul – TURKEY

PUBLICATIONS IN NATIONAL CONFERENCE PROCEEDINGS

İlker Balcılar, Abdullah Zararsız, Yakup Kalaycı, Güray Doğan, Gürdal Tuncel, 2013, “Investigation of Chemical Composition of Eastern Black Sea Atmosphere Aerosol”, 5. Uluslararası Katılımlı Hava Kirliliği ve Kontrolü Sempozyumu, Bildiri Özetleri Kitabı, pp 136, 18-20 Eylül, 2013, Eskişehir, Türkiye.

İlker Balcılar, Abdullah Zararsız, Yakup Kalaycı, Güray Doğan, Gürdal Tuncel, 2015, Doğu Karadeniz ve Batı Karadeniz Atmosferi Aerosolleri Kimyasal Kompozisyonunun Karşılaştırılması, 6. Ulusal Hava Kirliliği ve Kontrolü Sempozyumu-2015, Bildiri Kitabı, pp 262-272, 7-9 Ekim 2015, İzmir, Türkiye.

İlker Balcılar, Abdullah Zararsız, Yakup Kalaycı, Güray Doğan, Gürdal Tuncel, 2017, Türkiye'nin Doğu Karadeniz Bölgesindeki PM için Potansiyel Kaynak Analizi, 12. Ulusal Çevre Mühendisliği Kongresi, Bildiri Özetleri Kitabı, pp 89-90, 5-7 Ekim 2017, Ankara, Türkiye.

Ömer Ateş, İlker Balcılar, Gürdal Tuncel, 2017, Atmosferden Pm10, Pm2.5 ve Pm1 Parçacıkları Eş Zamanlı Olarak Toplayabilecek, Ekonomik Bir Örnekleme Sisteminin Geliştirilmesi, 12. Ulusal Çevre Mühendisliği Kongresi, Bildiri Özetleri Kitabı, pp 163-164, 5-7 Ekim 2017, Ankara, Türkiye.

Derya Deniz Genç Tokgöz, İlker Balcılar, Ali İhsan İlhan, Tülay Balta, Gürdal Tuncel, 2017, Batı Karadeniz Aerosolunun Zamansal Değişiminin Değerlendirilmesi, VIII. Ulusal Hava Kirliliği ve Kontrolü Sempozyumu, 1-3 Kasım 2017, Antalya, Türkiye.